THERMOTECTONIC EVOLUTION OF THE CONTINENTAL MARGINS OF THE BAY OF BISCAY: APPLICATION OF APATITE FISSION TRACK ANALYSIS

Ruth Siddall

A thesis submitted for the requirements
of the Degree of Doctor of Philosophy

Department of Geological Sciences
University College
University of London

September 1993

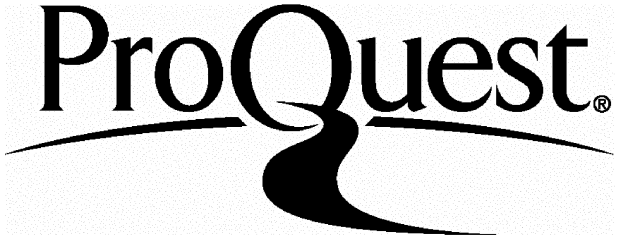

To my Mother and Father.

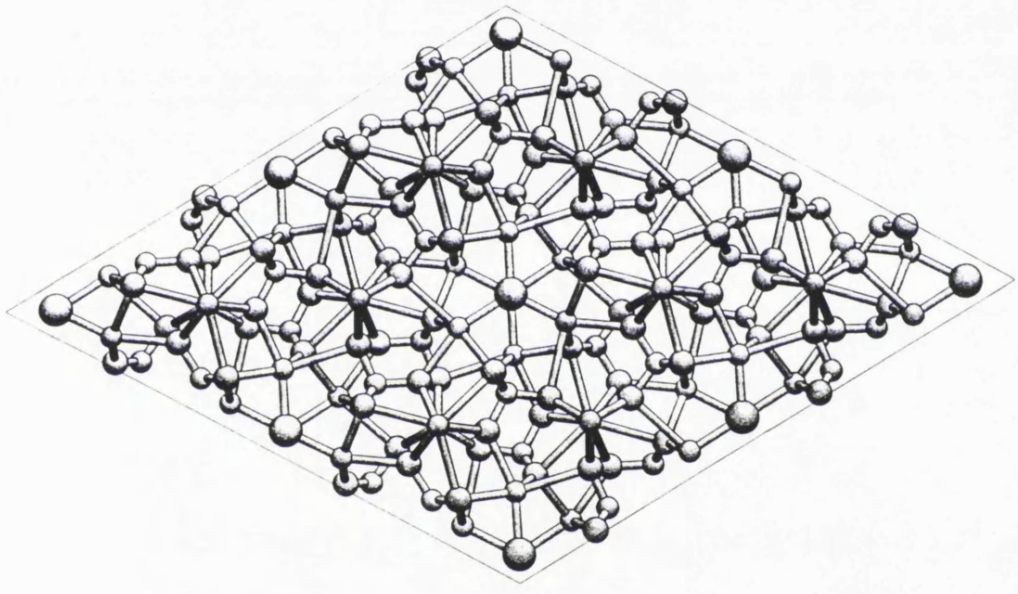

A mineral name has never been more appropriately selected than that of apatite, which is from απαταω (I deceive).

D. McConnell, 1938.

ERRATUM

The final sentence on page 18 (finishing on page 20) should read:-

In the North Atlantic region, a number of passive margin studies have been or are currently being compiled. The presence of eroded Precambrian and Palaeozoic basement on many of the western margins of Europe, bordered to the east by Mesozoic sediments, is indicative of denudation along the rifted margins.

Abstract

The sensitivity of apatite fission tracks to cooling and unroofing episodes in Earth history is particularly suited to the tectonic processes of rifting and the long term evolution of continental margins. Apatite fission track analyses have been made on ~70 samples of igneous, metamorphic and sedimentary rocks from coastal outcrops of Western France (the Armorican Massif) and north-western Spain (the Hesperian Massif) the aim being to unravel the potential thermal overprint associated with the opening of the North Atlantic Ocean, specifically in the Bay of Biscay.

This thesis reviews the geological evolution of the continental margins of the Bay of Biscay region and presents the fission track sampling strategies and analytical results. The fission track ages range from ~70 to 270 Ma, with the youngest ages towards the Atlantic coasts, and become progressively older eastwards. The data are interpreted in terms of the thermal histories resulting from the Mesozoic post-breakup exhumation of the rift flanks in the westernmost regions of Spain and France, whilst eastwards the earliest detectable cooling episode is Early Permian, reflecting the exhumation of the Variscan mountain chain.

The data from the Armorican Massif are consistent with 2 previously unrecognised periods of burial and subsequent exhumation during the Mesozoic. The most recent (Campanian) burial episode is inferred to represent the deposition of chalk. The data from north-western Spain do not appear to reflect this second burial, probably because at this time this region was outside the chalk depocentre.

A second major aspect of the research is an assessment of the role of chemical composition as a control on variation in single grain ages within a sample. In particular, annealing of fission tracks in apatites rich in chlorine is expected to be retarded relative to a more fluorine-rich crystal, resulting in an older fission track age. A new application of infrared microspectroscopy has been developed to determine the chemical compositions of apatites *in situ* on the grain mount, enabling the significance of the relationship of fission track age to apatite chemistry to be assessed directly. This method relies on the progressive shift of infrared spectral peaks towards lower wavenumbers with the increasing chlorine. This phenomenon indicates that it is the structural rather than chemical adjustment of the crystal to the substitution of a large ion such as Cl^- that is important to the annealing of fission tracks in apatite. The methodology is an important advancement to the technique of fission track analysis being rapid and non-destructive.

Acknowledgements

Many thanks go especially to the following people:

my supervisors;
Dr Tony Hurford and Dr Monica Mendelssohn

Everyone in the London FT Lab past and present: Kerry Gallagher, Andy Carter, Andy Yelland, Kit Johnson, Vijay Vohora, Alún O'Brien, Stuart Thompson, Susie Loates, Cherry Lewis and Rod Brown for help, tuition, support, information and ideas.

Mike Audley-Charles and Jason Lane for collecting samples for fission track dating when they should have been on holiday.

Dr Andy Tindle for invaluable use of the electron microprobe at the Open University. The British Museum (Natural History), Bart Kowallis, Paul Green and Rod Brown for the provision of apatite samples for the infrared data set and to Dave Harris for the use of sample TIM 655

At UCL thanks to Professor David Price, Dr Nancy Ross, Dr Judith Milledge, Professor Paul Henderson, Dr Ian Starmer, Dr John Stuart, Rex Galbraith, Janet Baker, Colin Stuart, Mike Gray, Ron Dudman, Ken Coventry, Leisa Clemente and Deborah Lewis for invaluable help, ideas and interest.

Professor Bernard Auvray and Bruno Reynard at the University of Rennes for excellent field advice and help with translations.

Dr Marcos Zentilli, Dr Chris Beaumont, Dr. Jakob Verhoef, Dennis Arne, Sandy Grist, Antonio, John Shimeld, Sarah Palmer and everyone else at Dalhousie University and the Bedford Institute of Oceanography, Nova Scotia, for letting me work there with all needs provided for.

And to everyone else at UCL Department of Geological Sciences, especially Charlie Bristow, Mark Cowgill, Phil Dolding, Chen-Hui Fan, Chris Hayward, Faz Jaffri, Nils and Anne Kågeson-Loe, Llynne McCarthy, Alit Ngakan, David Petley, Spencer Roberts, Andy Samuel, Steve Starkie and Lidunka Vocadlo for moral support, entertainment and the rest.

And NERC award GT4 / 89 / GS / 78

Contents

List of Figures

ADDENDA

List of Tables

ADDENDA

Chapter 1

Prologue.

1.1 Introduction

The aims of this thesis are twofold. Firstly, on a continental scale, a set of samples collected from the relicts of the Palaeozoic Variscan Orogeny in western France and Spain have been investigated using apatite fission track analysis in an attempt to refine the nature of thermotectonic processes in this geologically complex region. Although the continental margins of the Bay of Biscay are a key region for understanding the evolution of the eastern North Atlantic Ocean, the onshore Mesozoic and Cenozoic evolution of the area is poorly understood.

A second aim of this thesis, on a crystallographic scale, has been to develop the technique of Fourier Transform infrared microspectroscopy as a method for ascertaining the chlorine and fluorine contents of apatites used for fission track analysis. In the field of fission track research, the study of the sensitivity of fission track annealing in response to temperature, is far better understood in apatites than it is for zircon and sphene. However, there are still uncertainties within the interpretation of the annealing kinetics. The major stumbling block is the effect of chlorine as a major element substitution in apatite. Laboratory experiments and the study of geological situations have revealed that chlorapatites are more resistant to annealing than the more common fluorapatites. An aim of this project is to develop a routine method of compositional determination from which direct comparisons of apatite chemistry may be made with fission track age and length measurements, as a first step to understanding the problem.

1.2 Why use apatite fission track analysis?

Fission tracks accumulate in uranium-rich minerals, such as apatite, over geological time due to the spontaneous fission decay of ^{238}U **(Fig. 1.1)**. A fission track is essentially a string of defects in the crystal lattice, caused by the passage of a fission particle. They are not stable features, and can be erased (annealed) by heating, in a process that gradually shortens the tracks and then removes them totally over a temperature range of 60 - 120 °C over a timescale of 1 to 100 Myr. This temperature window is commonly known as the partial annealing zone. The degree of shortening of a track is directly related to the maximum temperature that track has reached and consequently, as tracks are continually forming in the crystal, regardless of

Fig. 1.1. A photomicrograph of a an apatite crystal showing etched fission tracks. The original photograph was taken at 1250x magnification.

geological events, an image of the thermal history suffered by the crystal and
by association, the host rock, is recorded. Measurement of the track lengths in a sample reveals an integrated thermal history of a sample from which the timing of maximum temperatures can be determined.

The uplift and denudation of rifted margins, such as those of the Bay of Biscay, both possibly accompanied by an increase in crustal heat flow, illustrates the links between plate tectonics and geomorphology. Rifted margins can be subdivided into those in which continental breakup and seafloor spreading have occurred, and those that have either failed or not yet developed a spreading centre, and remain as rift valleys. Fission track analysis has been applied to both rift margin types, and in each case, the reduced apatite ages observed have been interpreted as resulting from denudation and cooling, rather than enhanced heat flow.

Moore et al. (1986) produced some of the earliest and most influential fission track work on rift flanks, from the Palaeozoic basement adjacent to the Palaeogene separation of the Lord Howe Rise from SE Australia. Significantly, a clear trend was observed as the apparent fission track ages rapidly decreased from Permian dates to 80-120 Ma at approximately 130 km from the rift margin **(Fig. 1.2)**. Such a relationship between the geometry of rifted margins and the apatite fission track data, explained in this case by a *mild thermal event* associated with rifting coupled with the erosion of the upwarped rift flanks, cannot be ignored. Also, they noted the oldest ages were associated with the highest elevations in the hinterland.

Similar patterns of apatite fission track ages have been recognised from other rift margins, in a variety of tectonic settings, including the Rio Grande Rift (Kelley and Duncan, 1986), the Red Sea (Omar et al., 1987; Kohn and Eyal, 1981), the East Greenland Rift (Hansen, 1988; Gleadow and Brooks, 1979) the East African Rift (Foster and Gleadow, 1992), South-west Africa (Brown, 1990) and in the Transantarctic Mountains (Gleadow and Fitzgerald, 1987). All of these studies have indicated a pattern of uplifted and consequently denuded rift margins, the reduced apatite fission track ages representing the erosional episodes, and a general increase in apatite age moving away from the rift flanks. Rift margins are also occasionally characterised by a region of 'mixed ages' in the hinterland, representing uplift from various levels in the apatite partial annealing zone (Kohn and Eyal, 1981).

In the North Atlantic region, a number of passive margin studies have been or are currently being compiled. The presence of eroded

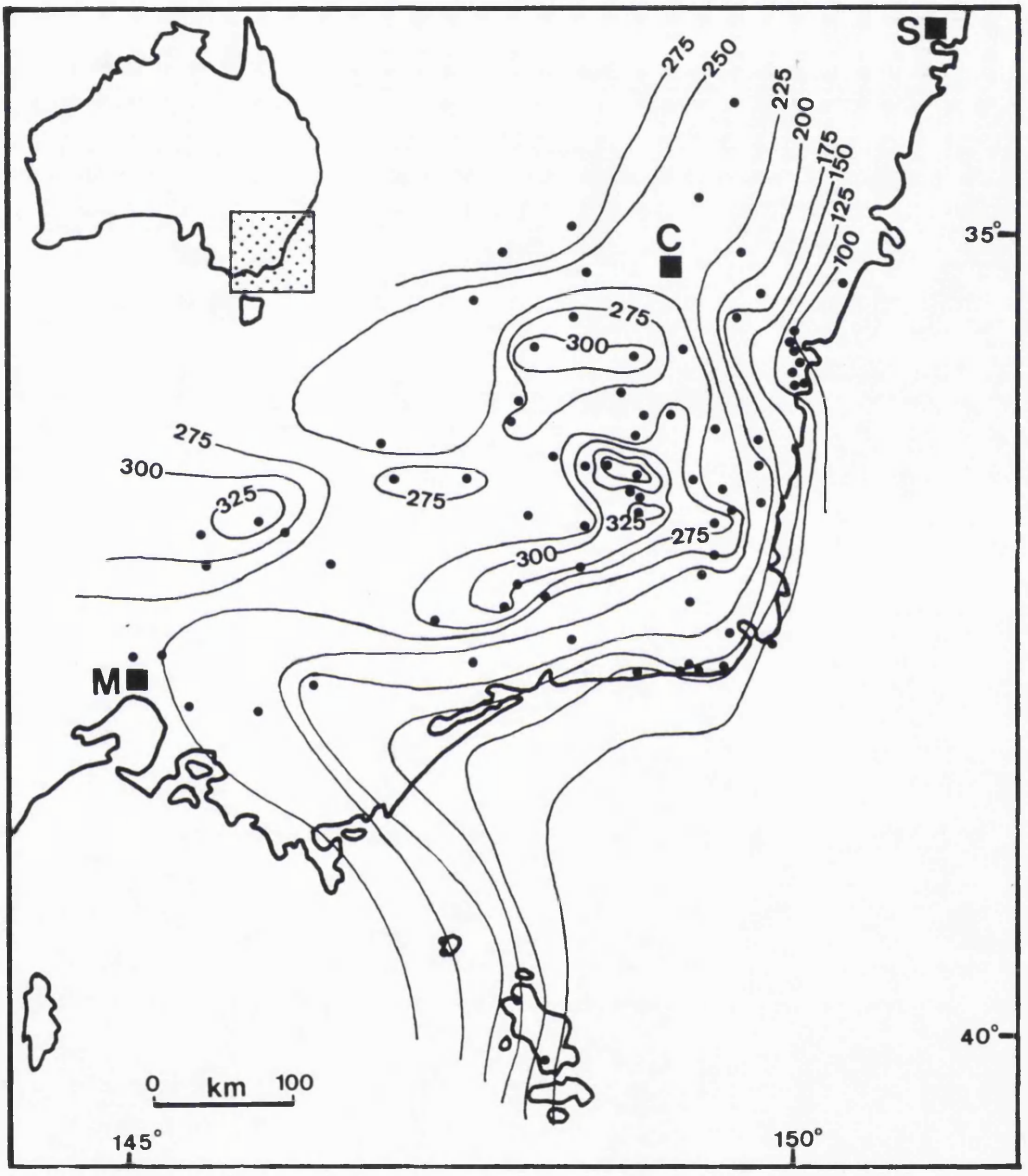

Fig. 1.2. Apatite fission track data from South-East Australia, contoured at 25 Myr intervals. Fission track age increases away from the rift axis (after Moore et al., 1986).

Precambrian and Palaeozoic basement on many of the western margins of denudation along the rifted margins. At present there is minor relief in these regions (the British Isles, Western France, Portugal and Northern Spain). The influence of localised thermal episodes, for example the intrusion of Tertiary igneous bodies in the British Tertiary Volcanic Province (Hurford, 1977a; Lewis et al., 1992b), again associated with the rifting, have produced localised thermal perturbations.

Existing fission track data from the Atlantic continental margins are compiled in **Figure 1.3,** showing the regions sampled and the apatite age ranges. It is the simplest scenario to interpret the fission track data from these continental margins as representing Mesozoic-Tertiary rifting coupled with the denudation of Palaeozoic basement complexes. However, as the scope and detail of sampling increases, the picture becomes more complex on both local and regional scales. All the areas have been affected by events possibly separate from Atlantic rifting and breakup; for example basin subsidence, hot fluid circulation and volcanism. However, the general trend apparent from the case studies compiled on the map is the decrease of the upper fission track age limit northwards (from ~145 - 15 Ma), whereas the lower limit remains within a similar range (~200 - 300 Ma), broadly following the inferred northward propagating opening of the North Atlantic Ocean. The ages are also representative of the periods of rifting and breakup in the region (Permian-Tertiary). The Palaeozoic margins of the Bay of Biscay thus provide an ideal location to further this field of active research.

1.3 The continental margins of the Bay of Biscay.

1.3.1 Introduction.

The Bay of Biscay is a deep indentation into the Atlantic coast of west central Europe, bounded to the north by the Armorican Peninsula of western France, and to the south by the northern part of the Iberian Peninsula. It has the steepest continental slope in Europe, reaching the 2000 m depth marine contour, in places, within 50 km of the north Spanish coast **(Fig. 1.4).**

Geologically, the continental margins of the Bay of Biscay comprise two Proterozoic to Palaeozoic basement complexes: the Armorican Massif of western France and the Hesperian Massif of NW Spain. These continental regions were chosen for this apatite fission track study. A simplified geological map of the region is illustrated in **Figure 1.5.**

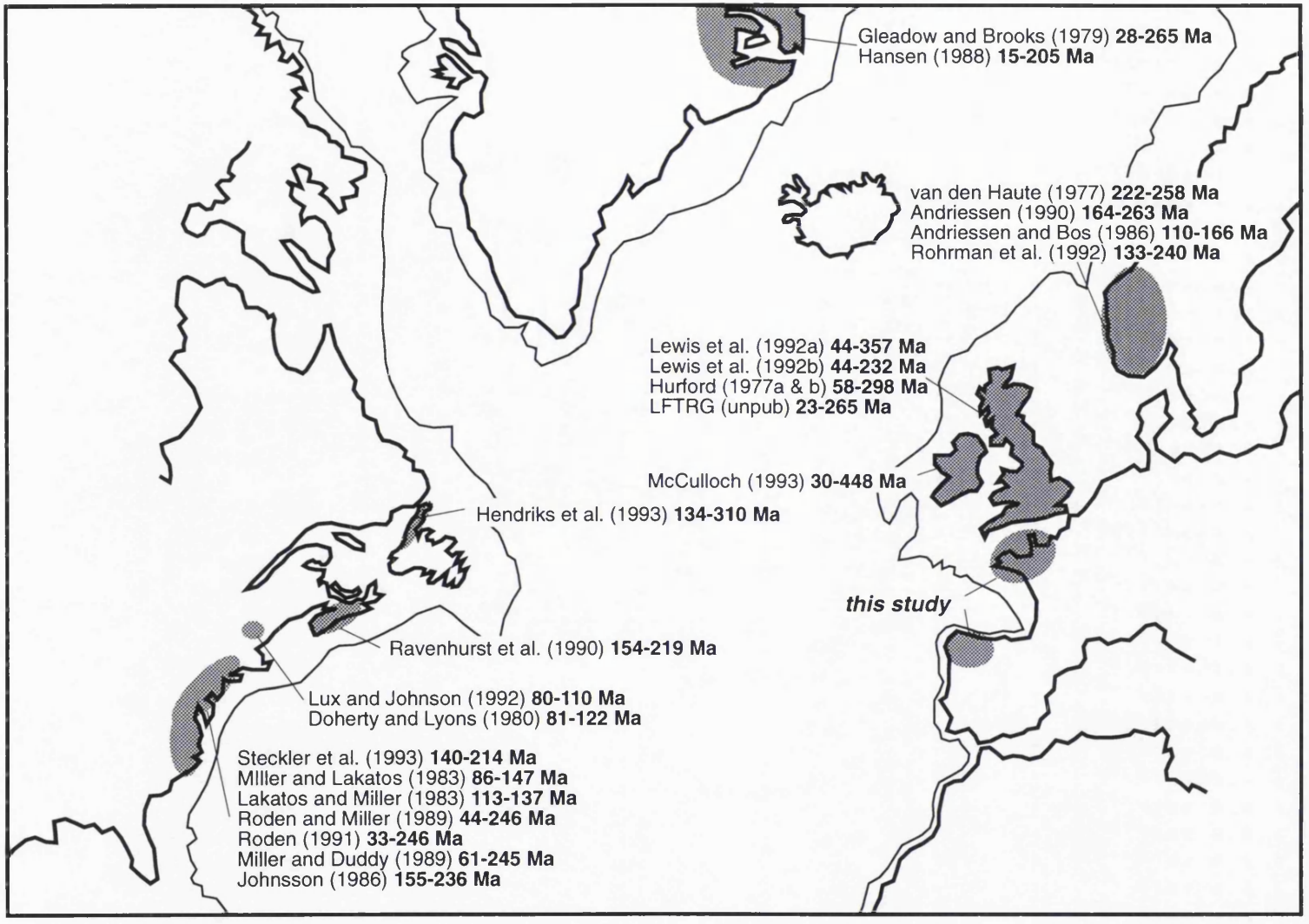

Fig. 1.3. Some recent apatite fission track studies from the North Atlantic Margins. Age-ranges are in bold type, areas studied are shaded.

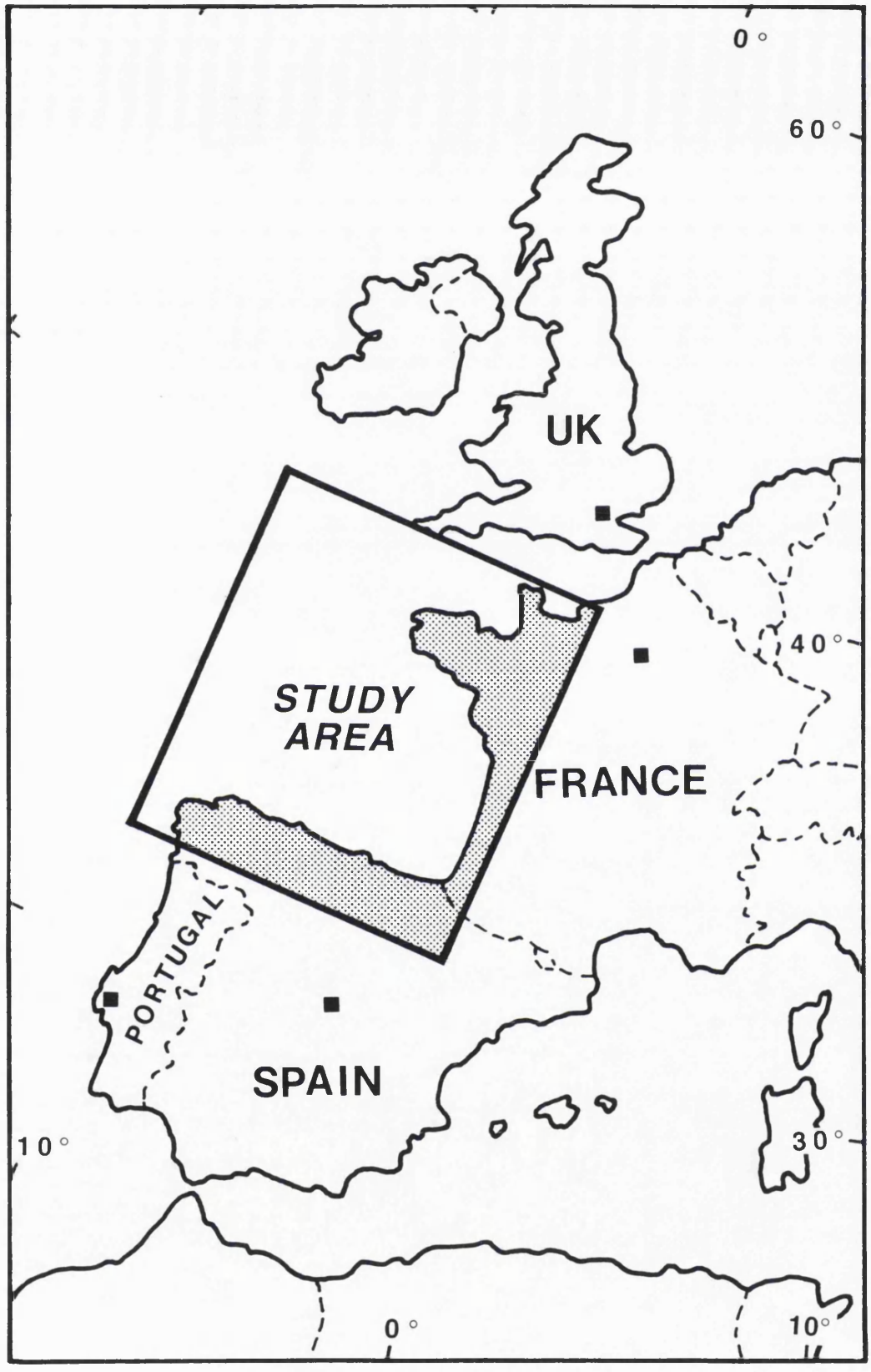

Fig. 1.4. The region studied in this thesis.

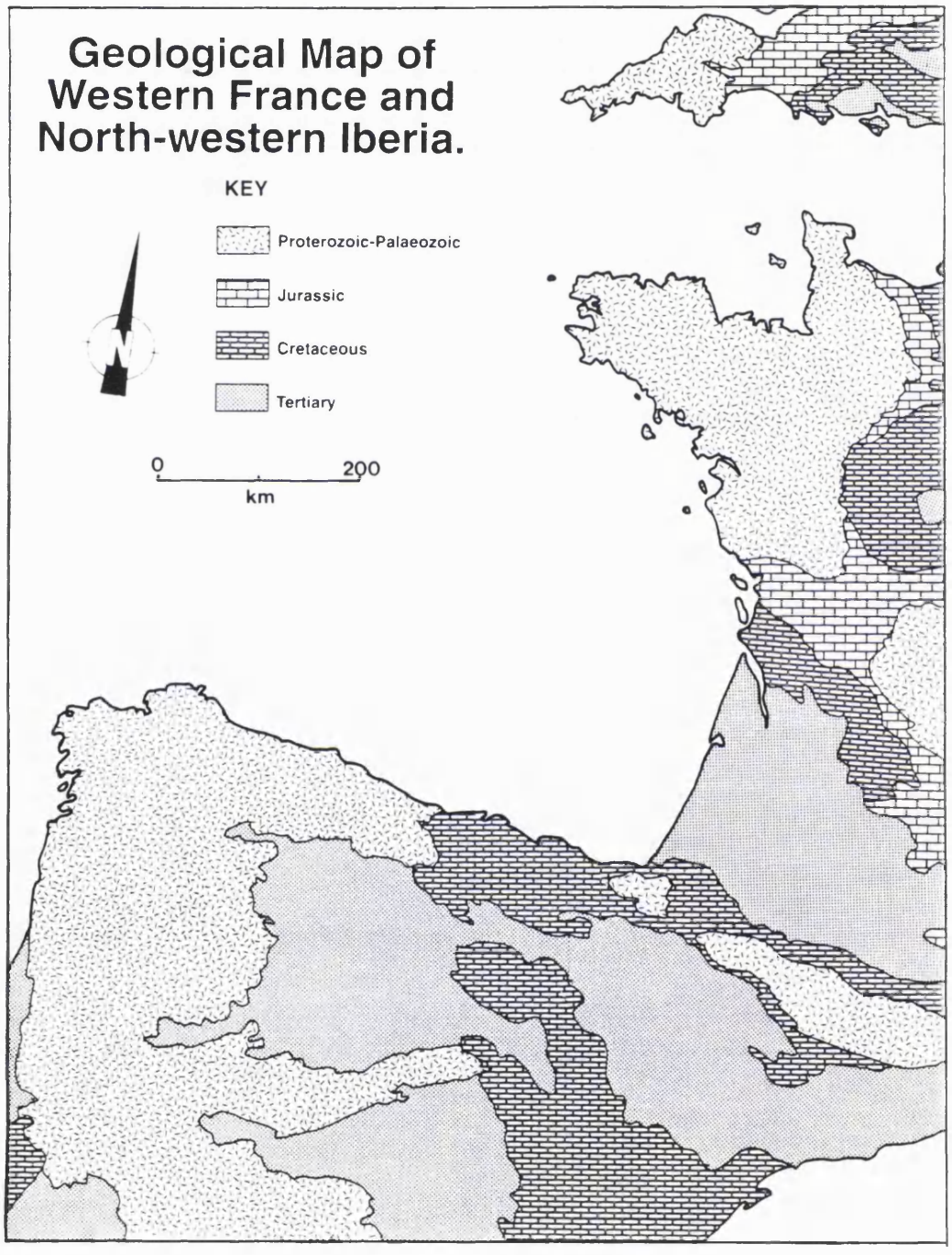

Fig. 1.5. A simplified geological map of Western Central Europe.

1.3.2 Geological evolution of the continental margins of the Bay of Biscay.

The Hesperian and Armorican Massifs are relicts of the Hercynian Orogeny that occurred as a result of the Palaeozoic convergence of Gondwana upon Laurasia, and its eventual collision, forming the supercontinent Pangaea during the late Carboniferous. Fragments of the older Proterozoic, Cadomian Orogenic Belt is also incorporated into these massifs. The Hesperian and Armorican Massifs are specifically segments of the Variscan Belt, the European arm of the Hercynian Orogeny. They form between them the Ibero-Armorican Arc, a major syntaxis in the Variscan Belt. As a consequence of this structure, the Variscan Belt strikes NW through the Iberian Peninsula and changes strike abruptly to approximately E-W through the Armorican Massif and Central Europe. The core is preserved in the highly tectonised Asturian Arc of Northern Spain.

The Mesozoic evolution of the region was dominated by the breakup of Pangaea, which was initiated during the Permo-Trias by the formation of rift valleys. Atlantic Ocean-related continental breakup ensued along some of these rifts during the Jurassic and Cretaceous. The Bay of Biscay formed as a failed arm of the Atlantic, synchronous with the separation of Iberia from North America during the Middle Cretaceous. The Mesozoic was also the time of the formation of the major sedimentary basins preserved today in west-central Europe. In France, these are the Paris basin, draining the rivers Seine and Loire, and the Aquitaine Basin, draining the Garonne-Dordogne system. In the interior meseta of Spain the Ebro and Duero basins drained by their eponymous rivers, onlap to the south of the Hesperian Massif, and the rift-related Cantabrian Basin, on the northern coast between the Hesperian Massif and the Pyrenées.

1.3.3 Geographical and cultural background.

Despite their geographical separation, there are many similarities in culture between the Armorican and Hesperian Massifs. Both are isolated due to their position on the western edges of Europe, suffering the unpredictable nature of the wet, marine climate forced by the presence of the Atlantic Ocean. Topography is dictated in both regions by an underlying similarity of geology, and is predominately of low relief. This is particularly true of Armorica; north-west Spain, like much of the country is of relatively high elevation and a greater relief **(Fig. 1.6)**.

The regions have suffered a similar history and are both rich in Neolithic remains and monuments. There are numerous dolmens, menhirs (standing stones) and henges. Most famous are the stone avenues

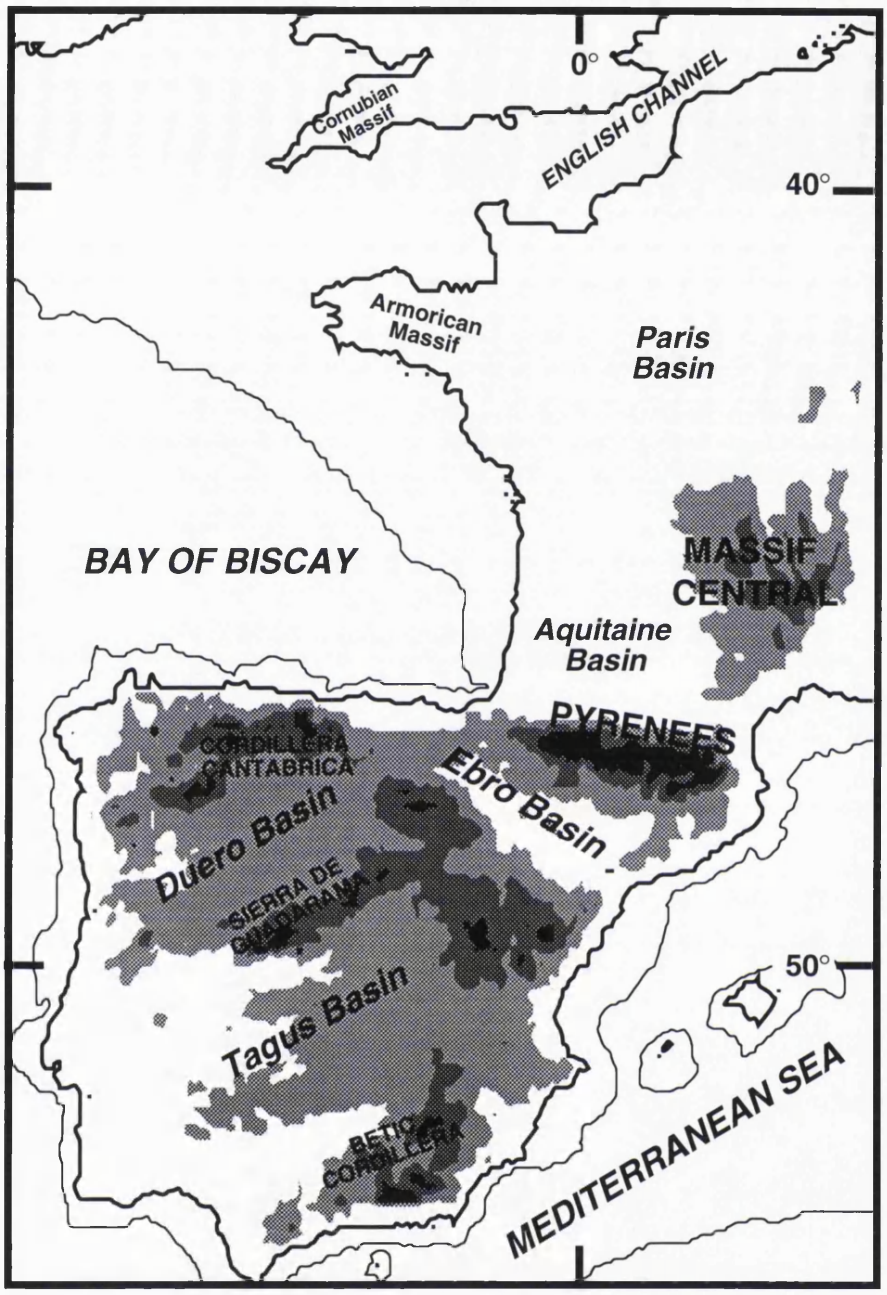

Fig. 1.6 A Map of the physical geography of western France and the Iberian Peninsula. Contours are at 500 m intervals, and the marine contour is at -500 m.

and burial grounds at Carnac, and in northern Spain, there are caves with fine examples of Neolithic paintings. Subsequently, like much of western Europe, the regions have fallen prey to a series of invasions and occupations from the Celts, Romans, Huns and Visigoths. The Moorish invasions of Spain from the 7th to 15th Centuries A. D. were resisted in the Basque Lands, Cantabria and Asturias, however Galicia eventually fell to the Moors after some resistance. Probably one of the strongest influences is the Celtic one, this being particularly so in Armorica. Both regions have managed to retain there own Celtic based languages and dialects, *Breton* in Armorica and *Gallego* in north-west Spain.

The political and administrative divisions of the studied regions and their major administrative centres are illustrated on **Figure 1.7**. Industry in the region has traditionally been dominated by agriculture and fishing, and in many regions these are still a major form of income. The Bay of Biscay is famous for its seafood and the regions are noteworthy for their more unusual crops such as maize and artichokes, as well as dairy produce and other vegetables. Vendée also produces sea salt gleaned from the many salt marshes along the coast. Manufacturing industries are growing in importance, particularly around the larger towns and ports. There are major coal deposits in Oviedo region of northern Spain, and the extraction of minerals and quarrying of stone for building is also important.

The sandy beaches and spectacular coastlines of the regions have meant that tourism is becoming more important in both regions, particularly so in the Armorican Peninsula which is very popular with British holidaymakers. Northwest Spain is less developed, but is increasing yearly as a popular destination for Spanish tourists.

1.4 Apatite fission track annealing and composition.

The second part of the thesis deals primarily with the development of a technique using Fourier Transform Infrared (FTIR) microspectroscopy to identify different chemistries within a population of apatite grains used for fission track analysis.

With the annealing of fission tracks taking place between 60 - 120 °C over geological time, there is still a strong need to increase the understanding of the thermal annealing of fission tracks in apatite. It is known that the end member composition of a crystal is a major determining factor on the rate of annealing and etching of the fission tracks. In early work on apatite samples from the Otway Basin, Victoria, Australia (Green et al., 1986), the conclusion was reached that an increase in chlorine atoms in the apatite provoked a resistance to the effects of annealing when

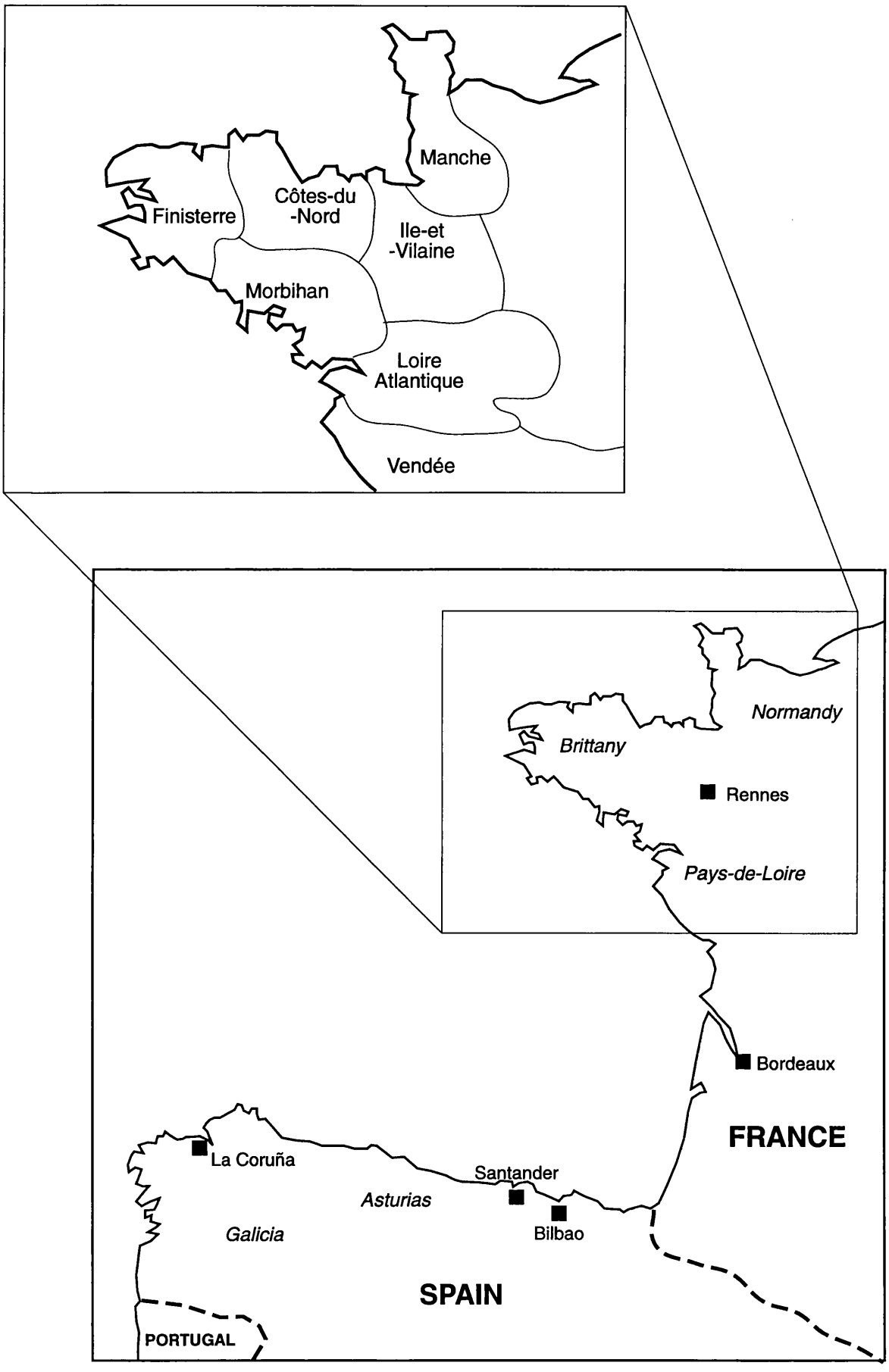

Fig. 1.7. Political regions in Spain and France. Inset Map shows the departements for the regions Brittany, Normandy and Pays-de-Loire.

the sample was subjected to a temperature increase. Thus, reduced levels of annealing in a fission track dataset, resulting from undetected variations in apatite chemical composition could be erroneously interpreted as indicating relatively low palaeotemperatures. It is therefore important to make compositional analysis a routine procedure for all fission track samples.

Primary magmatic apatite has the chemical formula $Ca_5(PO_4)_3(F, C, OH)$. The most stable component of this solid solution is fluorine, the chlorine and hydroxyl ions playing minor roles. The most widely accepted technique for chemical analysis is the electron microprobe, but it can prove a cumbersome procedure for routine use with samples for fission track analysis. A non-destructive and rapid analytical technique is required that can be applied to the individual crystals on which the fission track single grain ages are determined. Ideally the samples would not have to be treated in any way other than that used for apatite fission track analysis. Such a technique would have to be rapid, bearing in mind that at least twenty crystals per mount need to be measured in a thorough analysis. Spectroscopy using the FTIR method appears to be a suitable technique with which to resolve this problem. This technique fits all the necessary criteria with the major exception that it does not yield a truly quantitative result. Apatites are infrared active in the orthophosphate (PO_4) region, and it is the change in position of this band of the spectrum which is used to give a semi-quantitative handle on the end member ion.

1.5 Layout of the thesis.

This thesis is divided into nine chapters, dealing first with the geological aspects and data produced from the fission track case study and then the methodology and techniques used in enabling a method for the rapid determination of chlorine content of apatites.

Chapters 2 and 3 review the literature dealing with the geological evolution, both onshore and offshore, of the Bay of Biscay region of Western Europe, comprising the Armorican and Hesperian Massifs. The rocks analysed are themselves entirely collected from surface exposures, and **Chapter 2** deals with the geological evolution of the sampled rocks and the regions of the Armorican and Hesperian Massifs, as segments of the Cadomian and Variscan Orogenic belts. **Chapter 3** considers the formation of the Bay of Biscay, a failed Mesozoic rift occurring as part of the formation of the North Atlantic, and the adjacent regions of continental shelf. No offshore rocks were sampled; however it is the Mesozoic evolution of the region including the forming of the Bay of Biscay and the associated separation of the Galicia Banks (Northwest Spanish Shelf) from Flemish

Cap (Eastern Canadian Shelf) which were the most important tectonic and sedimentary influences during this time.

Chapter 4 describes the apatite fission track data in terms of age ranges, track length distributions and the geographical spread of the data. The apatite fission track ages and confined track length measurements are tabulated and the track length measurements and single grain age data are displayed graphically. The data are described in terms of their limits and ranges.

In **Chapter 5** the apatite fission track analyses described in Chapter 4 are interpreted using geological constraints (summarised from Chapters 2 and 3) and computer modelling techniques. The causes and effects of apatite fission track annealing are discussed and these are applied to the data. Finally, a thermal history for the evolution of the Armorican and Hesperian Massifs is derived from this combination of interpretative techniques.

Chapter 6 attempts to discuss the evolution of the Hesperian and Armorican Massifs derived from the results of the fission track analysis in terms of the structural and sedimentological evolution of Western Central Europe. Comparisons and variations of the proposed thermal history with the published literature, derived from other geological disciplines, are argued.

Chapter 7 outlines the present understanding of the formation and annealing of fission tracks in apatite with respect to the crystallographic structure and chemistry of the mineral. The importance of the presence of chlorine in the apatites causing a resistance to annealing is stressed.

Chapter 8 assesses the potential of infrared microspectroscopy as a routine, rapid and non-destructive method for the determination of chlorine content in apatites which are to be used or have been used for fission track analysis. Earlier work is briefly reviewed and the analytical techniques are discussed. A new semi-quantitative method for chemistry determination was designed and tested on apatite fission track samples.

Chapter 9 summarises the results, conclusions and implications of the thesis as an entirety and promotes ideas for further research in the fields.

The Appendices provide the reader with the techniques involved in sample preparation for fission track and electron microprobe analysis and infrared microspectroscopy (**Appendix 1**), and descriptions of the samples collected for apatite fission track analysis and infrared microspectroscopy (**Appendix 2 and 3**). **Appendix 4** lists symbols used in formulae and in other chemical and physical data mentioned in the text

1.6 Terminology and usage.

Throughout this work the geological timescale used will be that of Harland et al., (1989). The terms used for major tectonic events are defined in the relevant parts of the text. The 'Armorican Massif' refers to the Palaeozoic and older rocks of western France, outcropping in the political regions of Brittany, Normandy and Pays-de-la-Loire. Likewise the term 'Hesperian Massif' refers to similar lithologies in Galicia and Asturias, NW Spain. For the most part the stratigraphic names of the lithologies sampled are as in the language of their country of origin (i.e. Granite de Mont-St-Michel rather than Mont-St-Michel Granite).

Chapter 2

Geological and tectonic setting of the Ibero-Armorican Arc.

2.1 Geological setting.

The Armorican Massif of western France and its correlative, the Hesperian Massif of north-west Iberia, have experienced a long and complex geological history. They have been affected by two major collisional events, the late Precambrian Cadomian Orogeny, and the Palaeozoic Variscan (Hercynian) Orogeny. Both regions are dominated by Variscan structures, representing the continent-continent collision of Gondwana with Laurasia during the latest Palaeozoic, closing a series of E-W trending oceans **(Fig. 2.1)**. The geology and structure of the Armorican and Hesperian Massifs are summarised in **Figures 2.2** and **2.3**.

The Armorican Massif was divided into four structural zones by Cogné (1974) which are illustrated in **Figure 2.4**. The Domnonean Domain of north-west Brittany consists of a Precambrian basement that has undergone several phases of Cadomian deformation, plutonism and metamorphism. The region has only a minor Variscan overprint (Cabanis, 1974). The Mancellian Domain lying in the north-eastern part of the Massif, is composed of younger Precambrian rocks (Brioverian metasediments) that were folded during phases of Cadomian deformation. These sediments were intruded by granites during the early Palaeozoic, preceding the deposition of epicontinental deposits. This area represents a segment of the Variscan Externides, and was consequently only mildly deformed. The Domnonean and Mancellian Domains are bounded to the south by the North Armorican Shear Zone (NASZ). To the south of the NASZ, in the Central Armorican Zone, Palaeozoic cover was deformed by large-scale E-W folds and intruded by granitoids during the Variscan Orogeny, although it did not undergo a high grade metamorphism. The South Armorican Zones are separated from the Central Armorican Zone by the deep-seated South Armorican Shear Zone (SASZ). The South Armorican Zones are characterised by a vast thickness of Precambrian to Palaeozoic sedimentary rocks, which underwent a number of metamorphic and intrusive events from end-Cadomian to end-Variscan orogens. The area is divided into three subzones, separated by major shear zones through the central areas (Cogné, 1974). In the southernmost Ligerian Zone the basement can be clearly distinguished from the cover. To the north and west, the Cornuailles Anticlinal Zone is intensely affected by both deformation and granite

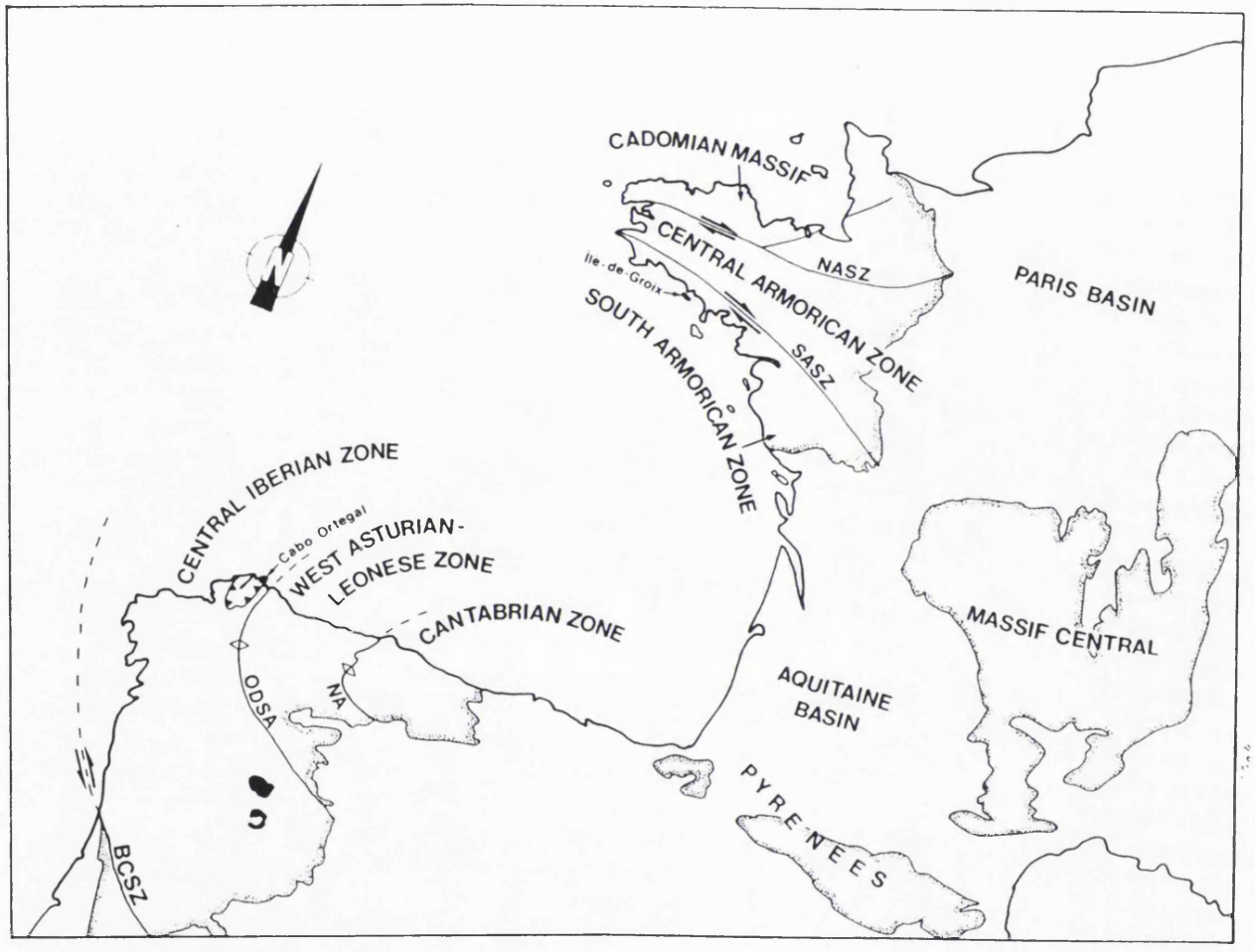

Fig. 2.1. The major structural and geological elements of west-central Europe, showing the juxtaposition of the Variscan Massiffs (stippled contact) with Mesozoic basins. NASZ: North Armorican Shear Zone; SASZ: South Armorican Shear Zone; NA: Narcea Anticline; ODSA: Ollo de Sapo Antiform; BCSZ: Badajoz-Cordoba Shear Zone; black patches: ultramafic rocks.

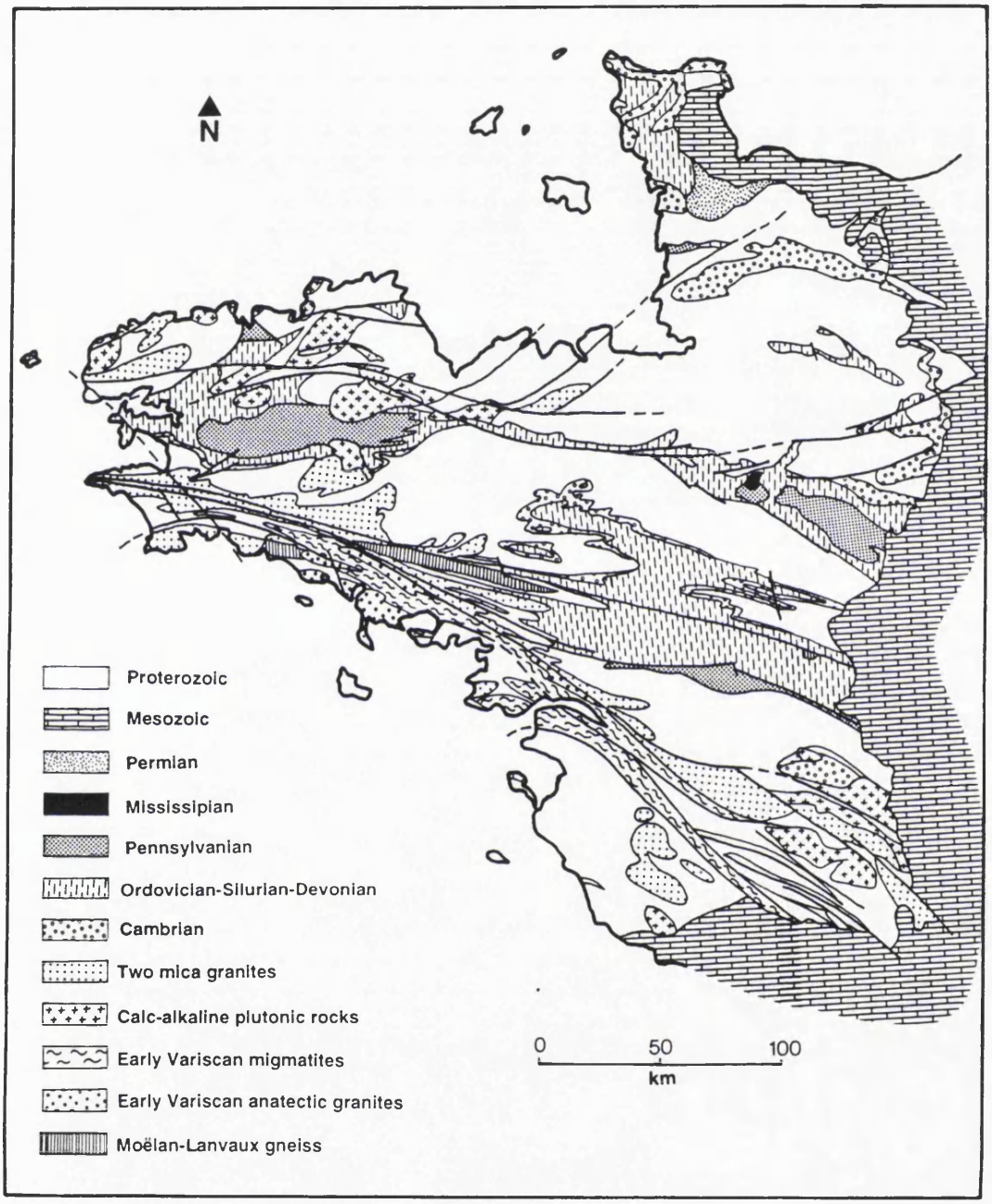

Fig. 2.2. Geological map of the Armorican Massif (after Cogné, 1974).

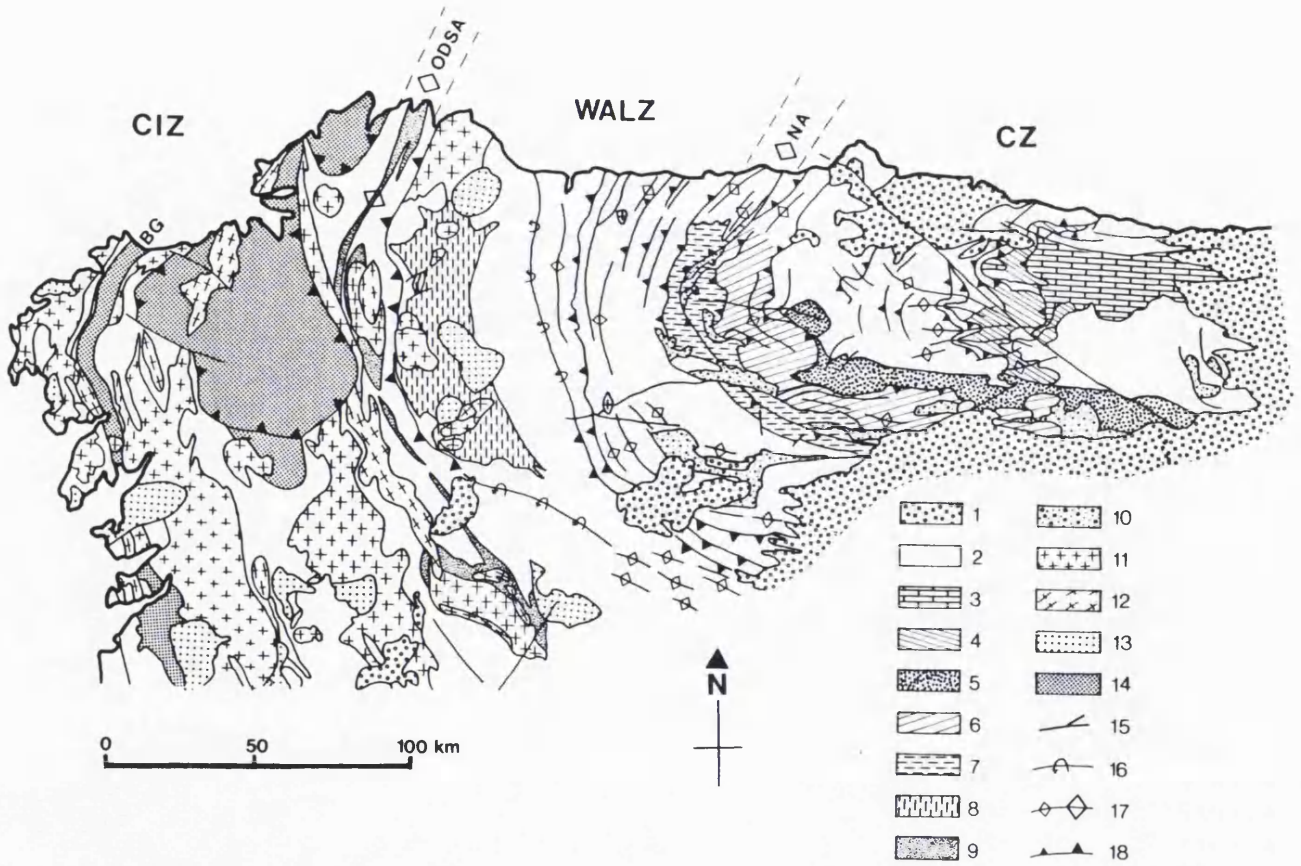

Fig 2.3. Structural and geological map of NW Iberia. CIZ: Central Iberian Zone; WALZ: Western Asturian-Leonese Zone; CZ: Cantabrian Zone; ODSA: "Ollo de Sapo" Antiform; NA: Narcea Antiform; BG: Blastomylonitic Graben; 1: Mesozoic and Tertiary cover; 2: Undifferentiated Palaeozoic and Proterozoic rocks; 3: Picos de Europa Unit; 4: Ponga Nappe; 5: Sobia-Bodon Unit; 6: Somiedo Correcilla Unit; 7: Precambrian core of the Narcea Antiform; 8: Precambrian core of Mondoñedo fold; 9: Precambrian core of "Ollo de Sapo" Antiform; 10: Upper Carboniferous (Gzelian) sediments; 11: two-mica granites; 12: older, sheared calc-alkaline plutonic rocks; 13: younger, calc-alkaline plutonic rocks; 14: Allocthonous terranes; 15: major faults; 16: recumbent fold; 17: antiforms (minor, major); 18: thrusts (minor, major) (after Julivert et al, 1980).

injection. This makes it very difficult to determine exactly what unit belongs to which orogenic event (i.e. Variscan or earlier Cadomian rocks). The South Armorican Crushed Zone (SACZ) probably represents one of the Variscan sutures; it is and distinguished by the intrusion of Variscan syntectonic granites and intense shearing.

In North Western Iberia, the Armorican Massif has its equivalent in the Hesperian Massif. This region forms the southern branch of the Variscan Ibero-Armorican Arc stretching through Galicia, NW Spain and Portugal. Cadomian rocks are exposed in the external Variscan zones of southern Portugal. The Iberian segment of the Variscides reveals an almost complete cross section through the Variscan Orogenic Belt, exposing five structural levels **(Fig. 2.5)**. Whilst some of these levels can be correlated across the Bay of Biscay to similar zones in the Armorican Massif, the complex nature of the SACZ causes problems with exact correlation of these zones. Recently Martinez-Garcia (1993) has proposed that parts of the Variscan Belt in Iberia correlate with the Variscan rocks in the Pyrenées and Montagne Noires (southern Massif Central) rather than the Armorican Peninsula.

The Cadomian and Variscan massifs are flanked by Mesozoic-Cenozoic sedimentary basins: the Paris, Aquitaine and Asturian basins onshore, and the Bay of Biscay, Western Approaches, English Channel and Lusitanian (Galicia Margins) basins offshore **(see Fig. 2.1)**. Exploration for hydrocarbon reserves has been successful in the Paris and Aquitaine Basins. The Aquitaine Basin is still undergoing active sedimentation, dominantly from windblown dune sands and the major fluvial systems of the Dordogne and the Garonne.

2.2 Pre-Cadomian Basement.

Patches of Proterozoic, pre-Cadomian 'Icartian' gneisses have been located in areas in the north of the Armorican Massif, notably the type locality of the Icart Gneiss of Guernsey, dated at 2018±15 Ma (U-Pb; Calvez and Vidal, 1978), and gneisses exposed at La Hague giving a 2600-2000 Ma Rb-Sr isochron age (Leutwein et al. 1973). There are enclaves of gneiss in the Perros-Guirec complex of Trégor that have been dated at 1790±10 Ma (U-Pb; Auvray et al., 1980a). Gneiss on Sark, which remains undated, but is thought to represent Pre-Cadomian basement.

An important recent classification of the stratigraphy is noted. The Penthievre Complex on the Baie-de-St-Brieuc was originally thought to be of Pre-Cadomian age (Cogné, 1964). However, it has since been dated at

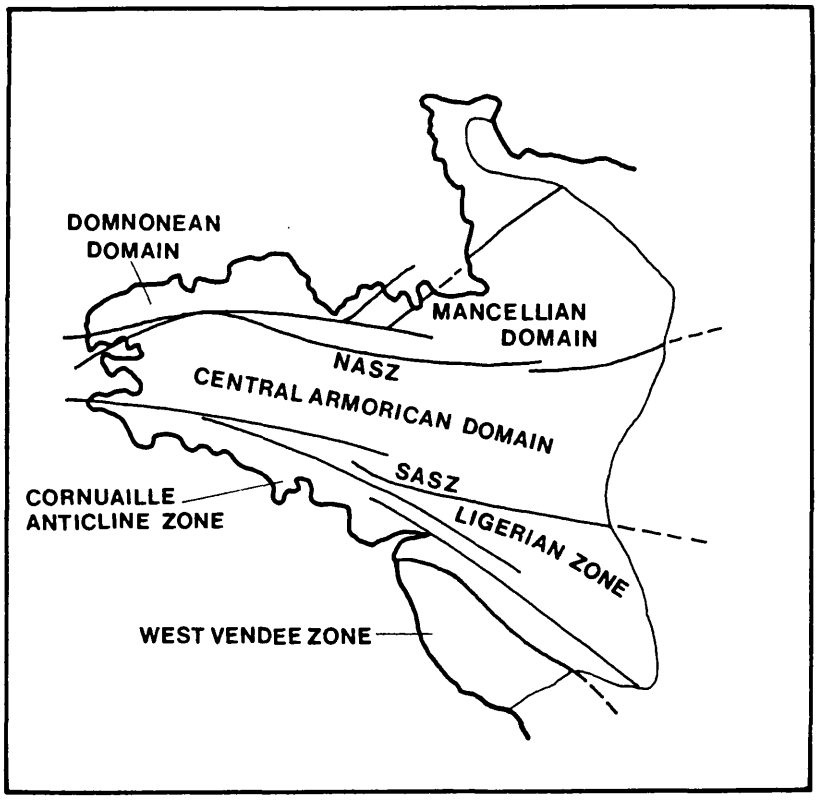

Fig. 2.4. The structural zones in the Armorican Massif. NASZ: North Armorican Shear Zone; SASZ: South Armorican Shear Zone.

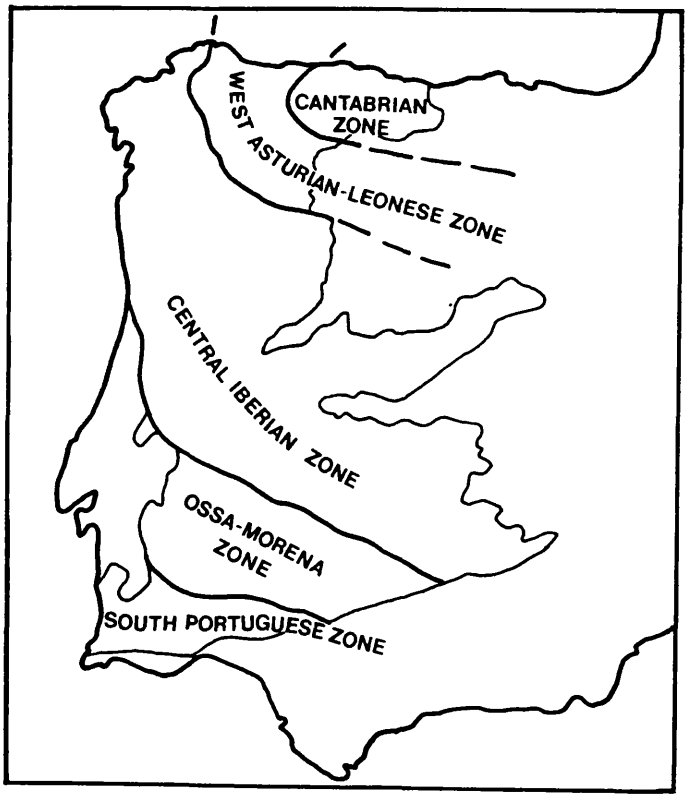

Fig. 2.5. The structural zones in the Hesperian Massif.

593±17 Ma by Vidal et al. (1974), indicating that the Penthievre Complex and its correlatives are of Cadomian age. The term 'Pentevrian' is now obsolete as a term defining pre-Cadomian basement that differs from the Icartian. All pre-Cadomian rocks are now attributed to the Icartian (D'Lemos et al. 1990).

2.3 The Cadomian Orogeny.

The Cadomian Orogeny *sensu lato* formed late Proterozoic rocks residing on the south-eastern continental margin of the evolving Iapetus Ocean. During the late Proterozoic, the north-western margin of Iapetus was affected by the Grenvillian Orogeny (1,000 Ma), the Morarian Orogeny (750 Ma) and the Grampian Orogeny (520-450 Ma; Wright, 1976). The evolution of the south-eastern continental margin of what was to become the Iapetus Ocean was independent and characteristically different from, but partly synchronous with that of the northern continental margins.

The northern part of the Armorican Massif is the type area of the Cadomian Orogeny (named after the Latin for Caen in Normandy, 'Cadomus'). The orogeny was first defined here by Bertrand (1921), who noticed that the Brioverian sedimentary sequence had been deformed and uplifted before the deposition of the lower Palaeozoic red beds around the Baie-de-St-Brieuc. The Cadomian *sensu stricto* is poorly defined elsewhere, but there is evidence for deformation of a comparable age in the Monian, Avalonian and other basement rocks of Central England, North Wales, south-east Ireland, south-west Iberia and Maritime Canada. The term 'Cadomian' is now used to include the rocks of the Monian and Avalonian terranes as well as the north Armorican type sections.

2.3.1 The Cadomian Orogeny in the Armorican Massif.

The Proterozoic rocks of the Cadomian orogeny are exposed mainly in the northern part of the Armorican massif in the Domnonean and Mancellian Zones **(Fig. 2.6)**.

The orogeny was dominated by extrusive and intrusive calc-alkaline magmatism, characteristic of an active margin, dominated by oblique subduction for a period of some 200 million years. Leutwein et al. (1973) dated the orogenic events to a span of 690-500 Ma (Rb-Sr, K-Ar). Peucat (1986) refined the timing to 650-425 Ma (U-Pb, Rb-Sr). More recent work proposed that Cadomian events spanned the latter part of the Proterozoic from *c.* 700 - 425 Ma (D'Lemos et al., 1990).

The pre-Cadomian Brioverian sedimentary succession consists of supracrustal rocks of Late Proterozoic age (Cogné and Wright, 1980). The

presence of a Cadomian 'event' was first recognised on discovery that the Brioverian had undergone mild deformation (Bertrand, 1921). The succession is represented by sandstones, siltstones and mudstones, with minor conglomerates, impure limestones and carbonaceous quartzites (phtanites) and occasional basic and acid volcanic horizons (Chauval and Mansuy, 1981). The sequence is interpreted as a submarine fan deposit by Denis and Dabbard (1988). Until recently, the Brioverian sequences were subdivided into the lower, middle and upper Brioverian. These subdivisions only exist on a local scale. The Brioverian was totally distorted by Cadomian events that make it impossible to correlate these units over the whole outcrop (Strachan and Roach, 1990). In Central Brittany, to the south of the NASZ, there is evidence that the Brioverian rocks are younger than those in the Domnonean and Mancellian Domains. It is thought that the sediments are derived from already deformed and uplifted earlier Brioverian sediments. However in this region, the deformation is dominantly Variscan rather than Cadomian (Hanmer et al., 1982).

Volcanism occurred in the northern marine basin margins of the Brioverian. The Erquy and Hillion Volcanic Formations in the Baie-de-St-Brieuc are metamorphosed submarine volcano-sedimentary rocks including pillow lavas and peperites (Roach et al., 1990). The volcanic rocks are presumed to predate the major Cadomian phases being synchronous with the Brioverian sediments and distorted with them (Shufflebotham and Roach, 1985). Coeval volcanic rocks at Trégor and the Baie de Douarnenez are of the same age (640-650 Ma). They are largely spilites but keratophyres are well developed at Trégor (in the form of bedded tuffs), but rare in the Baie de Douarnenez. The rocks at Trégor have a calc-alkaline affinity, although an enrichment in Fe in the intermediate stages of their evolution indicates the existence of a tholeiitic series. They are enriched in Rb, Sr, and K/Rb to values identical to those expected from island arcs. An enrichment in light rare earth elements also implies a mid-ocean-ridge or island arc origin. The volcanic rocks were erupted in either an island arc or continental margin environment.

Early Cadomian plutonic activity is characterised by the intrusion of quartz diorites in the Channel Islands, at Cap de La Hague, in the Coutances region and in the Baie-de-St-Brieuc, dated 700 - 580 Ma (Guerrot and Peaucat, 1990; Power et al., 1990). The intrusions are locally overlain by the Brioverian sequence (D'Lemos et al., 1990), and post-date the major deformative and magmatic phases. The dominant Cadomian structures deformed the Brioverian successions into E-W to NE-SW trending upright folds, that developed a strong cleavage and schistosity. Cadomian strain was

heterogeneous and concentrated in steep shear zones, like the St Cast shear belt. The prevalent movement along these was a sinistral strike-slip. Timing of folding is not well constrained, but has been placed at *c.* 590 - 540 Ma (Bale and Brun, 1983; D'Lemos et al., 1990).

Contemporaneous with the main Cadomian deformation events, the St. Malo, Dinan and St. Cast migmatites evolved directly as a result of deformation and magmatism **(Fig. 2.7)**. Granite anatexis occurred around 540 Ma (Peucat, 1986) by partial melting of Brioverian sediments (Treloar and Strachan, 1990). The relatively undeformed granites and granodiorites of the Mancellian batholith include the Vire-Carolles Granite dated at 541±5 Ma (U-Pb zi, Guerrot and Peaucat, 1990) and smaller intrusions yielding younger ages of 500 - 525 Ma (Jonin and Vidal, 1975; Guerrot and Peaucat, 1990).

The NASZ is dominantly a Cadomian structure with most of the strike-slip movement occurring between 600 and 340 Ma, with perhaps only 10 km of movement since that time (Watts and Williams, 1979). Latest Cadomian activity occurred in the Cambrian to Silurian, represented by tectonically controlled sedimentation. Late orogenic extension resulting in the formation of the Jersey dyke swarm occurred as recently as 425 Ma (Lees, 1990).

2.3.2 The Cadomian rocks outside the Armorican Massif.

Exposure of 'Cadomian' rocks *sensu lato* outside the North Armorican Massif are found as isolated inliers in the British Midlands, Wales, south-eastern Ireland, southern Spain and in Newfoundland, New Brunswick and Nova Scotia **(Fig. 2.8)**.

The Monian terranes of North Wales and their counterparts in Central England contain sequences of plutonic, volcanic, volcano-sedimentary and sedimentary rocks (Barber and Max, 1979; Gibbons and Horak, 1990). Each fault bounded terrane is tectonically and genetically separate from the adjacent terrane. Similar rocks occur in the Rosslare complex of south-east Ireland, where Monian-type sediments are docked onto the basement (Murphy et al., 1990). The 'Cadomian' rocks of Central England (the Longmyndian and others) represent successions of marginal sediments, deposited in an interarc basin type environment, lying to the north of a magmatic arc formed by the Uriconian volcanic rocks (Cogné and Wright, 1980; Pauley 1990).

The Avalon Terranes of New Brunswick, (Nance, 1990) and Nova Scotia (Murphy et al., 1990) eastern Canada show similarities to the Cadomian rocks of the north Armorican Massif. Calc-alkaline magmatism

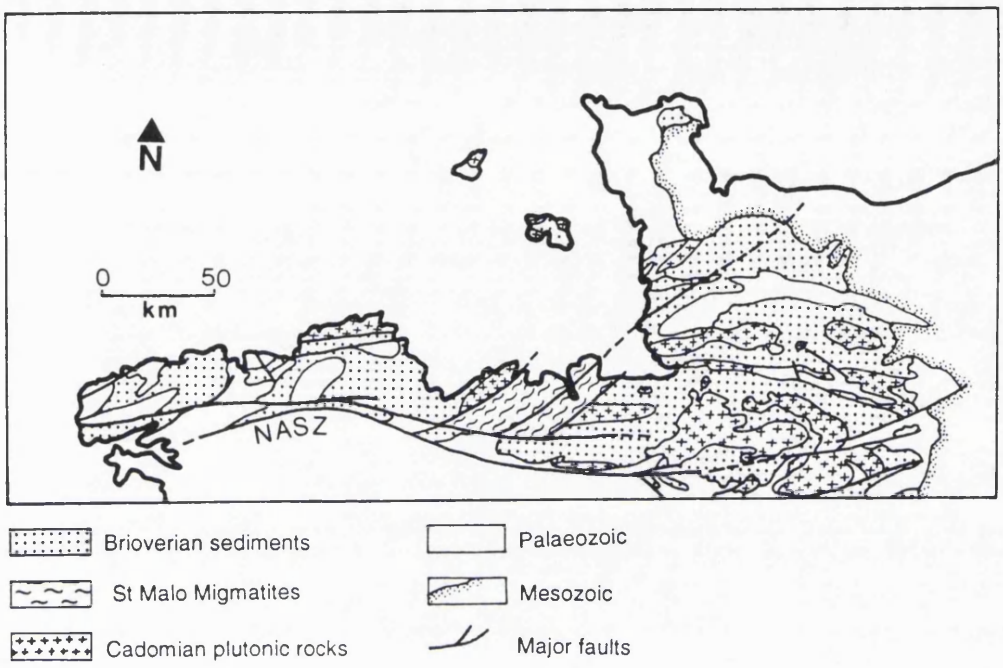

Fig. 2.6. A geological Map of the Cadomian Massif (North Armorican Massif) (after Vidal, 1980).

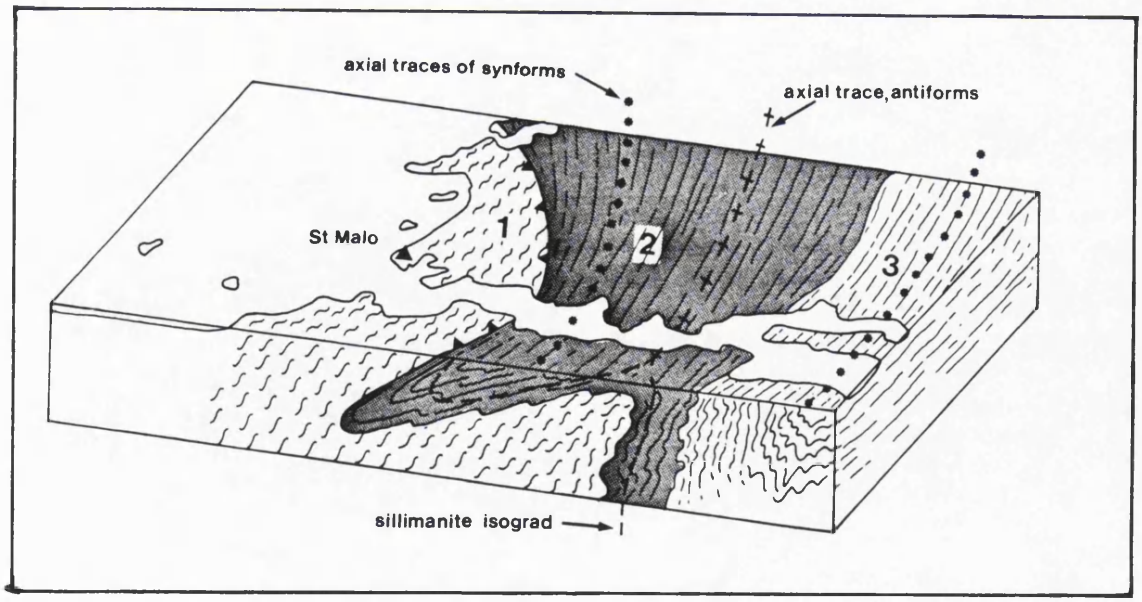

Fig. 2.7. A block diagram showing the structure of the St Malo Migmatite Belt across the Rance Valley. 1: migmatites; 2: cordierite-sillimanite gneiss; 3: mica- schists; 4: axial trace of synforms; 5: axial trace of antiforms; 6: sillimanite isograd (after Auvray and Martin, 1982).

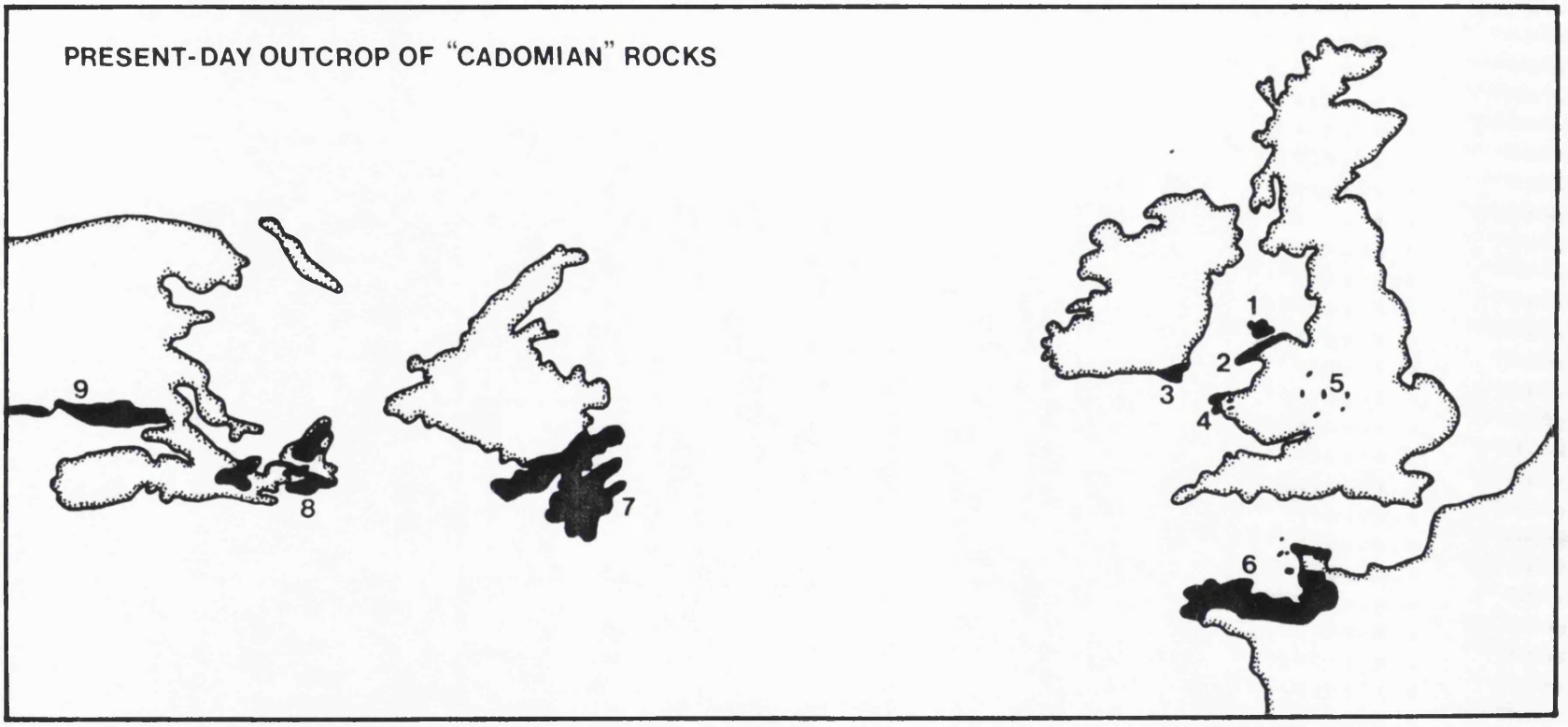

Fig. 2.8. Outcrop of Cadomian rocks in the North Atlantic region. 1: Anglesey; 2: Llyn Peninsula; 3: Rosslare; 4: Pembrokeshire; 5: British Midlands; 6: North Armorican Masif; 7: Newfoundland; 8: Nova Scotia; 9: New Brunswick (after Gibbons and Horak, 1990).

and associated arc-type volcanic rocks pass up into post-tectonic red beds and Lower Palaeozoic sandstones. There is no evidence for continent-continent style collision, but a series of terranes, representing an island arc, an interarc basin with calc-alkaline and continental tholeiitic rocks, possibly represents interarc rifting and a remnant arc.

In south-western Iberia, Cadomian rocks outcrop within the reactivated and exhumed rocks of the Palaeozoic Ibero-Armorican arc. Notably in the Ossa-Morena and South Portuguese Zones of the Variscan belt, Quesada (1990) has recognised at least two periods of Cadomian deformation, an early Cadomian event is represented by polyphase deformation and metamorphism associated with the collision of the island arcs with the continental plate, rather than an oceanic closure. A second Cadomian event appears to be a single phase of deformation.

2.3.3 Discussion.

It is agreed by most authors (Cogné and Wright, 1980; D'Lemos et al., 1990, and references therein) that the Cadomian orogenic belt represents an active plate margin, with subduction related volcanism, magmatism, and tectonism, lasting for some 150 Ma, and possibly adjacent to the evolving Precambrian-Lower Palaeozoic Iapetus Ocean (the 'Celtic Ocean' of Cogné and Wright, 1980, or the 'Uranian Ocean' of Gibbons, 1990). However, it must be remembered that the tectonic processes were distinctly different from those on the north-western continental margin of Iapetus. The Caledonian orogeny did not encroach upon the south-eastern continent until the two landmasses began to collide during the Palaeozoic. Cadomian activity had ceased prior to the beginning of the Cambrian.

Two major tectonic environments have been recognised within the Cadomian belt, an outer trench zone and an inner continental-arc zone **(Fig. 2.9)**. Continental collision apparently played no part in the Cadomian Orogeny; a modern analogue of such a situation is the Andean Cordillera of South America (M. Brown et al., 1990). Cadomian rocks are displaced along their outcrop in such a way that they have been interpreted as suspect terranes*. Similar situations have been recognised along the cordilleras of the west coast of the Americas. Suspect terranes are associated with oblique subduction encroaching upon a continental margin. Pigram and Davies (1987) have proposed that fragments of oceanic, continental and island arc crust are carried by the oceanic slab and then overthrust or obducted onto the continental plate. Although this is a reasonable explanation, there

*defined as 'a mappable unit characterised by a geological history different from that of adjacent units' (Jones et al., 1983).

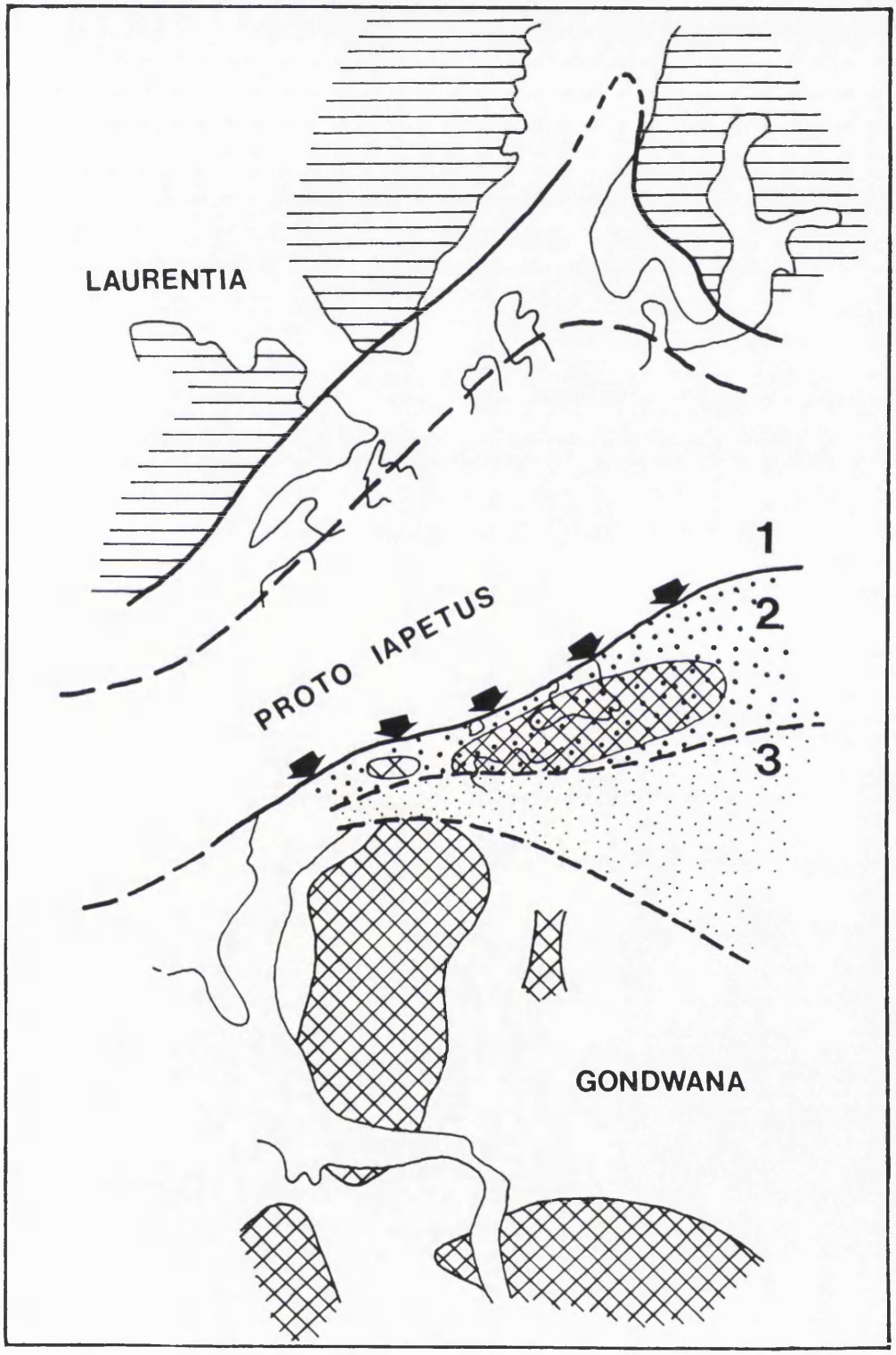

Fig. 2.9. A plate tectonic model for the Cadomian Orogeny. 1: convergence and subduction on the Gondwanan margin; 2: the active margin on the pre Cadomian basement microplate; 3: extension in the Brioverian marginal basin (after Cogné, 1990).

remain many observations which run contrary to the theory. Once accreted, a terrane can be moved thousands of kilometres and/or broken up by transcurrent faults, and may even rotated through angles of up to 60° (Cox, 1980). Such fault bounded units are common throughout the Cadomian. Gibbons and Horak (1990) have proposed that all the fragments of the chain are allochthonous.

2.4 Post-Cadomian Sedimentation and Volcanism.

The Cadomian Orogeny was succeeded by the deposition of Early Palaeozoic terrestrial sediments. These red-beds are dominantly immature sandstones, coarse-grained sandstones and conglomerates (Auvray and Martin, 1982), that are exposed in restricted outcrops in the northern part of the Armorican Massif. The probable depositional environment was an alluvial-fan draining E-W trending basins, towards southern Normandy into the Normanno-Breton Gulf (Auvray et al., 1980b; Went and Andrews, 1990). The reactivation of Cadomian structures controlling these basins marked the cessation of Cadomian movements (Went and Andrews, 1990). The sediments are barren of fossils, and this consequently makes dating difficult. However, the red-beds at Plouézec are intercalated with extrusive igneous rocks. Auvray et al. (1980) dated the andesitic Plourivo Formation at 472±5 Ma, (Rb-Sr wr isochron), thereby implying a Lowest Palaeozoic age for the red-beds.

The Palaeozoic sedimentary rocks were formed syntectonically with the Variscan Orogeny. Their outcrop is mainly restricted to the Central Armorican Zone where they form two major synclines. The northern syncline, the Châteaulin and Laval structures extend from Brest and the Presqu'Ile de Crozon to Laval; the southern syncline the Lanvaux, extends from south west of Rennes to Angers (Cogné, 1974). The sediments are the consummation of a Palaeozoic transgressive event, over the Brioverian basement. The depositional basin was subsiding along the South Armorican Shear Zone (SASZ) adjacent to the newly forming cordilleras of the South Armorican Crushed Zone, from whence the sediments were derived. The basin was finally deformed at the climax of Variscan collision (c.f. Pelhâte and Mirouse, 1980).

2.5 Variscan Deformation, Plutonism and Metamorphism.

The terms 'Variscan' or 'Variscides' are used here to define the European segment of the Hercynian foldbelt, extending through Iberia to the Bohemian Massif (Bard et al, 1980, Matte, 1991) and the terms 'Hercynian' or 'Hercynides' refer to describe features of the entire orogen,

across America, Africa and Europe. The term 'Variscan' arose because of major differences in the American and European parts of the orogen. In North America, deformation continued in the same sense of the Caledonian Orogeny, following the same NE-SW trend, whereas the European events were of a trend (~E-W) physically and spatially separate from the Caledonian belts of northern Europe.

There is considerable confusion surrounding terminology applied to the Hercynian foldbelt. This is due to the extent of the belt across North America, Africa and Europe, resulting in a diversity of multilingual literature. This problem is further compounded by the fact that much of the belt is overlain by Mesozoic sediments and/or overprinted by later deformation events, (i.e. the Alpine Orogeny in Europe) leaving incomplete, isolated segments. Matthews (1984) presents an excellent review and critique of the inconsistencies within the Variscan from the English, French and German literature, with reference mainly to the northern regions of the belt. There are several phases of activity requiring correlation; the Acadian, Bretonic, Ligerian, Sudetic, Asturian, Alleghanian, and so on, only apparently relevant to their type areas. For example the Acadian exists as an 'event' in the Appalachians, and although 'events' of comparable age (Devonian) occur in Europe (Bernard-Griffiths et al., 1977) they are plainly unrelated and spatially distinct (the 'Ligerian' of Autran and Cogné, 1980). In the United Kingdom, the Acadian exists as an end *Caledonian* 'event' (Soper et al., 1987).

The Palaeozoic Hercynian Orogeny comprises a major foldbelt stretching from the Ouachita-Alabama Transform Fault (Rast, 1988) through Appalachians in North America, through the West African Mauretanides and across Europe to the Bohemian Massif of Eastern Europe where it is terminated by the Russo-Scandinavian Shield, truncating against the Tornquist Line **(Fig. 2.10)**. The Orogeny was active between 500 and 250 Ma, the result of the convergence and collision between the continents Gondwana and Laurasia, events which led eventually to the suturing of the supercontinent Pangaea in the Early Permian.

The European Variscan belt is 3000 km long and between 700 - 800 km in width, and shows all the characteristics of a collision belt, including oceanic subduction and obduction, followed by continental collision with associated intracontinental deformations **(Fig. 2.11)**. Since the close of orogenic activity in the early Permian, the Variscan belt has undergone a period of deep exhumation. This has revealed five separate structural layers within the belt that have been used to construct a zonation of the western part of the belt (Bard et al., 1980). The belt has a distinct bilateral symmetry,

Fig. 2.10. The outcrop of Hercynian rocks and major structures associated with the orogeny from the Appalachians to North Central Europe. OA - Ouachita-Alabama Transform Fault; SA - South Atlas Fault; C - Chedabucto Fault; TL - Tornquist Line; segments of the belt numbered I to X; I - Southern and Central Appalachians; II - Northern Appalachians; III - Brito-Irish Variscan Belt; IV - North German Variscides; V - French Armorican and Central Variscides; VI - Central European Variscides; VII - Alpine-Mediterranean Variscides; VIII - Iberian Massif; IX - Algero-Moroccan Variscides; X - Mauritanides (diagram and segment names after Rast, 1988).

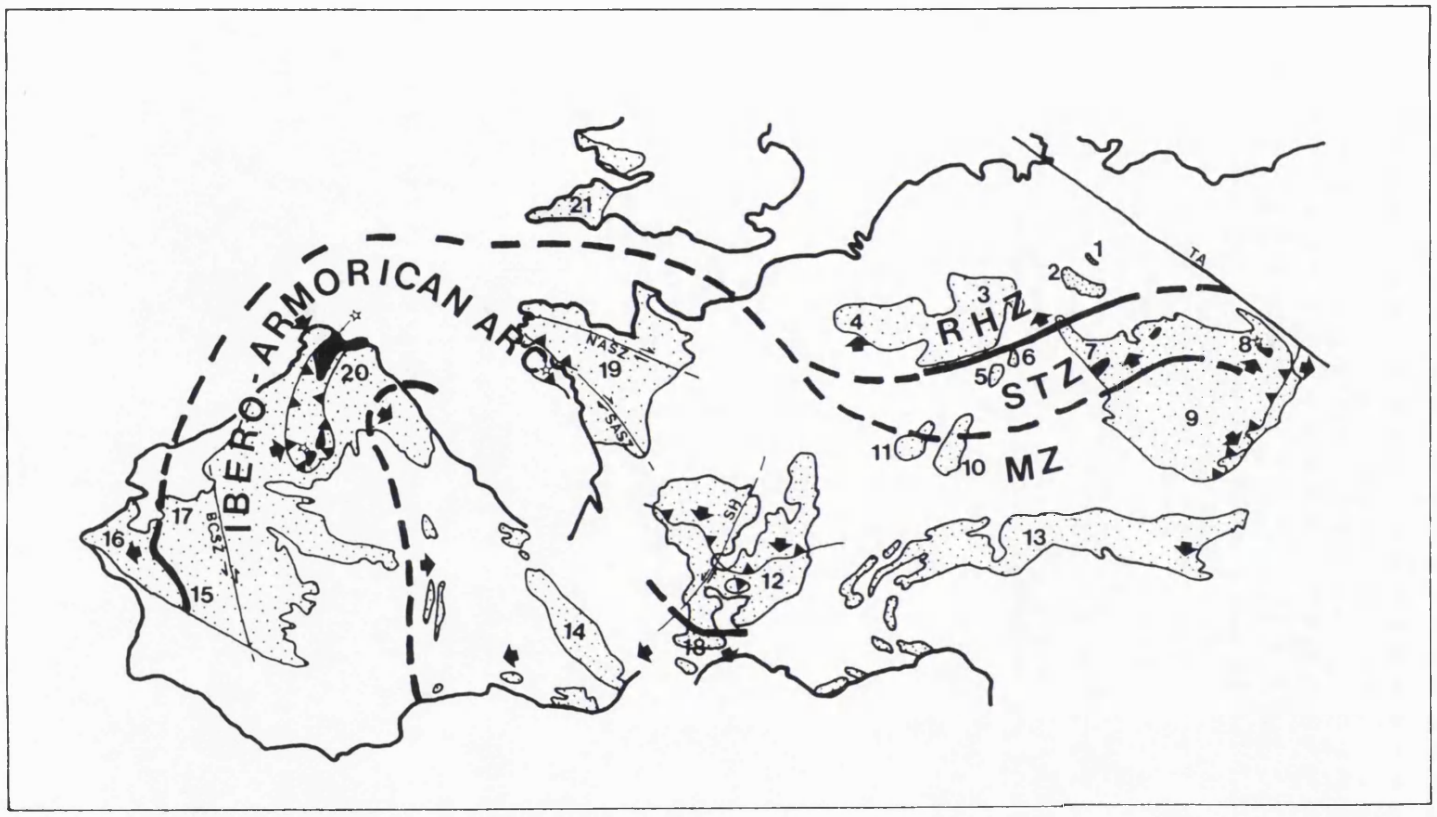

Fig. 2.11. The Variscan Belt through Europe. The exposed relicts of the belt (stippled) are 1: Flechtingen Hills; 2: Harz Mountains; 3: Rheinisches Schiefergebirge; 4: Ardennes; 5: Odenwald; 6: Spessart; 7: Thüringer Wald; 8: Eulengebirge; 9: Bohemian Massif; 10: Black Forest (Schwarzwald); 11: Vosges; 12: Massif Central; 13: Alpine external massifs; 14: Pyrenées; 15: Sierra Morena; 16: South Portuguese Basin; 17: Alto Alentejo; 18: Montagnes Noires; 19: Armorican Massif; 20: Hesperian Massif; 21: Cornubian Massif and South Wales; RHZ: Rhenohercynian Zone; STZ: Saxothuringian Zone; MZ: Moldanubian Zone; SH: Sillon Houiller Fault; NASZ: North Armorican Shear Zone; SASZ: South Armorican Shear Zone; BCSZ: Badajoz-Cordoba Shear Zone; TA: Tornquist Alignment; black patches: crystalline mafic-ultramafic nappe complexes; stars: blueschists; arrows: structural vergence; ticked lines: potential sutures. (redrawn after Engel and Franke, 1983)

with a central zone flanked to the north and south by mobile zones and external zones. One of the major features of the belt is the Ibero-Armorican Arc, a tight syntaxis possibly formed by indentation of Africa with Europe (Bard et al., 1980; Brun and Burg, 1982). Other attempts have been made to divide the Variscan belt into a series of well characterised, tectonically distinct zones. Kossmat (1927) devised a scheme of zones for the eastern European segments of the Variscides; a northern Rhenohercynian Zone (RHZ), a central Saxothuringinian Zone (STZ) and a southern Moldanubian Zone (MZ). When extrapolated into the western part of the belt, Kossmat's zones begin to loose their definition, (for example SW England with the Lizard Complex, Cornubian Batholith and Devono-Carboniferous sediments exhibit characters of all three (Matthews, 1984). Corresponding zones exist for the division of the Appalachian Alleghenian* belt of North America

2.5.1 A Plate Tectonic model for the Hercynian Orogeny.

It is now thought that the Hercynian orogeny was the result of the Palaeozoic collision of the continents Laurasia and Gondwana leading to the suturing of the supercontinent Pangaea during the latest Carboniferous to Early Permian **(Fig. 2.12)**.

The terminal stages of the Caledonides sutured the Laurentian and Baltic plates to form the supercontinent Laurasia with the closure of the Iapetus Ocean. True Hercynian deformation commenced during the Devonian, with northward subduction of the Proto Tethys-Proto Atlantic ('Rheic') Ocean along the length of the Hercynian Belt from the Appalachians to the Caucasus (Ziegler, 1990). This was accompanied by northward movement of the Gondwana derived Traveler-Avalon-Meguma and the Cantabrian-Aquitaine Terranes as well as many other microplates including the Iberian, Austroalpine, Cadomian and Carolinas blocks (Johnson and van der Voo, 1990). These terranes collided with a Laurasian subduction arc complex in the Emsian-Givetian, forcing closure of Massif Central ocean basin (Matte, 1986). By the mid-late Devonian, dextral, oblique, clockwise rotational convergence of Gondwana on the relatively stationary Laurasia was well developed. Temporary hiatuses occurred in the Laurasian back-arc extensional area in Mid-Devonian and latest Devonian due to preliminary collisions (Ziegler, 1989). The Fammenian saw the beginning of collision between Laurasia and Gondwana and full scale Himalayan-type collision between Laurasia and

*'Alleghanian' refers to the terminal phase of collision in the Appalachians whereas 'Alleghenian' is a lithostratigraphic term

Gondwana began in the Visean, terminating back-arc extension. During the Late Visean-Namurian, the collision front propagated westward and eastward. Closure of the proto-Atlantic Ocean occurred in the Lower Pennsylvanian. The terminal Alleghanian Orogeny ceased in the Gzelian and with the dissection of the Variscan foldbelt by a system of conjugate fractures in response to dextral translation between Africa and Europe, Hercynian deformation ceased (McKerrow and Scotese, 1990).

The Variscan belt exhibits a distinct bilateral symmetry with structures in the northern segments having a northward vergence, and those in the southern segments having a southward vergence. Similar activity formed the structures on both sides, and that must have been related to lithospheric convergence and associated subduction. Weber, (1984) proposed that this subduction must retreat because equilibrium was not possible due to the lack of mid-ocean ridges during the upper Devonian. He suggested that a mechanism for this could be a forced convection cell initiated by subduction, as described by Andrews and Sleep (1974). Such a cell would shift towards the margins of the orogen as subduction retreated. The symmetrical Variscan belt would require two such cells, moving in opposite directions. This in turn would produce compressive stress fields which would be transmitted into the crust, this would account for SE verging folds in the northern parts of the orogen.

2.5.2 Sutures in the Variscides.

Evidence for sutures within the Variscan belt are found within the internal zones of the orogen and rests upon the existence of isolated ultramafic massifs situated along the belt. In particular these are the Lizard Complex (SW England), the Munchberg Massif (S Germany), Ordenes, Cabo Ortegal, Tras-os-Montes (NW Iberia), Ile-de-Groix (Brittany), and smaller ultramafic outcrops in Brittany, Vendée and the Massif Central. There are probably two major sutures, a northern one, the Lizard-Munchberg Suture (Bard et al., 1980), and a more prominent southern suture. There are also many minor sutures associated with the closure of small oceanic basements between microplates.

This major Variscan collision suture (the southern suture) is assumed to be situated in south Brittany, continuing through northern Spain, westwards, and through the Massif Central to the east (Bard et al, 1980, Lefort, 1979). In NW Iberia the ultramafic massifs of Cabo Ortegal, Tras-os-Montes, Ordenes and Braganca are related to this major suture and are composed of metagabbros, amphibolites (retrogressed from granulites), basic granulites, eclogites, peridotites and pyroxenites, with associated

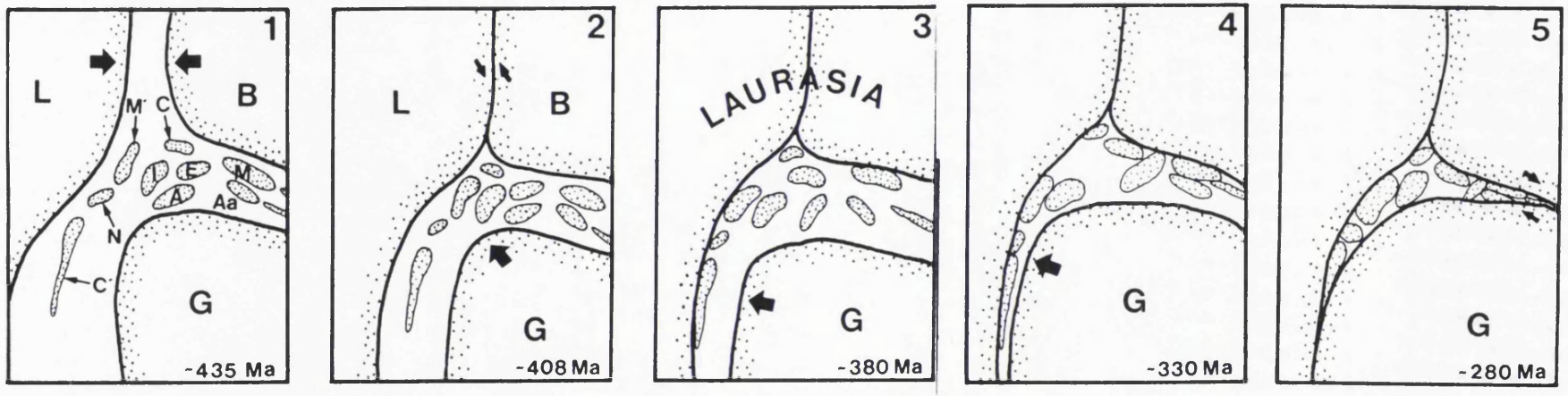

Fig. 2.12. Plate tectonic model for the convergence of Gondwana upon Laurasia. 1. Early Silurian (pre-Caledonian collision), Laurentia approaches Baltica. 2. Late Silurian-earliest Devonian (Caledonian Orogeny): collision of Laurentia and Baltica to form Laurasia, and late Caledonian transpression. 3. Middle Devonian to early late Devonian; collision of large microplates with Laurasia, and the initiation of movement of Gondwana. 4. Early to middle Carboniferous; a northward push of Gondwana, possibly partly rotational. Early phases of the Variscan orogeny. 5. End Carboniferous-early Permian full collision of Gondwana with Laurasia forming the supercontinent Pangaea. Key; L: Laurentia; B: Baltica; G: Gondwana; C': Carolinas Microplate; N: New Brunswick Microplate; M': Meguma Microplate; I: Iberian Microplate; C: Cadomian Microplate; E: East Armorican Microplate; M: Mont Blanc Microplate; Aa: Austroalpine Microplate (redrawn from Rast, 1988).

metasediments. However the region is definitely allochthonous and is associated with the accretion of the Iberian microplate to Laurasia. The presence of low pressure-high temperature (LP/HT) metamorphism to the north of the suture and high pressure (HP) granulites with glaucophane schists along the suture have lead to comparisons of the Southern Suture with Andean- and Himalayan-type collisions (Matte and Burg, 1981).

However, the Ile-de-Groix does not necessarily mark a suture. The blueschists here, like those in the Central Iberian Zone described above, are allocthonous, and there is no evidence of them being deeply rooted (Lefort and Ségoufin, 1978); making nappes or obduction a likely form of transport.

The evidence for the Lizard-Munchberg Suture is found from the fragments of ultramafic material in the Lizard Complex of Cornwall, SW England, and in the Munchberg Massif in Southern Germany. The ultramafic rocks of the Lizard Complex were probably obducted in the early Devonian. This is a region of dubious origin, with theories relating it to a southward dipping subduction zone south of the region (Shackleton et al., 1982) or the closure of a back-arc basin in between the RHZ and STZ (Leeder, 1982). The model of Leeder (1982) better fits the theory of an Andean-type collision. The high rates of exhumation that occurred in the Variscan chain from the Permian onwards are likely to have removed other features of an Andean-type collision, for example high level andesitic volcanism.

The geology of the European Variscan belt are described here in terms of the external and internal zones of the orogen *sensu lato*, rather than a coherent attempt to correlate the zones of Kossmat (1927) with those of subsequent authors working in other segments of the belt. The bilateral belt can be summarised as having a central internal zone, flanked on each side by two mobile zones, which are in turn flanked by the external zones.

2.5.3 The evolution of the pre-Variscan basement.

Prior to the Variscan Orogeny, the European basement was affected by two other major periods of activity, the Cadomian and the Caledonian Orogenies. The Caledonides were a major event in northern Europe, however, the consequences upon west-central Europe were limited to minor intraplate transpression, and the crustal shortening it produced was negligible. However, there were significant intrusions of calc-alkaline and peralkaline magmatism in the pre-Variscan basement (for example, the Moélan, Lanvaux and Douarnenez gneiss bands of central Armorica; Autran et al., 1980). These rocks were consequently metamorphosed to orthogneisses and are a characteristic part of the Variscan belt. Early

Variscan granulite facies metamorphism occurred during the Ordovician in many areas of the belt, including Saxony (the Granulitegebirge, Jäger, 1977), the Waldviertal granulites of Austria (Weber, 1984) and in the Hesperian Massif (Kuijper, 1979).

2.5.4 The Central Zone.

In Armorica and Iberia, the Central Zone runs through the Hesperian Massif, Central Armorican Zone and into central Europe.

In the Central Armorican Zone, Brioverian and Palaeozoic sediments rest unconformably upon the Precambrian basement. The zone is intruded by a number of earliest Variscan (Cambrian and lower Ordovician) granites. The sediments are weakly metamorphosed with minor deformation. This contact metamorphism was accompanied by the formation of a cleavage influenced by the intrusion of the granites (Hanmer et al., 1982). Later syntectonic Lower Pennsylvanian-Mississippian intrusions (the Granite-de-St Renan and the Granite-de-Brignognan) form large batholiths forcefully intruded into the Cadomian basement. These grade into migmatised granitic rocks (Migmatites de Plouguerneau). The Northern parts of the massif witnessed later Variscan magmatism.

In the Central Iberian Zone (CIZ), metamorphism is medium to high grade, and there is abundant granitic plutonism. Three phases of plutonism are recognised; an early calc-alkaline phase of biotite rich granodiorites (Capdevila and Floor, 1980) and a second phase of two mica granites, related to Variscan metamorphism and migmatisation and a third group of varying geochemical affinity intruded in the late Variscan (Bastida et al., 1986).

The eastern edge of the Iberian internal zones comprises the polyphase Mondoñedo Nappe Complex **(Fig. 2.13).** This is an eastward verging stack of thrusts that moved late Precambrian-lower Palaeozoic sediments tens of kilometres creating a 3 km thick shear zone at the base of the nappe pile, deforming syntectonic granites (Bastida et al., 1986). The nappe is cut by the Vivero Fault, a major disruption with an estimated 10 km throw. On the eastern portion of the nappe, the basal Mondoñedo Thrust can be traced along strike for some 165 km.

The CIZ also contains several allochthonous ultramafic complexes. These include Cabo Ortegal, Bragança and Morais massifs. The largest of these, Cabo Ortegal **(Fig. 2.14)** is found on the north-western coast of Spain. The complex is composed of ultramafic and ultrabasic rocks, and also shows other rocks associated with ophiolites. The Moeche Group is composed of low grade metamorphic rocks including cherts, basalts,

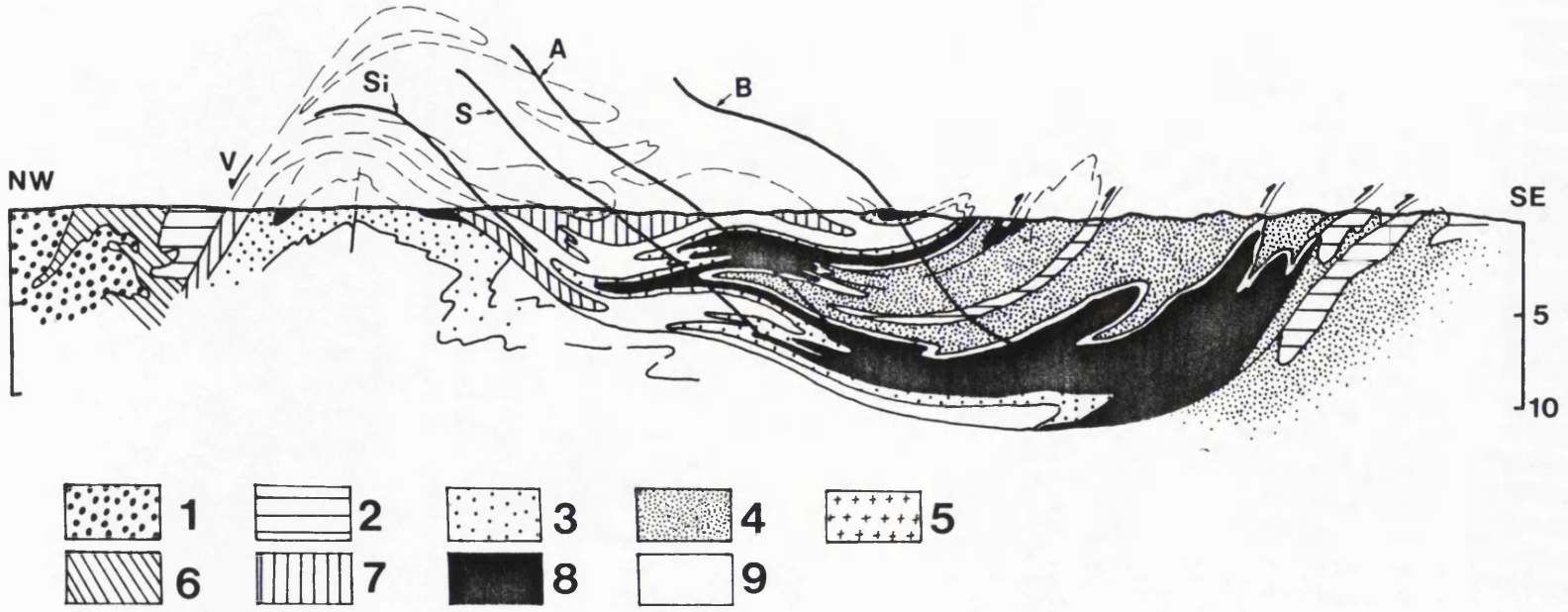

Fig. 2.13. A cross section through the polyphase Mondoñedo Nappe, the section line is taken just to the south of Mondoñedo. Key; V: Vivero Fault; Si: sillimanite isograd; S: staurolite isograd; A: almandine isograd; B: biotite isograd; 1: Ollo de Sapo Formation; 2: Luarca Slates; 3: Candana and Gistral Quartzites; 4: Cabos Series; 5: Varsican 2-mica granite; 6: Montes Slates; 7: Villalba Series; 8: Upper Candana Group transition beds; 9: Lower Candana Group slates and quartzites. (after Bastida et al., 1986).

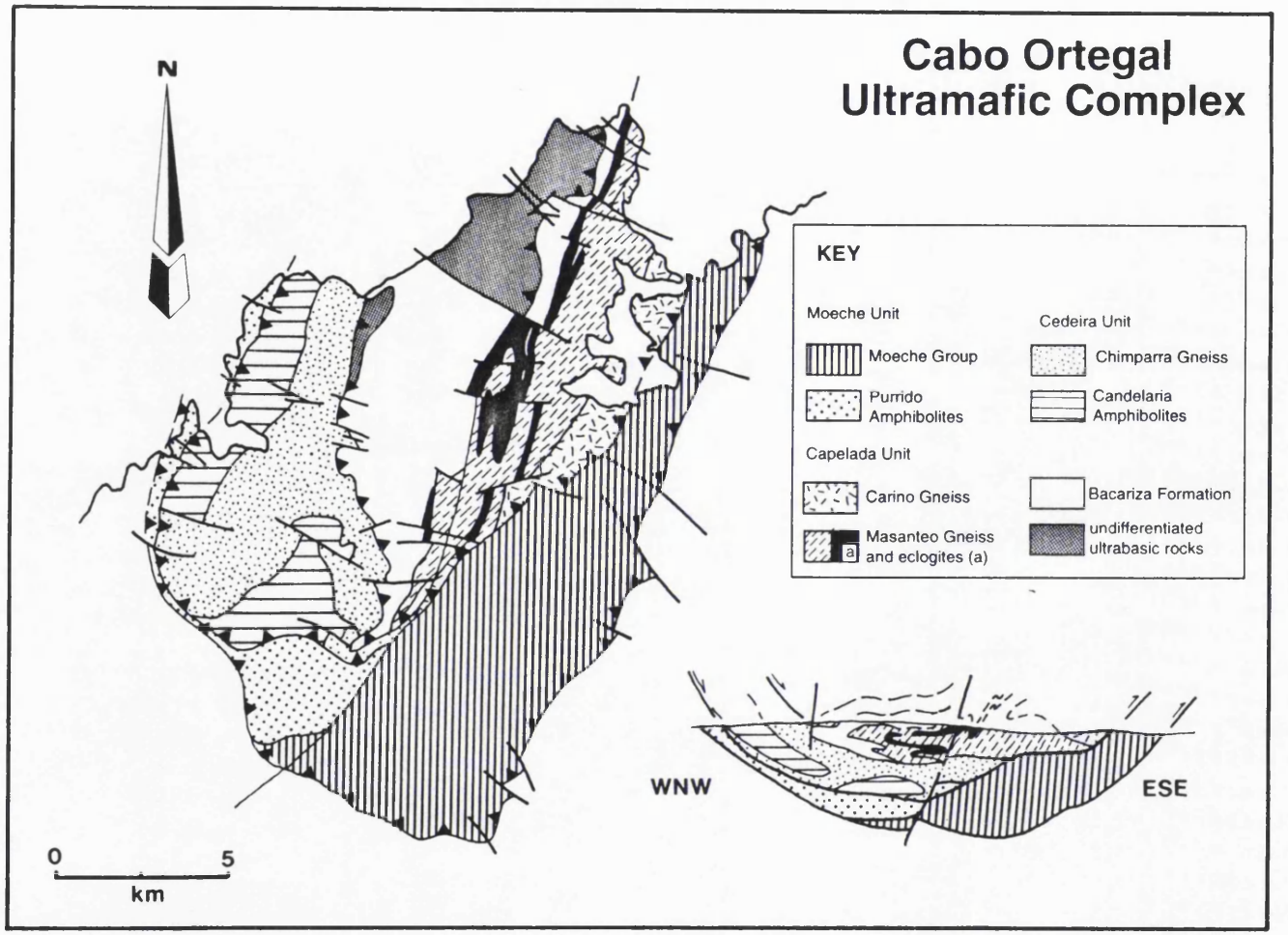

Fig. 2.14. A map showing the units of the Cabo Ortegal Ultramafic Complex, North-West Spain with a cross-section (after Bastida et al., 1984).

volcanic breccias and slates. Eclogites occur within the Capelada Unit as layers within gneisses (Bastida et al., 1984)

2.5.5 The Mobile Zones.

The Mobile Zones occur to both the north and the south of the Central Zone and have reactivated poorly differentiated Precambrian and Palaeozoic strata. The most characteristic features of these zones are large-scale thrusts and nappes, which Bard, et al. (1980) proposed formed due to tangential stress fields. Metamorphism occurred between the upper Silurian and the upper Visean. They contain a high density of syn-, late- and post-tectonic intrusions. The Northern Mobile Zone extends to the South of the British Isles and includes the 'sub-Iberian segments' of the Alentejo and Sierra Morena massifs. The Southern Mobile Zone extends from the Badajoz-Cordoba axis to the south of the Bohemian Massif, including Galician, South Armorican Crushed Zone, Massif Central, Pyrenean and Corso-Sardinian massifs. It is a complex region, with large nappes verging towards the core of the Ibero-Armorican Arc.

The SASZ is a major lithospheric fracture exposed for over 400 km from the Baie des Tréspasses, westernmost Finistérre to the Pays-de-la-Loire (Arthaud and Matte, 1975). Intrusive rocks were progressively deformed in the shear zone into orthogneiss and mylonitised by continuous-discontinuous shearing and flattening episodes (Berthé et al., 1979). The SACZ witnessed the earliest phases (mid-Devonian-earliest Carboniferous) of magmatism. The region was totally sheared during Carboniferous post-collisional episodes. The resulting 'Migmatites de Morbihan' are anatectic 'granodiorites' associated with formation of an early Variscan cordillera, the Ligerian Zone of Autran and Cogné (1980). These intrusions are coarse grained biotite-quartz-monzonites with associated biotite-sillimanite gneisses.

The West Vendéean Zone to the south-east of the Armorican Massif has suffered less tectonic disturbance. Typical Variscan nappes are exposed, unaffected by the Carboniferous strike-slip tectonics deforming the SACZ. The nappes moved westward along ductile shear zones (Vauchez et al., 1987) and were emplaced upon deformed sub-autochthonous lower Palaeozoic strata (Brun and Burg, 1982). Rb/Sr wr isochron ages on post-thrusting anatectic granites has given an age of 370 Ma (Vidal, 1980) placing the thrusting as occurring after the Silurian but before the Upper Devonian.

2.5.6 The External Zones.

The Variscan external zones comprise the northern North Variscan Foredeep and the southern Asturian-Cantabrian Basin. The

external zones show negligible metamorphism and tectonism, with small folds and superficial nappes which represent the latest Variscan structures to form (Gzelian). The Anglo-Germanic 'North Variscan Foredeep', is a 2500 km long, arcuate basin, which forms the Externides of the Variscan foldbelt. It stretches across southern Ireland, England, Belgium, northern Germany, Poland and eastern Czechoslovakia. The basin contains a shallowing northward sequence of Devonian to Carboniferous sedimentary rocks that were folded and thrusted in the southernmost areas. The basin developed within an extensional stress regime limited to the north by the Welsh and London-Brabant Massif, and to the south by the Normannian high (an uplifted Cadomian Platform comprising the Domnonean and Mancellian Domains). The Cornubian Batholith of SW England was intruded 290-280 Ma Rb/Sr (Darbyshire and Shepherd, 1985). It has a geochemical affinity pointing to S-type, syn-collisional granites, similar to those found in the North Armorican Massif, for example the Ploumanac'h Ring complex (303±15 Ma, Rb-Sr whole rock, Auvray and Martin, 1982) and the Granite de Flammanville (315-320 Ma, Rb-Sr, K-Ar, orthoclase and biotite).

The northern Variscan Front can be traced with some certainty as the northern boundary of the North Variscan Foredeep. From the Tornquist Line, the front is observed as overthrusts upon the Coal Measures of South Wales and the Brabant Massif. There are problems in correlating the front across the Irish Sea. Here the NW trending Dingle-Dungarvon Line represents the northern limit of the Variscides. However, it is a transcurrent fault zone rather than a thrust, and there is some offset with the structures in South Wales. Such dislocations of the front are evident on the other side of the Atlantic Ocean, and indeed there are problems in tracing the Front across the Atlantic. In the Southern Appalachians, the front is well defined as the Allegheny Front terminating against the Ouachita-Alabama Transform Fault. Moving northwards, in New England the front is more obscure but may well be represented by the Honey Hill thrust belt (Wintsch and Lefort, 1984). Between here and Southern Ireland the Front is further dislocated and may follow one of two major fault systems across Maritime Canada, either the Cabot or Chedabucto Fault Zones. It is the latter system that is favoured in this case, as it would mean that the front, deflected around Newfoundland would have concentrically followed the Ibero Armorican Arc (Rast, 1988) **(Fig. 2.15)**. The separate geological evolutions of the Galicia and the Avalon Terrane of eastern Canada which are Atlantic conjugate margins can be interpreted by either the existence of a plate suture

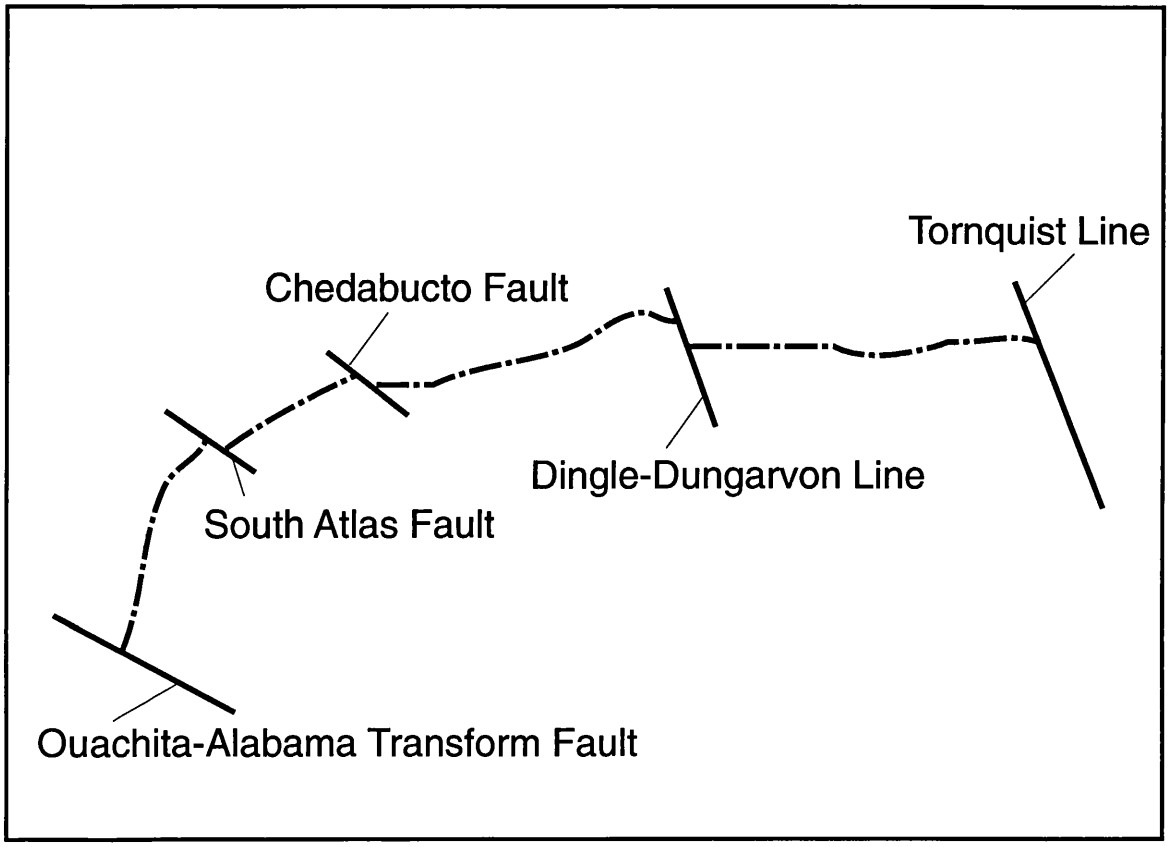

Fig. 2.15. A sketch of the Northern Hercynian Front, and the major structures disrupting it (after Rast, 1988).

or the Variscan frontal thrust separating them (Boillot et al., 1989). To join with the Cabot Fault Zone, the front is carried to the northern parts of Newfoundland. Here the rocks may be matched with that of Southern Ireland and South Wales, but the structure is of a distinctly separate N-S rather than E-W trend. It is likely that the Cabot Fault system is linked with the Caledonian Front.

The southern Variscan Front is difficult to define due to the strong overprint of the Alpine Orogeny. Nevertheless, the external zones are recognised in the core region of the Ibero-Armorican Arc. The Asturian Arc forms the core of the Ibero-Armorican Arc, it includes the Western Asturian-Leonese Zone (WALZ) and the Cantabrian Zone, now separated by the large structure of the Narcea Antiform. The structural units are as follows: the WALZ comprises an almost complete record of Cambrian to Silurian sedimentation, with lower Devonian locally exposed. Dominantly the sediments are shallow water, with the exception of an upper Ordovician transgressive event producing turbidite facies. It is also intruded by late Variscan granitic intrusions (i.e. Plúton de Salave). The subsequent formation of the Narcea Antiform exposes Precambrian schists and the imbricated, dominantly Carboniferous, Cantabrian Zone (CZ). The CZ has a sedimentary succession similar to that of the northern Variscan Externides of South Wales and central England, with well developed coal bearing deposits, the Namurian-Lower Pennsylvanian Central Coal Basin containing up to 6 km of sedimentary fill. The limestones of the Picos de Europa (the Escalada Limestone) are spectacularly exposed as complex duplex structures near the top of the nappe pile (Perez-Estaùn et al., 1988) **(Fig. 2.16 and 2.17)**.

The core of the Ibero Armorican Arc is characterised by thin skinned tectonics (the thrust roots are often less than 4 km deep). This tectonism occurred under shallow crustal conditions and resulted in the formation of a weak slaty cleavage and a low grade metamorphism. The region represents an intraplate environment, suffering transpression style tectonics related with the tightening of the Ibero Armorican Arc, and not associated with its orogenic formation (Bastida et al., 1986).

The first thrusts were emplaced in a NE direction during the Early Bashkirian. Thrust related folds were also formed at this time. Sediments then covered this unconformable surface, only to be deformed by a second phase (Gzelian) of thrust emplacement. This time the transport direction was to the SW, and possibly associated with strike-slip movement (Nijman and Savage, 1989) Associated deformation tightened the folds formed earlier and caused some reactivation of the structures (Alonso, 1989).

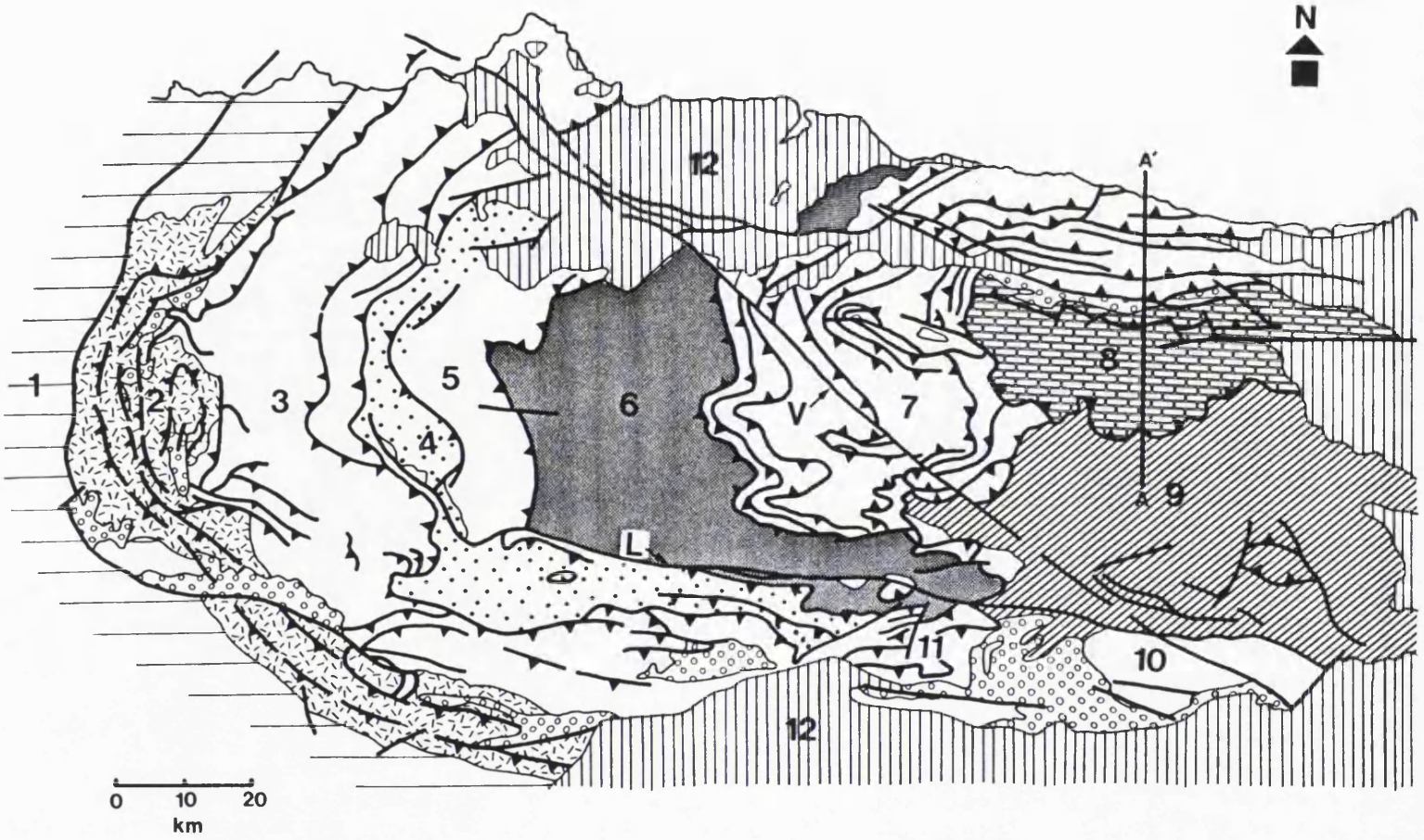

Fig. 2.16. A geological map of the Asturian Arc and Cantabrian Zone. 1: West Asturian-Leonese Zone; 2: Precambrian Rocks in the core of the Narcea Anticline; 3: Somiedo-Correcilla Unit; 4: La Sobia-Bodon Unit; 5: Aramo Unit; 6: Central Coal Basin; 7: Ponga Unit; 8: Picos de Europa Unit; 9: Pisuerga-Carrion Unit; 10: Valsurvio Unit; 11: Esla Unit; 12: Mesozoic-Tertiary cover; V: Ventaniella Fault; L: Leon Line; A-A'; line of section in fig. 2. (after Perez-Estaun et al., 1988).

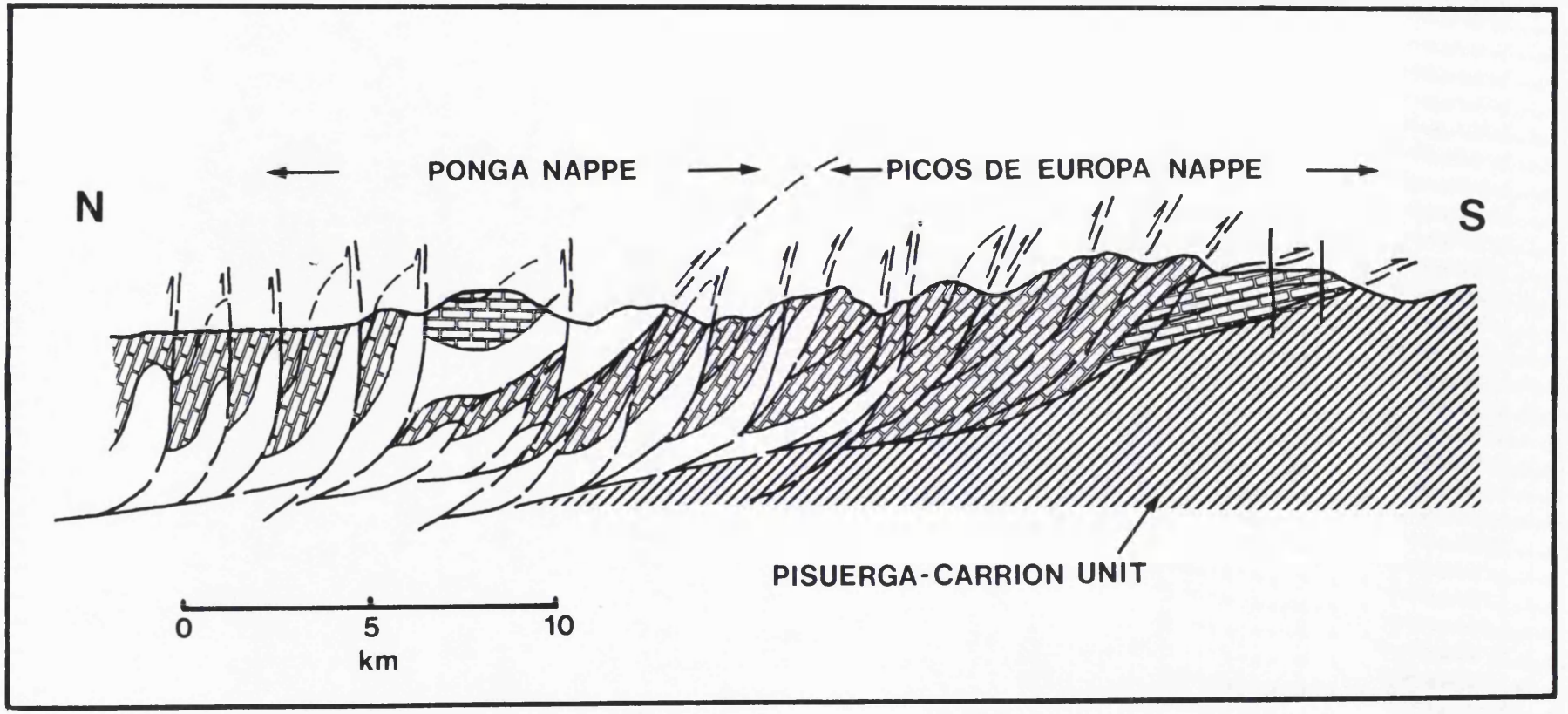

in Fig. 2·16

Fig. 2.17. Cross-section along the line A-A′ showing the imbricate structure of the Ponga and Picos de Europa thrust sheets (after Perez-Estaun et al., 1988).

Whether or not the nappes were emplaced by gravity-glide mechanisms along a flat decollement surface or as thrust sheets over an unconformable sequence is a matter of continuing debate (Nijman and Savage, 1989; Alonso et al., 1991; Nijman and Savage, 1991), as is the timing of the emplacement of the sheets. It is now thought that tectonism and sedimentation were synchronous and that sedimentation was frequently tectonically controlled throughout the Pennsylvanian. The deformation was highly influenced by transpression in the Iberian microplate.

Post orogenic Permo-Triassic redbeds (conglomerates overlain by sandstones and siltstones) form unconformable sequences overlying the eastern border of the Cantabrian Zone. Dating of these deposits has proved difficult due to the absence of fauna. However, magnetic data obtained by Schott and Peres (1987) has revealed that the tectonic history of these red beds is complex. They recognised two main phases of remagnetisation subsequent to the primary magnetisation of the beds. The first of these was associated with the precursors to opening of the Bay of Biscay during the Jurassic to Early Cretaceous. A second remagnetisation during the Eocene is linked to transpression due to the convergence of the Iberian Block on Europe. The authors attribute the remagnetisations to the circulation of mineralising fluids and their consequent deposition of authigenic minerals; no evidence for regional metamorphism of this age is present. The occurrence of hot fluids within the Cantabrian Zone has been independently noted using conodont colour alteration indices (CAI) by Raven and van der Pluijm (1986). They estimated palaeotemperatures in excess of 300°C, that are attributed to Pennsylvanian Variscan metamorphism. However, metamorphism is weak, and the high CAI is not necessarily associated with Palaeozoic lithological and structural divisions, and thus could feasibly have occurred after the cessation of Variscan events.

2.5.7 The structure of Ibero-Armorican Arc.

The most characteristic feature of the Variscan belt is the Ibero-Armorican Arc, a vast syntaxis that is now bisected by the Bay of Biscay and cross-cut by the SACZ (Lefort, 1979). The structure is an example of a non-rotational arc as defined by Marshak (1988). Such a structure formed as an arc with no change of the original strike of the rocks. This is contrasted with an orocline where the structure was formed as a direct result of deformation. The Ibero-Armorican Arc does exhibit evidence of compression after its formation, but the tightening of the structure this produced was minor compared to the geometry of the arc itself.

Although recognised as an arcuate structure since the early parts of this century, Matte and Ribeiro (1975) were the first to give an explanation of the formation of the Ibero-Armorican Arc as a configuration formed by the collision of a continent moving from the south-east with one in the north. The tectonic structures are associated with two phases of deformation, a transpressive phase followed by a compressive phase, although these phases are difficult to discern. This theory was revised and improved upon by Brun and Burg (1982), applying the recent advances in Himalayan geology to the Ibero-Armorican Arc. They observed that the South Armorican Crushed Zone (SACZ) is contemporaneous with and has a correlative in the Coimbra-Cordoba Shear Zone, the geometry fitting the rigid-plastic indentation tectonics model of Tapponier and Molnar (1976). A model of indentation of Africa with Europe (Bard et al., 1980; Brun and Burg, 1982) or indentation of the Iberian Microplate with stable Europe (Quesada, 1991) has been proposed to account for the structure, and comparisons with Hazara and Jijal syntaxes of the Himalaya formed by the collision of the Kohistan Arc (Tapponier and Molnar, 1977) may be made **(Fig. 2.18)**.

During a phase of late Carboniferous tightening of the arc at the climax of collision, conjugate shear zones developed in the core, accompanied by sinistral wrenching in Coimbra-Cordoba Shear Zone and dextral wrenching in SACZ (Brun and Burg, 1982). The inner regions of the arc which are the Variscan external Cantabrian Zone, display a complex series of thrusts, imbrications and duplexes. Two major phases of tectonism are exposed in the Cantabrian Zone; early nappes developed along a basal Palaeozoic décollement surface which young in a clockwise sense around the arc (Perez-Estaún et al., 1988, 1991), the amplitude of this continental overthrusting increases towards the hinge of the Ibero-Armorican Arc. Dextral transpression developed here due to the oblique angle of collision (Ribeiro et al., 1991b), and the nappes were stacked towards the east with a flake geometry due to this oblique collision, illustrating typical thin-skinned tectonics (Ribeiro et al., 1991a). Later phases of folding occurred deforming the nappes. A first parallel to the nappe fronts and another perpendicular to them and therefore radial to the arc (Perez-Estaún et al., 1991, 1988), was succeeded by strike-slip fault movements (Julivert, 1971). These structures indicate a late Carboniferous tightening of the Ibero-Armorican Arc. The faults were later reactivated in the Mesozoic as a response to early extension and rifting in the Bay of Biscay (Lepvrier and Martinez-Garcia, 1990)

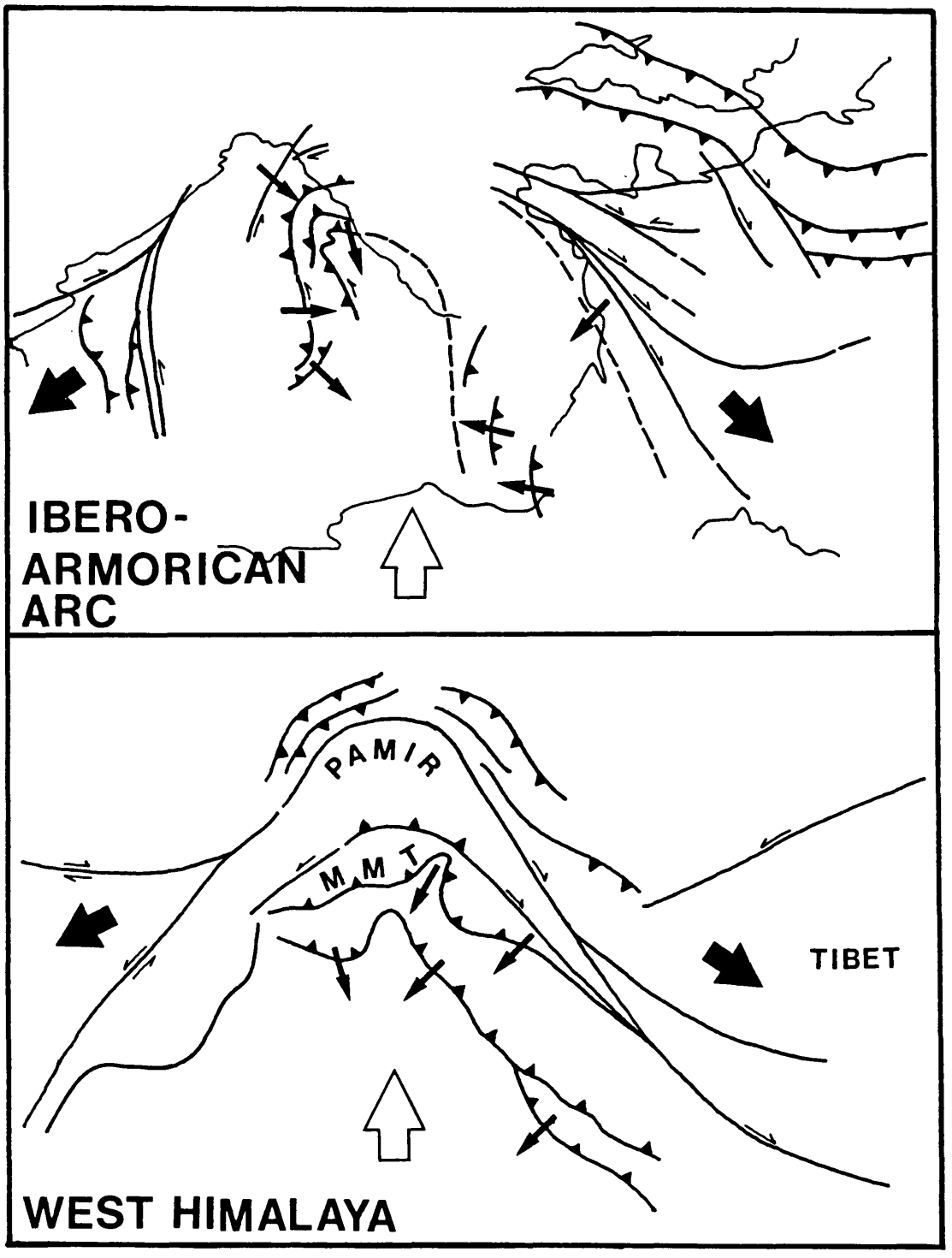

Fig. 2.18. Comparison of the structure of the Ibero-Armorican Arc with the western Himalaya (after Matte, 1991).

2.5.8 Summary.

The Palaeozoic Hercynian Orogeny formed as a result of the suturing of the supercontinent Pangaea as a consequence of collision of northward moving Gondwana with the recently accreted and relatively stable Laurentian and Baltic cratons which formed the continental mass of Laurasia.

The European arm of the Hercynian orogeny, the Variscides is summarised as a sequence of events typical of most collision orogens; early subduction along the South Armorican margin was superseded by the accretion of several microplates, including the Iberian plate to the Laurasian margin, followed by full-scale continental collision between Laurasia and Gondwana. The compression resulted in tightening of the Ibero-Armorican Arc and was accompanied by the formation of the South Armorican and Coimbra-Cordoba shear zones.

2.6 Post Variscan Evolution.

2.6.1 Permian and Triassic.

The termination of the Variscan Orogeny in the earliest Permian culminated in the formation of the supercontinent Pangaea **(Fig. 2.19)**. This led to subsequent peneplaination and deep exhumation of the Armorican, Hesperian and other Variscan massifs during the Permian and Triassic (den Tex and Floor, 1971; Cogné, 1974, Smith et al., 1974,). The Early Permian is consequently regarded as an erosionary period. The continental nature of the Permian sediments has made them difficult to date, floral or faunal remains being sparse. Designating the base of the Permian has therefore, occasionally, proved difficult. In some regions the major erosional phase is pre-Gzelian (latest Cretaceous) where a major unconformity exists between Gzelian sediments and the Variscan molasse **(cf. Fig. 2.16)**. However, in many places the Gzelian-Permian boundary is diffuse (i.e. onlap to the Cornubian Massif; Smith et al., 1974). Semi-arid to humid climatic conditions were prevalent throughout most of this time which led to a reddening of the exposed basement (Hay et al., 1981; Smith et al., 1974) and the formation of lateritic horizons (Cogné, 1974). Permian and Triassic sedimentation in the western Variscan massifs was reduced to the deposition of substantial amounts of dominantly terrigenous clastic sedimentary rocks in, amongst others, the Cantabrian Basin (1 km; Ziegler, 1990), the Aquitaine Basin (2 km; BRGM et al, 1974), and the Western Approaches Basin (5 km; Chapman, 1989). Evaporites developed in restricted, newly formed shallow marine basins, of which the Bay of Biscay rift zone was one (Ziegler, 1990).

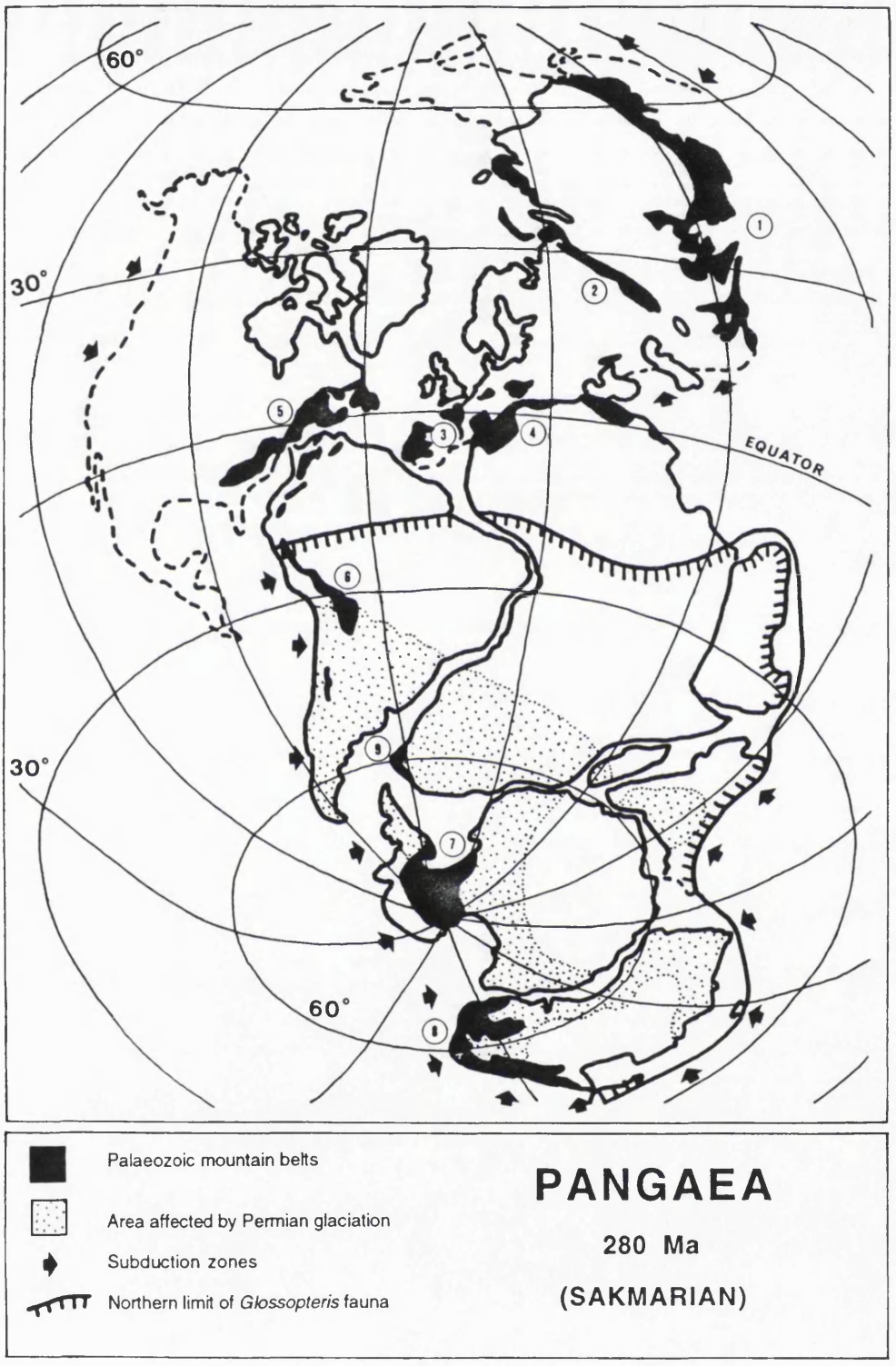

Fig. 2.19. The super continent Pangaea in the early Permian, showing position and climate. The Palaeozoic mountain belts are 1: Mongolian; 2: Urals; 3: Variscan; 4: Mauretanides; 5: Appalachians; 6: Pampean; 7: Transantarctic; 8: Tasman; 9: Cape (redrawn after Windley, 1986, and Dott et al., 1976).

2.6.2. Sedimentation in the Jurassic and Cretaceous.

Major marine transgressions during the Rhaetian and Hettangian brought about the formation of marine basins (Ziegler, 1990). The Bay of Biscay rift was a restricted basin, and conditions there produced evaporites, the Aquitaine and Cantabrian Basins were shallow water carbonate environments (BRGM et al., 1974). The Paris Basin initially developed a sequence of deltaic material, sourced from the London-Brabant and Rhenish Massifs that deepened into shales and marls (Rosenfeld, 1978). Sea level rose during the Sinemurian and Toarcian (Vail et al., 1977). This led to the development of widespread seas that allowed connections between Tethyan and Boreal faunal realms, and marine conditions were developed in the Bay of Biscay rift zone (Enay and Mangold, 1982). At this time, minor clastic sedimentation continued in the Paris Basin, again the main source region being the London-Brabant and Rhenish Massifs rather than the Armorican Massif (Ziegler, 1990). Clastic sedimentation ceased in the Aquitaine Basin, and here the dominant deposits, as in the forming Western Approaches and English Channel Basins was of carbonates and shales (BRGM et al., 1974). Extension in the basins caused movement on reactivated Palaeozoic structures, and the sedimentation was affected by this with abrupt changes in thicknesses of beds (Mégnien, 1980a). Warm, shallow seas in the Bajocian and Bathonian produced extensive shallow marine carbonates in the basins. At least parts of the Armorican Massif were emergent at this time as marginal reef facies are located upon its north-eastern margins. Similar reefs covered parts of the Massif Central (Mégnien, 1980b). The late Jurassic and early Cretaceous were more important times in the evolution of the Armorican Massif. A transgression occurred in the Callovian to mid-Kimmeridgian followed by regression in the later Kimmeridgian and Tithonian (Vail et al., 1977). The formation of a high around the Biscay triple junction prior to continental breakup (Bott, 1992) allowed the west European Variscan Massifs and particularly uplift of the Hesperian Massif, to play a more important role as a source region for clastic input into the surrounding basins (Mégnien 1980a, 1980b). Igneous activity occurred along fault systems in the Western Approaches and English Channel Basins.

The Cretaceous was a period of major sea-level fluctuations. The lower Cretaceous was a time of regression, with a retreat of seas and the deposition of the continental "Wealden" facies (Allen, 1981). This emergence of land was influenced by the continued upwarping of the Biscay rift dome, which continued to shed clastic sediments eastwards. Around 4 km of continental-type sediments were deposited in the Duero and Parentis

Basins (Choukroune and Mattauer, 1978). Parts of the Paris and Western Approaches Basins were emergent, whilst the English Channel Basin continued collect sediment from the Armorican and Cornubian Massifs. Eventual subsidence of the dome began with the onset of seafloor spreading in the Mid-Cretaceous (Mégnien, 1980a, 1980b).

Throughout the Aptian-Albian, sea level was similar to that today (Vail et al., 1977). Eustatic rise in sea level commenced in the Albian and the Armorican Massif was probably submerged during the maximum transgression in the Campanian, at the greatest extent of the chalk seas (Hancock, 1987). The small areas of land remaining during this time produced little erosional material, and the chalk extended well onto the continental shelves. Up to 1 km of chalk was deposited in the basins around the Variscan Massifs. The possibility of chalk deposition on these massifs is not documented. Sea level subsided abruptly during the Maastrichtian (Vail et al., 1977).

2.6.3. Cenozoic sedimentation and tectonism.

The Tertiary evolution of the Armorican Massif is represented by several brief transgressive events. The massifs became emergent in the late Palaeocene, and continental lacustrine and fluvial sedimentation occurred in the Paris and English Channel Basins. Palaeogene deposits occur near the coasts of southern Brittany and in Vendée, representing two transgressions in the Stampian and Lutetian (Cogné, 1974). Neogene deposition began with the Miocene Helvétian conglomerates and limestones traversing the Normanno-Breton Gulf, linking the Bay of Biscay with the English Channel. The final transgression in the Pliocene left the Redonian deposits consisting of montmorillonite-rich, red sands which were synchronous with Alpine (Laramide) tectonic episodes gently folding these sediments, again reactivating Variscan structures (Cogné, 1974).

The Iberian Plate was tectonically active during the Tertiary, and also underwent copious sedimentation in the Ebro, Duero and Tagus Basins. The effects of the Pyrenean convergence and collision were important causes of intraplate deformations. There were two major compressive events associated with the Pyrenéan Orogeny. The first, a NW-SE oriented phase was linked to the NW translational movement of the Iberian plate occurring during the late Cretaceous to Lower Eocene (Grimaud et al., 1982). Collision in the Eocene forced a major compression responsible for the emplacement of the largest Pyrenéan nappe complexes i.e. the Gavarnie and Montsec Nappes (Julivert et al., 1974). This compression continued during the Oligocene when at the end-Oligocene

there was a reversal in tectonic regime in the Iberian Plate from compression to extension (Guimerà, 1984).

The history of Mesozoic and early Cenozoic basin sedimentation and the importance of the Variscan Massifs as source regions is summarised in Table 2.1.

MESOZOIC BASIN SEDIMENTATION				
Stage	**Ma**	**tectonic (T) & volcanic (V) episodes**	**environment *(sediments)***	**clastic source region**
Rhaetian - Hettangian	225	V Aquitaine Basin	deep marine	London-Brabant & Rhenish Massifs
Sinemurian - Aalenian	204		transgression *(shales & carbonates)*	London-Brabant & Rhenish Massifs *(reduced clastic input)*
Bajocian - Bathonian	183		*(carbonates)*	*negligible clastic input*
Callovian - Tithonian	169	?V English Channel T formation of the Biscay rift dome	regression *(sands)*	London-Brabant, Rhenish & Variscan Massifs
Berriasian - Aptian	144		rapid sea-level change	London-Brabant, Rhenish & Variscan Massifs
Albian - Maastrichtian	113	T subsidence of Biscay rift dome; start of seafloor spreading.	transgression *(chalk)*	*negligible clastic input*
Palaeocene	66	T Laramide Orogeny	regression *(terrestrial, lacustrine)*	London-Brabant, Rhenish & Variscan Massifs

Table 2.1 A summarised and generalised history of the sedimentary and tectonic controls on the Paris, Aquitaine, English Channel, Western Approaches, Asturian and Duero Basins (compiled from BRGM et al., 1974; Mégnien, 1980a; Mégnien, 1980b; Ziegler, 1990).

2.7. Summary and Conclusions.

The Armorican and Hesperian Massifs represent Proterozoic to Palaeozoic Andean- and Himalayan-type mountain building events, finally bisected by the rifting and ultimate seafloor spreading in the Bay of Biscay and the opening of the North Atlantic.

Oblique subduction and eventual dissemination of the Cadomian Cordillera during the late Proterozoic (Sinian) was succeeded by the

Hercynian Variscan Orogeny, as Gondwana and Laurasia collided to form the supercontinent Pangaea. These events concluded at the end of the Palaeozoic when, prior to and during Mesozoic collapse of the Variscan Belt, the massif underwent deep exhumation during the Early Permian. The geological history of the region during the Mesozoic was dominated by rift controlled sedimentation in basins forming around the edges of the massifs. Only minor marine incursions occurred during these times onto the landmasses. Tertiary translation, convergence and eventual collision of the Iberian Microplate with stable Europe culminated in the formation of the Pyrenées as part of the early Alpine closure of Tethys, resulting in the geological and geographical arrangement of the continent as it remains today.

Chapter 3.

The Bay of Biscay: Mesozoic rifting in the Variscan Belt

3.1 Introduction.

Continental rifting, occurring as a result of crustal extension and the associated thinning of the continental crust is an active field of research in geological, geochemical and geophysical disciplines and an ideal field of tectonics in which to apply fission track analysis to aid in the determination of crustal evolution.

The majority of rift valleys originate along lines of relative crustal weakness (much of the East African Rift follows intercratonic mobile belts), often generated by a relaxation of compressive stresses after continental collision (Molnar and Tapponier, 1975; Coward, 1992). As a result, many rift valleys form approximately perpendicular to, and soon after the formation of major orogenic belts; for example the Baikal Rift in response to the Himalayan Orogeny, and the Rhine Graben after the Alpine Orogeny. Similarly, continental rifting forming the Bay of Biscay and other rift basins in the Atlantic Ocean began soon after the cessation of plate collision in the earliest Permian **(Fig. 3.1)**.

Rift valley systems share similar structural characteristics. Typically, the margins consist of tilted blocks sequences. The deep structure of these blocks and bounding faults is problematic, but it is assumed that the faults are planar in their upper regions, becoming listric and soling out at lower crustal depths, grading into low angle detachment zones. Brun and Choukroune (1983) propose that gravity gliding is a dominant mechanism for block tilting along low angle normal faults at depth, once rifting has been initiated.

A series of models have been proposed to explain the mechanisms of rifting, involving either pure shear or simple shear mechanism or a combination of these two end members. The models are summarised in **Figure 3.2** In the pure shear model as described by McKenzie (1978), crustal extension is achieved by uniform thinning of the lithosphere in response to extensional forces, with any detachment zones and slip being horizontal **(Fig. 3.2a)**. Wernicke (1985) proposed a simple shear model involving asymmetric rifting caused by extensional slip along a single detachment zone. This is the simple shear model **(Fig. 3.2b)**. It is too simplistic a scenario to assume that rifting is one or other of these

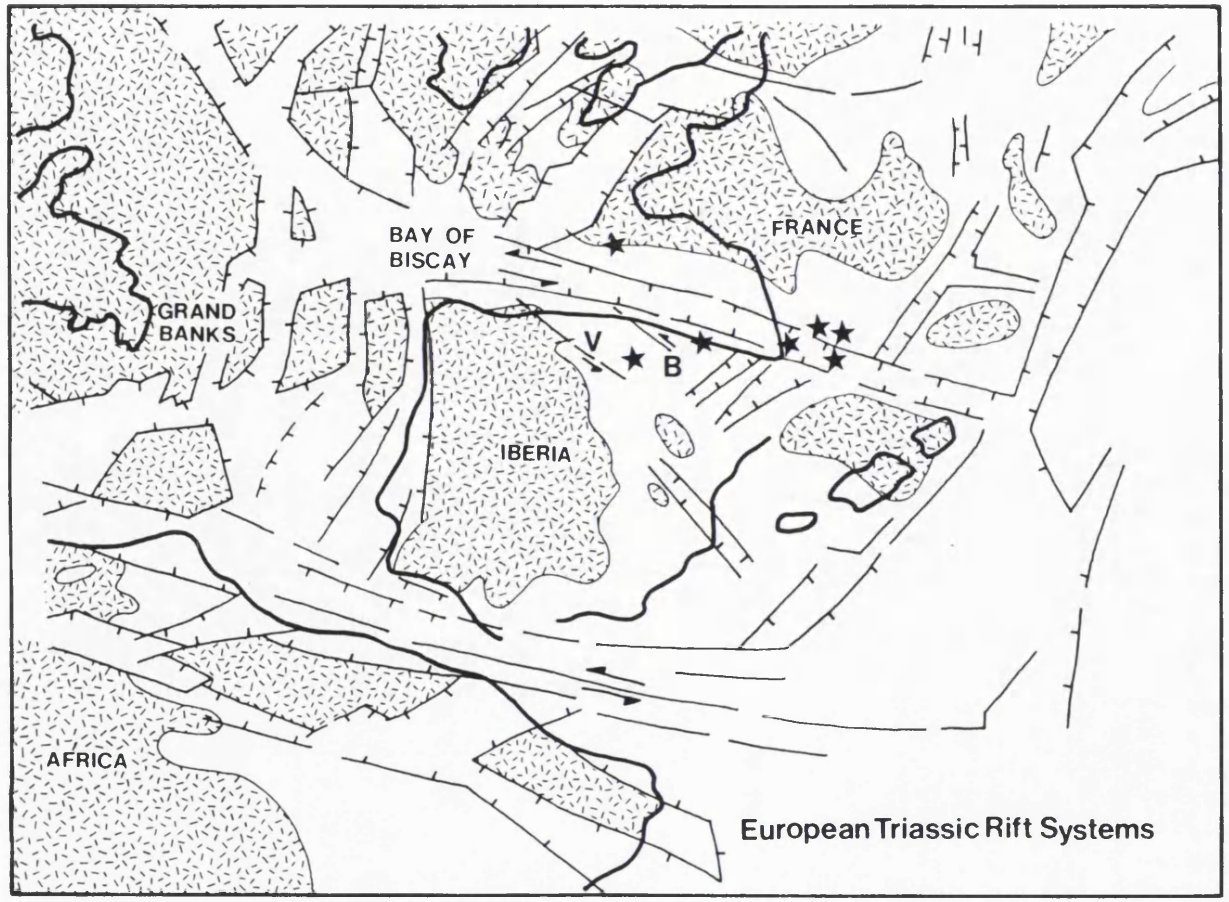

Fig. 3.1. European Triassic rift systems. The map shows the Bay of Biscay in context with neighbouring Triassic rifts. Shaded areas represent upstanding blocks. V: Ventaniella Fault; B: Bilbao Fault. Both faults are Variscan structures reactivated at the time of breakup. Black stars indicate regions of tholeiitic volcanism associated with rifting in the Bay of Biscay (after Garcia-Mondejar, 1989).

mechanisms, particularly as the two are not necessarily mutually exclusive events. Both models exist as end members, but the majority of rifting is most likely to result from some combination of the two regimes. The lithosphere is layered thermally and therefore rheologically, and cannot be expected to behave as a homogenous mass. Lister et al. (1991) propose combinations of the McKenzie and Wernicke models **(Fig. 3.2c and 3.2d)**. Simple shear is probably the predominant extensional mechanism in the brittle upper crust and lithosphere, with extension being achieved through pure shear in the lower ductile lithosphere. Most authors agree that this is a likely case; McKenzie (1978) accepts that graben formation occurs only in the upper 10-15 km of crust.

Rift valleys are discrete regions some tens of kilometres wide and a few 100 kms in length, and are in contrast with broad regions of continental extension such as the Basin and Range Province in the western United States. The Basin and Range is an unusual extensional environment on tectonically thickened crust, which possibly resembled the Tibetan Plateau in its pre-rift stage (Braun and Beaumont, 1989). Direct comparison with the continental margins of the Atlantic, is therefore difficult.

Despite the broad symmetry of modern rift valleys (as a downfaulted central graben bounded by two near vertical fault systems flanking horsts) geophysical exploration has made it possible to ascertain strong asymmetries in rift structures, particularly sediment thickness, rift flank topography gravity anomalies and fault morphology. The asymmetry suggests that one of the rift walls is bounded by a listric fault, becoming approximately planar at depth. It is not possible for this asymmetry to change its sense between rift basins (Bosworth, 1985; **Fig. 3.3**).

As crustal thinning occurs isotherms will become compressed, locally increasing the geothermal gradient. Uplift may occur as hotter, and therefore less dense material rises (Mareschal, 1983). This thermal uplift is not necessarily a permanent phenomenon of passive margins, and a thermal dome, if present will subside upon cooling. However, such upwarping of the crust can become permanent features. Elevated escarpments parallel to the rift axis exist on continental margins in the South Atlantic (South America and southern Africa), the margins of the Red Sea, the Western Ghats of India and in eastern Australia **(Fig. 3.4 and 3.5)**. These rift flanks up to 1000 m high and 300 km wide, separate the continental interior from the coastal plain (Summerfield, 1991). Their persistence is not well understood. Gilchrist and Summerfield (1990) have postulated that up to 600 m of topography may be created by the isostatic

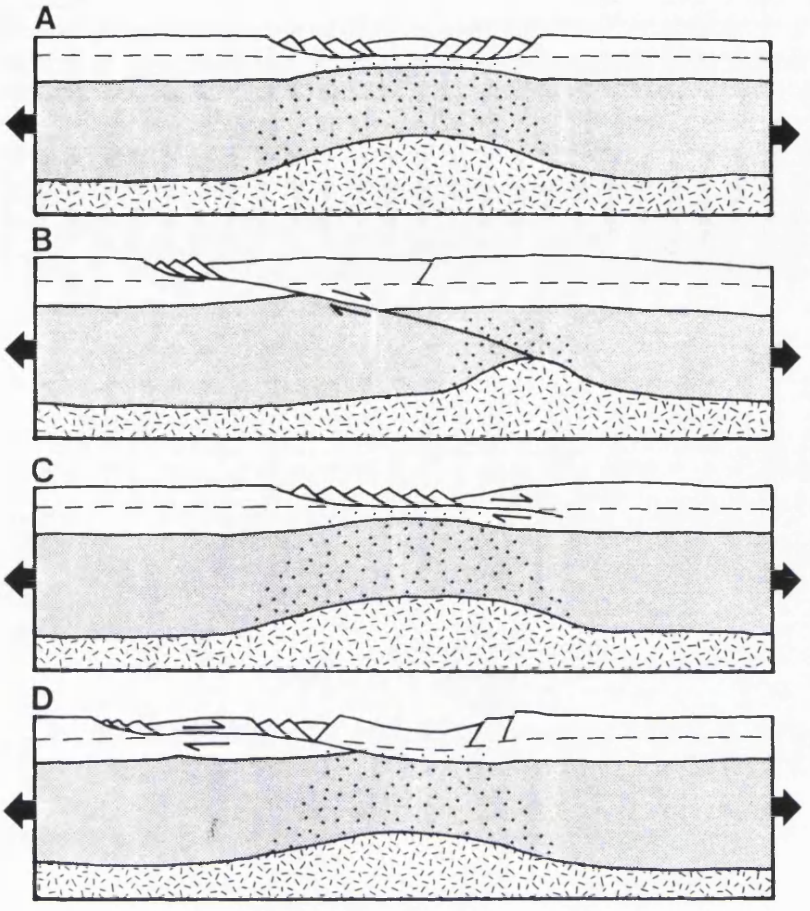

Fig. 3.2. Models for extension of the lithosphere, leading to the formation of passive margins. On all diagrams, areas of ductile stretching are indicated by stippling. A: Pure shear (McKenzie, 1978) model. This would give rise to symmetrical conjugate passive margins; B: Simple shear (Wernicke 1985) model; C: Asymmetrical fault wedges in the brittle upper crust, directly underlain by pure shear ductile stretching; D: Delamination model with complicated stretching of the brittle upper crust and a strongly offset zone of pure shear stretching of the underlying ductile part of the lithosphere after Bott, 1992).

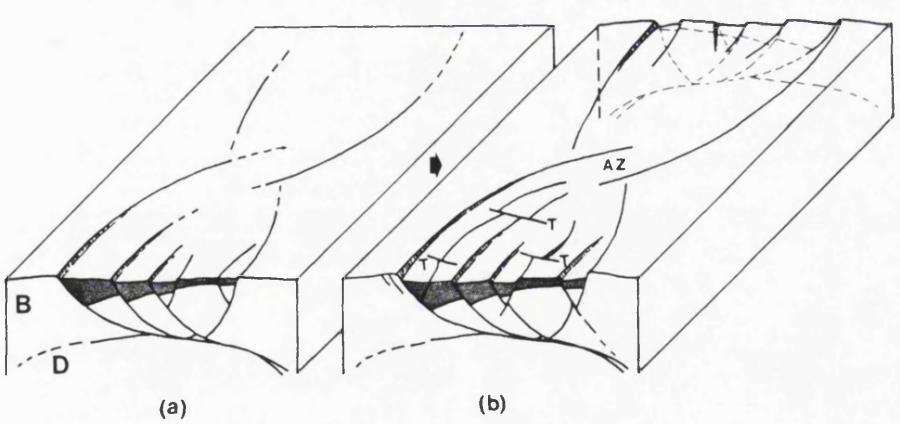

Fig. 3.3. A model for the propagation of a continental rift. (a): a zone of diffuse faulting is initiated due to upper crustal extension, these faults become listric at depth, the base of the system being marked by a detachment zone. Opposing detachments may form, and if these are larger, a reversal of rift symmetry may occur. (b): the detachment system may overlap or merge at an 'accommodation zone' (AZ), which would have the appearance of a small graben. Transfer faults (T) would also act as small scale accommodation zones (after Bosworth, 1985).

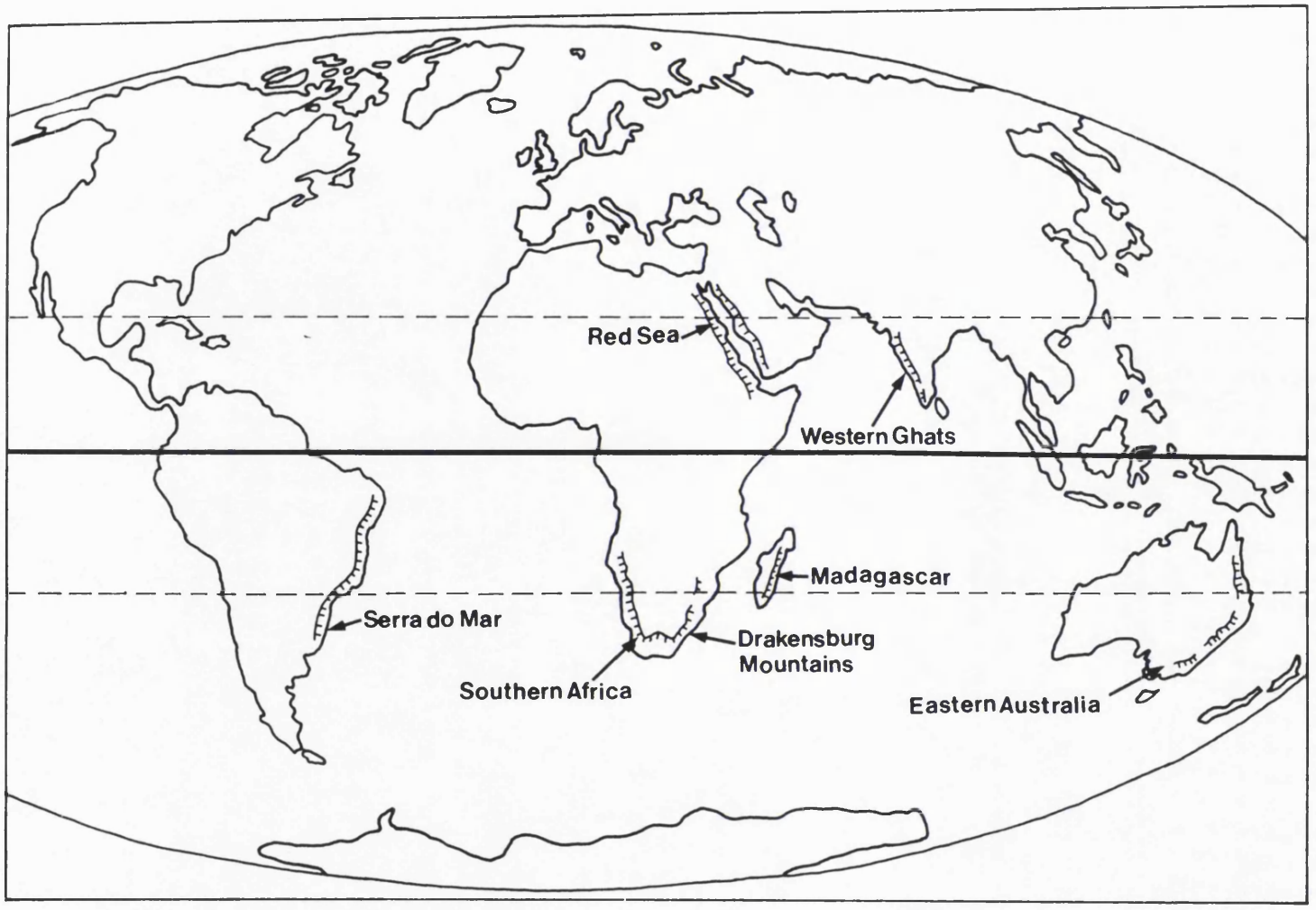

Fig. 3.4. A World Map showing the localities of great rift escarpments (after Summerfield, 1991).

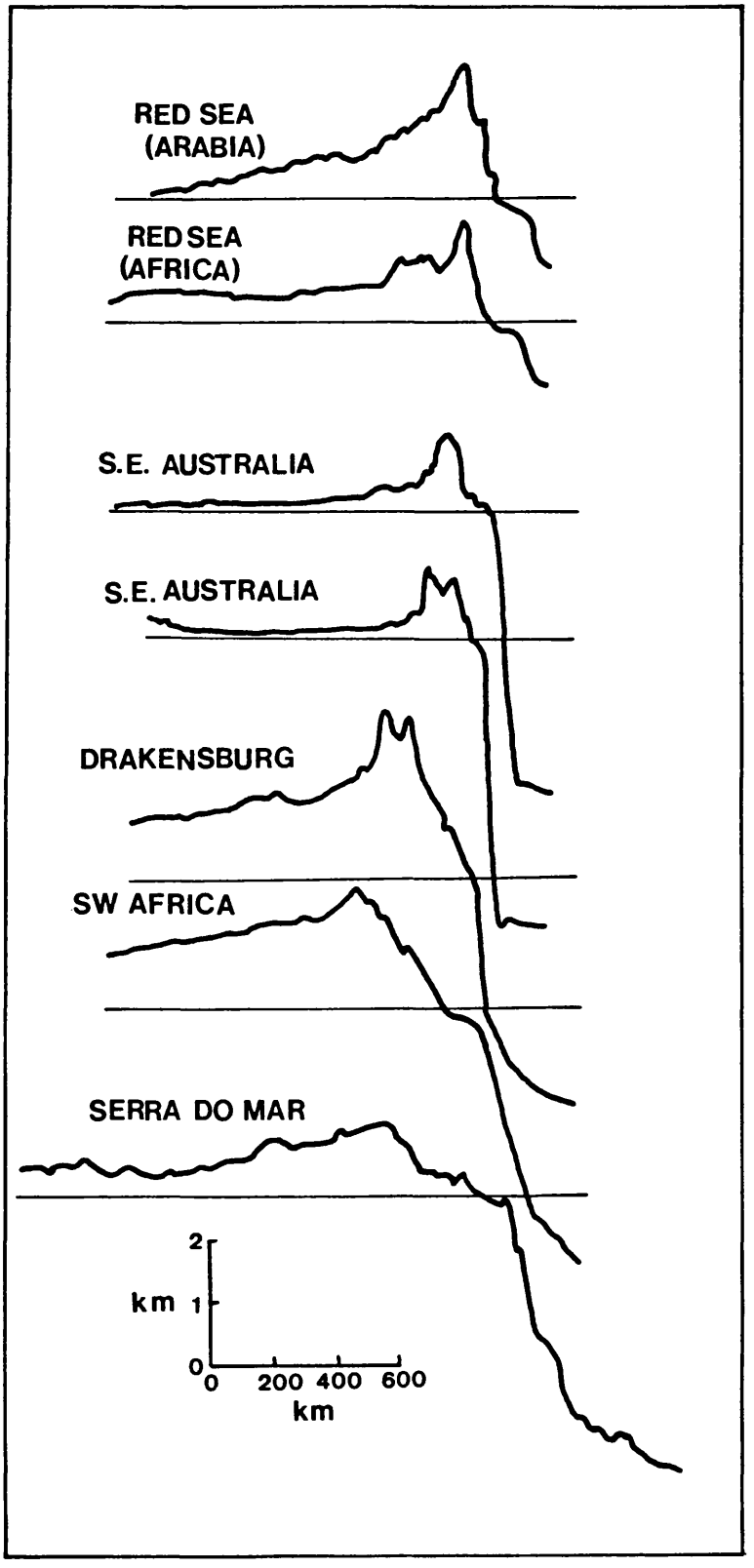

Fig. 3.5. Elevation profiles across selected passive margins of the Gondwana continents (after Weissel and Karner, 1989).

response to unloading by denudation alone. The mechanisms responsible for the long term elevation of rift flanks is not well understood. Although prominent features of some passive margins, especially those in Gondwana derived continental plates, they are certainly not a feature of all rift zones. For example the southern Australian margin is of low elevation despite rifting between Antarctica in the early Mesozoic. The North Atlantic region and in particular the Bay of Biscay show no recognised rift escarpments. The Proterozoic-Palaeozoic Caledonian mountains in Norway (Skogseid and Edholm, 1988) and in the north-western UK (Lewis et al., 1992b; White and McKenzie, 1989) are probably elevated as a result of North Atlantic rifting (C. Beaumont *pers. comm.*).

A possible mechanism for the continued elevation of rift flanks is magmatic underplating by partial melting in the underlying mantle (White et al., 1987). This hypothesis may account for the presence of flanks on the South Atlantic margins and the Western Ghats of India, both of which are associated with large volumes of continental flood basalts. It is also conceivable that elevated flanks exist in these regions because the rifts were formed in thickened intra-plate cratonic crust which had a high pre-rift elevation (R. Brown *pers. comm.*) although the cause of this high elevation remains unknown.

The present absence of characteristic rift escarpments on the northern margin of the Bay of Biscay is probably the result of denudation and thermal subsidence before the onset of seafloor spreading in the Aptian-Albian. Bott (1992) has estimated a Biscay rift dome with upwarping of around 3 km, which was present during the Oxfordian (Hiscott et al., 1989). This was followed by erosional cooling then crustal thickening which has produced an estimated subsidence of the region of 2.3 km since the end of rifting in the Aptian to the present day (Bott, 1992).

As continental rifting progresses, the crust is thinned and heat flow in the rift axis is increased. However, as close as 25 km to the rift axis the thermal effects are minor, and are undetectable at around 50 km away (Gallagher et al., 1993). Such conclusions depend somewhat on the nature and rate of rifting. Once the crust breaks up, and rifting gives way to seafloor spreading, the passive margins of the rift flanks are moved away from the heat source and are no longer subjected to any rift related heating. Seafloor spreading may or may not take place after the rifting phase. The conditions for this change over in tectonic regime are dependent on the occurrence of significant extension to thin the crust sufficiently for lithospheric decoupling to take place (Montadert et al., 1977).

Passive margins are defined from active subduction related margins as being seismically inactive, and have continental and oceanic crust welded together as part of the same plate (Bott, 1992). As non-seismically active environments, the implications of sedimentation and subsidence along continental margins and the responses of the lithosphere are the subject of much ongoing research, especially in the North Atlantic region. The sediment 'starved' nature of the passive margins forming the Central European Atlantic seaboard, and the region around the Bay of Biscay and Galicia Banks, reveal the tectonic structures associated with continental extension, rifting and breakup that are often buried by post-rift sedimentation.

3.2 The opening of the North Atlantic Ocean.

The opening of the Atlantic Ocean between Africa and South America, then Europe and North America, was a gradual northwards propagating process, in action from the Mesozoic to the present day. Clockwise rotation of Pangaea resulting in the northward movement of North America and southward movement of Asia occurred in the early Jurassic. The South Atlantic Ocean opened during the Jurassic, and was associated with mantle plumes and the extrusion of continental flood basalts prior to breakup. These have left spectacular rift escarpments in the Parana and Etendeka provinces of Brazil and South Africa.

The formation of the Central Atlantic was associated with limited volcanism and the formation of rift flank escarpments is not readily obvious. The North Atlantic margins are typical passive (non-volcanic) margins, some sediment starved (i.e. Galicia Bank) and others undergoing large amounts of sedimentation and subsidence (i.e. offshore North America). The early Tertiary to present day formation of the North Atlantic in the region north of 55°N was probably plume related (White, 1988), with extensive flood basalts onshore and offshore in the Thulean and British Tertiary Volcanic Provinces (BTVP, **Figure 3.6)**.

Breakup of the supercontinent Pangaea began after relative tectonic stability during the Permian. However, there is evidence for Late Palaeozoic dextral shear causing a translational movement of the Eurasian, Iberian and African plates (Arthaud and Matte, 1975, Bullard et al. 1965, Le Pichon et al. 1977). There is still disagreement with the translations and timing of these movements. Sibuet (1973) proposed that some of this Palaeozoic translation was accommodated by strike-slip movement along

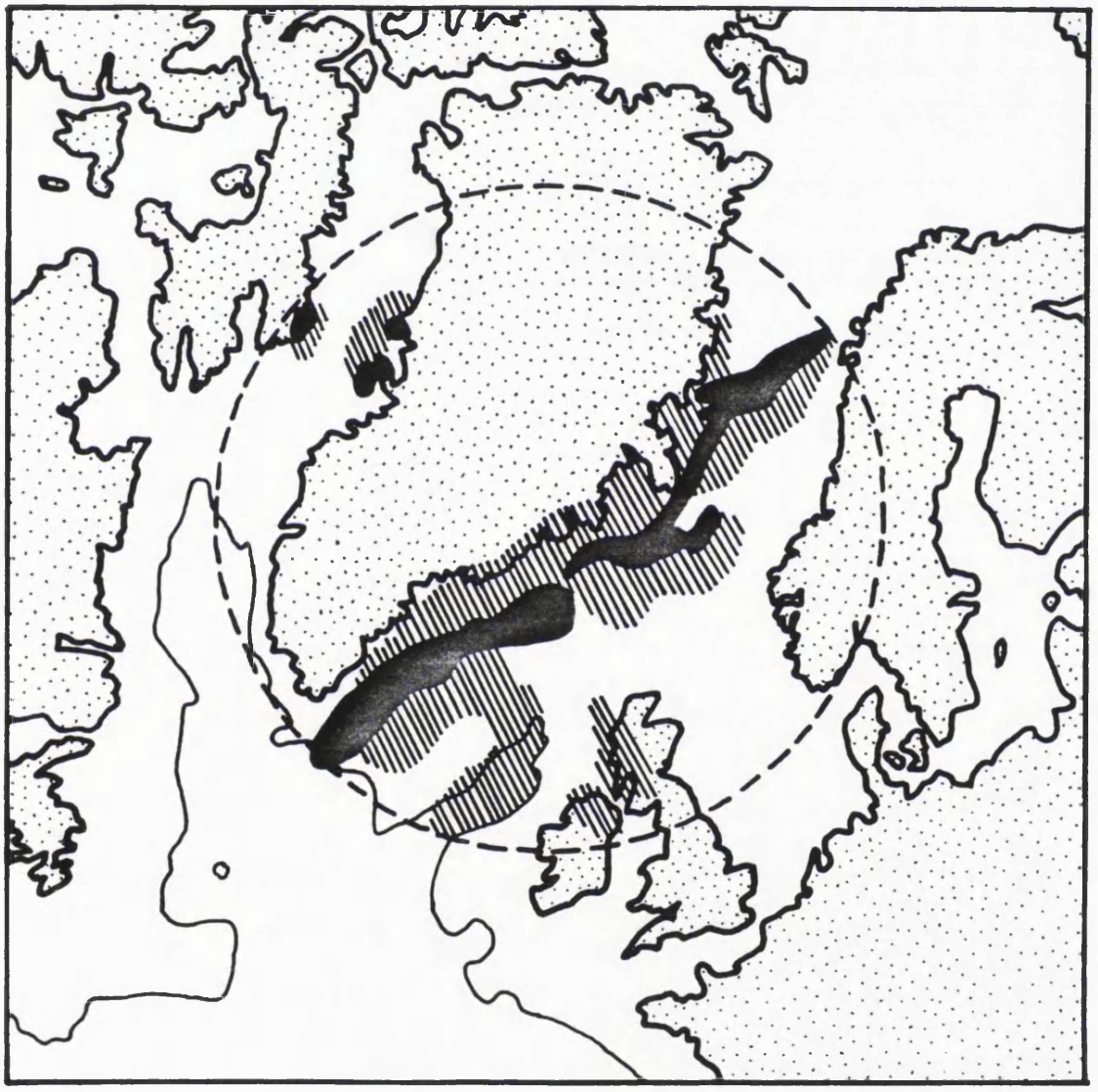

Fig. 3.6. The North Atlantic region at anomaly 23, showing the position of the proposed mantle plume at this time. The plume is approximately 2000 km in diameter. Solid black areas indicate areas of extrusive volcanic rocks, and hatching indicates the extent of volcanic activity. An equal area projection centerd on the plume, after White and McKenzie, 1989.

the North Pyrenéan Fault and the perhaps the South Armorican Shear Zone (SASZ).

Incipient rifting began during the early Triassic in response to a change in plate motion from NW-SE compression to NE-SW to E-W extension and inducing post orogenic collapse of the Variscan belt. This process was probably aided by delamination of the lithosphere (Coward, 1992) assisting softening of the crust as a precursor to extension and rifting. Collapse began in the latest Carboniferous, leading to the formation of basins throughout the Variscan Belt, and its partial dissemination (Parnell et al., 1992). These basins, controlled by Variscan and Caledonian structural lineaments, have NW-SE to N-S trends. Chadwick et al. (1992) described two major extensional episodes in the late-Permian and mid-Triassic. The North Sea (Coward, 1992), English Channel and Western Approaches basins (Coward et al., 1992) began to form around this time. The rifting in the North Sea was initiated by southward propagation of the Arctic Ocean (e.g. Doré, 1992) accompanied by the intrusion of late Carboniferous sills and dykes, prior to Permo-Triassic extension (Coward, 1992). Rifting continued during the later Triassic to early Cretaceous*. By the Earliest Jurassic in the South Atlantic and Late Jurassic in the North Atlantic, a number of these grabens had become significant tectonically active regions. The Hercynian megasuture between Gondwana and Laurasia, became a major line of weakness, forming the Tethys-Central Atlantic-Caribbean Wrench system, initiating the detachment of Gondwana away from Laurasia and opening the Central Atlantic and proto-Mediterranean basins (Ziegler, 1990) **(Fig. 3.7)**. Triassic evaporites and Jurassic marine sediments on the developing Armorican and Northern Spanish continental margins gave evidence of an early Mesozoic Atlantic Ocean (Montadert et al., 1971).

The formation of aulacogens and other failed rifts are a common feature of the Atlantic Ocean and the breakup of Pangaea (Burke, 1977) **(Fig. 3.8)**. Although the propagation of the Atalntic Ocean was essentially northward, there were attempts to alter its path, usually along pre-existing structural lineaments. The formation of the Bay of Biscay is a direct result of this process.

The separation of North America from Europe is characterised by the pattern of magnetic anomalies in the oceanic crust originally described by Pitman and Talwani (1972). Their work enabled the calculation of spreading rates. The most active phases of rifting were during the

---

*The term 'Cimmerian' *sensu lato* is often used defining rift unconformities of this age, and it should not be confused with the Cimmerian *sensu stricto* orogenic cycle in Turkey and the Middle East (c.f. Zeigler, 1990).

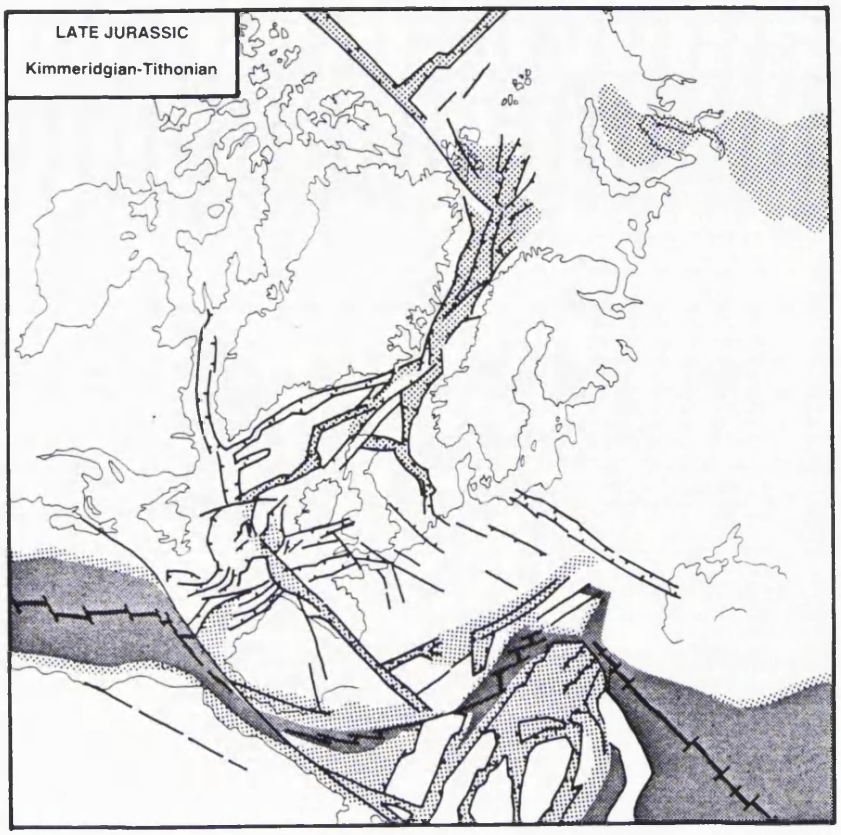

Fig. 3.7. The Late Jurassic tectonic framework of the North Atlantic region, illustrating the Tethys-Central Atlantic-Carribean Megashear, running E-W across the lower part of the map. Dark stipple indicates oceanic basins; light stipple indicates deep marine basins (after Ziegler, 1990).

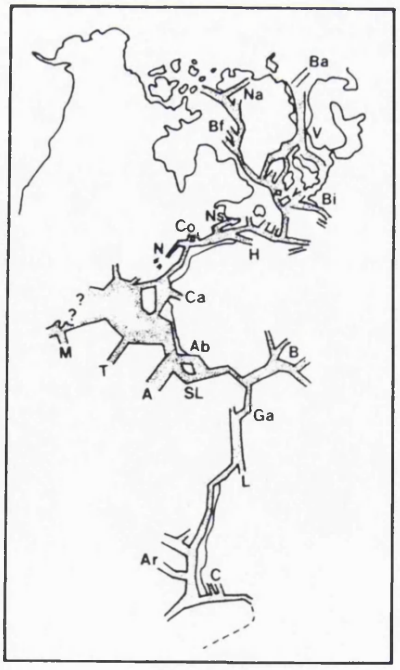

Fig. 3.8. Atlantic rifting and failed rifts. C: Cape; Ar: Argentina; L: Luanda; Ga: Gabon; B: Benue Trough; SL: Sao Luis; A: Amazon; Ab: Abidjan; T: Takatu; M: Maracaibo; Ca: Casamance; N: Newark; Co: Connecticut; Ns: Nova Scotia; H: Haha; Bi: Bay of Biscay; V: Viking Graben; Ba: Barentz; N: Nares; Bf: Baffin (after Burke, 1977).

Cretaceous when the continents diverged at rates of 4.0 cm y^{-1}. The present rate of divergence is approximately 2.0 cm y^{-1} (Pitman and Talwani, 1972; Foulger et al., 1992).

3.3. Plate kinematics

The fit of the plates and microplates (North America, Eurasia and Iberia) around the North Atlantic region prior to and during seafloor spreading, has been constrained with palaeomagnetic data. The fit made by Bullard et al. (1965) although one of the earliest attempts, still remains one of the most acceptable interpretations. More recent work on palaeomagnetism and continental fit, incorporating the importance of basin formation and evolution has been carried out by Srivastava and Verhoef (1992).

The original uncertainty with the Bullard et al. (1965) fit is that there is a considerable amount of continental overlap at all stages prior to seafloor spreading. Verhoef and Srivastava (1989) and Srivastava and Verhoef (1992) have shown that at chron M25 (156 Ma, Kimmeridgian, the start of earliest breakup of Iberia from North America) there was substantial overlap centred around Flemish Cap and Galicia Bank **(Fig. 3.9)**. This overlap had decreased by the time of separation in this region (chron M0, 118 Ma, Aptian) **(Fig. 3.10)**. An explanation for this phenomena involves the hypothesis that separation between plates is not geologically instantaneous as assumed in most models. This theory is discussed by Srivastava and Verhoef (1992) who propose that the plates were stretched prior to their separation at the onset of seafloor spreading. Therefore there is a diachroneity between rifting at various points in the North Atlantic. For example, at chron M0 there is no overlap in the Galicia Bank-Flemish Cap region, and seafloor spreading had already been initiated in this region. However further north in the Bay of Biscay and to the west of the Porcupine Bank there is still considerable overlap. It is assumed that at this time these regions were being stretched prior to breakup. The amount of overlap describes the amount by which the plates were extended. 'Destretching' of these plates to their original geometry was modelled by Srivastava and Verhoef (1992) using the simplest assumption that the plates were destretched uniformly in directions obtained from the rotation poles of the plates. Deformations of continental fragments (i. e. Flemish Cap and Galicia Bank) were also omitted. However, the hypothesis proposes that the rift basins were extended between the Kimmeridgian and the Aptian, and that there was extension and dislocation between Flemish Cap and Galicia Banks and their associated continental plates. Evidence for this are arcuate

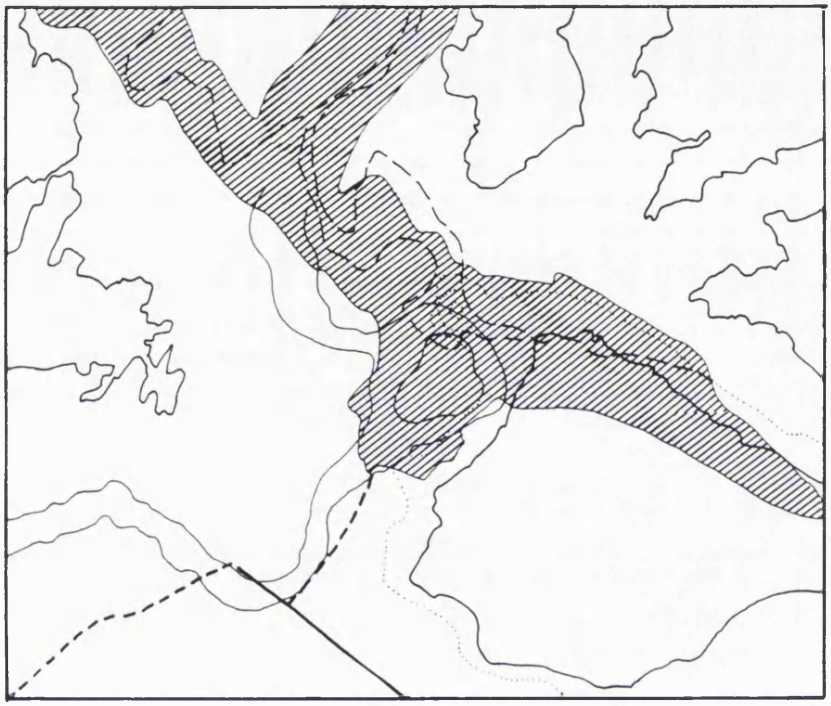

Fig. 3.9. Continental fit overlap at M25 (Srivastava and Verhoef, 1992).

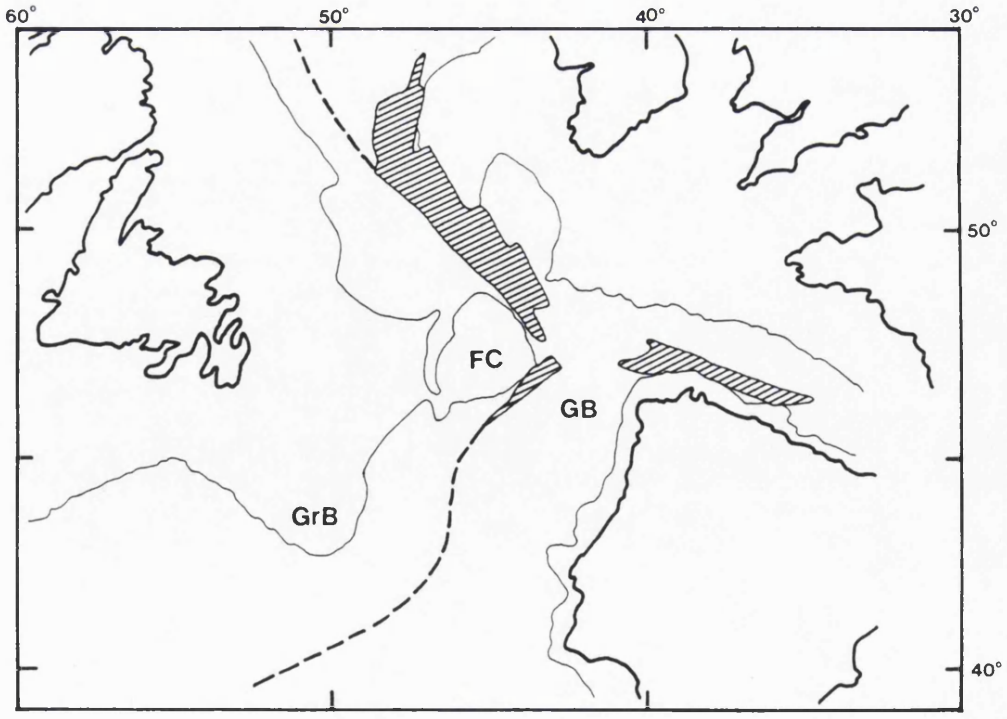

Fig. 3.10. Continental fit overlap at M0 (Verhoef and Srivastava, 1989).

magnetic anomalies in the eastern Grand Banks region at M0 which are subparallel to the Ibero-Armorican Arc. These do not exist in Srivastava and Verhoef's (1992) reconstruction at the initiation of basin formation in the Triassic. This suggest that they are a feature caused by a later rotation and movement of Flemish Cap **(Figs. 3.11 and 3.12)**.

Argand (1924) was the first to suggest that northern Spain and Brittany were once connected and were then separated by the opening of the Bay of Biscay. The region was subsequently somewhat neglected until Carey (1958) proposed that the Bay opened by the anticlockwise rotation of the Iberian peninsula by some 40°, involving a scissor-like movement causing sea-floor spreading in the Bay, and compression in the Pyrenées **(Fig. 3.13)**. However, subsequent geophysical and geological research (reviewed by Ries, 1978 and Garwin, 1985) implies that the Bay of Biscay opened by an anti-clockwise rotation of the Iberian plate away from the stable Eurasian plate, followed by a translational movement culminating in the formation of the Pyrenées. The Iberian plate itself moved independently to a certain extent, but was also driven by the African plate for much of the time (Srivastava et al., 1990b). The rifting was initiated by the opening of the North Atlantic Ocean, in which sea-floor spreading took place in a series of steps, moving progressively northwards (Malod and Mauffret, 1990). The onset of oceanic spreading between North America and Eurasia is generally assumed to be contemporaneous with the end of rifting and extension on the continental margins, occurring from Late Jurassic to the Early Cretaceous (Masson and Miles, 1984). Two triple junctions on the North Atlantic Rift allowed the movement of the Iberian plate as a separate entity. Two models exist as to the positioning of these junctions. It is accepted that the most northerly, the Biscay Triple Junction, a ridge-ridge-ridge arrangement between the Galicia Rift, Biscay Rift and the Celtic Rift, changed to three spreading centres after continental breakup occurred **(Fig. 3.14)**. Malod and Mauffret (1990) believe that the Tethys Triple Junction lies to the south, a ridge-ridge-ridge or ridge-ridge-transform system active from the late Jurassic to early Cretaceous. The differential rotation of Iberia against Africa caused the formation of pull-apart basins along the Tethyan rift through strike-slip movement. This ridge became inactive after 118 Ma, after which time the Iberian Plate can no longer be considered as separate from the African Plate. Sibuet and Collette (1991) believe that a ridge-ridge-fault triple junction existed north of the proposed Tethys Triple Junction of Malod and Mauffret (1990). This 'dead' triple junction lay just to the south of the Biscay Triple Junction, with a NW-SE trending fault moving into the Tethyan transtensional zone

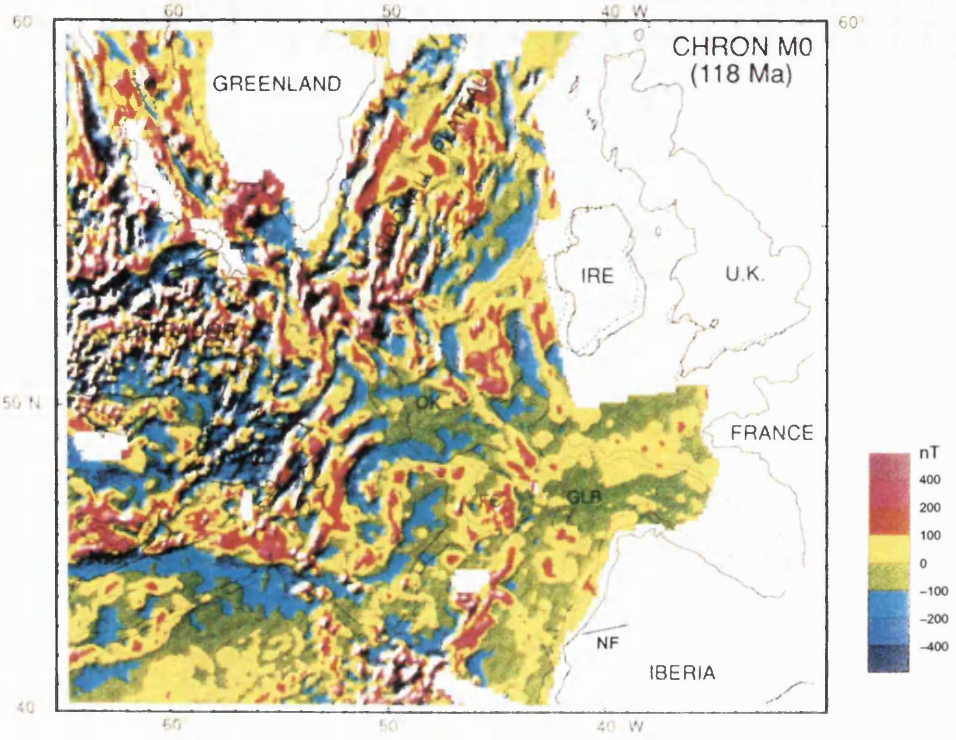

Fig. 3.11. Shaded relief map of reduced to the pole magnetic anomalies showing positions of the destretched plates at chron M0. OK, Orphan Knoll; FC, Flemish Cap; GLB, Galicia Bank; NF, Nazare Fault (Srivastava and Verhoef, 1992). Note the anomalies west of Flemish Cap are curved roughly concentric to the Iberian Coast.

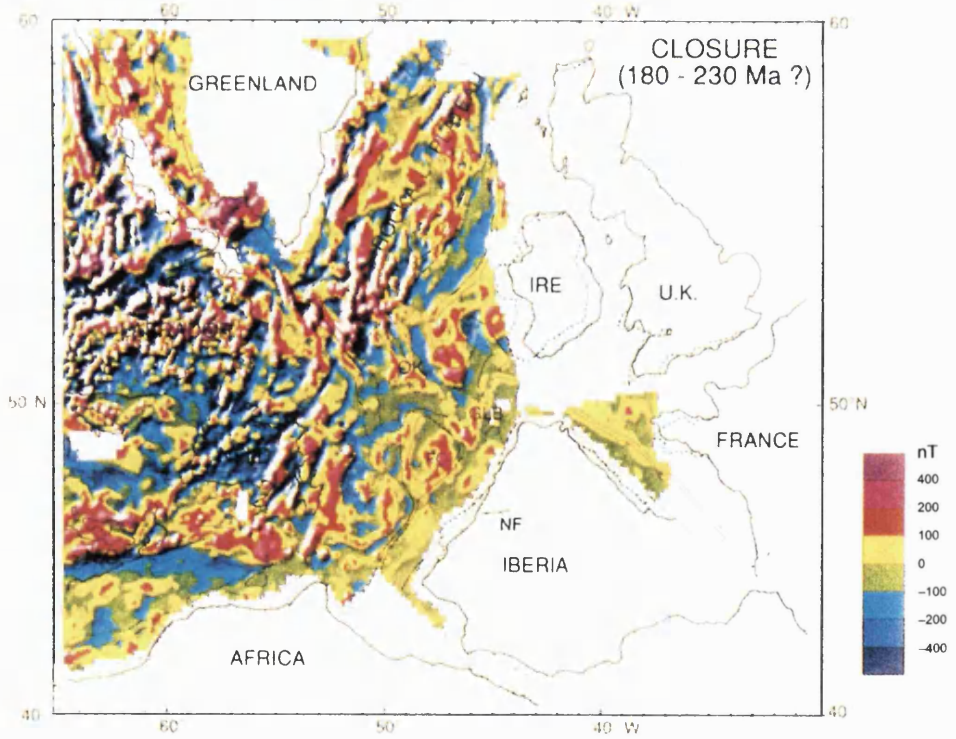

Fig. 3.12. Shaded relief map of reduced to the pole magnetic anomalies showing positions of the destretched plates at closure. OK, Orphan Knoll; FC, Flemish Cap; GLB, Galicia Bank; NF, Nazare Fault (Srivastava and Verhoef, 1992). Note that the the anomalies west of Flemish Cap have lost their curvature.

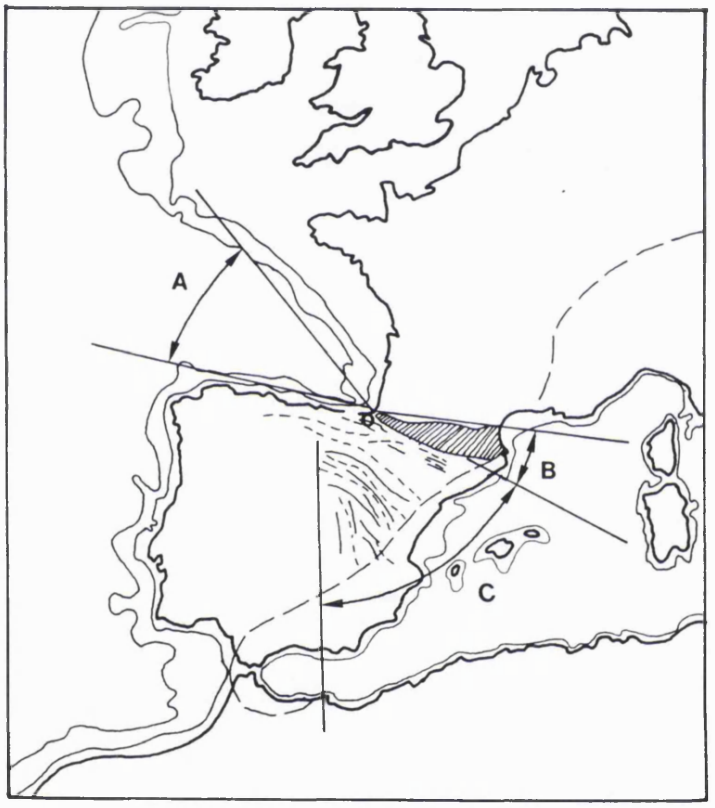

Fig. 3.13. Carey's (1958) 'sphenochasm' hypothesis. Pivoting of Iberia about O opens the Bay of Biscay and causes simultaneous compression in the Pyrenées. It was later that these two events were found to be chronologically separate.

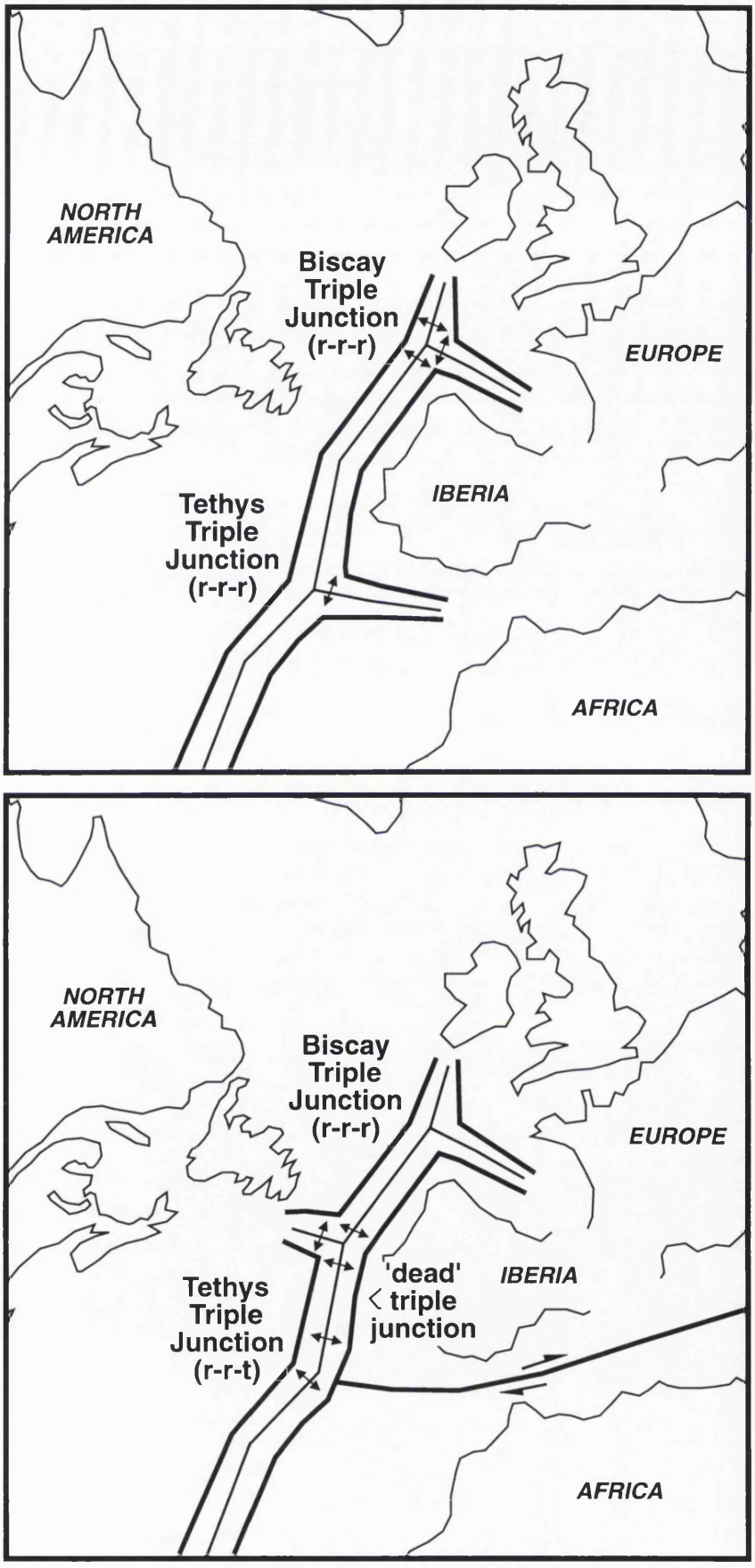

Fig. 3.14. Spreading centres between Europe, North America, Iberia and Africa during the Early-Middle Cretaceous. a). a Biscay r-r-r triple junction, and a Tethys r-r-r triple junction (Malod and Mauffret, 1990) and b). a third 'dead' triple junction north of a r-r-f Tethys triple junction (Sibuet and Collette, 1991).

between Africa and Eurasia. This fault follows a prominent morphological boundary.

Palaeomagnetic studies in the Iberian Meseta and in the eastern Pyrenées (van der Voo, 1967; van Dongen, 1967) concluded that there was a post-Permian rotation of Spain of approximately 30°. Further palaeomagnetic studies in Iberia (Van der Voo, 1969), proposed that rotation of the Iberian Peninsula probably occurred between the late Triassic and the late Cretaceous, and that the total angular rotation between Iberia and Eurasia from the Permian to the Aptian is approximately 35°.

Magnetic anomalies from the oceanic crust of the Bay of Biscay **(Fig. 3.15)** have given some of the most conclusive information describing the timing and relative motion of the Iberian plate as it separated from the Armorican Massif and stable Europe. Williams (1975) recognised a disruption in the sequence of magnetic anomalies in the North Atlantic. Here, Pitman and Talwani (1972) had recognised a complete sequence of anomalies dating from the present back to 80 Ma (anomaly 32). There is a discontinuity in anomalies 31-32, which exhibit a eastward verging kink in the otherwise regular pattern of anomalies. This is accompanied by an apparent E-W striking lineation converging with the apex of this kink. Williams (1975) interpreted this as a ridge-ridge-ridge 'Biscay Triple Junction' located at 45°N, 13.75°W, and proposed seafloor spreading had been initiated before 80 Ma, when the Mid Atlantic Ridge began to move northwards, and that the Biscay Ridge had ceased spreading by 73 Ma. The long Cretaceous normal magnetisation (the "Mesozoic quiet zone", Aptian-Santonian) forced difficulties in timing the onset of seafloor spreading. However, the magnetic anomaly data coupled with knowledge of the sedimentary cover constrained rifting between 113 and 73 Ma. Pitman and Talwani's (1972) anomalies 27-31 were re-identified as anomalies 30-34 by Cande and Kristofferson (1977) although the relative ages remain the same. Sullivan (1983) using these revised figures showed that rifting of North America and Iberia was in action from at least 115 Ma, before the spreading centre migrated north of the Biscay Triple Junction.

Tectonic activity associated with the Pyrenean collision was apparent in the Bay of Biscay. Eocene compression reactivated Cretaceous E-W trending rift-related faults on the Armorican Margin (Montadert et al., 1979) and in the region of the Porcupine Seabight (Masson and Parson, 1983). Sediment sampling in the Biscay Abyssal Plain as the result of dredging and ocean drilling projects concluded that the oldest sediments were Palaeocene in the region of the Cantabrian Seamount (Ewing et al., 1971). On these grounds, some early Eocene rotation was proposed. This

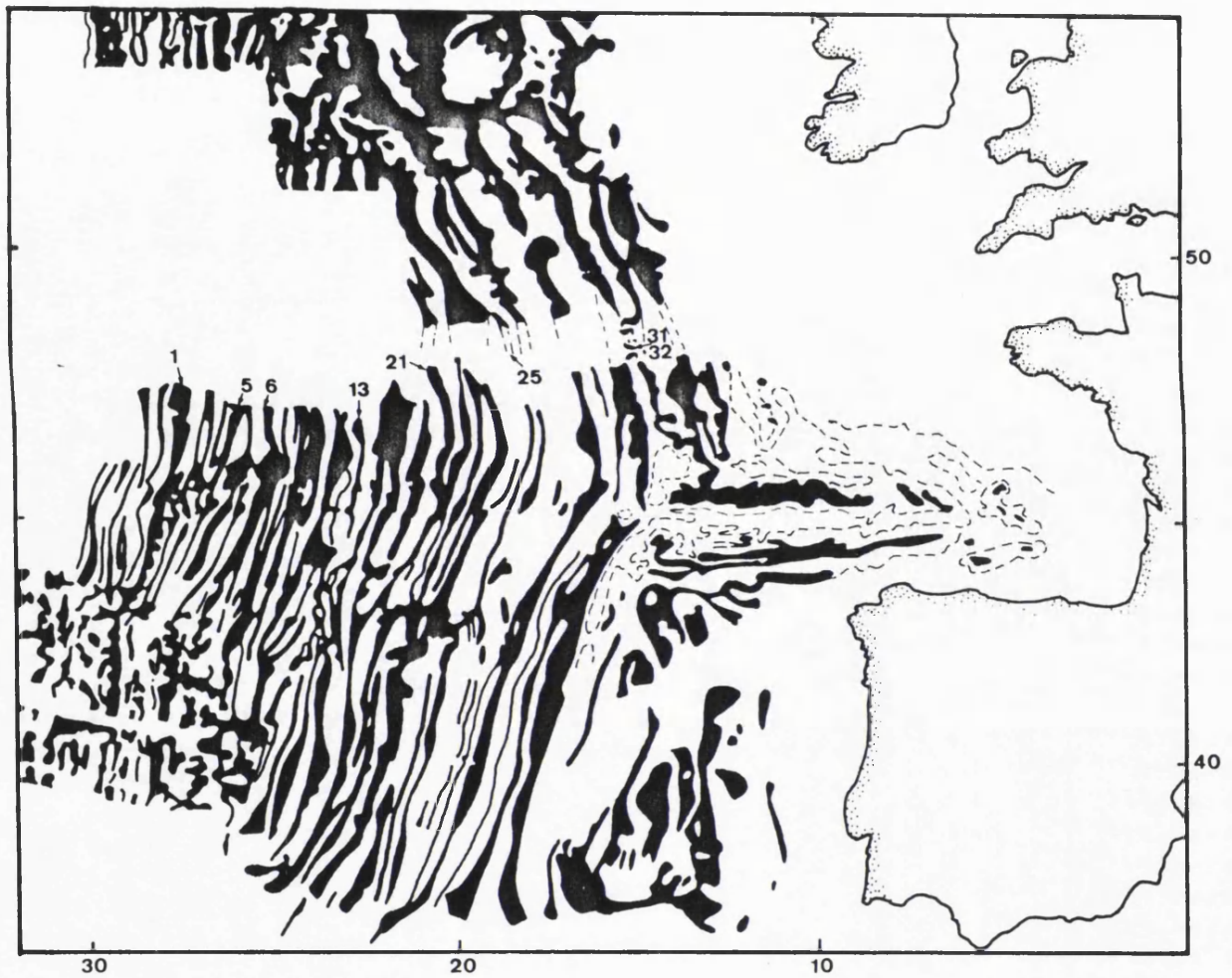

Fig. 3.15. Magnetic anomaly pattern in the Bay of Biscay and adjacent Atlantic Ocean (after Williams, 1975 and Cande and Kristofferson, 1977).

theory is supported by that of Laughton and Berggren (1971) whose drilling recovered no sediments older than the Palaeocene.

3.4. Evolution of the margins of the Bay of Biscay.

The Bay of Biscay forms the easternmost region of the North Atlantic Ocean. It is situated between the Charlie Gibbs and Azores Fracture Zones, at 40-50° N and 0-10° W, incised into south-western continental Europe **(Fig. 3.16)**. The Biscay Abyssal Plain (maximum depth 5251 m) is bounded to the north and east by the ~150 km wide Celtic, Armorican and Aquitaine Shelves **(Fig. 3.17)**. The North Spanish Shelf is less than 50 km wide in many places. The Biscay Seamount, Cantabria and Gascony Knolls form prominent elevated regions on the Abyssal Plain. The south-westernmost part of the Bay of Biscay terminates against the Galicia Bank, a platform extending approximately 200 km into the North Atlantic forming the conjugate margin to Flemish Cap on the Newfoundland Shelf.

The basins on the Atlantic margins, namely those along the North American and Western European seaboards, have many stratigraphic elements in common, including, importantly, unconformities in the Mid Oxfordian, pre-Valanginian (usually in the Kimmeridgian) and in the Aptian, this latter being the most prominent. These three major hiatuses in deposition represent respectively, thermal upwarping during rifting (Hiscott et al., 1989), renewed stage of extension and the post rift, breakup unconformity at the commencement of seafloor spreading (Hiscott, et al., 1989; Montadert et al., 1979; Boillot et al., 1989) which was synchronous in much of the region **(Fig. 3.18)**. Although similarities exist, these basins do not have identical geological histories. Most have Triassic evaporite deposits and consequently the overlying stratigraphy may be deformed by halokineses; also periods and rates of extension are likely to have varied. The following sections describe the geological evolution of the margins of the Bay of Biscay and the stratigraphy of their associated basins; the Armorican Margin-Western Approaches Basin, North Spanish Margin-Asturian Basins and the Galicia Basin (North Lusitanian Basin).

3.4.1. Armorican Margin.

The Armorican Margin trends NW-SE, running parallel to the coast of the Armorican peninsula. It is dissected by many submarine canyons, most of which cut the slope obliquely, trending WSW or SSE **(see Fig. 3.17)**. The disparate trends of these canyons when compared to the NW-SE trending continental margin are explained by being controlled by pre-rift structural lineaments. Across the ~150 km wide margin there is a gradual

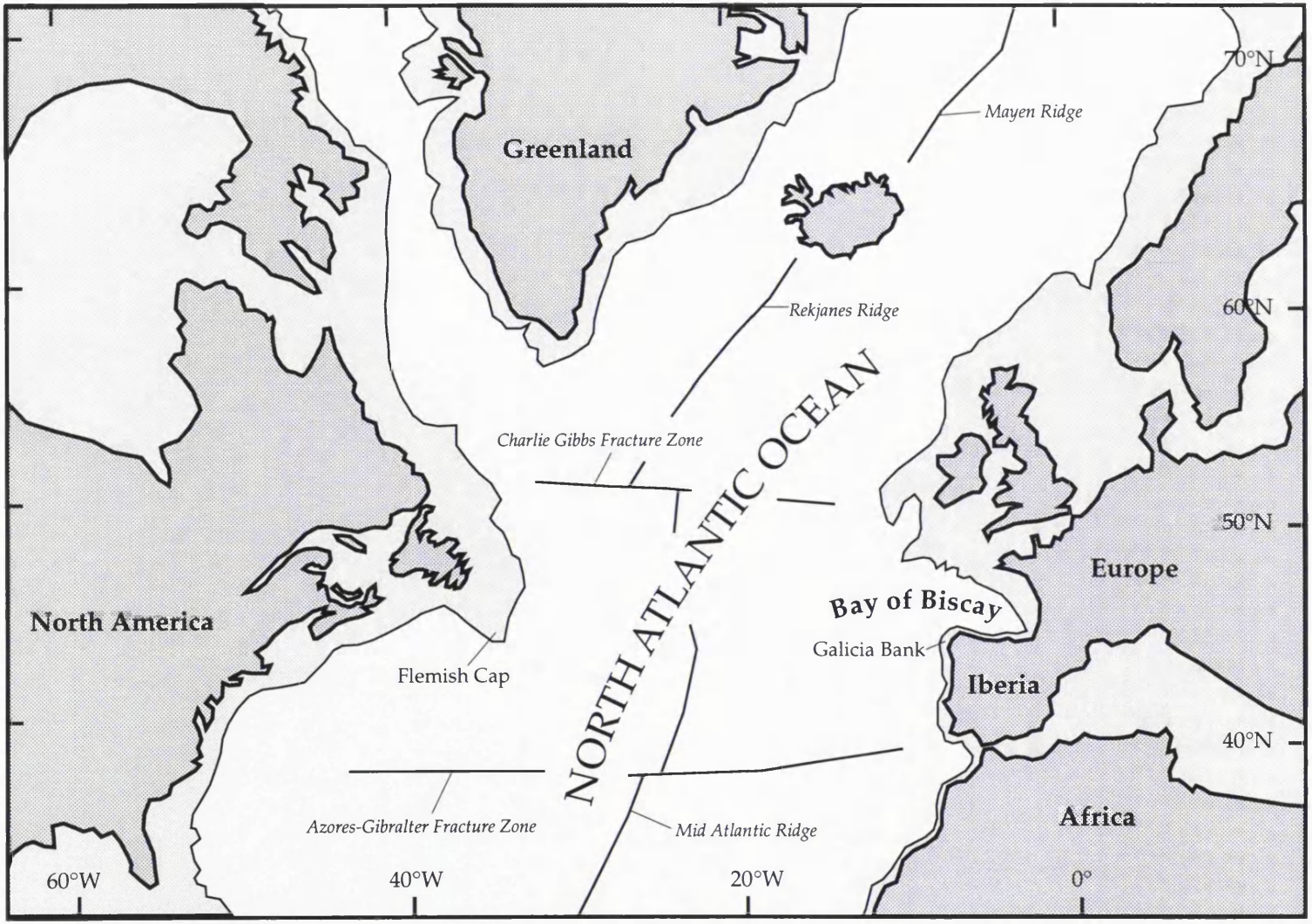

Fig. 3.16. The locality of the Bay of Biscay in the North Atlantic Ocean. Major present-day marine features are shown. Key: land - dark grey; continental shelf - light grey; ocean - white.

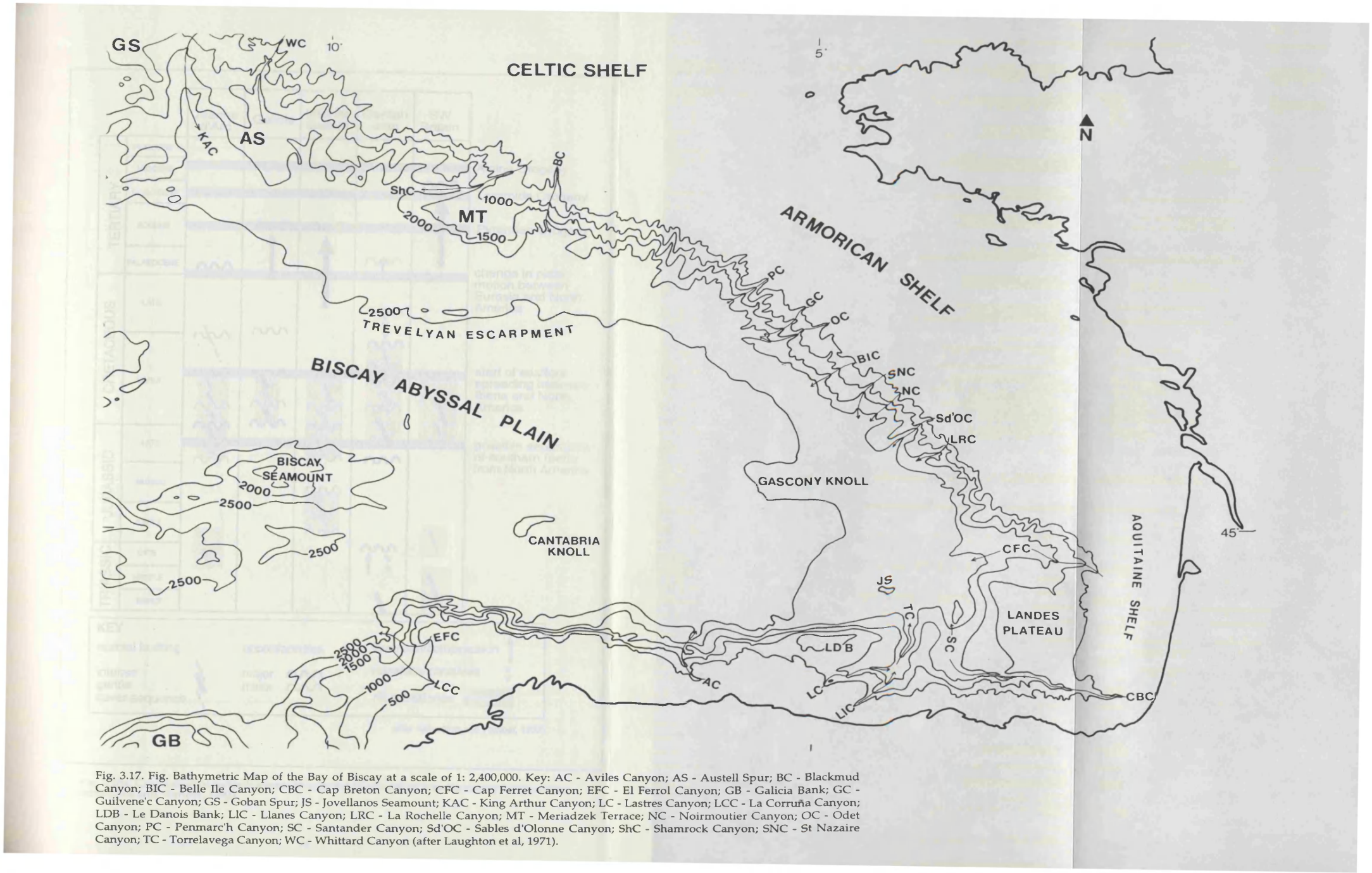

Fig. 3.17. Fig. Bathymetric Map of the Bay of Biscay at a scale of 1: 2,400,000. Key: AC - Aviles Canyon; AS - Austell Spur; BC - Blackmud Canyon; BIC - Belle Ile Canyon; CBC - Cap Breton Canyon; CFC - Cap Ferret Canyon; EFC - El Ferrol Canyon; GB - Galicia Bank; GC - Guilvene'c Canyon; GS - Goban Spur; JS - Jovellanos Seamount; KAC - King Arthur Canyon; LC - Lastres Canyon; LCC - La Corruña Canyon; LDB - Le Danois Bank; LlC - Llanes Canyon; LRC - La Rochelle Canyon; MT - Meriadzek Terrace; NC - Noirmoutier Canyon; OC - Odet Canyon; PC - Penmarc'h Canyon; SC - Santander Canyon; Sd'OC - Sables d'Olonne Canyon; ShC - Shamrock Canyon; SNC - St Nazaire Canyon; TC - Torrelavega Canyon; WC - Whittard Canyon (after Laughton et al, 1971).

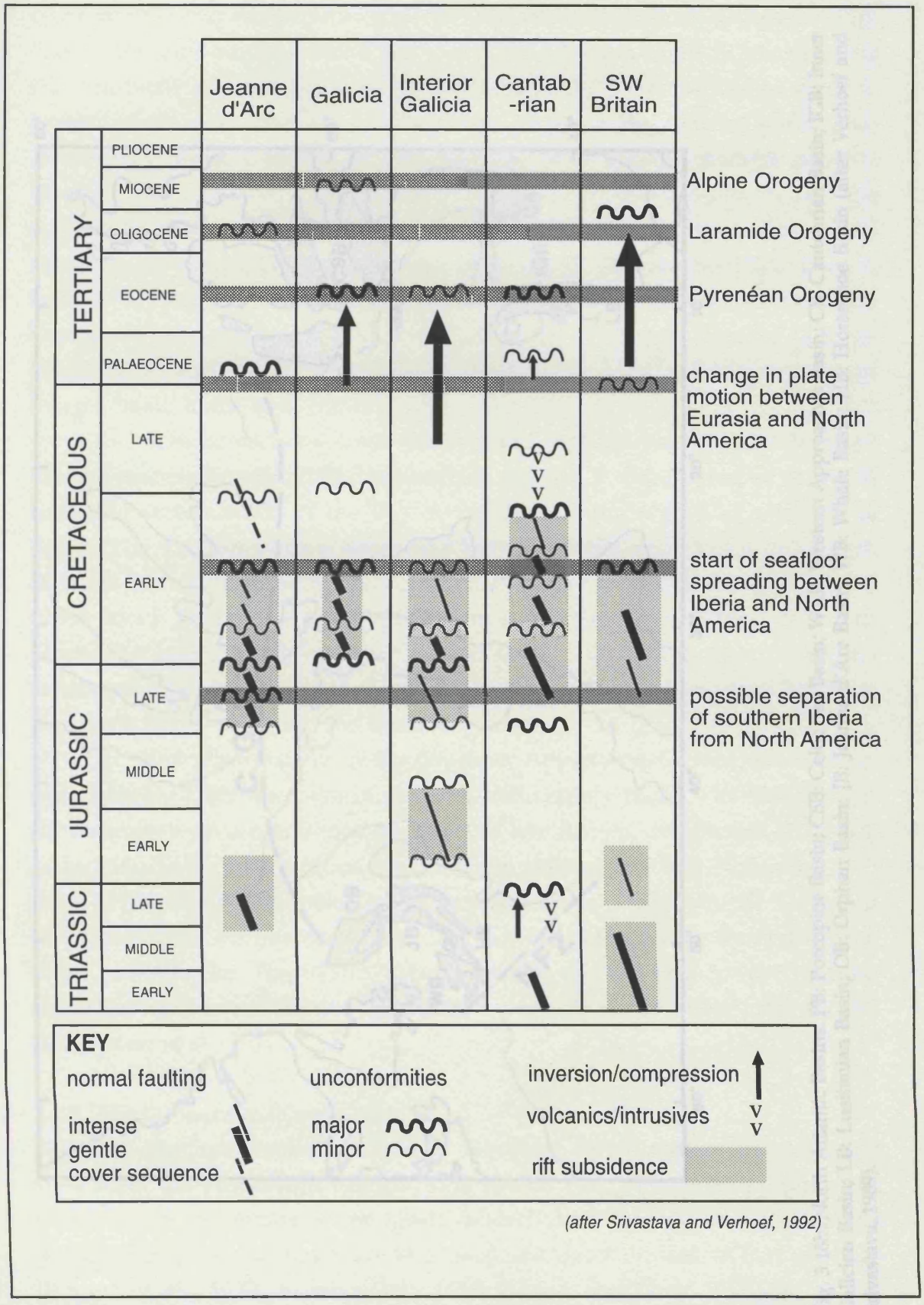

Fig. 3.18a. Correlation of tectonic events in selected North Atlantic sedimentary basins (after Srivastava and Verhoef, 1992).

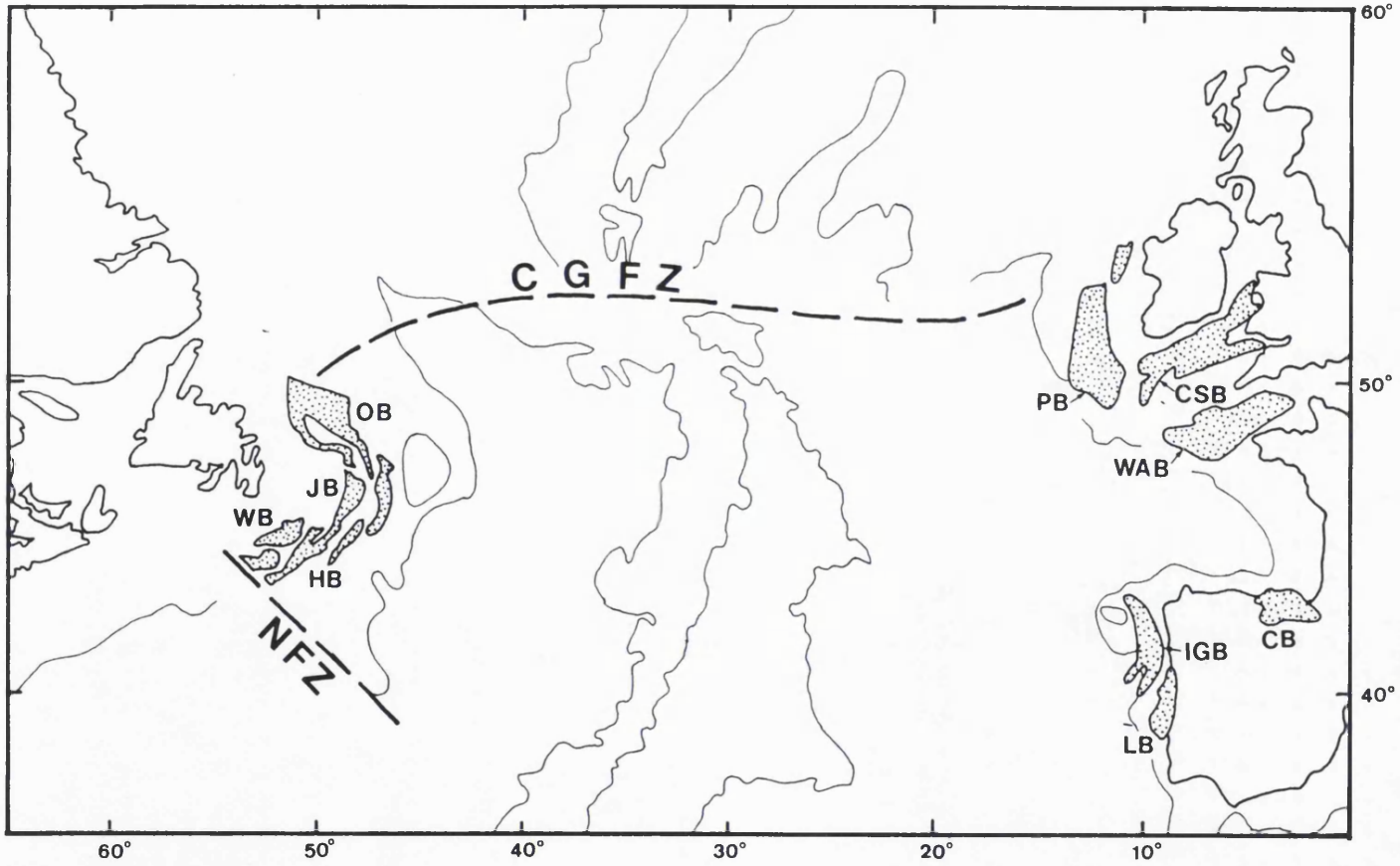

Fig. 3.18b. North Atlantic Basins. PB: Porcupine Basin; CSB: Celtic Sea Basin; WAB: Western Approaches Basin; CB: Cantabrian Basin; IGB: Inner Galician Basin; LB: Lusitanian Basin; OB: Orphan Basin; JB: Jeanne d'Arc Basin; WB: Whale Basin; HB: Horseshoe Basin (after Verhoef and Srivastava, 1989).

thinning of crust from 30 km thick continental crust to 6 km thick oceanic crust (Bott, 1992) encompassing a characteristic tilted block sequence **(Fig. 3.19)**. The fault blocks increase in height from 3-4 km to 10-12 km towards the continent and are tilted to an angle of 25-30°. The faults dip with a present angle of 15° and are mostly planar, except at their lowest parts. The Armorican Margin shows all the features of a typical starved passive margin. The most recent major seismic section to be obtained across the Armorican margin is described by Barbier et al. (1986), studying the crustal structure between 2°W and 11°W and between 43°30'N and 48°15'N. This survey stops just short of the ocean-continent limit as defined by Derégnaucourt and Boillot (1982), including the Meriadzek Terrace (a large tilted block) and the Trevelyan Escarpment to the west and the Armorican margin basin to the east.

Seismic sections from the Western Approaches margin detected the deepest continuous reflecting horizon named 'S' (Montadert et al. 1979) traceable across much of the Bay and the adjoining region of the Galicia Banks. The S reflector has a depth of 8 km on oceanic crust, but is at a depth of 13-14 km at the base of the continental slope. 'S' lies at the base of the tilted block layer, the faults of which either stop at, or just above it. Montadert et al. (1979) and de Charpel et al. (1978) have interpreted the reflector 'S' as a mid-crustal discontinuity, marking the boundary between the brittle upper crust and the ductile lower crust.

The stratigraphy of the Western Approaches-Armorican margin is as follows: there are 2 km of post-rift sedimentary rocks. The oldest post-rift sediments are a ubiquitous sequence of late Aptian, deep water (2000 m), calcareous and carbonaceous black shales (Montadert and Roberts, 1976; Bott, 1992). The black shales unconformably overly thin syn-rift Lower to Mid Cretaceous sedimentary rocks infilling the half grabens formed by the tilted fault blocks. The blocks themselves are pre-rift mid to late Jurassic sedimentary rocks. Triassic evaporites possibly exist below the blocks (Montadert et al., 1971).

3.4.2. North Spanish Margin.

The continental margin of Northern Spain differs in structural style from the Armorican Margin. It is narrow, only some 30-40 km wide, with a steep continental slope (10-12 % declivity). Seismic and gravimetric profiles have shown that there is a deep sediment infilled trench offshore (Boillot et al., 1979; Bacon et al., 1969; Bacon and Gray 1970), in which Triassic to lower Jurassic sediments are apparently absent, although there are evaporites located towards the inner part of the margin. A major feature

of the margin is Le Danois Bank. This is a shallow (500 m water depth) platform, to the north of the Picos de Europa, composed of Late Jurassic to Cretaceous sedimentary rocks overlying Variscan basement. The innermost regions of the margin are possibly underlain by Triassic and pre-Mesozoic sedimentary rocks (Boillot et al., 1979). The appearance of Triassic salt diapirs implies that this region is part of the pre break-up area of which the Aquitaine basin was also once part.

Evidence for tilted block sequences are less obvious, although Le Danois Bank represents the upper regions of such a block and the inner trough between it and the coast a half graben. The stratigraphy of the area is similar to that of the Armorican margin. However, the North Spanish Margin appears to have been tectonically active since the end of the main phase of seafloor spreading in the late Cretaceous. Boillot et al. (1979) have proposed that there was a short lived late Cretaceous-Eocene subduction event related to the Pyrenéan convergence and collision, thus transforming the passive margin into a temporarily active one, until the Oligocene when it returned to being passive **(Fig. 3.20)**. The evidence for this event is not particularly convincing. Boillot et al. (1979) describe centimetre scale deformation observable in late Jurassic to early Cretaceous limestones, and seismic sections of the region are inconclusive. Cloetingh et al. (1982) have suggested that subduction may be initiated in the lithosphere adjacent to a passive margin as a response to extreme downwarping because of sediment loading. An estimated sediment thickness of between 10 - 16 km may be sufficient to achieve subduction. The north Spanish margin has a thick sediment wedge, possibly of this order of magnitude. However, it is simpler to propose the theory of Bacon and Grey (1970) that the North Spanish marginal trench is a fault scarp, possibly a correlative of the North Pyrenean fault and its associated trough in southern parts of the Aquitaine Basin.

The North Spanish Basins exist as an onshore extension of the North Spanish continental margin. Stretching from Oviedo to Santander, the basins take in the reactivated Variscan Asturian Basin (reactivation of Ventaniella and Bilbao faults) and the Mesozoic Basque-Cantabrian Basin. The sedimentary succession here is from Gzelian to Neogene. The youngest Basque-Cantabrian Basin formed synchronously with the precursors to rifting in the Bay of Biscay during the Permian, reactivating Variscan lineaments, and underwent a major extensional phase during the Kimmeridgian (Lepvrier and Martínez-García, 1990). At this time extension was NE-SW oriented, producing a series of tilted blocks. During the Eocene, the Asturian Basin underwent compression and then further extension associated with the convergence and eventual collision of Iberia with

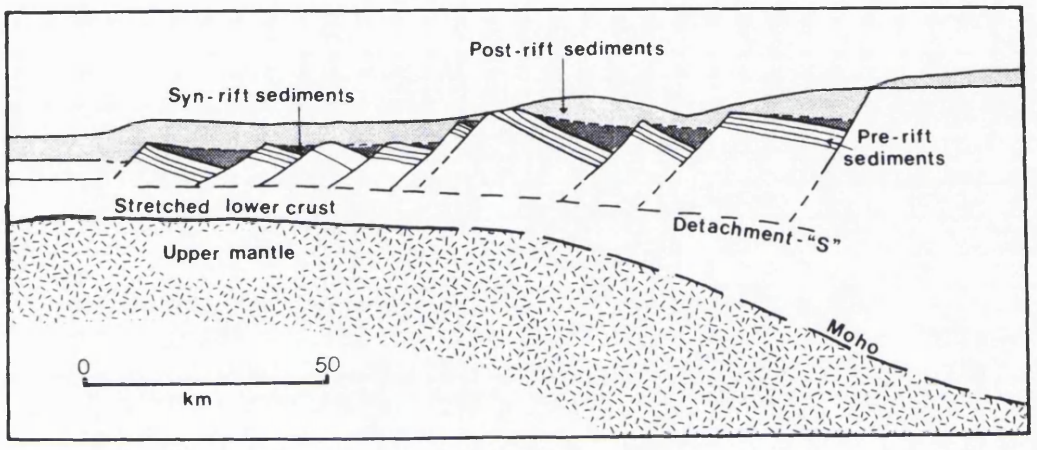

Fig. 3.19. Simplified section across the Armorican (Northern) Margin of the Bay of Biscay (after Bott, 1992).

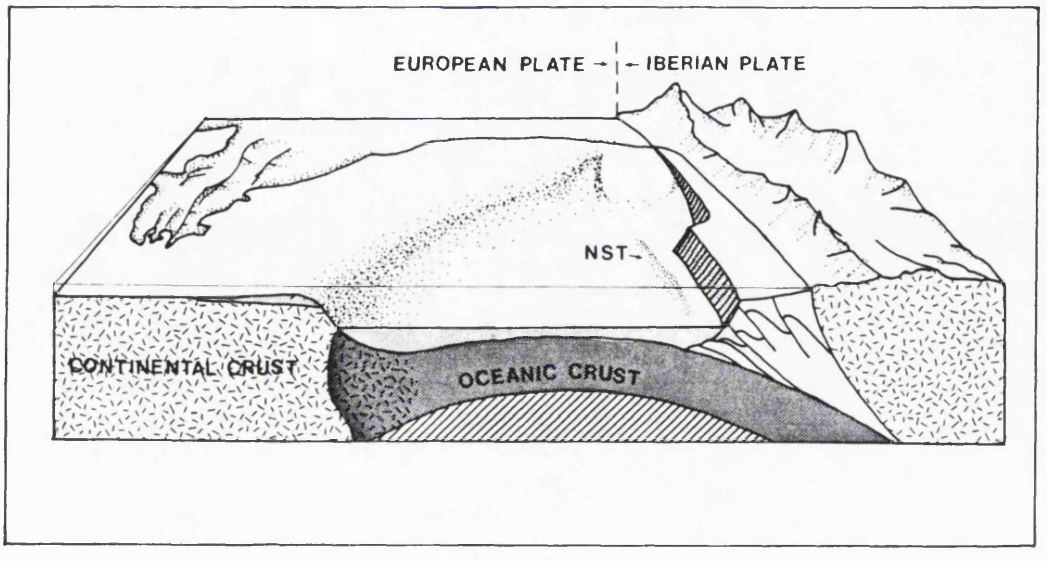

Fig. 3.20. Schematic cross section across the Bay of Biscay showing Boillot's hypothesis of subduction of the European plate under the Iberian Plate. The position of the North Spanish Trough (NST) is marked (after Boillot, 1984).

France. This initiated a reactivation of the fault system, and caused minor inversion.

3.4.3. The Galicia Banks.

The West Galicia Margin is a North Atlantic passive margin trending N-S, and paralleled by rows of domino faulted tilted blocks which are traversed by E-W faults **(Fig. 3.21 and 3.22).** The major phase of rifting at this margin was in the Valanginian to latest Aptian (Boillot et al., 1989). Like the Biscay margins, the West Galicia Margin formed during Permo-Triassic incipient fracturing of Pangaea.

The Galicia margin is starved, with a maximum 4 km of sedimentary cover, and consists of a sequence of east-dipping tilted fault blocks **(Fig. 3.23)**. The Galician coastline is bounded by a 30 km wide platform, which is flanked to the seaward by an offshore basin. This basin has a landward continuation to the south in the form of the Lusitanian Basin of central and southern Portugal (Wilson et al., 1989). The basin is bounded to the west by a ring of plateaus: the Galicia Banks, Vasco de Gama, Vigo and Porto Seamounts. Continental basement samples have been obtained from these mounts, which formed as blocks along reactivated Variscan structures. The seamounts are rimmed to the west by an unusual feature, the Peridotite Ridge, and the Iberian Abyssal Plain. The Peridotite Ridge is a sublinear feature which probably exists for around 130 km, although it only outcrops for around 70 km in the region between 41.5° N and 12.8° W and 43.5° N and 12.8° W to the western side of Galicia Banks. The ridge is composed of serpentinized peridotite probably emplaced diapirically just prior to the onset of seafloor spreading as a response to the highly attenuated crust (Sibuet, 1992).

The reflector 'S' is prominent in the Galicia Basin, at depths of around 2-3 km (de Charpal et al., 1978). It deepens towards the east, but is undetectable beneath the Peridotite Ridge. It possibly represents the contact between the basement and the peridotite. The dominant mechanism for crustal extension is probably detachment faulting (Sibuet, 1992) which led to the unroofing of the Upper Mantle, allowing the uprising of the peridotite (Boillot et al., 1989). The 'S' reflector may well be the trace of this fault. Tilted blocks formed along the décollement surface created by the underlying serpentinites. The stratigraphy of the region, similar to that on other margins of the Bay of Biscay, is illustrated in **Figure 3.24.** The post rift unconformity is of late Aptian Age (114 Ma), and is marked as on the Armorican Margin by the black shales designating the transition to deeper waters (Boillot et al., 1989).

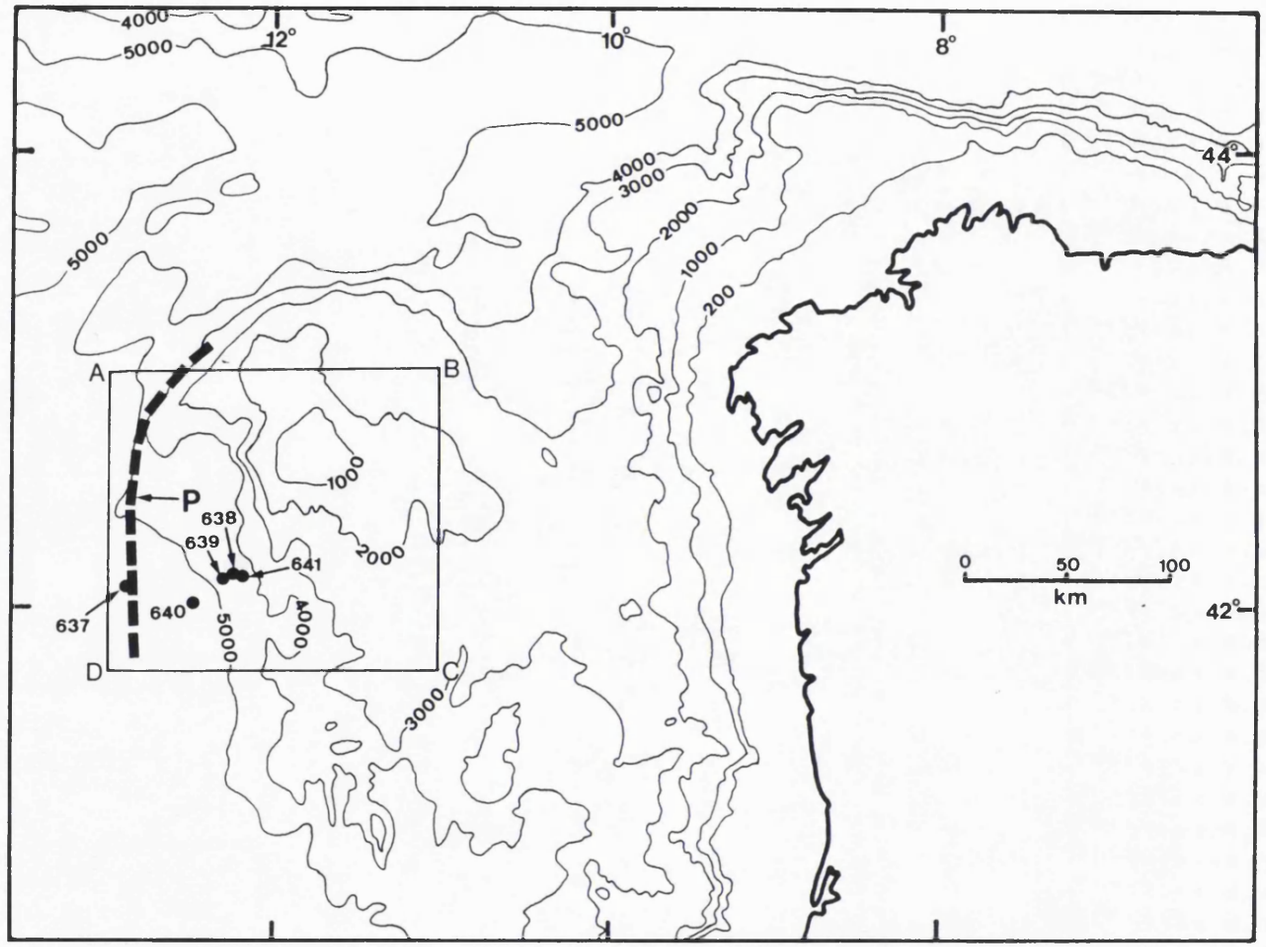

Fig. 3.21. Bathymetric map of the Galicia Banks region, showing the outcrop of the Peridotite Ridge (P), the area drawn in Fig. 3.22 (ABCD) and the ODP drill holes used in Fig. 3.24 (adapted from Boillot et al., 1989).

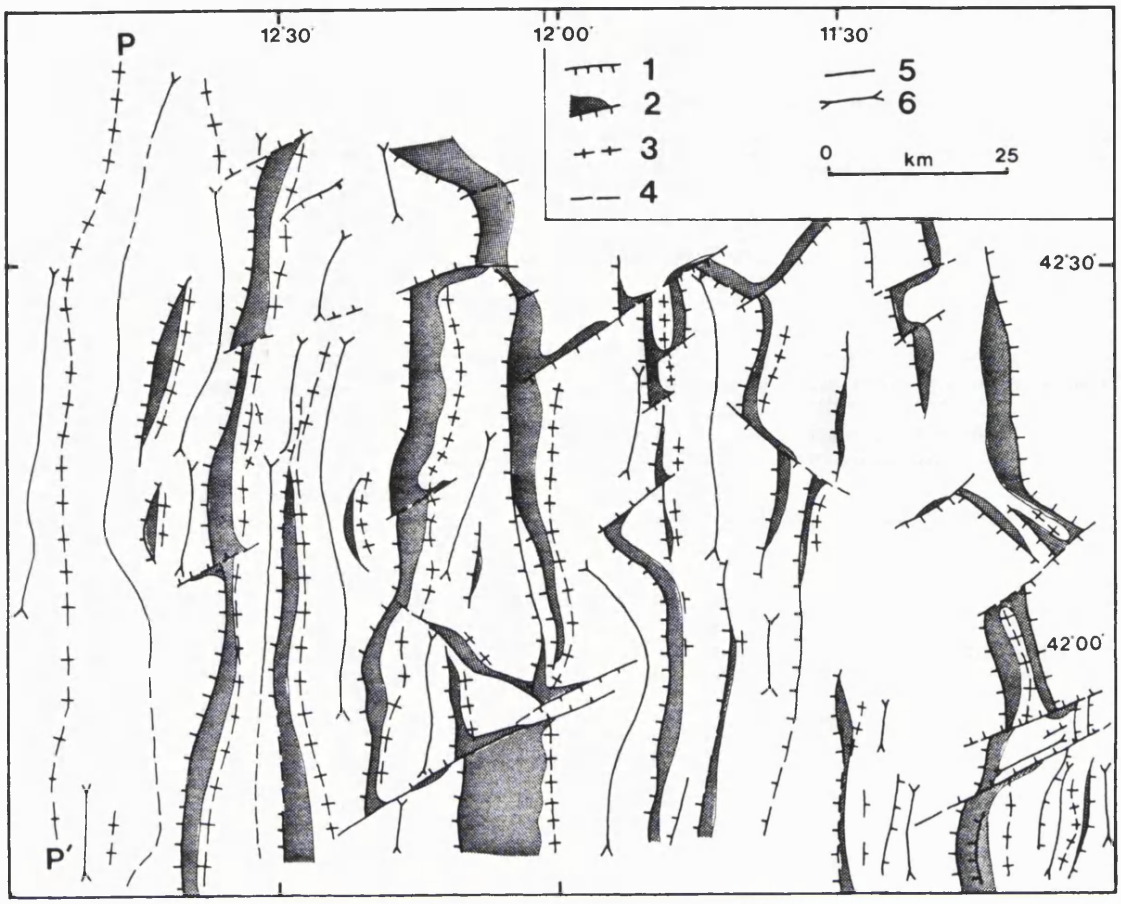

Fig. 3.22. Structural map of the deep Galicia Margin. Located on Fig. 3.21 as the area ABCD. Key; 1: normal fault; 2: fault escarpment (above syn-rift sediment); 3: tops of tilted blocks, ridges or horsts; 4: presumed fault; 5: transverse fault; 6: basin axis; PP': Peridotite Ridge (after Thommeret et al., 1988).

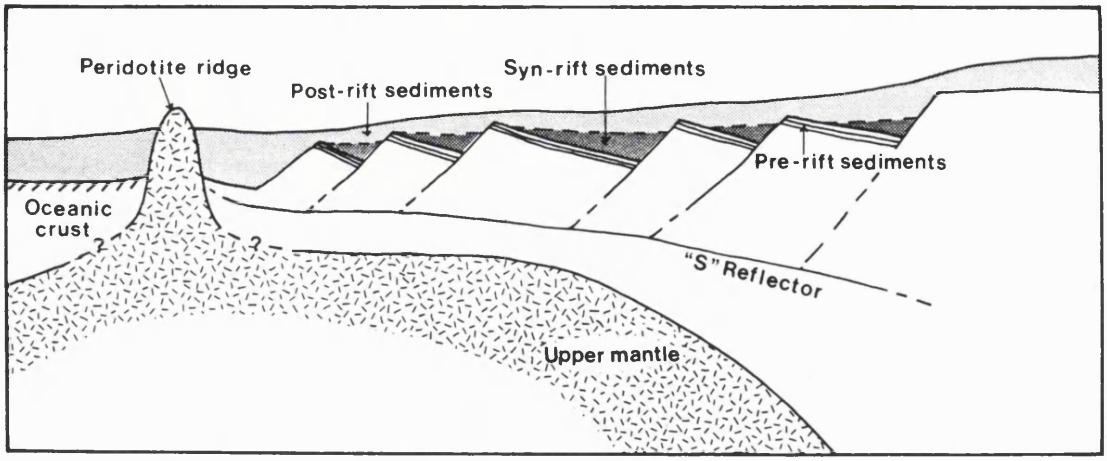

Fig. 3.23. Schematic cross-section across the Galicia Margin, showing the Peridotite Ridge (adapted from Sibuet, 1992).

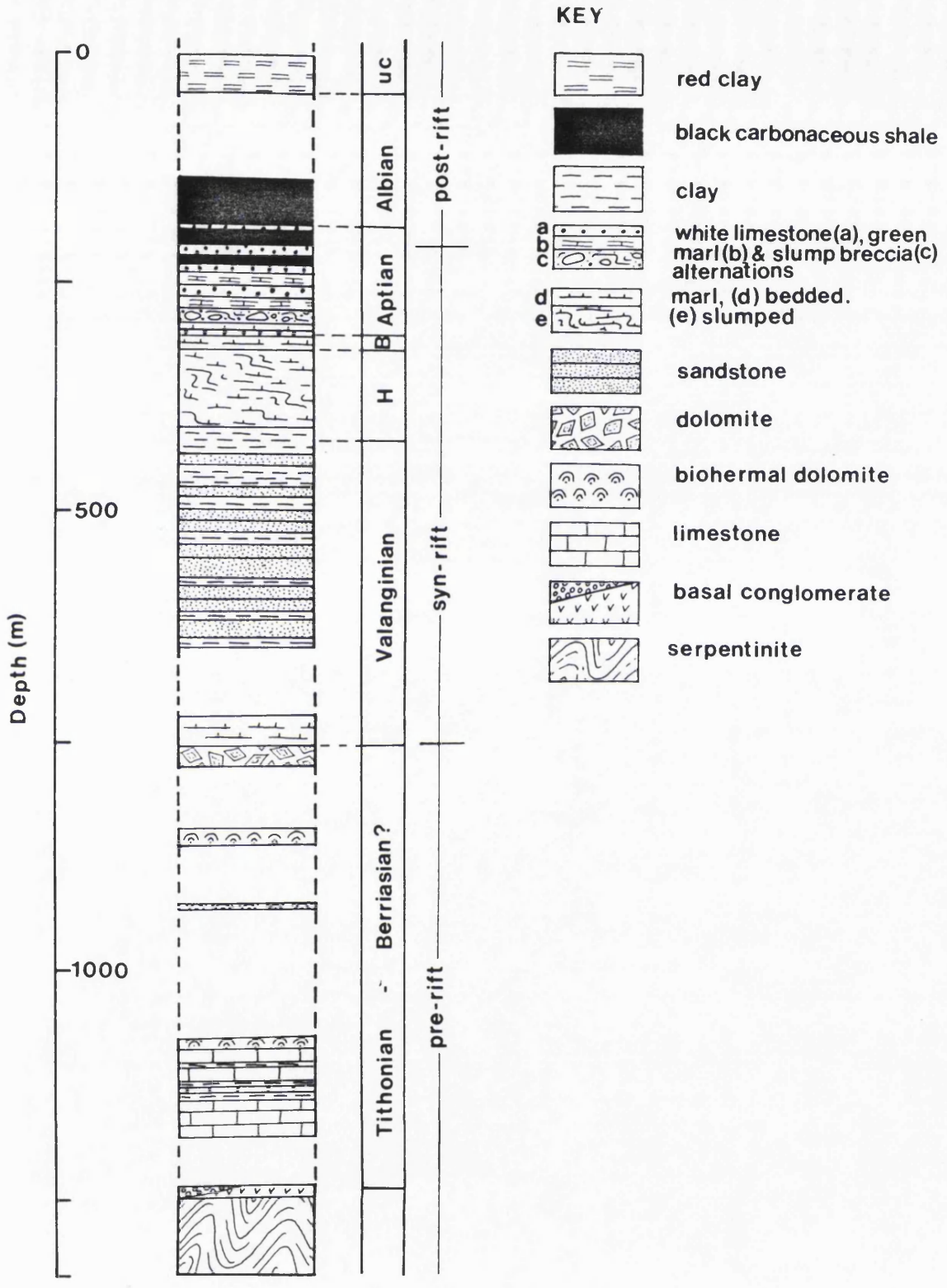

Fig. 3.24. Stratigraphic log of the Galicia Margin (after Boillot et al., 1989). The data is compiled from the drill holes in Fig. 3.21.

3.5. Summary.

The evolution of an ocean basin, such as the Bay of Biscay is linked to a sequence of tectonic developments; a). continental rifting as a first response to extension; b). the formation of passive margins as continental decoupling takes place; c). the initiation of seafloor spreading.

Rifting throughout western Europe began in the early Triassic as a result of the collapse of the Variscan mountain belt. Grabens controlled by reactivated Variscan or Caledonian structures, commonly formed perpendicular to the trend of maximum compression (in Europe this is ~N-S). This rifting was apparently penecontemporaneous throughout the North Atlantic region (Hiscott et al., 1989).

Most workers agree that rifting and seafloor spreading in the Bay of Biscay caused anticlockwise rotation of the Iberian Plate through an angle of approximately 35° away from the stable European plates, the major movements occurred during the late Triassic to the late Cretaceous, with a rift dome forming during the Upper Jurassic. True seafloor spreading commenced c. 120 Ma, during the early Aptian, achieving the highest activity around 115 Ma. Further movements occurred during the Eocene as a response to the Miocene Pyrenean collision. This sinistral translation of the Iberian block may be accommodated by two possible mechanisms: Boillot et al. (1989) proposed a shortlived subduction event to compensate for the NW movement of the Iberian Plate, followed by its eastwards translation. Evidence for this event is not conclusive. Alternatively, Tertiary translational movements of Iberia may have occurred along a strike-slip fault. Eocene compression causing fault reactivation in the region of the Bay of Biscay has been documented by Montadert et al. (1979) and Masson and Parsons (1983).

The stratigraphy of the shelf regions surrounding the Bay of Biscay contain many similar elements, with correlatives in other basins on the North Atlantic Margins. The oldest post rift sediment is an Aptian black shale marking the appearance of deep marine conditions (Hiscott et al., 1989). The seismic reflector 'S' is a prominent marker below the tilted block sequence of the Galicia and Armorican Margins, possibly marking the transition between brittle and ductile crust.

The Mesozoic formation of the Bay of Biscay is the most important geological episode to affect the Armorican and the Hesperian Massifs since the end of the Variscan Orogeny, despite the fact that there is negligible Mesozoic stratigraphy preserved onshore. However, the influence of this rifting and seafloor spreading, coupled with the formation of a rift dome and the associated sedimentological controls cannot be

overlooked when it comes to the interpretation of apatite fission track data acquired from the Variscan Massifs.

Chapter 4

Apatite fission track analysis of samples from the continental margins of the Bay of Biscay.

4.1 Introduction.

A total of 106 surface exposed samples were collected from the Armorican Massif (Western France) and Northern Spain. Sixty-nine of the samples yielded apatite on which fission track ages and length distributions were determined.

For the purpose of this and the following chapters, the understanding of the geological implications of fission track data, and the methods of calculation and interpretation of data are more important rather than the physical and chemical aspects of track behaviour. The mechanisms of fission decay, the formation of fission tracks in a crystal and the kinetics of track annealing are described in further detail in Chapter 7.

4.2 Apatite Fission Track Analysis

Fission tracks are the result of spontaneous fission decay of ^{238}U in apatites which occurs at a constant rate over time. This decay forms the basis of apatite fission track analysis in a similar fashion to other conventional radiometric dating techniques. However, the major difference is that instead of measuring daughter isotopes, the number of fission tracks are measured. This fission damage can be repaired (or annealed) and the rate of annealing is a strong function of temperature. Natural annealing of tracks in apatites is typically a gradual process taking place over a geological timescale of 1 to 10 Myr. at temperatures of 60 to 120°C. Such temperatures are typical of upper crustal temperatures and thus fission tracks in apatites have the property of recording upper crustal thermal history. In a simple history where a rock is slowly and monotonically cooled tracks (which form continuously over time) begin to be preserved at temperatures of <120°C. In samples with more complex histories, reheating to temperatures of 60-120°C will cause partial to complete annealing of the tracks formed up to that time, the degree of annealing being dependent on the temperature reached. Because tracks are constantly being produced, they provide an integrated record of the thermal history in the low-temperature range below ~120°C. Only very rarely does an apatite fission track age represent an absolute formation age, typical cases being undisturbed, sub-aerial volcanic rocks (Hurford and Green, 1983).

Two distinct datasets are obtained from the measurement of fission tracks in apatite, an apparent fission track age and a confined track length distribution. These two observed parameters should not be interpreted individually but must be combined to give a picture of the thermochronological evolution of the sample. Further constraint is put on the thermal history by geological parameters such as stratigraphic age and geological history of the region. These include the proximity and timing of igneous intrusions, tectonic events and the appearance of prominent unconformities within the stratigraphic record indicating times of denudation and surface exposure.

Fission track analysis can provide a thermal history of a rock sample provided that it contains a suitable uranium bearing mineral, usually apatite, zircon and sphene; more rarely used are natural glasses and uranium-bearing garnet. Fission decay of ^{238}U occurs spontaneously throughout geological time with a Poissonian distribution* of decay events, as with all radioactive decay mechanisms. The density of spontaneous fission tracks (ρs) within a sample is directly dependent on the uranium content of the mineral which, for apatites is typically 20 - 40 ppm. Over time tracks will form continuously in a crystal. To obtain meaningful data, the uranium content must be determined, and consequently the sample is irradiated to produce an induced density of fission tracks (ρi). This population of induced fission tracks formed by thermal neutron bombardment of the sample in a nuclear reactor, with the neutron fluence calibrated using standard dosimeter glasses of known uranium content (i.e. Corning CN-5, 11 ppm uranium). The measured ratio $\rho s/\rho i$ thus provides an assessment of the fraction of total uranium which has fissioned and is used with the rate of fission decay in a modified version of the general age equation of Rutherford and Soddy (1902) to yield an apparent fission track age. The process of annealing may erase previously formed tracks, but will not affect formation of new tracks either during or subsequent to the thermal event.

All the analyses in this work were calculated from fission tracks in apatite using the external detector method (EDM; Hurford and Green, 1982) and this procedure is summarised in **Figure 4.1**. The EDM involves the use of non-uranium bearing white mica, placed on top of the sample during thermal neutron irradiation. This acts as a detector for the fission of

---

* The Poissonian distribution represents a series of events that are randomly scattered in time and space, having a mean number of occurrences λ in a given interval of time (or space), and if X is the random variable "the number of occurrences in a given interval", then $X \sim Po(\lambda)$.

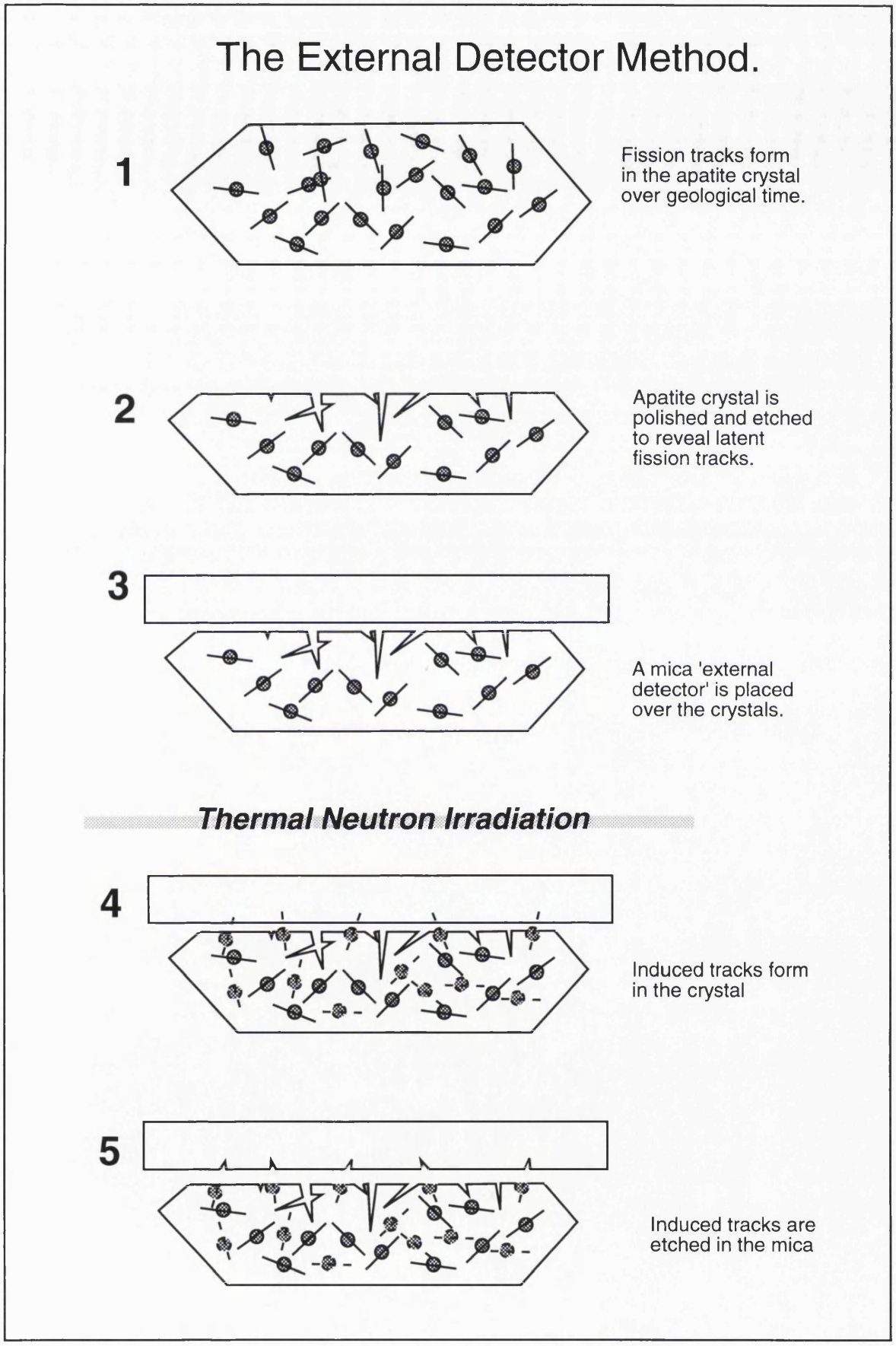

Fig. 4.1. A flowchart illustrating the external detector method for calculating fission track ages.

uranium induced in the crystals by thermal neutron bombardment and thus yields the value of ρi. Neutron fluence is calibrated from the density of induced tracks in the dosimeter (ρd) by using a similar mica detector placed against the dosimeter glass.

All the apatite fission track samples in this study were analysed using a Zeiss Axioplan microscope at a magnification of 1250x with a dry objective and a Märzhauser motorised stage. The computer application 'Stagemover' allows for the selection and alignment of the apatite grains and corresponding micas and the rapid return to any selected apatite in the grain mount or its mirror image with a precision better than 1 μm.

The methods of extraction of the apatites and their subsequent preparation for analysis are outlined in Appendix 1. The samples are analysed from a polished and etched grain mount, the fission tracks in approximately twenty crystals being counted. Individual single grain ages (SGAs) and errors are calculated for each crystal. These ages are averaged to produce a single apparent age which can be compared with the distribution of fission track lengths.

4.2.1 The Zeta Calibration Factor and the use of Age Standards.

In fission track analysis, zeta (ζ) represents a personal calibration factor which circumvents the necessity for absolute values for the thermal neutron fluence and the decay constant for the spontaneous fission of ^{238}U* (Hurford and Green, 1983). With the use of this calibration factor, only three measured variables are used to determine a fission track age: ρs, ρi and ρd.

An individual SGA (t_{samp}) is calculated using the fission track age equation (1).

$$t_{samp} = \frac{1}{\lambda_{D8}} \ln\left\{\left(\frac{\rho s}{\rho i}\right)_{samp}.\lambda_{D8}.g\,.\rho d.\zeta+1\right\} \qquad (1)$$

where λ_{D8} is the total decay constant for ^{238}U (1.55125×10^{-10} yr^{-1} ; Jaffey et al., 1971); ρs is the spontaneous track density in the sample; ρi is the induced track density in the corresponding mica; g is a geometry factor, $g \approx 0.5$; ρd is the induced density in the dosimeter and ζ is a personal calibration factor. To determine ζ equation (1) is rearranged:

---

* Problems arise in the disparities between measured values for the uranium fission decay constant, λ_{f8}. Fleischer and Price (1964a) calculated it to be 6.9×10^{-17} yr^{-1}, whereas Spadavecchia and Hahn (1967) arrived at the value 8.42×10^{-17} yr^{-1}. The majority of other estimates lie around these two values (see Bigazzi, 1981). More recently Garwin (1985) calculated a value of 8.7×10^{-17} yr^{-1}.

$$\zeta = \frac{e(\lambda_{D8} \cdot t_{std})-1}{\left(\frac{\rho s}{\rho i}\right)_{std} g.\rho d.\lambda_{D8}} \quad (2)$$

where t_{std} is the known age of a standard sample. The presence of a geometry factor, g, in the equations is to compensate for the fact that potentially there are twice as many spontaneous tracks formed per unit area than corresponding induced tracks. **Figure 4.2** shows that the polished plane selected for counting reveals fragments of etched fission particle paths derived from uranium atoms originally situated either above or below this plane. The induced tracks are formed after the part of the crystal above the plane has been removed by polishing. Hence the induced fission tracks are derived only from uranium atoms below this plane (cf. Gleadow and Lovering, 1977; Naeser et al., 1980).

To be used as an age standard, an apatite must be assumed to have undergone no annealing and consequently must fit certain criteria; it must have been, on a geological timescale, instantaneously formed, be accurately datable by several techniques, both stratigraphic and radiometric, and must not have witnessed any subsequent thermal or geological phases. It must also contain abundant apatite thus making it available as an internationally usable standard. In this rare case, the apatite fission track age corresponds exactly to those obtained by other methods. Such samples are relatively scarce: at present three apatite standards are routinely available, and have been used for the evaluation of the zeta calibration factor in this thesis **(Table 4.1).**

4.2.2 The apparent apatite fission track age.

For each sample the measured data consist of ~20 Single Grain Ages (SGAs), one for each individual crystal dated, and a Central Age, which is a weighted mean age of the SGAs. The SGAs are best illustrated in the form of a radial plot (Galbraith, 1990). This presents each single grain age on a radius to an arc, the age becoming more precise as it approaches the arc, and less precise as it approaches the origin. The age range increases around the arc from bottom to top **(Fig. 4.3a and b)**. The radial plot provides an immediate visual representation, of the range of distribution of the SGAs and their precision. Consequently, they can be readily compared with each other and with the stratigraphic or formation age and the apparent fission track (central) age. In this way trends and spreads within the data are readily discernible.

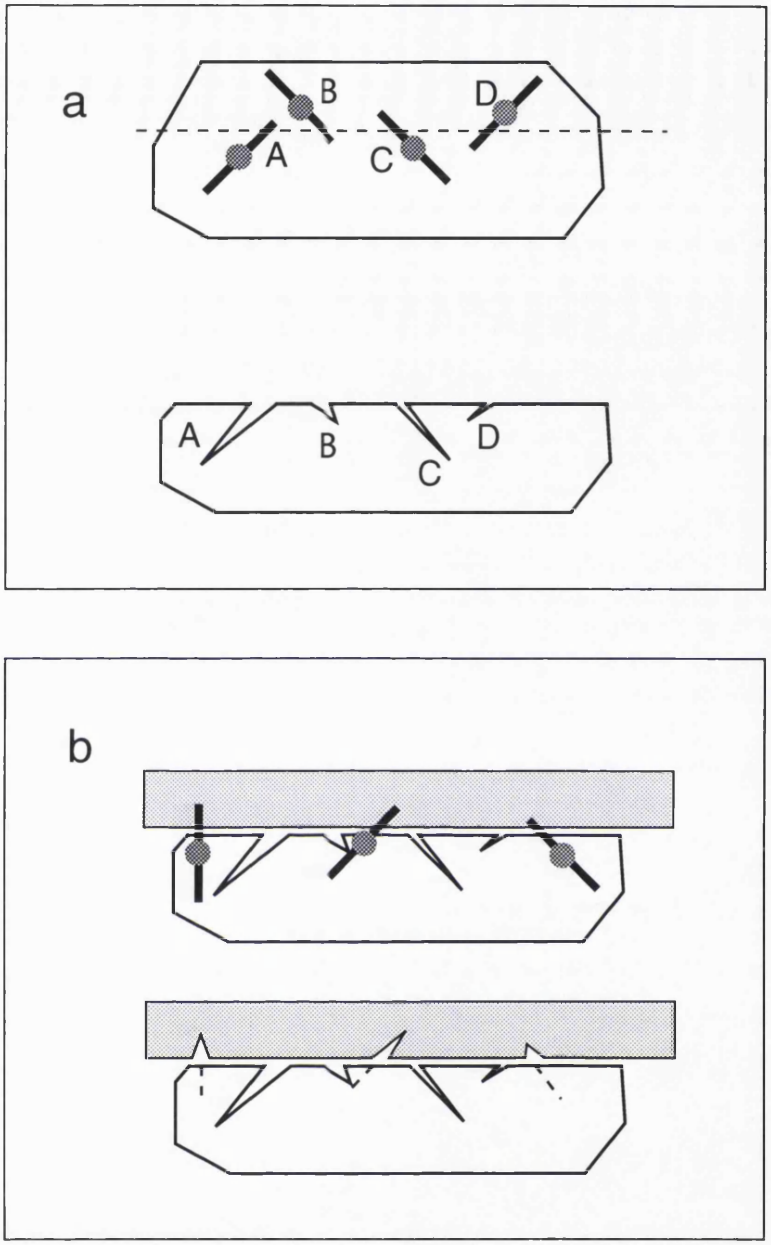

Fig. 4.2. The need for the use of a geometry factor in fission track analysis. The diagram illustrates how there are potentially twice the density of spontaneous fission tracks with respect to induced fission tracks. a). fission tracks etched on the poilished plane are derived both from nuclei *above* and *below* the plane. b). induced fission tracks revealed in the mica are only derived from nuclei *below* the plane.

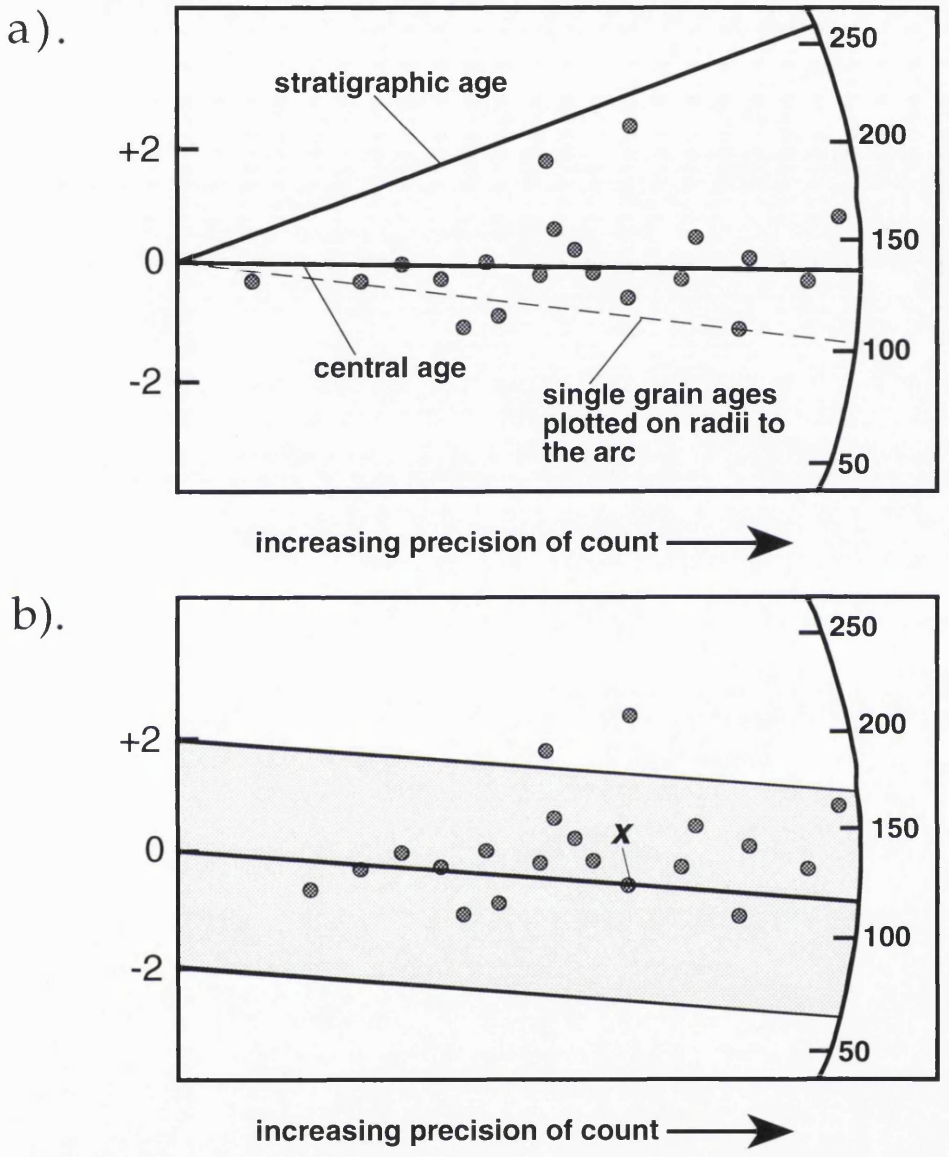

Fig. 4.3. a). The principal elements of the radial plot, used for displaying the distribution and precision of single grain ages. Precision is represented in a relative value and is a function of the number of spontaneous tracks counted in each crystal. The placing of the arcuate axis is a function of the plotting application. b). the 2σ error bars can be applied to each individual grain age. Typically 20 crystals are counted, selected from the apatite yield of approximately 5 kg of rock. A spread in ages is expected especially in cases where partial annealing has taken place.

In a sample such as an age standard, the single grain ages would be expected to have little non-Poissonian variation. In such a sample a *mean age* is an accurate measure of these single grain ages. In simplest terms this assumes that the crystals counted are all fragments of one large, homogenous crystal (which is true in the case of Durango Apatite). However, in heterogeneous samples, this assumption cannot be made and the spread of single grain ages is extremely important to the interpretation of the thermal history. In such a case to quote an mean age can be misleading.

Apatite age standard	Locality	Age (Method)	Reference
Fish Canyon Tuff	Colorado, USA.	27.8±0.2 Ma (^{40}Ar-^{39}Ar sa) 27.9±0.7 Ma (K-Ar sa, bi, hb, pl)	Hurford & Hammerschmidt, 1985 Steven et al., 1967
Mount Dromedary	Tilba Tilba, NSW.	98.8±0.6 Ma (Rb-Sr, bi) 96.0±2.0 Ma (K-Ar, bi) 98.7±0.6 Ma (mean)	Williams et al., 1982. McDougall & Wellman, 1976. Green, 1985*.
Durango	Durango, Mexico.	31.4±0.5 Ma (K-Ar)	McDowell & Keizer, 1977.

Table 4.1. Apatite fission track age standards showing independent radiometric ages, and method used. * a weighted mean age from published ages; all independent ages calculated or recalculated using I.U.G.S. constants (Steiger and Jäger, 1977). Mineral abbreviations are in Appendix 4.

The *pooled age*, calculated from the ratio of the sum of spontaneous tracks in all crystal to the sum of all individual tracks, has been the most frequently used measure of sample age. Dispersion of the data has been assessed by use of a chi-squared criterion to detect no Poissonian variations. Chi-squared (χ^2) is a measure of the departure of observed values from expected values, in the case of frequencies that arrive from any classification of data in which each specimen is put into one, and only one class. In the case of fission track analysis, this is the difference of a single grain age from the pooled mean age. Recent examinations of data have

highlighted the appearance of different age populations within a sample, that may be a result of provenance or differential annealing. Therefore, all the single grain ages should be considered in interpreting the results of an analysis. Since a single measure of sample age is also useful, the *central age* is used, quoted with an age dispersion. This is a weighted mean age of all the crystals (Galbraith, 1992). The age dispersion is a coefficient of variation of the ages of the individual grains, expressed as a percentage of the central age. A central age is equivalent to the pooled age when the age dispersion is zero. The central age and age dispersion is used for the representation of fission track data in this work. The chi-squared value is also stated for comparison with earlier results.

4.2.3 Track Length Measurements.

Each fission track formed at a different time in the history of the crystal and its host rock, and therefore each track represents an individual record of part of the thermal history, being shortened to the length corresponding to the highest temperature it has experienced. Together the track lengths represent an integrated picture of the sample's thermal history.

To avoid bias with truncated tracks intersecting the surface, the track length distribution is obtained by measuring horizontal, confined fission tracks. Confined track lengths occur within the crystal and are not truncated by the polished surface on which the track density is measured. To be revealed, these confined tracks must intersect a feature through which they are accessed by the etching fluid (HNO_3). Such a feature can be a fission track that intercepts the polished surface ('track-in-track'), or a fissure in the crystal ('track-in-crack') **(Fig. 4. 4)**.

In practice, 100 confined tracks are measured using a drawing tube adaptation to the microscope. This allows a view of a digitising tablet placed next to the microscope, to be superimposed on the magnified image of the grain mount. The track lengths are measured using a mouse fitted with a small LED, operated on the digitising tablet. This LED, viewed through the drawing tube, is placed at each end of a track and hence the co-ordinates are recorded on the digitising tablet. The microscope image is calibrated to the tablet using a graticule with divisions of known length, which allows an absolute measurement of track lengths. The uranium content and the degree of annealing are important factors in governing the number of measurable confined track lengths. As the tracks are only optically visible if etched and therefore need to be cut by a feature intersecting the surface, the number of etched confined tracks is directly related to the number of features along which the etchant can pass. Consequently a low uranium

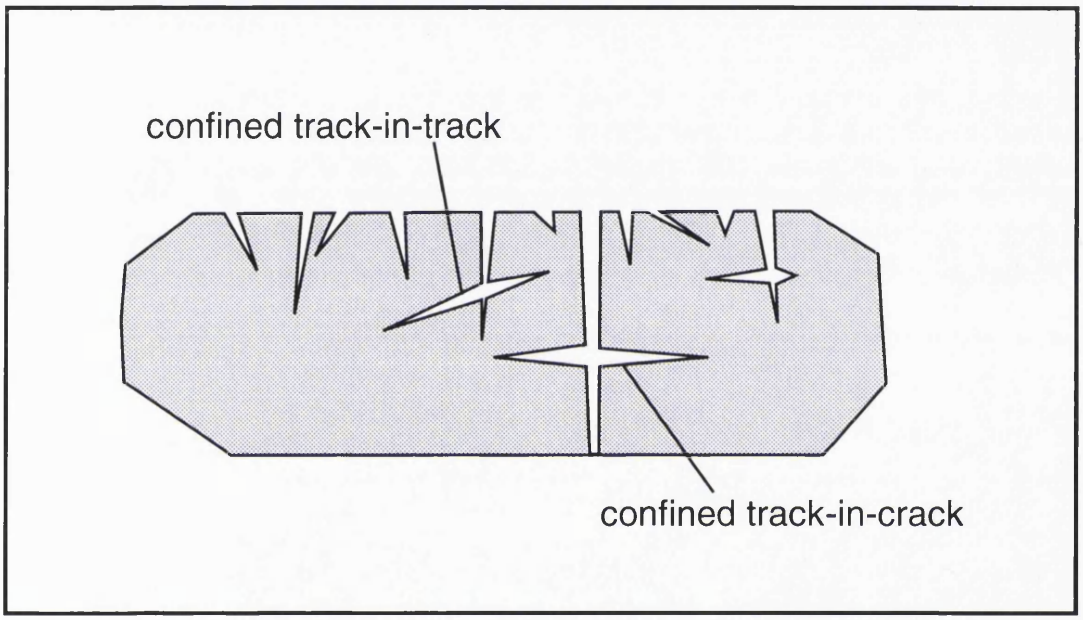

Fig. 4.4. A cartoon showing how confined tracks are revealed by etchants within a crystal, either as tracks-in-tracks or tracks-in-cracks.

content means that the chances of a confined track intersecting a projected track (i. e. a surface outcropping track) are diminished. The same is true when dealing with samples that have been partially annealed. The probability of a short track intersecting a projected track is less than that for a long track intersecting a projected track. This develops an unavoidable bias to measuring longer tracks, potentially giving a distorted view of the degree of annealing. Consequently the appearance of short tracks (< 10 μm) in a sample is significant, even if there are relatively few of them.

The track length measurements are generally presented as a histogram, the shape of the distribution being the most important diagnostic of the thermal history (Gleadow et al., 1986b). The conventionally quoted parameters are the mean track length (MTL) and the standard deviation (σ) of the distribution. The appearance of short (< 10 μm) and long (> 14 μm) tracks is of paramount importance, because they are a direct measure of the severity of annealing and/or the time of residence at ambient temperatures since the cessation of any thermal perturbation. Gleadow et al. (1986b) defined three main track length distributions that can be ascribed to particular thermal histories **(Fig. 4.5)**. A rock which has cooled rapidly, and remained thermally undisturbed since that cooling event will have a narrow symmetrical track length distribution, with the MTL will be 14 to 15.5 μm, with σ between 0.8 - 1.2 μm (Fig. 4.5 a). Extrusive volcanic rocks are the most likely candidates to fall into this 'undisturbed volcanic' category, although high level intrusions and volcanogenic sediments may also have very similar characteristics. The track lengths measured for the apatite age standards exhibit this type of pattern. A more common situation is that of a slowly and monotonically cooled and unroofed basement terrane. The distribution widens and is likely to develop a negative skew, with a MTL of 12.5 - 13.5 μm and σ between 1.3 to 1.7 μm. This has been termed an 'undisturbed basement distribution' (Fig. 4.5 b). Essentially, these two distributions exhibit the major difference in track length distributions occurring as a result of rapid or slow cooling.

A sample with a bimodal distribution of track lengths (Fig. 4.5 c) is representative of a more complex thermal history. The observation of this sort of distribution is a result of the sample being lowered into the PAZ and then being raised out of it either due to burial and exhumation, or to thermal perturbations. The bimodal distribution can be regarded as two separate distributions, each reflecting an independent part of the sample's thermal history. When partial annealing has taken place followed by cooling, the two populations represented are the shortened, 'older' tracks and the long, more recently formed tracks.

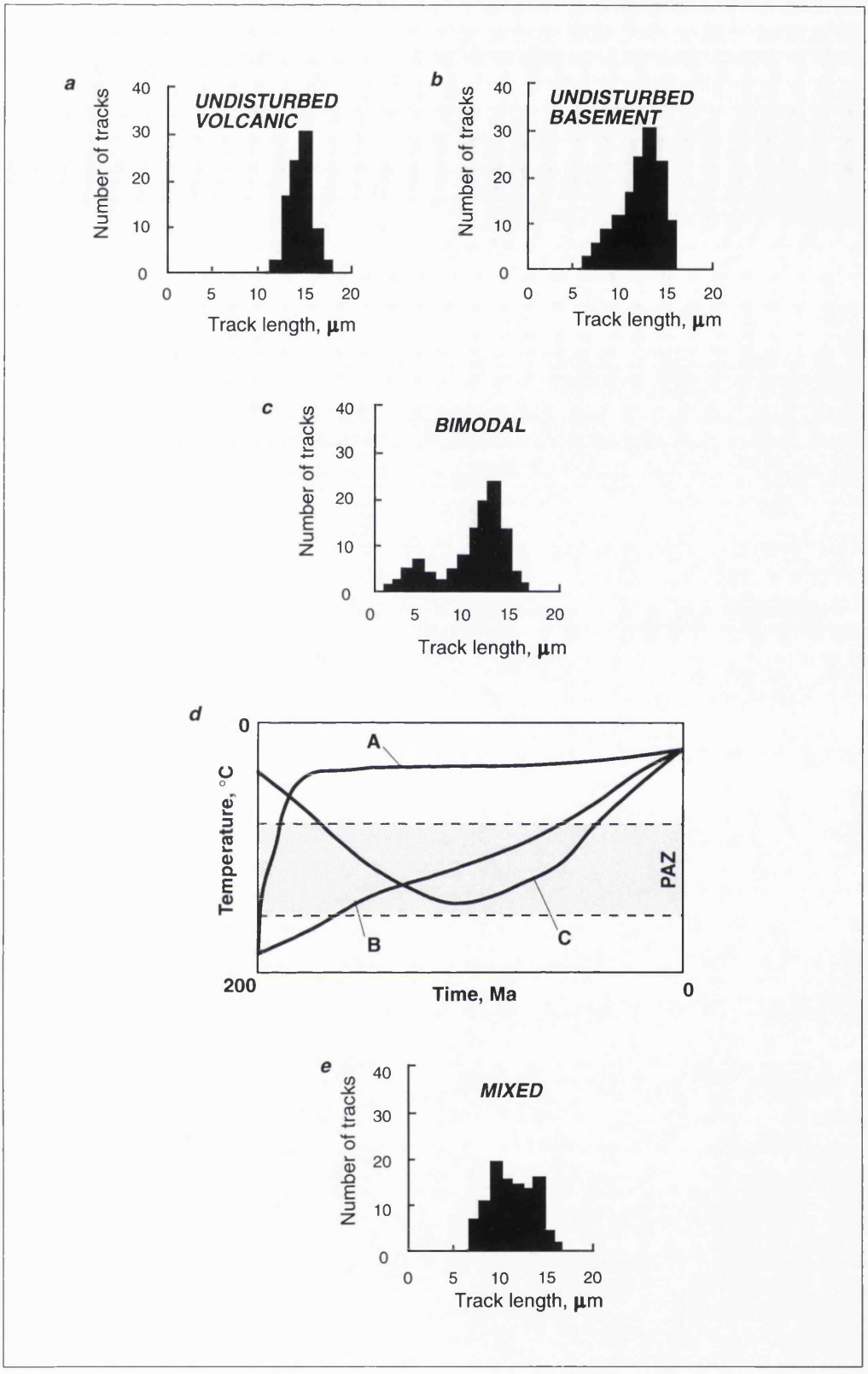

Fig. 4.5. Track length distributions (after Gleadow et al., 1986b). a). Distribution of tracks found in an undisturbed volcanic sample (and that of age standards) having suffered only ambient thermal annealing. b). The track length distribution expected from a monotonically cooled and unroofed basement complex. c). A bimodal track length distribution occurs when a sample has undergone partial annealing during some period in its history. d). Thermal history scenarios A, B, C, result in the track length distributions a, b, c. e). A track length distribution of mixed lengths, a result of differing sedimentary provenances.

The thermal histories that result in these track length distributions are summarised graphically in Figure 4.5 d. Thermal histories A, B and C correspond to the track length distributions a, b, and c.

Mixed length distributions (Fig. 4.5 e) generally occur in samples of clastic sedimentary rocks wherein the sample has a set of different provenance areas, each representing a different age and/or chemical composition. The significance of inherited ages is apparent only when samples have undergone little or partial post depositional annealing. Chemical composition will affect the annealing rates of the apatites and therefore the lengths of the individual tracks. The importance and implications of this concept are discussed in Chapter 7.

4.3 Sampling Strategy.

From previous description of the geological evolution of the Bay of Biscay it is clear that much of the area represents a denuded basement complex, exposing the roots of the Cadomian and Variscan mountain belts. With the exception of the Picos de Europa (around 2 km of elevation) both the Armorican and Hesperian Massifs are relatively low lying landscapes. Inland exposures are uncommon and although a few quarries and road cuttings exist, the majority of the samples were gathered from the rocky, indented coastline. Northern Spain is somewhat more mountainous than western France, and more inland exposures were sampled from the Hesperian Massif. **Figure 4.6** presents topographic sections across parts of the Armorican and Hesperian massifs. The 106 sample localities for the Armorican Massif are on **Figures 4.7 to 4.9,** and those for Northern Spain are illustrated on **Figure 4.10**. Approximately 5 - 10 kg of sample were collected in each case, to allow for sufficient apatite yield. The geology and petrography of each sample is detailed in Appendix 2, and summarised in **Table 4.2**. An attempt was made to collect a representative selection of the lithologies across the separate tectonic and chronological groups of the region. The variation in lithologies sampled and their corresponding yields are plotted in **Figure 4.11**.

The dominant lithologies collected were acid to calc-alkaline plutonic rocks. These are mostly two-mica granites (both Variscan and Cadomian) and Variscan leucogranites. Basic rocks are more rare and are dominantly Variscan. The gneisses are the distinctive Variscan biotite-sillimanite banded gneisses. The schistose rocks are all of metasedimentary origin and unusually are of higher apatite yield than those of the sediments from which they were possibly derived (the Brioverian Supergroup). The migmatites are deformed Variscan granites and the highly sheared

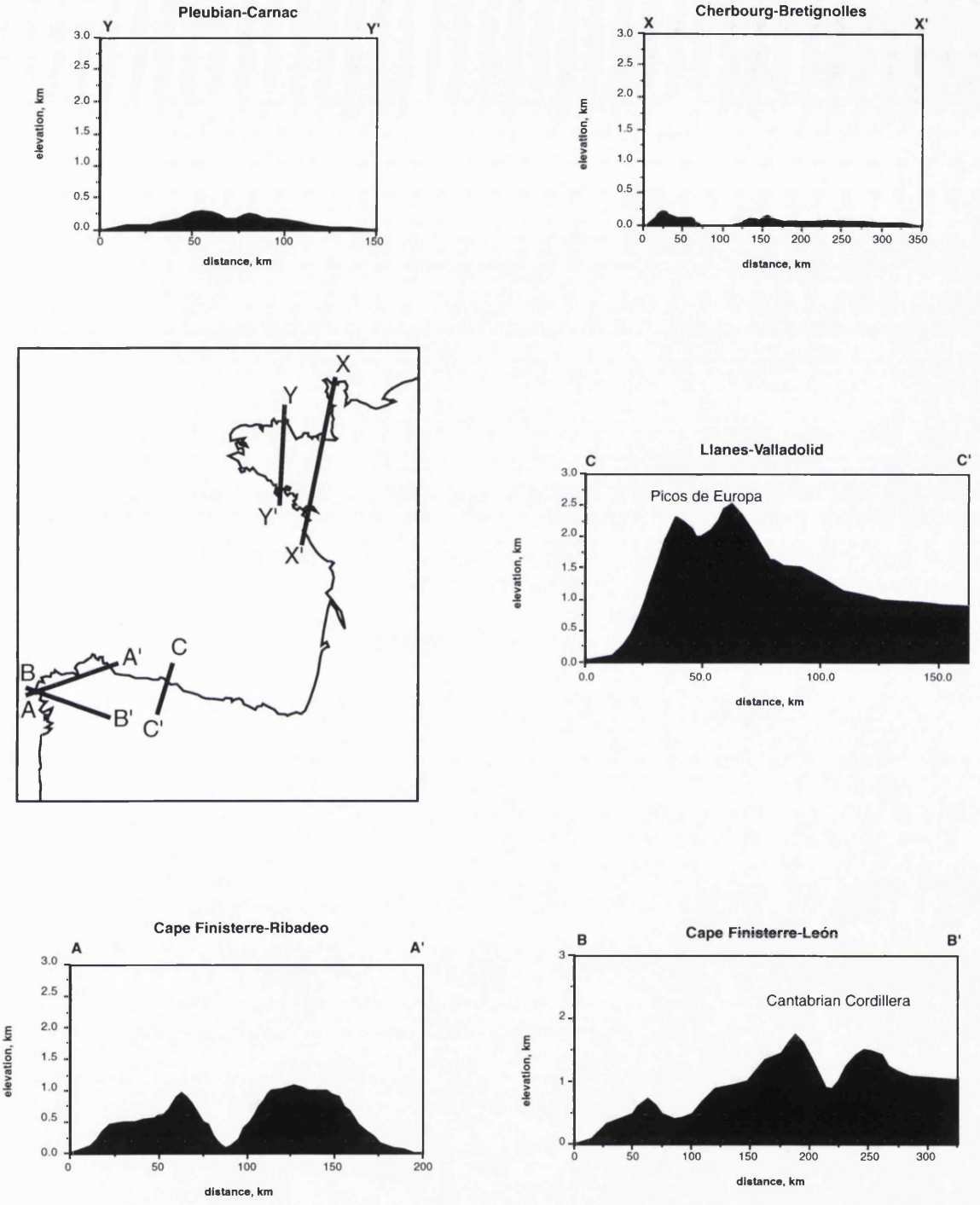

Fig. 4.6. Simplified topographic cross sections across the Armorican and Hesperian Massifs. X-X': A N-S transect from Cherbourg to Bretignolles across Normandy and Vendée. Y-Y': N-S transect across the central part of the Armorican Massif, from Pleubian to Carnac. A-A': SW-NE transect across North-west Galicia from Cape Finisterre to Ribadeo. B-B': E-W transect across the Cantabrian Cordillera from Cape Finisterre to Léon. C-C': N-S transect across the Cantabrian Cordillera in the vicinity of the Picos de Europa, from Llanes to the central plane north of Valladolid. Position of transects are shown on the map.

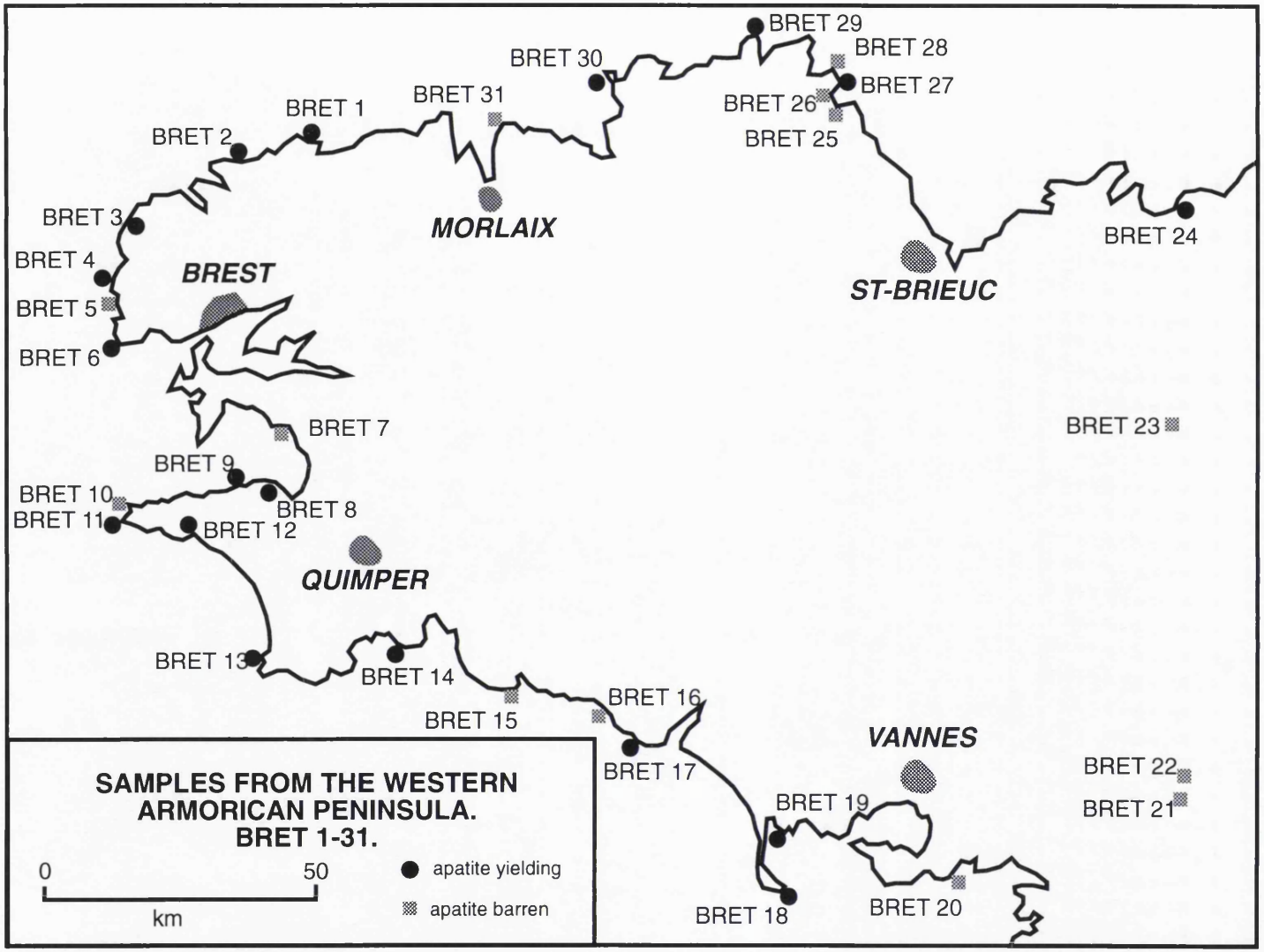

Fig. 4.7. The samples collected for fission track analysis from the Western Armorican Massif (BRET 1 - BRET 31).

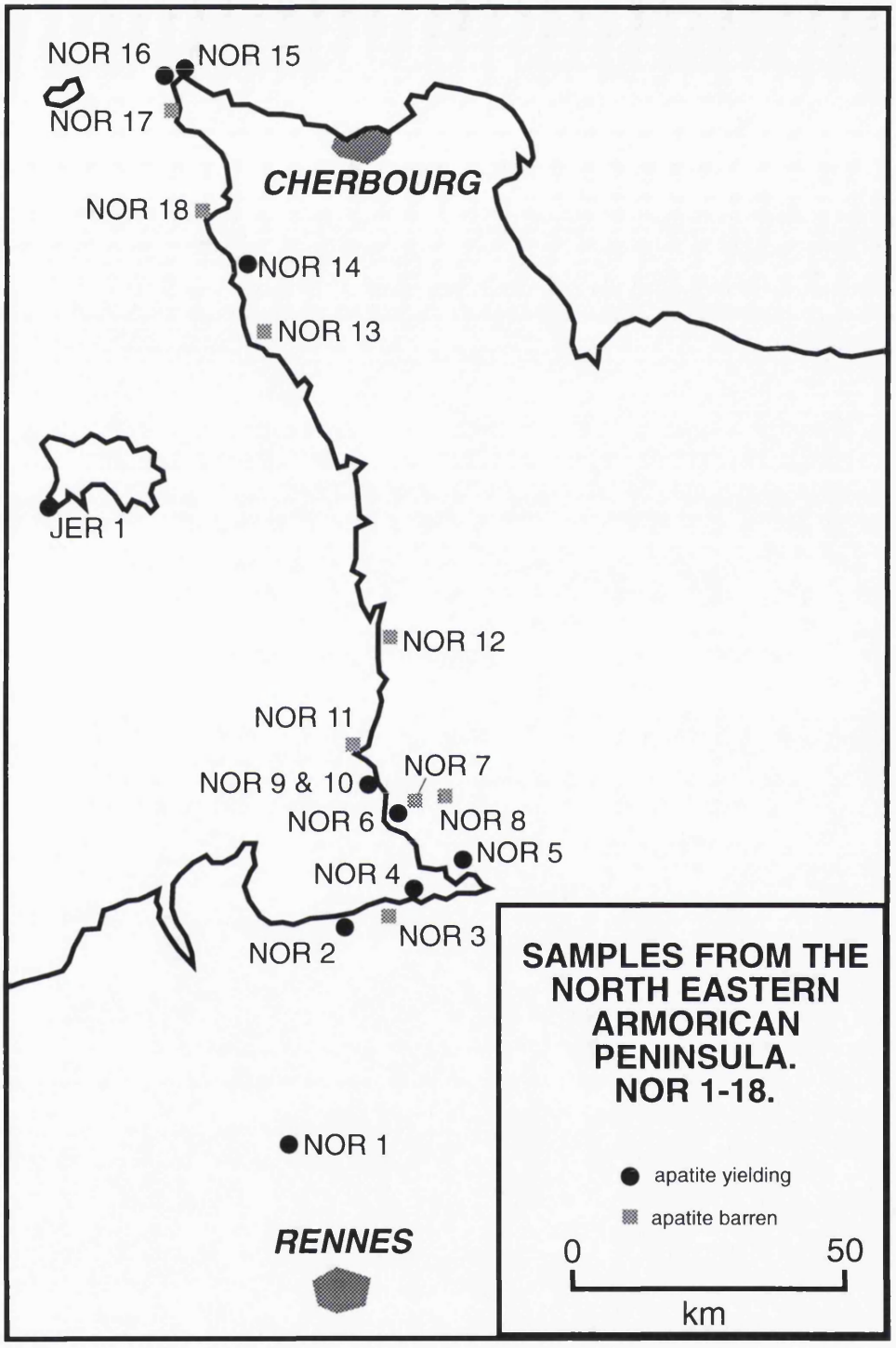

Fig. 4.8. The localities of samples collected for fission track analysis from the North-eastern Armorican Peninsula (Cotentin Peninsula). Samples NOR 1 - NOR 18.

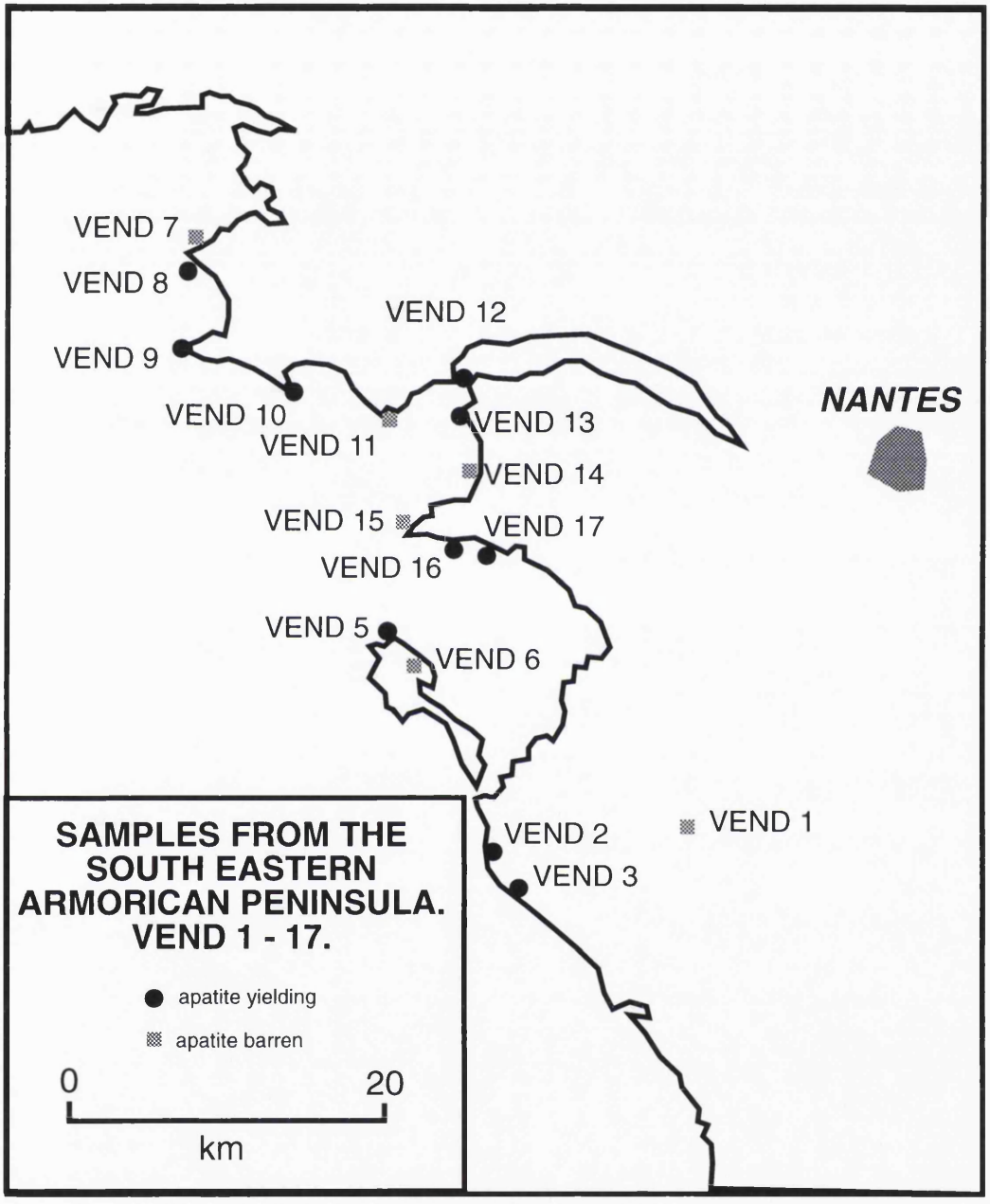

Fig. 4.9. The localities of samples collected for fission track analysis from the South-eastern Armorican Peninsula (VEND 1 - 17).

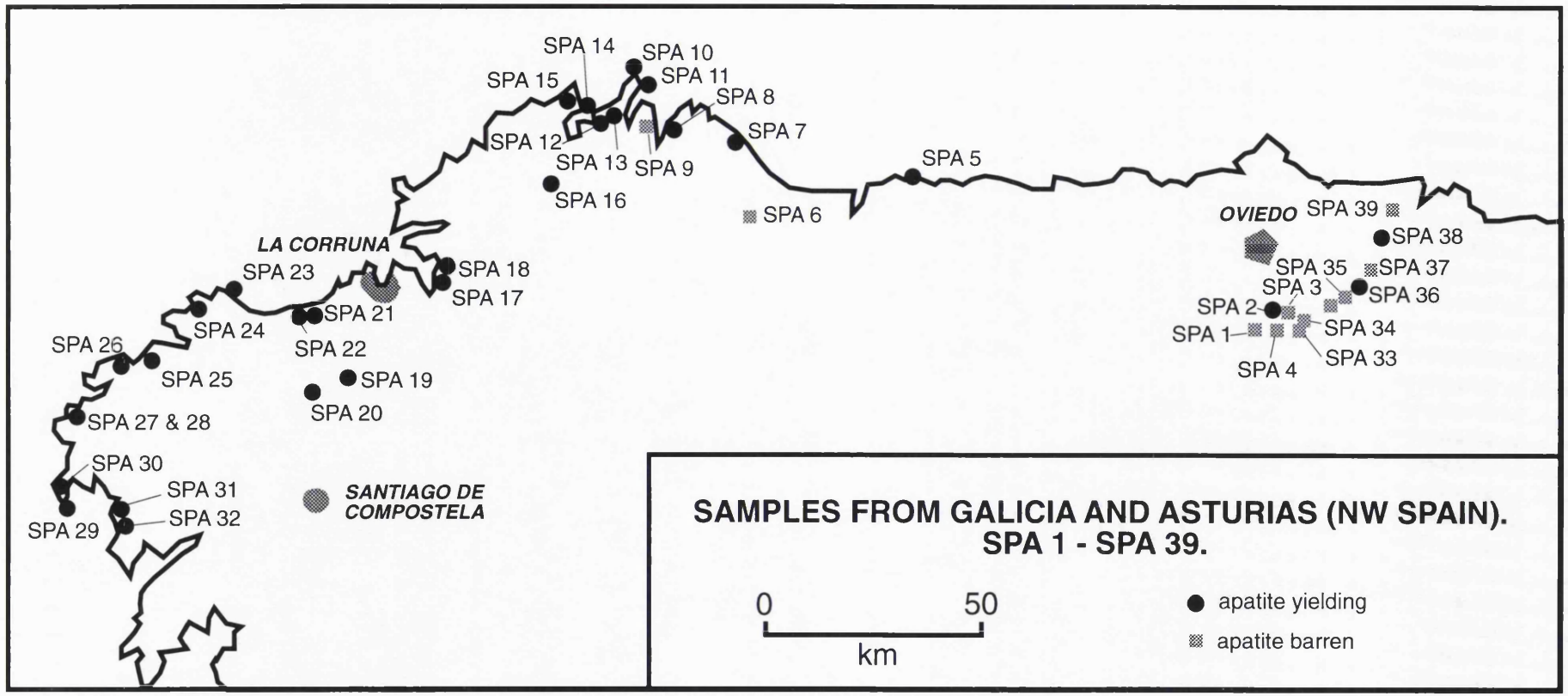

Fig. 4.10. The localities of samples collected from Galicia and Asturias, NW Spain (SPA 1- 39).

Table 4.1 Localities and lithologies of samples collected for apatite fission track analysis.

Sample No.	Locality	Lithology Name	Lithology Type	Age	Apatite?	Collector
BRET 1	Brignognan-Plage	Granite de Brignognan	granite	Variscan (345 Ma)	Y	RS / SG
BRET 2	St Michel Chapel	Migmatites de Plouguerneau	sheared granite	Cadomian	Y	RS / SG
BRET 3	Argenton	Migmatites de Plouguerneau	sheared granite	Cadomian	Y	RS / SG
BRET 4	Phare de Trezien beach	Granite de St Renan	tourmaline granite	Variscan (331 Ma)	Y	RS / SG
BRET 5	Baie de Porsmouguer	Gneiss de Lesneven	bi-si gneiss	Variscan	N	RS / SG
BRET 6	Pointe St Mathieu	Micaschistes du Conquet	qtz-mu schistes	U. Proterozoic	Y	RS / SG
BRET 7	Pentrez-Plage	Brioverian Supergroup	metagreywackes	U. Proterozoic	N	RS / SG
BRET 8	Tréboul	Granite de Douarnenez	granite	450 Ma	Y	RS / SG
BRET 9	Pointe de Beuzec	Granite de Douarnenez	granite	450 Ma	Y	RS / SG
BRET 10	Baie de Tréspassés	Granite de Douarnenez	granite	450 Ma	N	RS / SG
BRET 11	Pointe du Raz	Granite de Pointe du Raz	granite	Variscan (320 Ma)	Y	RS / SG
BRET 12	Anse du Loc'h		bi-si gneiss	Variscan	Y	RS / SG
BRET 13	Pointe de la Torche	Granite de Pont-l'Abbé	granite	Variscan (320 Ma)	Y	RS / SG
BRET 14	Mousterlin	Granite de Pont-l'Abbé	granite	Variscan (320 Ma)	Y	RS / SG
BRET 15	Raguenez-Plage	Brioverian Supergroup	qtz-mu schistes	U. Proterozoic	low U	RS / SG
BRET 16	Le Pouldu	Brioverian Supergroup	metagreywackes	U. Proterozoic	N	RS / SG
BRET 17	Kerroc'h	Granite de Guidel	granite	Variscan (312 Ma)	Y	RS / SG
BRET 18	Port Haliguen	Granite de Quiberon	foliated granite	Variscan (312 Ma)	Y	RS / SG
BRET 19	Carnac beach	Granite de Carnac	granite	Variscan (303 Ma)	Y	RS / SG
BRET 20	Pointe de Kervoyal	Migmatites de Morbihan	foliated granite	Variscan (375 Ma)	N	RS / SG
BRET 21	Aucfer quarry	Grés Armoricain	Fe-rich arkose	Arenig	N	RS / SG
BRET 22	Redon quarry	Grés de Redon	arkose	Lower Palaeozoic	N	RS / SG
BRET 23	St-Jouan-de-l'Isle		sandstone	Pliocene	N	RS / SG
BRET 24	Port Hué	St Malo Migmatites	migmatite	Cadomian(541 Ma)	Y	RS / SG
BRET 25	Abbey de Beaufort	Series Rouges de Plouézec	red sandstone	Llanvirn	N	RS / SG
BRET 26	Pointe de Guilben	Spilites de Paimpol	spilitic pillow lava	Cadomian (640 Ma)	N	RS / SG
BRET 27	Porz-Even	Tuffs de Tréguier	keratophyric tuffs	Cadomian (640 Ma)	Y	RS / SG
BRET 28	Pointe de l'Arcouest	Microgranite de l'Arcouest	porphyritic microgranite	Cadomian (615 Ma)	N	RS / SG
BRET 29	Castel-Meur	Microgranodiorite de Pleubian	granodiorite	Cadomian (615 Ma)	Y	RS / SG

Sample No.	Locality	Lithology Name	Lithology Type	Age	Apatite?	Collector
BRET 30	Grande-Ile	Granite de Ploumanac'h	granite	Variscan (290 Ma)	Y	RS / SG
BRET 31	Pointe de Primel.	Granite de St-Jean-de-Doight	granodiorite	Cadomian (615 Ma)	N	RS / SG
JER 1	St Peter's Quarry	St Peter's Granite	granite	Cadomian (483 Ma)	Y	JL
VEND 1	Challans	Brioverian Supergroup	qtz-mu schist	U. Proterozoic	Y	RS / AJH
VEND 2	La Paree beach	Arkose du Marais-Girard	meta-arkose	Lower Devonian	Y	RS / AJH
VEND 3	Bretignolles quarry	Granite de St Martin-de-Brem	microgranite	Variscan (320 Ma)	Y	RS / AJH
VEND 4	Sion-sur-l'Ocean	Série de St Gilles-sur-Vie	schist	U. Proterozoic	N	RS / AJH
VEND 5	La Madelaine	Granite de Noirmoutier	granite	Variscan (320 Ma)	Y	RS / AJH
VEND 6	Bord-de-la-Chaise		quartzite	Eocene	N	RS / AJH
VEND 7	Port au Loup	Schistes de la Vilaine	schist	U. Proterozoic	N	RS / AJH
VEND 8	Piriac	Granite de Guerande	granite	Variscan (320 Ma)	Y	RS / AJH
VEND 9	Pointe-du-Croisic	Granite de Croisic	granite	Variscan (320 Ma)	Y	RS / AJH
VEND 10	Pointe-de-Penchâteau		gneiss	Variscan	Y	RS / AJH
VEND 11	Pointe de Chermoulin		migmatite	Variscan	N	RS / AJH
VEND 12	Mindin	Granite de St Brevin	granite	Variscan (320 Ma)	Y	RS / AJH
VEND 13	St Brevin-les-Pins		bi-si gneiss	Variscan	Y	RS / AJH
VEND 14	Le Redois		schist	Silurian	N	RS / AJH
VEND 15	Pointe-St-Gildas		schist	Silurian	Y	RS / AJH
VEND 16	Plage-de-la-Meleu		meta-rhyolite	Silurian	Y	RS / AJH
VEND 17	St Marie-sur-Mer		schist	Silurian	Y	RS / AJH
NOR 1	Hedé	Mancellian Batholith	granodiorite	Cadomian (541 Ma)	Y	RS / AJH
NOR 2	Mont-Dol	Granite de Mont-St-Michel	granite	Cambrian (550 Ma)	Y	RS / AJH
NOR 3	St Broladre	Granite de St Broladre	diorite	Cadomian (541 Ma)	N	RS / AJH
NOR 4	Mont-St-Michel	Granite de Mont-St-Michel	granite	Cambrian (550 Ma)	Y	RS / AJH
NOR 5	Avranches	Granite d'Avranches	granite	Cadomian (541 Ma)	Y	RS / AJH
NOR 6	Les Perrieres	Granite de Vire	granite	Cadomian(542 Ma)	Y	RS / AJH
NOR 7	St Michel-des-Loups	Brioverian Supergroup	meta-arkose	U. Proterozoic	Y	RS / AJH
NOR 8	Carriere Semery	Granite de St Pierre-des-Langers	leucogranite	Cadomian(541 Ma)	N	RS / AJH
NOR 9	Pointe-de-Thar	*sill*	?dolerite	U. Proterozoic	Y	RS / AJH
NOR 10	Pointe-de-Thar	Formation de St Pair	meta-sandstones	U. Proterozoic	Y	RS / AJH
NOR 11	Pointe-du-Roc	Formation de Granville	meta-sandstones	U. Proterozoic	N	RS / AJH
NOR 12	Robillard	Grés de Robillard	sandstone	Tournaisian	N	RS / AJH

Sample No.	Locality	Lithology Name	Lithology Type	Age	Apatite?	Collector
NOR 13	Barneville-Carteret	Grés de Moitieres-Alonne	sandstone	Llanvirn	Y	RS / AJH
NOR 14	Les Pieux	Grés de Rozel	sandstone	L. Cambrian	Y	RS / AJH
NOR 15	Cap-de-la-Hague	Cap-de-la-Hague Granodiorite	granodiorite	Cadomian (477 Ma)	Y	RS / AJH
NOR 16	Goury	Granite de St Germain	granite	Cadomian (515 Ma)	Y	RS / AJH
NOR 17	Baie Ecalgrain	Grés de May	sandstone	Llandeilian	N	RS / AJH
NOR 18	Dielette	Granite de Flamanville	granite	Variscan (316 Ma)	N	RS / AJH
SPA 1		Sabero Unit	sandstone	Gzelian	N	MAC
SPA 2		Sabero Unit	sandstone	Gzelian	Y	MAC
SPA 3		Nocedo Formation	sandstone	Frasnian-Fammenian	N	MAC
SPA 4		Nocedo Formation	sandstone	Frasnian-Fammenian	N	MAC
SPA 5	Salave	Plúton de Salave	granite	Variscan (284 Ma)	Y	RS / CSB
SPA 6	Santa Cecilia	Macizo de la Tojiza	granite	Variscan	N	RS / CSB
SPA 7	Cabo Burela	Granito de San Ciprian	granite	Variscan (310 Ma)	Y	RS / CSB
SPA 8	Viveiro	Granodiorita de Viveiro	granite	Variscan (269 Ma)	Y	RS / CSB
SPA 9	Praia de San Román	Cuarzitas Armoricain	sandstone	Arenig	N	RS / CSB
SPA 10	Punta de la Estaca de Bares	Macizo de Estaca de Bares	granite	Variscan (269 Ma)	Y	RS / CSB
SPA 11	Porto de Barquero	Granito de el Barquero	granite	Variscan (280 Ma)	Y	RS / CSB
SPA 12	Picón		metarhyolite	Silurian	Y	RS / CSB
SPA 13	Picón	*sill*	porphyry sill	Silurian	Y	RS / CSB
SPA 14	Cariño	Neises de Cariño	gneiss		Y	RS / CSB
SPA 15	Cabo Ortegal	Neises de Masanteo	gneiss		Y	RS / CSB
SPA 16	As Pontes	Granito de Forgoselo	leucogranite	Variscan (303 Ma)	Y	RS / CSB
SPA 17	Playa de Ber	*dyke*	porphyry	Cambro-Ordovician	Y	RS / CSB
SPA 18	Playa de Ber	Esquitos de Ordenes	schist	Cambro-Ordovician	Y	RS / CSB
SPA 19	Mt Cedeira	Macizo de la Coruña	granodiorite	Variscan (300 Ma)	Y	RS / CSB
SPA 20	Anxeriz	Macizo de Monte Castello	gabbro	Variscan	Y	RS / CSB
SPA 21	W of Puerto del Razo	Unidad de Malpica-Tuy	gneiss	Cambro-Ordovician	Y	RS / CSB
SPA 22	E of Puerto del Razo	Macizo de Monte Neme	granite	Variscan (310 Ma)	Y	RS / CSB
SPA 23	Cabo San Adrian		augen granite	462 Ma	Y	RS / CSB
SPA 24	Punta Nariga	Macizo de Lage	foliated granite	Variscan (310 Ma)	Y	RS / CSB
SPA 25	Playa de Traba		foliated granite	462 Ma	Y	RS / CSB
SPA 26	Sierra de Peña Forcada	Macizo de Traba	granite	Variscan (280 Ma)	Y	RS / CSB

Sample No.	Locality	Lithology Name	Lithology Type	Age	Apatite?	Collector
SPA 27	Muxia	Macizo de Muxia	leucogranite	Variscan (310 Ma)	Y	RS / CSB
SPA 28	Muxia	Macizo de Muxia	pink granite	Variscan (310 Ma)	Y	RS / CSB
SPA 29	Cabo Fisterra		granite	460 Ma	Y	RS / CSB
SPA 30	Cabo Fisterra summit	Macizo de Fisterra	granite	Variscan (280 Ma)	Y	RS / CSB
SPA 31	El Pindo	Macizo de el Pindo	granite	Variscan (280 Ma)	Y	RS / CSB
SPA 32	Punta de Caldebarcos	Macizo de el Pindo	granite	Variscan (280 Ma)	Y	RS / CSB
SPA 33	Sabero	Sabero Unit	lithic arenite	Gzelian	Y	RS / CSB
SPA 34	Las Salas		lithic arenite	Upper Devonian	N	RS / CSB
SPA 35	Riano		sandstone	Ordovician	N	RS / CSB
SPA 36	Riano		conglomerate	Ordovician	Y	RS / CSB
SPA 37	La Vega		wackestone	Pennsylvanian	N	RS / CSB
SPA 38	Linnares		micaceous sandstone	Permo-Triassic	Y	RS / CSB
SPA 39	Panes		sub-lithic arenite	Albian	N	RS / CSB

NOTES.

i). Sources of geological and geochronological data are referenced in Appendix 2, otherwise see Vidal (1973), Lameyre and Autran (1980), Gonzalez-Lodeiro et al. (1984) and Bastida et al. (1984).

ii). For crystalline rocks, the orogenic phase during which they formed or were emplaced is given, together with a radiometric age (where available). The radiometric age in some cases refers to the intrusion of a suite rather than the specific rock. Pre- and post-orogenic crystalline rocks have a radiometric age only. Stratigraphic ages of sedimentary rocks are given as accurately as is available.

iii). Further information on the apatite yielding samples is given in Appendix 2.

iv). The abbreviations of those who aided in sample collection are as follows: RS, Ruth Siddall; SG, Susan Garnish; JL, Jason Lane; AJH, Tony Hurford; MAC, Mike Audley-Charles; CSB, Charlie Bristow.

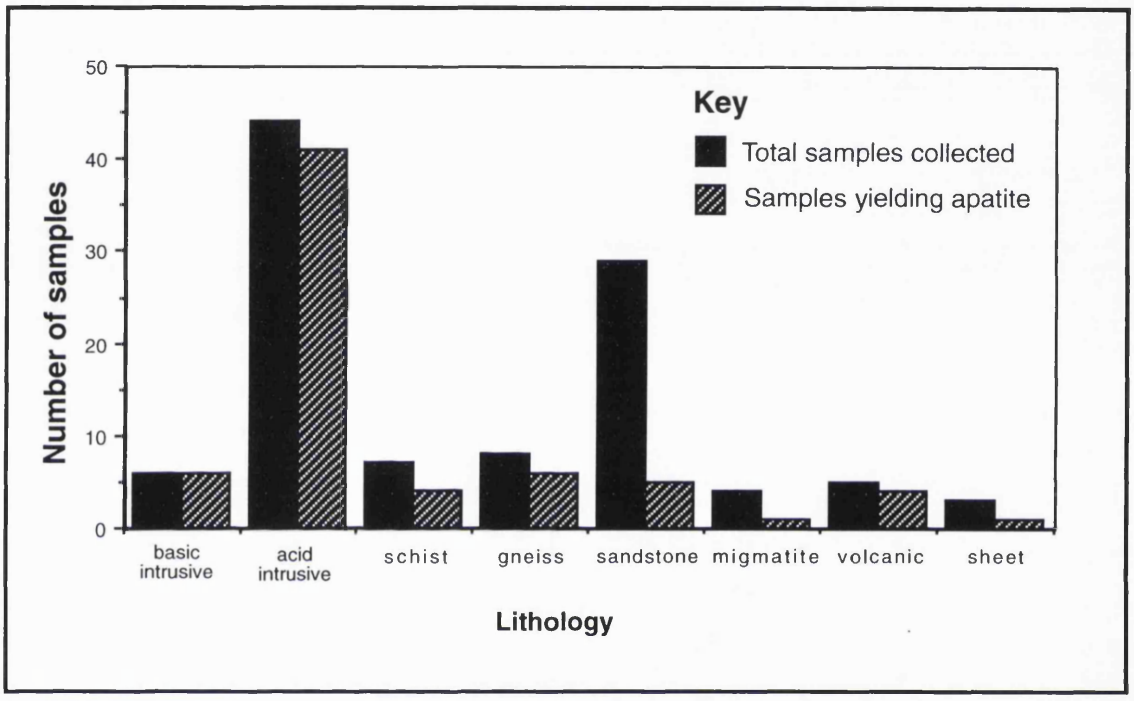

Fig. 4.11. A histogram showing the lithological groups sampled and the proportion of those groups to yield apatite. The clastic sedimentary rocks sampled were the most likely to be apatite-barren. This is often the case in mature sandstones, or those with an apatite-poor provenance. The sediments sampled were dominantly from this type of rock, there being little else.

Cadomian St Malo Migmatites. Volcanic rocks are uncommon in these old massifs due to the depth of erosion. Those that do exist are the product of Cadomian calc-alkaline magmatism. The sheet intrusions are Variscan, and vary from lamprophyres to basic dykes. Many sampled sediments yielded a disappointing quantity of apatite grains and this lack of apatite-bearing sediments contributed to the discrepancy between samples collected and samples analysed.

4.4 A qualitative evaluation of the data.

4.4.1 Geological constraints on the fission track data.

The accepted geological and tectonic background of the region has been summarised in Chapters 2 and 3. In summary, continental collision ceased at the end of the Variscan Orogeny, and rifting and eventual seafloor spreading ensued during the Mesozoic. Apatite fission track analysis has the ability to reveal denudational, uplift and heating events that may not be otherwise apparent in the rock record, and therefore have not been previously discussed. Accordingly it was not expected that any apatite fission track age should represent an absolute age determined in the study. Such is the conclusion of previous fission track analysis studies of undisturbed basement complexes. The stratigraphic ages of the rocks analysed spanned late Precambrian to early Mesozoic*. The range of apparent apatite ages spans from Lower Permian (Rotliegendes) to mid Eocene (267 ± 19 Ma, VEND 10, to 42 ± 2 Ma, SPA 36, respectively).

The apatite fission track data collected from the samples from the Armorican and Hesperian Massifs are presented in **Table 4.3**. The table allows for comparison between the age dispersion of the central age and the chi-squared probability value. When $\chi^2 > 5\%$, it is broadly equivalent to a age dispersion of < 10%.

Geographically, the data show a general decrease in apatite ages moving westwards. With the exception of those samples in the Picos de Europa (SPA 36 and 38), the youngest ages (in the interval around 70 - 115 Ma) are located in western Galicia. Although such young ages are not encountered in Brittany, there is a definite decrease in age here from around 250 Ma in Normandy and Vendée to around 140 Ma in Finistérre.

The ages obtained from the samples from Normandy are slightly younger than those from Vendée. These are similar to ages from the northern parts of Brittany and Jersey, which are slightly younger than those

* The oldest rocks sampled where from the Sinian Cadomian Belt, and the youngest sample from which a fission track apparent age was calculated were Permo-Triassic red beds. Younger samples (Cretaceous and Tertiary sands) were collected, but these unfortunately failed to yield apatite.

Table 4.3. Apatite fission track results of samples from the Armorican and Hesperian Massifs.

Sample Number	Lithology	No. of xtls	Spontaneous ρ_s x10^7 (N_s)	Induced ρ_ix10^7 (N_i)	Pχ^2	Dosimeter ρ_dx10^7 (N_d)	FT Central Age Ma (±1σ)	Age Dispersion %	Apatite Mean Track Length (μm)	Length Standard Deviation (μm)	No. of Lengths
JER 1	Granite	12	0.1473 (246)	0.1809(302)	30%	0.1083 (7503)	152.6±15	11.64	11.85±0.32	2.44	58
BRET 1	Granite	17	0.3264 (1415)	0.5455(2425)	0.001%	0.1233 (8310)	131.4±9	23.37	10.29±0.33	2.53	61
BRET 2	Granite	20	0.3316 (2979)	0.398(3578)	0.001%	0.1229(8310)	182.6±7	12.06	11.91±0.19	1.94	102
BRET 3	Granite	16	0.4446 (3792)	0.4852(4138)	0.05%	0.1224(8310)	196.0±6	7.36	10.98±0.23	2.42	112
BRET 4	Granite	20	0.2524 (1362)	0.3145(1697)	0.001%	0.1220(8310)	171.0±10	20.30	12.42±0.21	2.12	100
BRET 6	Schists	19	0.2979 (1850)	0.4572(2839)	0.001%	0.1215(8310)	143.2±8	17.90	11.33±0.26	2.28	77
BRET 8	Granite	18	0.5449 (2530)	0.5094(2365)	0.001%	0.1211(8310)	225.4±18	30.08	11.54±0.20	2.07	108
BRET 9	Granite	20	0.2724 (1323)	0.3181(1545)	25%	0.1207(8310)	182.6±8	6.26	11.72±0.36	2.38	45
BRET 11	Granite	19	0.5503 (1420)	0.8293(2140)	0.001%	0.1202(8310)	143.3±9	23.49	11.04±0.21	2.14	103
BRET 12	Gneiss	20	0.5283 (2610)	0.7360(3636)	0.001%	0.1198(8310)	153.0±7	14.29	12.60±0.15	1.53	109
BRET 13	Granite	18	0.4412 (1912)	0.6326(2741)	0.01%	0.1082(7503)	135.2±6	11.80	11.92±0.20	1.99	105
BRET 14	Granite	20	0.4987 (3104)	0.6401(3823)	0.001%	0.1193(8310)	166.0±8	16.00	11.66±0.20	2.00	100
BRET 17	Granite	20	0.3178 (2846)	0.4269(2189)	0.001%	0.1185(8310)	154.0±8	17.40	11.83±0.23	2.33	104
BRET 18	Granite	20	0.8100 (2079)	0.8528(957)	20%	0.1180(8310)	197.4±7	5.83	12.13±0.14	1.41	100
BRET 19	Granite	10	0.1939 (915)	0.2028(1791)	90%	0.1176(8310)	197.5±9	0.00	11.97±0.25	1.71	47
BRET 24	Migmatites	20	0.5443 (1675)	0.5820(219)	55%	0.1167(8310)	192.2±7	0.73	11.95±0.20	1.96	101
BRET 27	Tuff	20	0.0490 (234)	0.0458(446)	80%	0.1207(8310)	226.5±21	0.71	11.92±0.33	2.51	60
BRET 29	Granodiorite	20	0.1284 (411)	0.1393(2773)	99%	0.1803(7503)	176.0±12	0.00	10.21±0.32	3.16	100
BRET 30	Granite	18	0.4536 (2773)	0.4536(3065)	50%	0.1083(7503)	190.6±6	1.34	9.44±0.47	3.24	48
NOR 1	?Tuff	19	0.9801(2513)	1.1950(3065)	0.001%	0.1384 (9594)	192.0±12	23.28	12.47±0.17	1.77	105
NOR 2	Granite	20	0.2742(1453)	0.3159(1674)	0.05%	0.1383(9594)	215.1±10	12.16	13.18±0.13	1.32	100
NOR 4	Granite	17	0.1224(599)	0.1936(947)	0.001%	0.1383(9594)	154.2±15	29.94	12.73±0.17	1.59	93
NOR 5	Granite	20	0.2951(1751)	0.3237(1921)	0.01%	0.1382(9594)	220.2±11	15.08	13.04±0.21	1.45	50
NOR 6	Granodiorite	20	0.4859(3232)	0.6519(4336)	0.001%	0.1381(9594)	183.4±9	18.57	13.04±0.13	1.35	108

Sample Number	Lithology	No. of xtls	Spontaneous ρ_s x10^7 (N_s)	Induced ρ_ix10^7 (N_i)	Pχ^2	Dosimeter ρ_dx10^7 (N_d)	FT Central Age Ma (±1s)	Age Dispersion %	Apatite Mean Track Length (μm)	Length Standard Deviation (μm)	No. of Lengths
NOR 9	dolerite	20	0.2287(1035)	0.2428(1099)	0.01%	0.1380(9594)	235.4±17	21.39	12.8±0.17	1.73	101
NOR 10	sandstone	19	0.1611(898)	0.1781(993)	0.05%	0.1379(9594)	219.6±14	17.04	12.74±0.19	1.58	70
NOR 14	sandstone	19	0.1293(907)	0.1529(1072)	75%	0.1339(9281)	199.3±9	0.30	12.01±0.18	1.79	100
NOR 15	Granite	19	0.4753(2240)	0.5581(2630)	0.001%	0.1337(9281)	200.4±10	17.20	12.7±00.15	1.61	110
NOR 16	Granite	18	0.2997(918)	0.3448(1056)	60%	0.1336(9281)	206.3±10	6.54	12.02±0.31	2.53	68
VEND 2	Schist	14	0.2776(804)	0.2976(862)	0.01%	0.1391(9594)	228.6±19	22.97	12.58±0.26	1.89	53
VEND 3	Granite	20	0.1917(1015)	0.2132(1129)	60%	0.1390(9594)	219.7±10	2.02	12.81±0.15	1.41	86
VEND 5	Granite	20	0.6145(6967)	0.7436(8431)	0.001%	0.1390(9594)	204.3±6	10.78	12.58±0.19	1.92	100
VEND 8	Granite	16	0.2956(2065)	0.3758(2625)	60%	0.1389(9594)	192.3±6	0.16	12.45±0.11	1.13	100
VEND 9	Granite	19	0.6911(3573)	0.8060(4167)	0.01%	0.1388(9594)	210.7±8	11.61	12.84±0.19	1.91	105
VEND 10	Gneiss	9	0.5071(984)	0.4721(916)	0.02%	0.1388(9594)	267.3±19	14.94	13.13±0.17	1.21	49
VEND 12	Granite	20	0.3146(1417)	0.3144(1416)	0.02%	0.1387(9594)	247.1±14	15.76	12.62±0.19	1.90	100
VEND 13	Gneiss	20	0.3250(3401)	0.4060(4248)	20%	0.1386(9594)	195.4±5	4.89	13.8±0.13	1.37	120
VEND 16	Metarhyolite	12	0.1020(222)	0.4072(886)	0.1%	0.1385(9594)	58.7±6	20.91	13.29±0.68	1.36	5
VEND 17	Schist	12	0.0427(142)	0.0538(179)	50%	0.1385(9594)	187.2±25	16.94	12.32±0.23	1.22	28
SPA 2	sandstone	1	0.1734(134)	0.2006(155)		0.1233(8310)	187.6±22*		11.80±0.59	1.76	10
SPA 5	granite	20	0.0856(374)	0.0962(420)	90%	0.1336(9250)	209.0±15	0.03	13.51±0.21	0.98	22
SPA 7	granite	20	0.5728(4625)	1.006(8075)	0.001%	0.1320(9143)	134.9±5	13.80	13.66±0.11	1.12	102
SPA 8	granodiorite	20	0.2126(1435)	0.4551(3072)	0.001%	0.1338(9330)	113.1±6	15.26	11.75±0.18	1.75	100
SPA 10	granite	19	0.2504(1305)	0.3421(1783)	0.001%	0.1339(9330)	175.7±10	17.43	12.63±0.20	1.97	100
SPA 11	granite	20	0.4092(2830)	0.6871(4725)	0.001%	0.1340(9330)	139.6±6	14.05	12.79±0.16	1.61	100
SPA 12	metarhyolite	20	0.2287(1864)	0.2810(2290)	15%	0.1320(9143)	188.7±7	7.58	13.39±0.16	1.59	100
SPA 13	granite	20	0.2218(1334)	0.2372(1427)	0.2%	0.1342(9330)	224.0±12	14.55	13.12±0.16	1.61	100
SPA 14	gneiss	20	0.1138(511)	0.1679(754)	80%	0.1320(9143)	157.8±9	0.03	12.61±0.43	1.91	21
SPA 15	gneiss	20	0.1210(775)	0.1887(1208)	65%	0.1343(9330)	152.0±7	0.08	12.91±0.22	2.16	102
SPA 16	granite	20	0.2987(1598)	0.8744(4678)	0.2%	0.1320(9143)	80.5±3	10.47	12.97±0.23	2.25	100
SPA 17	'felsite' dyke	5	0.4613(927)	0.9210(1851)	0.05%	0.1320(9143)	117.0±5	0.00	13.29±0.48	1.99	18
SPA 18	schists	20	0.1103(376)	0.2930(999)	0.001%	0.1344(9330)	97.2±9	30.14	12.38±0.25	2.36	89
SPA 19	granodiorite	20	0.1829(1835)	0.5155(5173)	0.001%	0.1320(9143)	83.7±3	12.35	13.27±0.15	1.53	100

Sample Number	Lithology	No. of xtls	Spontaneous ρ_s x10^7 (N_s)	Induced ρ_ix10^7 (N_i)	Pχ^2	Dosimeter ρ_dx10^7 (N_d)	FT Central Age Ma (±1s)	Age Dispersion %	Apatite Mean Track Length (μm)	Length Standard Deviation (μm)	No. of Lengths
SPA 20	gabbro	11	0.0808(205)	0.1853(470)	40%	0.1354(9330)	104.3±9	7.07	15.32±0.44	1.78	17
SPA 21	gneiss	20	0.0334(183)	0.0753(412)	96%	0.1346(9330)	105.9±9	0.00	13.06±0.35	1.76	26
SPA 22	granite	20	0.0695(919)	0.1988(2626)	10%	0.1320(9143)	82.4±4	8.40	12.81±0.16	1.68	105
SPA 23	granite	20	0.0997(882)	0.3291(2910)	10%	0.1320(9143)	70.5±3	10.13	12.37±0.21	2.14	105
SPA 24	granite	20	0.1522(1517)	0.3709(3696)	0.001%	0.1346(9330)	98.7±5	18.83	12.24±0.24	2.39	100
SPA 25	granite	20	0.5663(1405)	0.9230(2290)	25%	0.1348(9330)	146.3±5	5.54	13.25±0.22	1.81	105
SPA 26	granite	17	0.05811(331)	0.1392(793)	0.01%	0.1349(9330)	103.6±10	26.96	12.85±0.19	1.92	100
SPA 27	granite	20	0.3232(1438)	0.8137(3620)	60%	0.1320(9143)	93.0±3	4.60	13.23±0.15	1.50	100
SPA 28	granite	20	0.3537(1809)	0.7360(3764)	0.001%	0.1350(9330)	114.6±6	15.89	12.52±0.20	2.03	102
SPA 29	granite	20	0.2231(1249)	0.4347(2434)	0.02%	0.1351(9330)	123.9±6	11.23	12.07±0.18	1.80	105
SPA 30	granite	20	0.0797(569)	0.1586(1132)	10%	0.1320(9143)	117.5±8	14.77	11.76±0.42	2.61	39
SPA 31	granite	18	0.0754(346)	0.1877(861)	0.001%	0.1352(9330)	98.2±12	39.59	12.54±0.41	1.95	24
SPA 32	granite	20	0.0735(670)	0.1508(1375)	0.02%	0.1320(9143)	114.8±8	18.67	12.98±0.17	1.74	100
SPA 33	sandstone	1	0.0548(76)	0.1130(156)		0.1320(9143)	116.7±16*		No lengths		
SPA 36	conglomerate	17	0.0132(82)	0.0681(424)	99%	0.1320(9143)	45.4±5	0.00	14.47±0.78	2.21	9
SPA 38	sandstone	20	0.0995(414)	0.5620(2337)	30%	0.1320(9143)	41.6±2	0.41	12.71±0.75	2.70	14

NOTES.

i). Ages marked * are calculated from single apatite crystals, and should be treated with caution.

ii). Ages are calculated with zeta-factor of 356±6

iii). N_s is the number of spontaneous fission tracks; Ni is the number of induced fission tracks and Nd is the number of tracks on the dosimeter. Similarly ρ refers to the track densities in the crystals and dosimeters.

from the southern coast. Therefore, another minor trend of decrease in apatite age occurs moving northwards across the Armorican Massif from the Bay of Biscay coast to the English Channel. The youngest ages encountered are derived from two samples from the Picos de Europa, samples SPA 36 and 38, giving mid Eocene ages.

The track length data are similar over the study area. The distributions are broader than expected from rapid cooling, (σ > 1.5 μm) and the MTLs are somewhat shorter than expected from an 'undisturbed basement' type cooling model (Gleadow et al., 1986b). The mean track lengths range between 9.44 ± 0.47 μm (BRET 30) and 15.32 ± 0.44 μm (SPA 19). These two end-member values are, however, outliers, based on a low number of length measurements, and the MTL for the majority of the samples is between 11 and 13 μm. The shortest MTLs are encountered in the Armorican Massif, particularly in Brittany (around 10 - 12 μm; lengths for Normandy and Vendée are around 0.5 - 1 μm longer). The Spanish MTLs are in the range 12 - 15 μm. The appearance of track lengths longer than 16 μm is rare.

Detailed description and interpretation of the data is presented for separate regions because of the diversity of apatite fission track age and tectonic environment of each area. However, there is no apparent link between geological structures and the apatite fission track data. The exception to this is in the Picos de Europa region where there is reactivation of Variscan nappes and fault systems (i.e. the Ventaniella Fault; Garcia-Mondéjar, 1989) at the time of rifting and opening of the Bay of Biscay, and probably a second reactivation involved with the Pyrenean Collision episodes (Ziegler, 1990).

4.4.2 Variscan basement adjacent to the Bay of Biscay and the North Atlantic.

The majority of samples come from the Variscan basement exposed on the southern coasts of the Armorican Massif, and the northern coast of Spain; samples BRET 8 - 19, VEND 1 - 17 and SPA 5 - 32. Although most of the rocks are Variscan or older in age, they have been structurally juxtaposed by the opening of the Bay of Biscay.

The fission track ages range from 267±19 Ma to 71±3 Ma. The younger ages are found in the west of Finistérre, Brittany and north-west Galicia, whilst the oldest are from Vendée. The ages can be subdivided into three groups, moving westwards across the region from Vendée to Galicia. The Vendéean samples have 'old' ages (187±25 Ma to 267±19 Ma); in southern Brittany and northern Spain, the ages are late Triassic - Early

Cretaceous (226±18 Ma to 135±6 Ma); and in western Galicia the ages are upper Cretaceous (118±8 to 71±3 Ma).

The radial plots of the Vendée, southern Brittany and northern Spain data show that there is often a considerable spread in SGA with the oldest ages being around Carboniferous and the youngest ages being mid-Cretaceous. The individual grains are, however, generally within 2 σ error of each other. The younger ages from western Galicia have single grain age distributions ranging from mid-Cretaceous to Palaeogene with no evidence of older 'Variscan' ages. Many samples fail the χ^2 test and have high age dispersions, often between 10 to 20 %. This is rather unusual for crystalline basement rocks which are generally assumed to have homogenous chemistry, and obviously no variation in provenance.

The track length distributions have mean track lengths in a range of 11.50 µm to 15.32 µm. This latter value is based on only 17 length measurements, and is imprecise. Apart from this value, the longest MTL in this group of samples is 13.80 µm. The distributions are dominantly symmetrical with standard deviations in the range of 1.5 to 2.5 µm. A weak negative skew is apparent in most samples. Samples BRET 27 - BRET 30 have a weakly bimodal distribution.

An anomalously young age from the Bay of Biscay coast of the Armorican Massif is from sample VEND 16 (59±6 Ma), a metarhyolite. This is particularly incongruous as it is surrounded by some of the oldest ages encountered. Unfortunately the low uranium content of this sample allowed only the measurement of 5 track lengths for this sample.

The data for this region are summarised on **Figure 4.12** and the radial plots and track length histograms are on **Figures 4.13** and **4.14**.

4.4.3 Cadomian and Variscan basement adjacent to the English Channel and Western Approaches Basins.

Samples from the North Coast of the Armorican Massif, including Brittany, Normandy and the Channel Islands are numbered JER 1, BRET 1 - 6, BRET 24 - 30 and NOR 1 - 16. This is the Cadomian Massif, and many of the rocks sampled are of Precambrian stratigraphic age, with the exception of the external Variscan granites. The Western Approaches and English Channel basins lie on submerged continental shelf to the north of the massif. Although involved in the incipient Triassic breakup of the North Atlantic region, extension in this region never progressed beyond the rifting and subsidence stage. Therefore the tectonic environment responsible for the formation of this margin was different from that forming the southern Armorican Margin. In spite of this, the data analysed

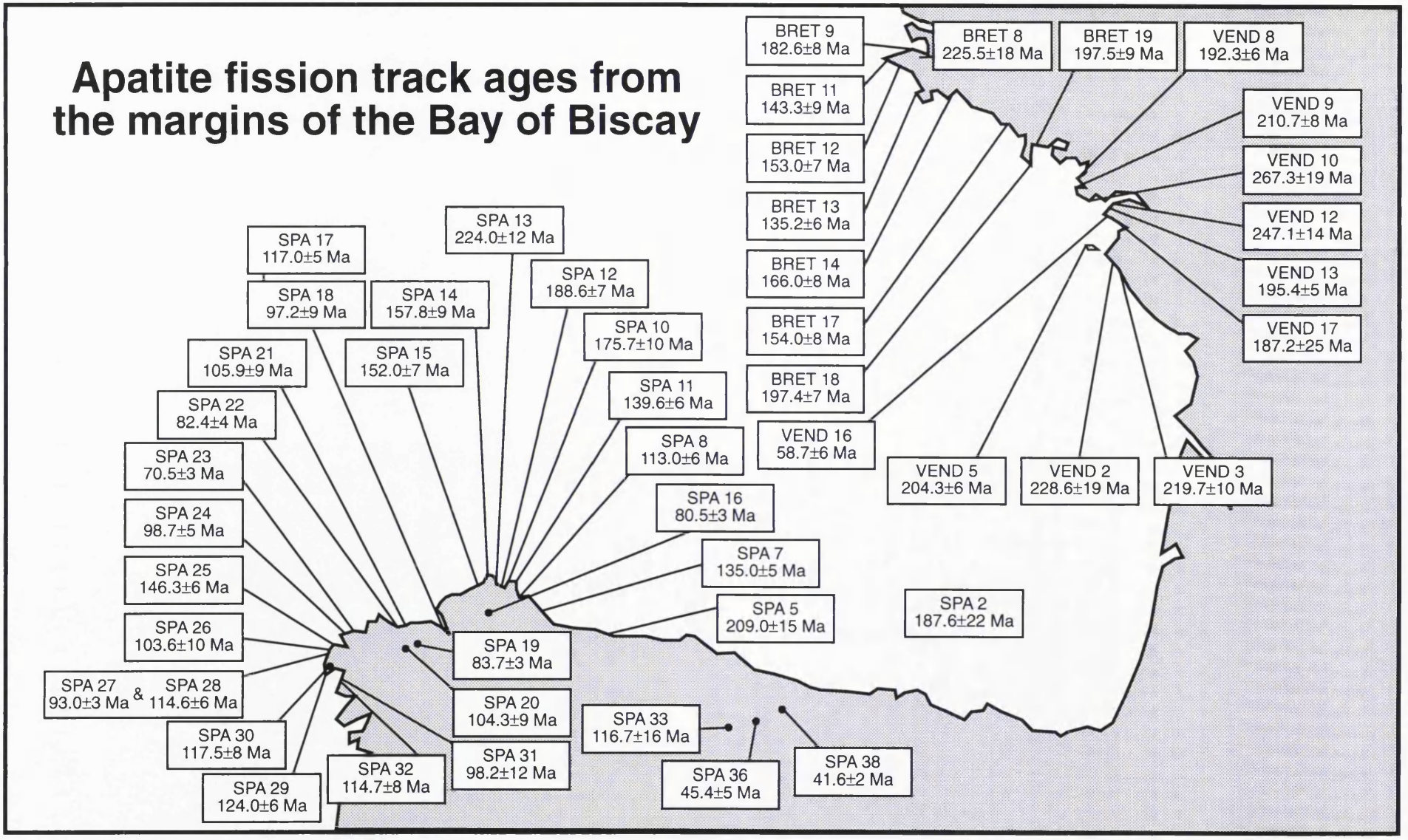

Fig. 4.12. Apatite fission track ages from the continental margins of the Bay of Biscay.

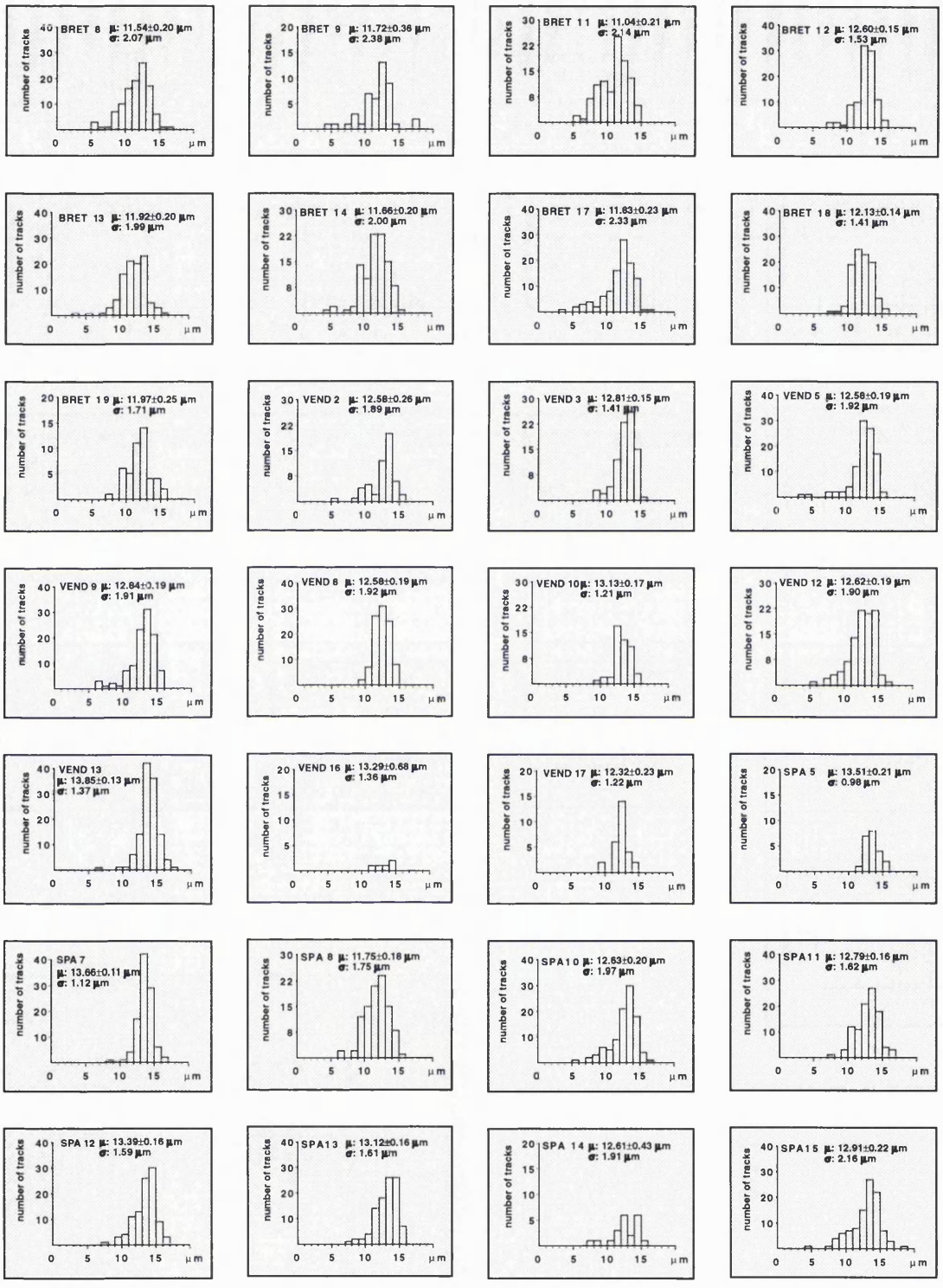

Fig. 4.13a. Confined track length histograms for samples from the French and Spanish coasts of the Bay of Biscay. An inset map showing the location of these samples is illustrated on fig. 4.13b (regions 1 and 2).

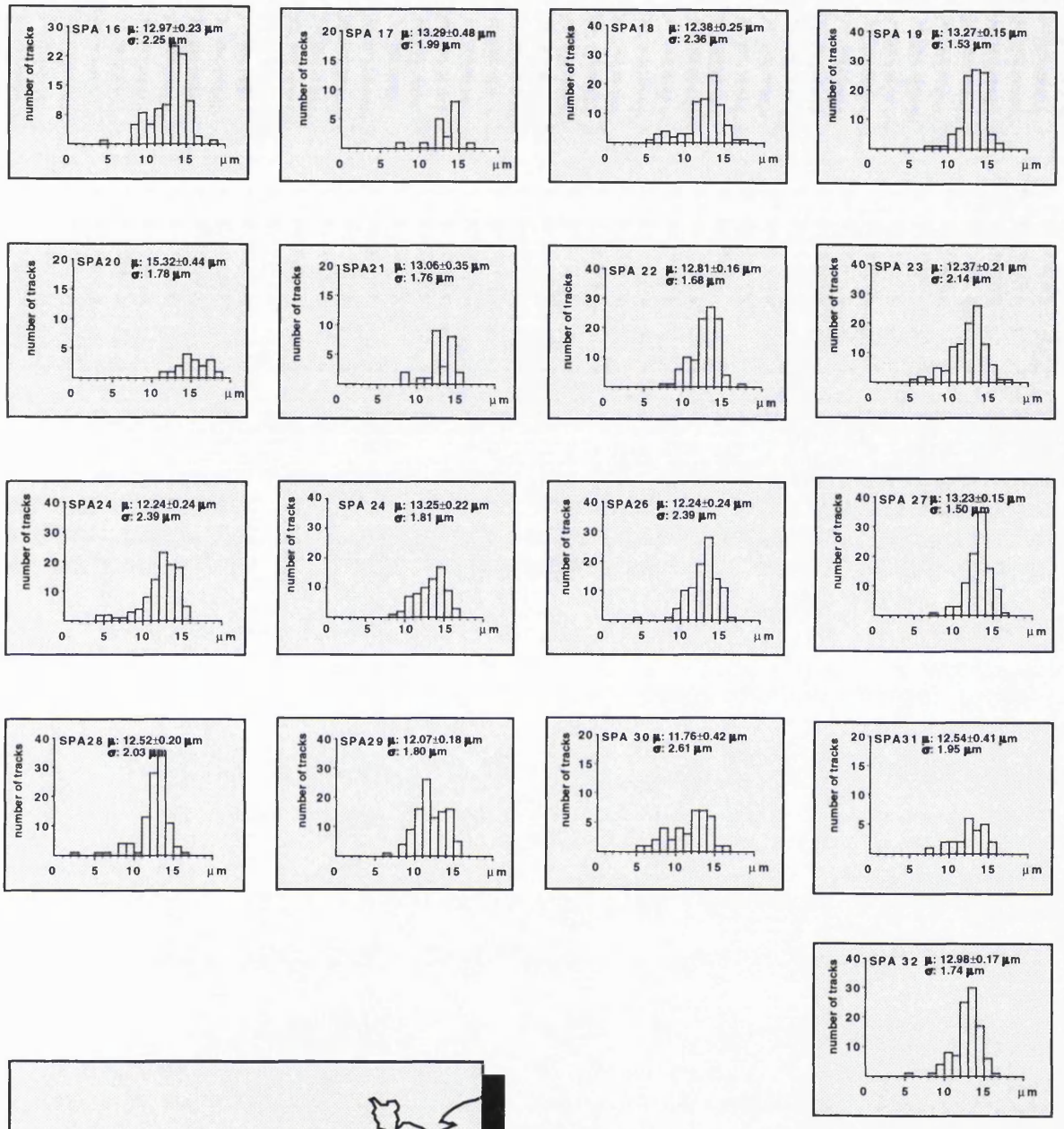

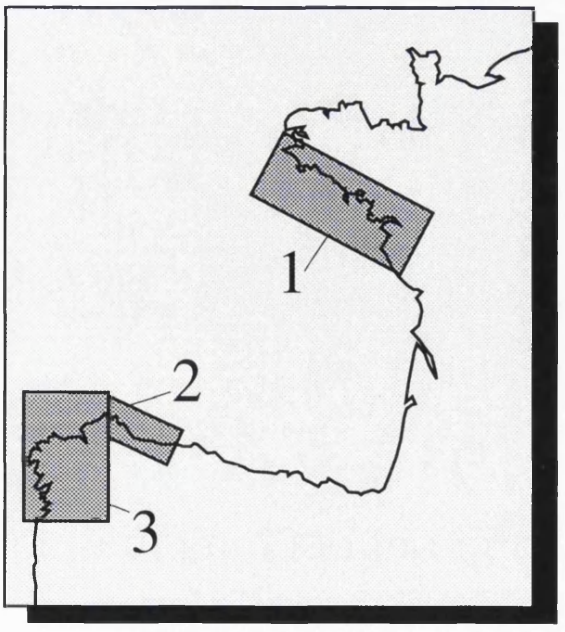

Fig. 4.13b. Track length histograms of samples from the continental margins of the Bay of Biscay. The histograms on this page are from the region 3 on the inset map.

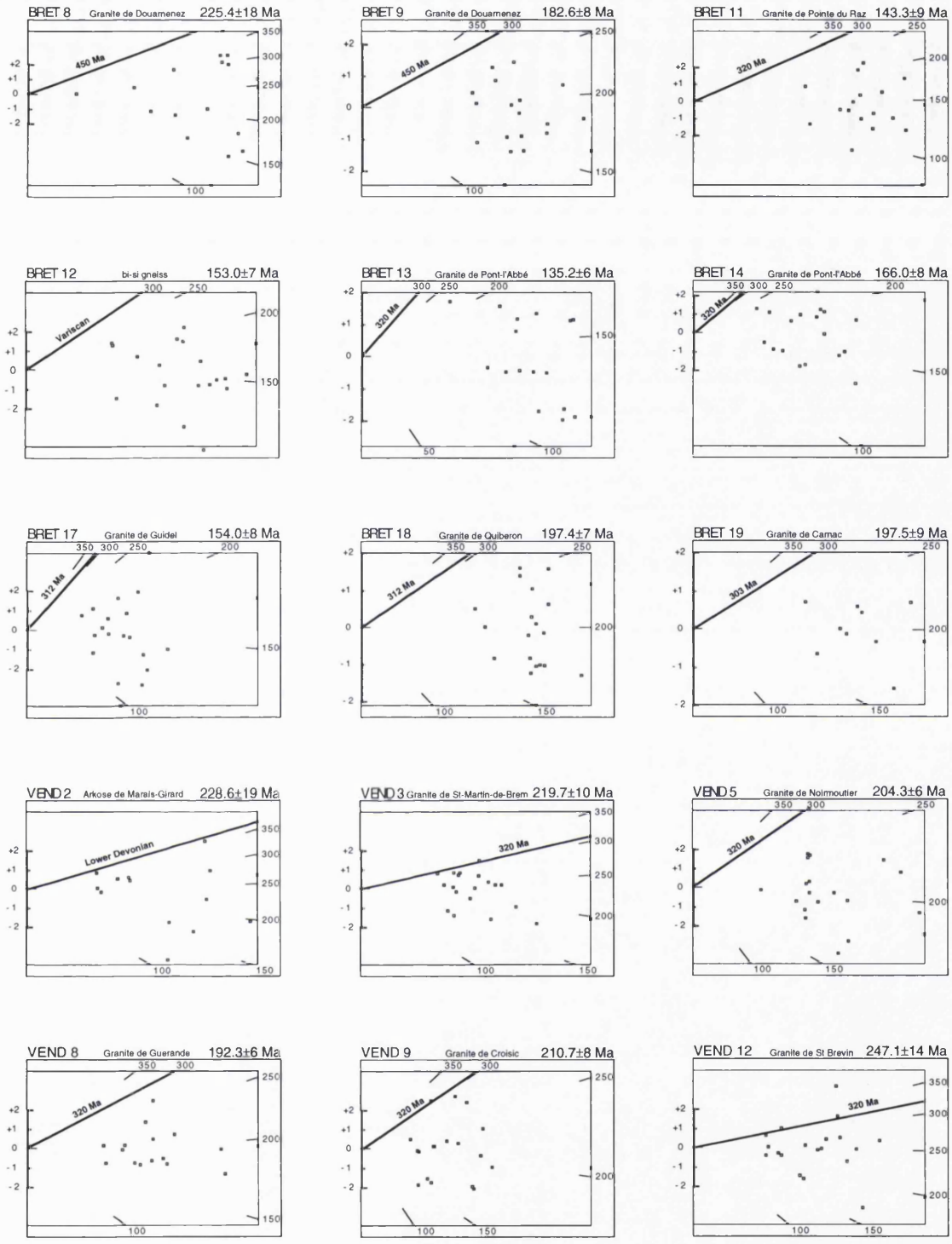

Fig. 4.14a. Radial plots of apatite fission track single grain ages from the continental margins of the Bay of Biscay. The stratigraphic age is marked by a solid line and the apatite fission track central age is on the top right hand side.

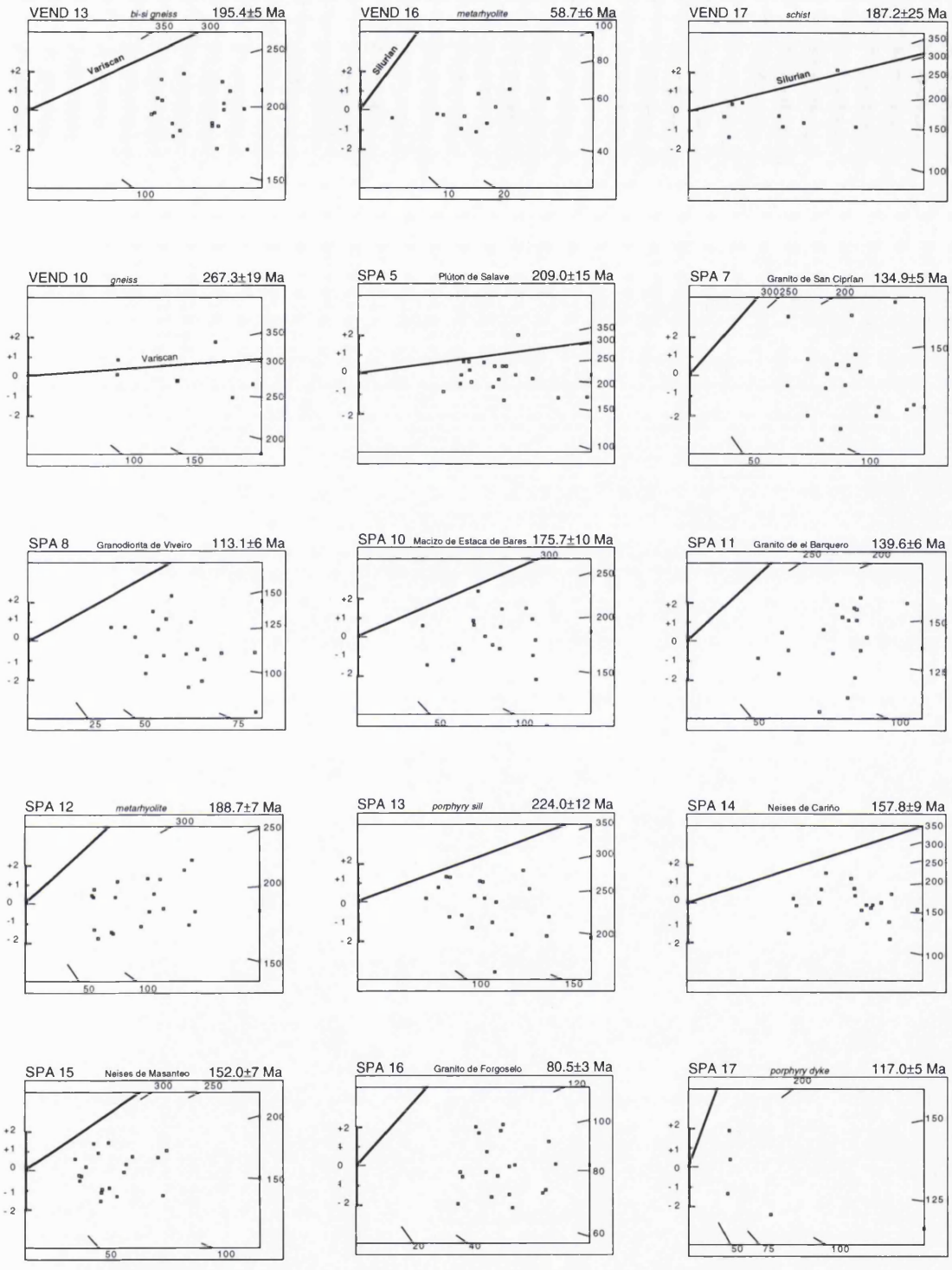

Fig. 4.14b. Radial plots of apatite fission track single grain ages from the continental margins of the Bay of Biscay. The stratigraphic age is marked by a solid line and the apatite fission track central age is on the top right hand side.

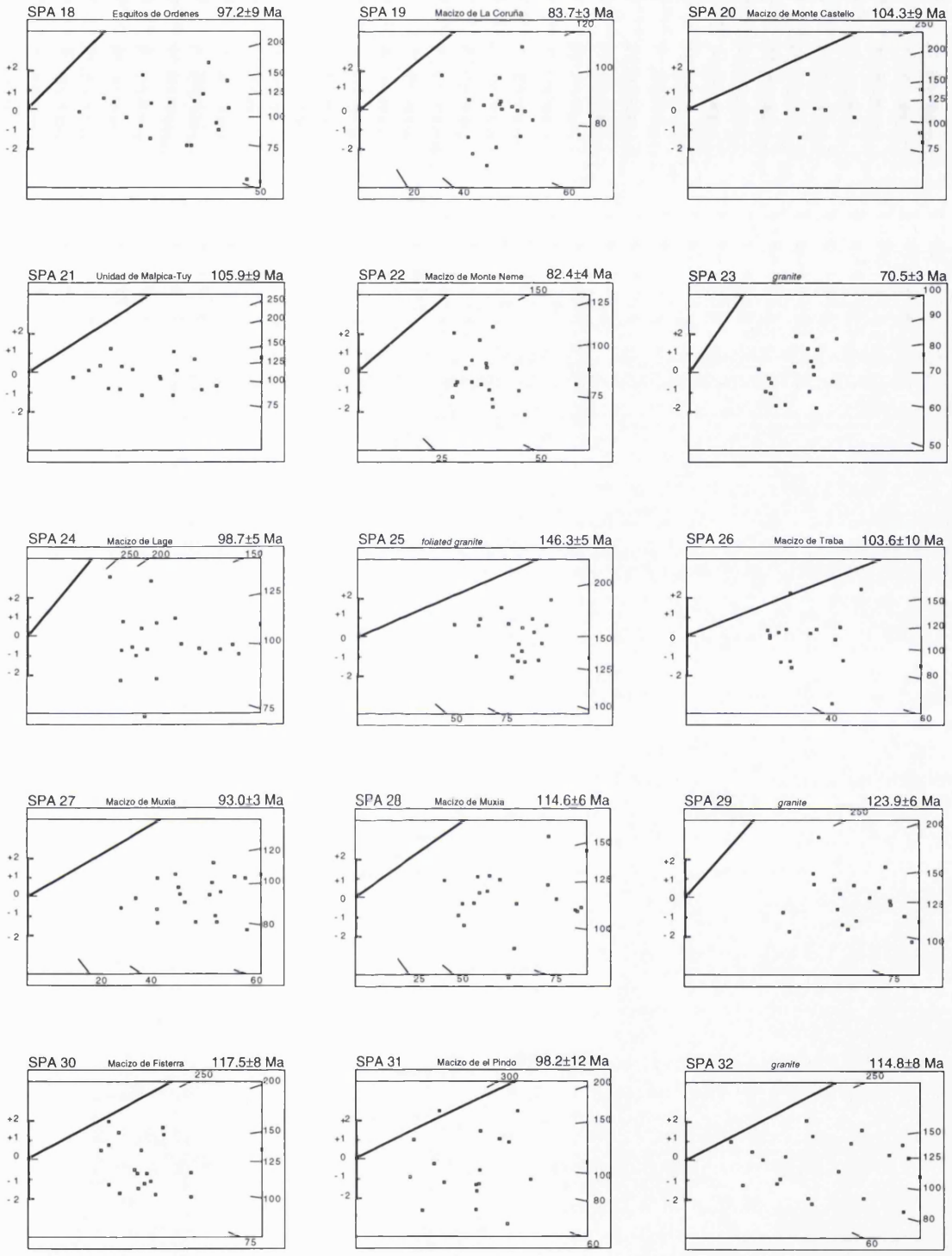

Fig. 4.14c. Radial plots of apatite fission track single grain ages from the continental margins of the Bay of Biscay. The stratigraphic age is marked by a solid line and the apatite fission track central age is on the top right hand side.

from this region are very similar to those from southern Brittany and Vendée.

Apatite fission track apparent ages range between 131±9 Ma to 235±17 Ma. There is no particular trend in this data except that the younger ages are derived from the western coast of north Finistérre.

On a radial plot, single grain ages spread between Variscan and mid to upper Cretaceous. The grains are generally within 2 σ error of each other. Like the data from the Bay of Biscay coast, many samples have an age dispersion of 10 to 20 %.

The track length data fall into two groups. Those from the northern Brittany have broad distributions (standard deviations of greater than 2.5 μm) with mean track lengths of between 9.44 μm and 12.42 μm, the majority being ~11 μm. Unannealed long (> 16 μm) confined track lengths are rare. The shortest lengths encountered are 3 to 5 μm and distributions often have a negative skew, but this is not pronounced. Some of the samples exhibit weakly bimodal distributions.

Samples from Normandy and the Channel Islands have similarly shaped distributions with significantly longer mean track lengths ranging from 11.85 μm to 13.2 μm. Ages for this region are plotted on **Figure 4.15** and their track length distributions and radial plots are plotted on **Figures 4.16** and **4.17.**

4.4.4 The Asturian Arc.

These samples were collected along a transect across the core of the Asturian Arc from the edge of the Central Coal Basin, across the Ponga Nappe and to the south of the carbonate Picos de Europa to the Mesozoic onlap to the east of the Variscan foreland nappes (see Fig. 2.16). Unfortunately, only four of the eleven samples yielded apatites (SPA 2, SPA 33, SPA 36 and SPA 38). Two of these produced insufficient apatite yields to give a statistically reliable age, and track length measurements were limited for all of the samples. SPA 36 and 38 produced mid-Eocene ages (45±6 Ma and 42±2 Ma respectively), within error of each other, The fission track ages were calculated on rocks of Ordovician and Permo-Triassic stratigraphic ages. The radial plots both showed the single grain ages to be within 1 σ error of each other with a range in singles grain ages for both samples being from 23 Ma to 63 Ma. Both ages had low age dispersions (0.00 % and 0.41 % respectively). One crystal gave an anomalously old age of 97 Ma. Track length measurements from the crystals were sparse. The mean track lengths of 14.47±0.78 μm and 12.71±0.75 μm are not precise as both were the result of few measurements (only 9 and 14 tracks respectively). SPA 2 yielded only

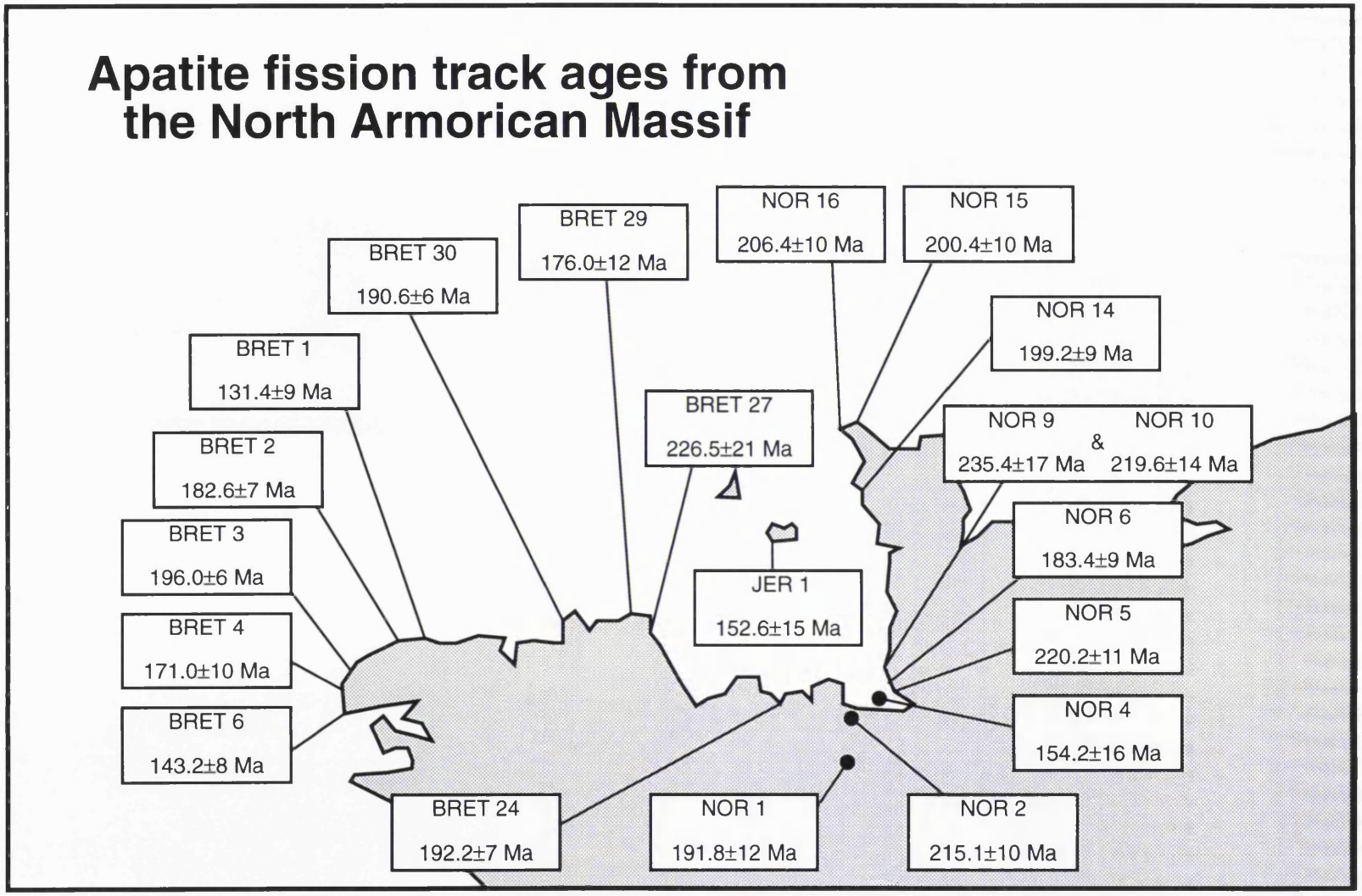

Fig. 4.15. Apatite fission track ages from the North Armorican (Cadomian) Massif.

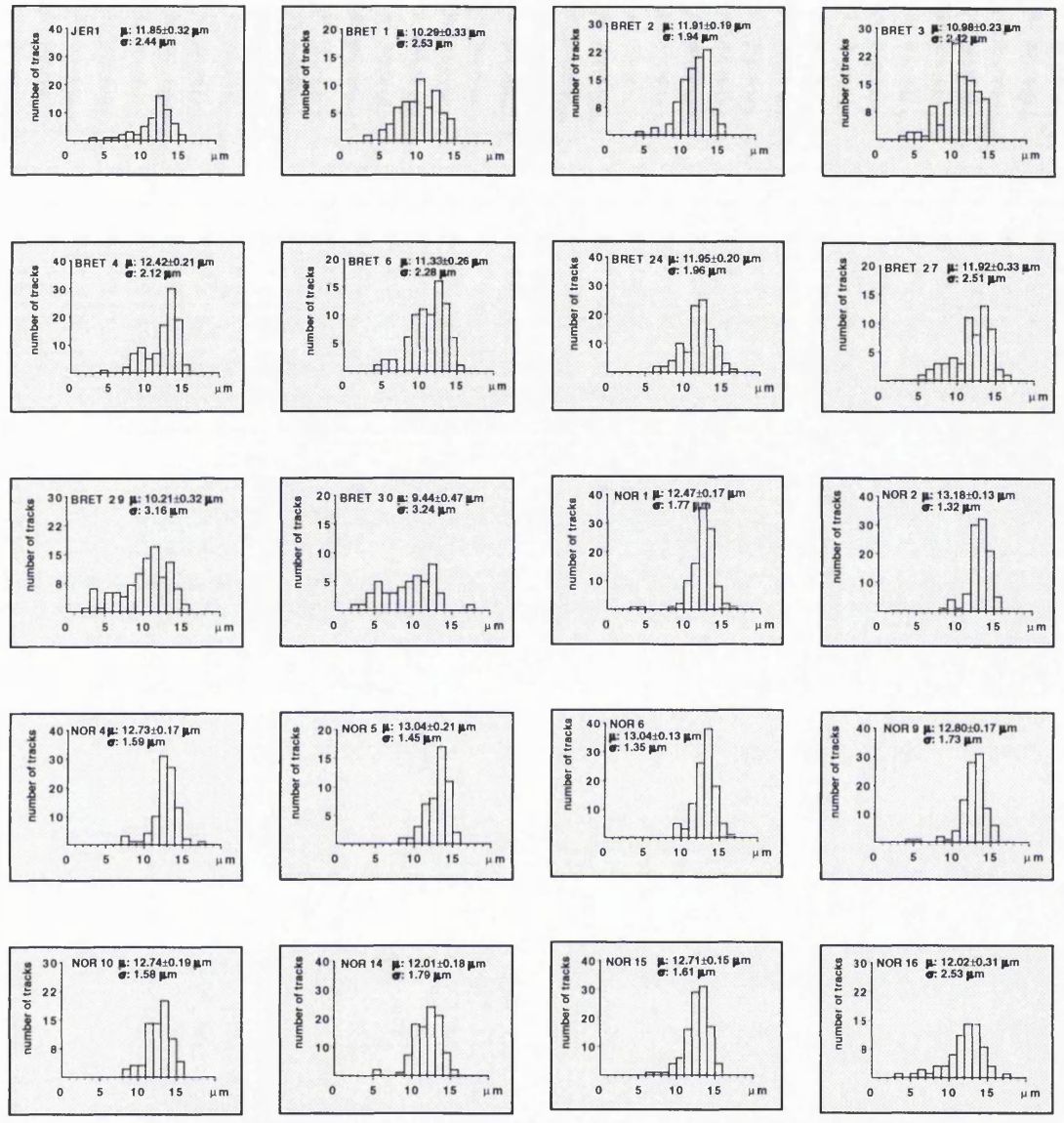

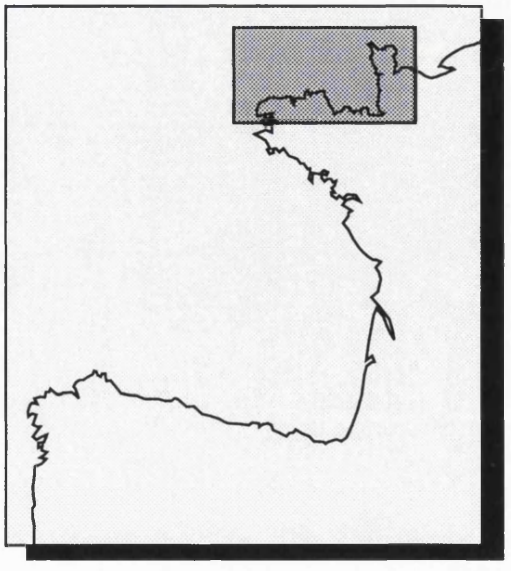

Fig. 4.16. Apatite fission track confined length histograms for the samples from the English Channel - Western Approaches coast of the Armorican Massif. Inset map (left) shows the area of collection of these samples.

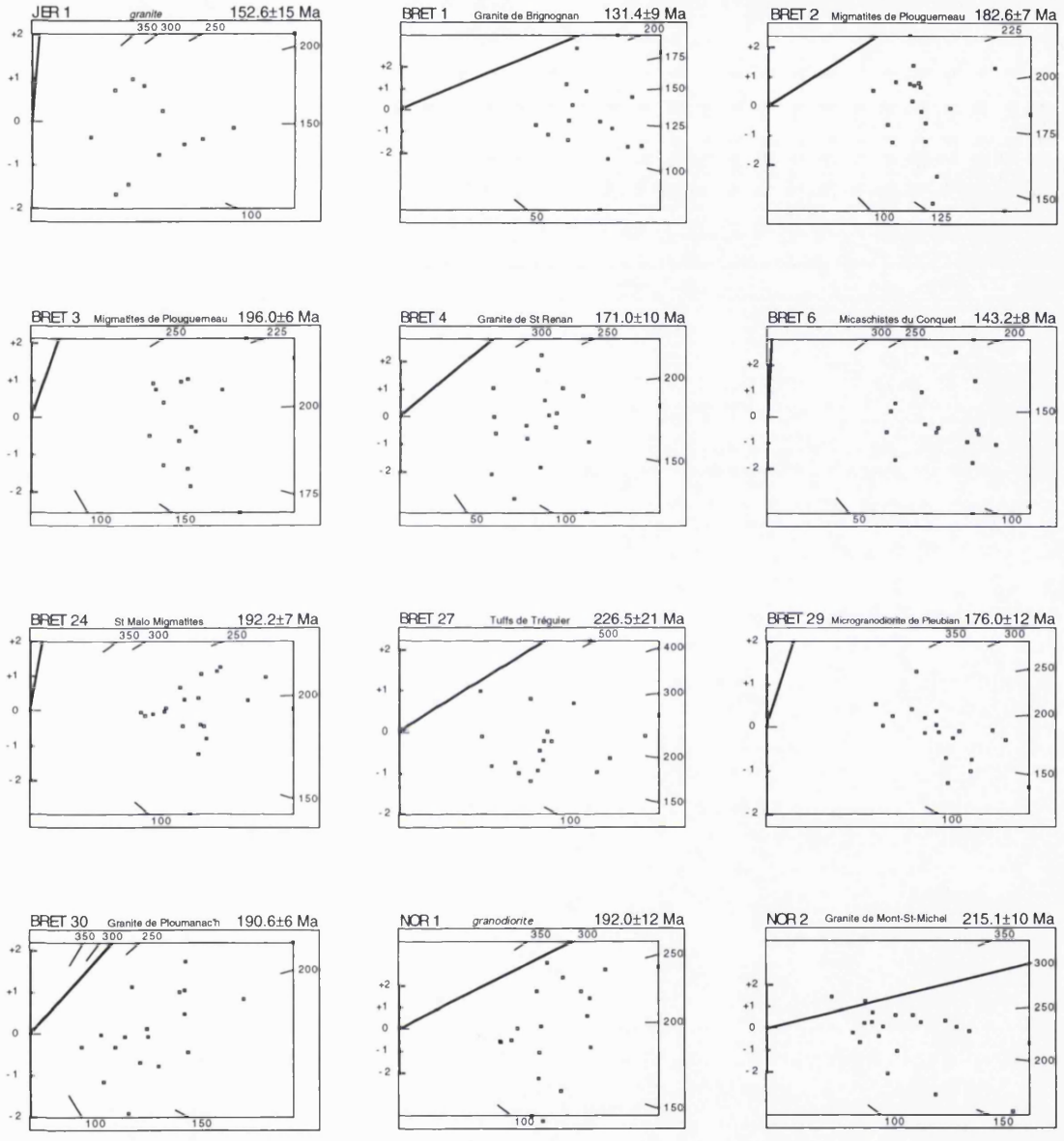

Fig. 4.17a. Radial plots of apatite fission track single grain ages from the northern margin of the Armorican Massif. The stratigraphic age is marked by a solid line and the apatite fission track central age is on the top right hand side.

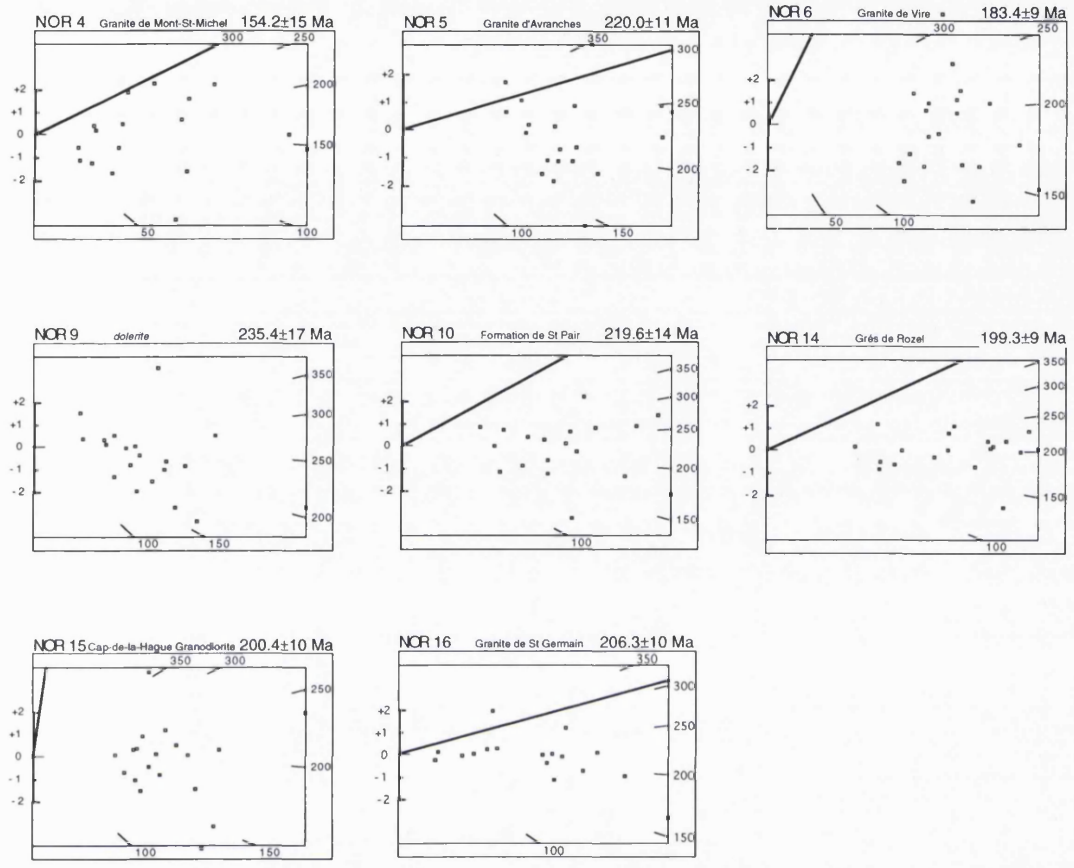

Fig. 4.17b. Radial plots of apatite fission track single grain ages from the margin of the Armorican Massif. The stratigraphic age is marked by a solid line and the apatite fission track central age is on the top right hand side.

one crystal which gave a lower Jurassic age This lone crystal however yielded ten track lengths with a mean of 11.80±0.59 μm. The same is true for SPA 33 which yielded a mid-Cretaceous age.

Radial plots and track length histograms for these samples are presented on **Figure 4.18**.

4.5 Discussion.

The data show a variation in apatite fission track apparent ages from Lower Permian (Rotliegendes) to Mid Eocene. All the ages are younger than the formation age of the crystalline basement sampled which has Palaeozoic or older formation ages. A first conclusion is that these fission track ages have no relation to the time of formation of the rocks from which they were sampled.

Many of the rocks sampled, especially those from granitic rocks, have a high uranium content giving large values for spontaneous track densities and induced track densities (generally between 2×10^6 and 1.2×10^7 tracks cm^{-2}). For the majority of samples analysed in this thesis, ρs is of the same order of magnitude as ρi and is often a similar value. This causes problems with counting as it is often difficult to determine the number of tracks present as many will intersect the surface of the crystal at effectively the same point. It is postulated that this may have been the basis for some of the large single grain age spreads, causing the samples to fail the χ^2 test and have age dispersions greater than 10 %. This hypothesis was tested by plotting uranium content, in the form of ρi, against age dispersion for all the samples. This graph is shown in **Figure 4.19.** It can be seen that there is a scatter of points with no clear trend of any sort relating error to a high ρi. The seeming random nature of these data indicate that there is no human error associated with high uranium density in the samples.

The entire data set is summarised on **Figure 4.20** and **Figure 4.21.** On both maps, the positioning of the 'contours' separating the age or length groups are arbitrary, representing broad groupings rather than precise ones. Figure 4.20 demonstrates the broad trend of decrease in age towards and parallel to the Mid Atlantic Ridge. The region of westernmost Galicia, where the apatite fission track ages are Upper Cretaceous, forms a discrete region with no samples having apparent ages older than 120 Ma. However, the transition from this region to the north is abrupt. The region of the northern Central Iberian Zone has ages from 113-224 Ma and this region appears to compare with that of western Brittany, where the ages are from 131-226 Ma. Both regions are characterised by broad age range. To the east, the ages increase. All the samples yielded apparent ages in the range 180 to

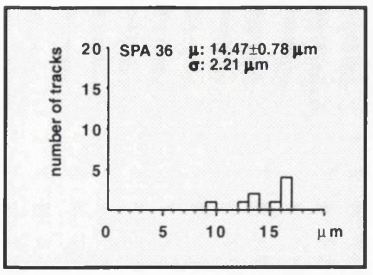

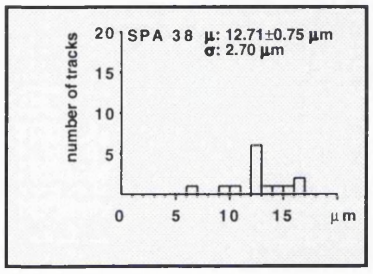

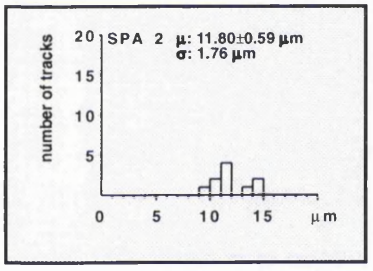

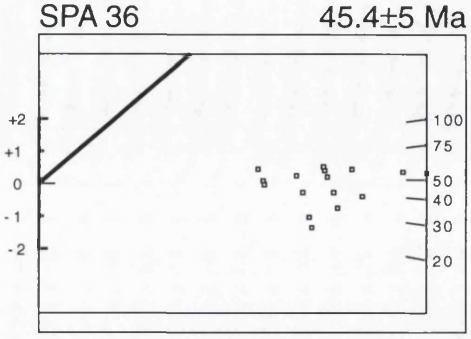

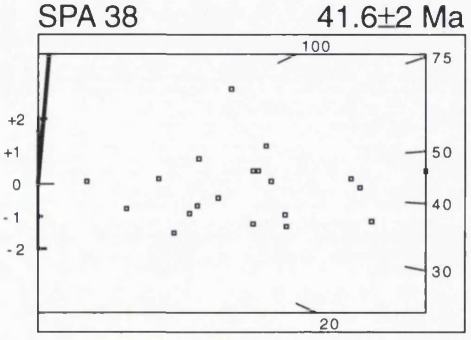

single grain age only = **116 ± 16 Ma**

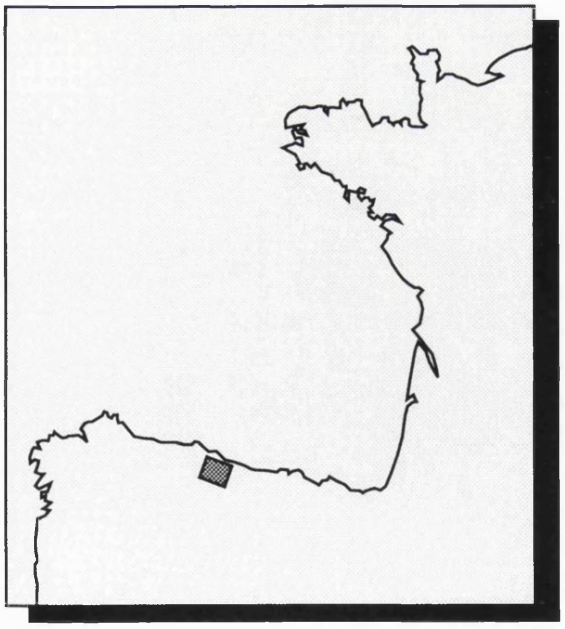

Fig. 4.18. Apatite fission track ages, radial plots and confined track length histograms from the Asturian Arc. The region is shown on the inset map.

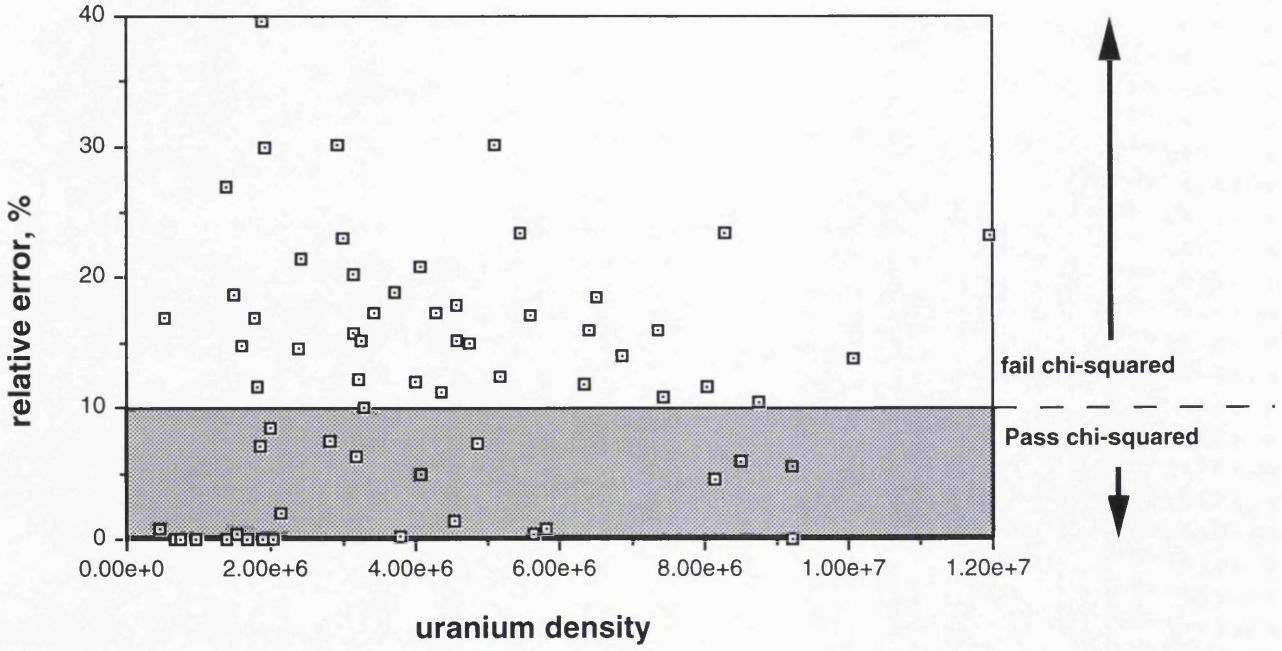

Fig. 4.19. A graph of uranium contents of apatites (ρi) versus age dispersion for all the apatite samples analysed. An age dispersion of 10% approximates to a failure of the chi-squared test.

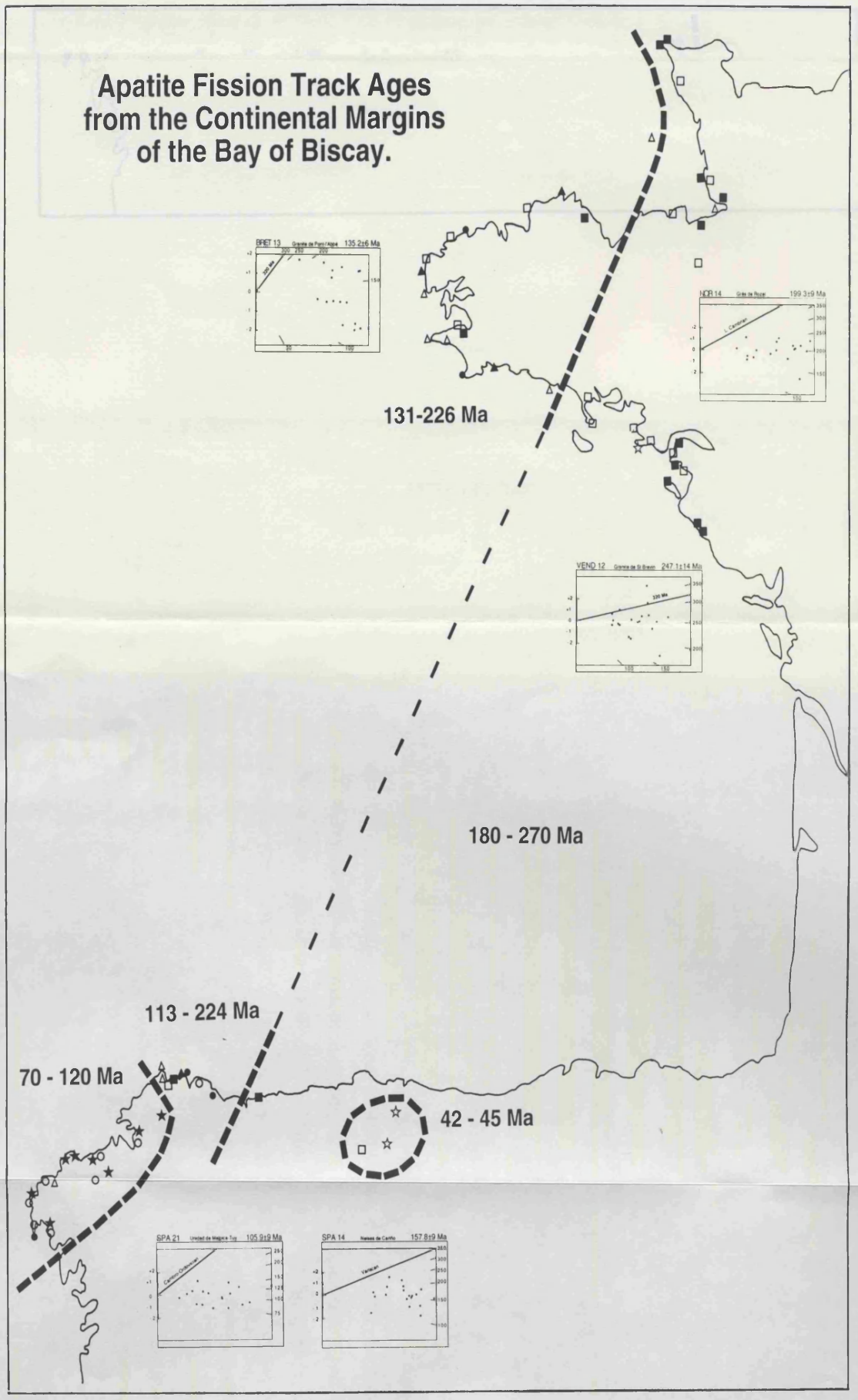

Fig. 4.20. All apatite fission track ages plotted on a map of the Bay of Biscay region, showing major age groups arbitrarily divided and selected representative radial plots. Key: black stars, <100 Ma; white circles, 100-120 Ma; black circles, 120-140 Ma; white triangles, 140-160 Ma; black triangles, 160-180 Ma; white squares, 180-200 Ma; black squares, > 200 Ma.

Fig. 4.21. All apatite confined track lengths measurements from the continental margins of the Bay of Biscay, with selected representative length distributions. Symbols represent the mean track length. Key: black stars, <10.5 µm; white stars, 10.5-11.0 µm; black circles, 11.0-11.5 µm; white circles, 11.5-12.0 µm; black triangles, 12.0-12.5 µm; white triangles, 12.5-13.0 µm; black squares, 13.0-13.5 µm; white squares, > 13.5 µm.

270 Ma. Despite the seemingly large age range, only three of these ages are greater than 230 Ma (NOR 9, VEND 12, VEND 10). It is not possible to incorporate the anomalously young ages from samples collected in the elevated region of the Picos de Europa.

The map illustrating the trends in mean track length values (Fig. 4.21) shows a similar trend with lengths increasing eastwards. The shortest track lengths are found along the north-western coast of Brittany, with them becoming progressively longer across the Armorican Massif. The samples from the Hesperian Massif all have track lengths greater than 12 μm. The mean track lengths from the Asturian Arc region are estimated from far too few measurements to be regarded as reliable in any way. The 'contours' on the mean track length data are not parallel to the Mid Atlantic Ridge, but in the North Armorican Massif, shorter lengths occur in the region of the Western Approaches margin of the massif.

4.6 Summary.

The samples for fission track analyses were collected on a reconnaissance basis from the west-central margins of continental Europe, surrounding the Bay of Biscay, and from the French coasts of the English Channel. The rocks collected were from basement complexes and their sedimentary cover, with stratigraphic ages from Upper Proterozoic to Permian.

The apatite fission track results represents a range in apparent ages from Lower Permian (Rotliegendes) to Mid Eocene, with track length distributions indicating a more complex thermal history than simple monotonic cooling of the Variscan basement. The mean track lengths are mostly between 11 and 13 μm. The distributions are broadly symmetrical about these means, with a small negative skew.

There is a strong regional trend in the data with fission track ages decreasing moving westwards across the Bay of Biscay region towards the Atlantic Ocean. There is a second minor trend moving from south to north across the Armorican Massif, with a decrease in ages from the Biscay to English Channel coasts.

Chapter 5.

A quantitative interpretation of the data from the Armorican and Hesperian Massifs.

5.1 Introduction.

In Chapter 4, apatite fission track data for the continental margins of the Bay of Biscay were presented as a distribution of single grain ages (in the form of radial plots), a central age (weighted means of these distributions) and track length histograms. These data were discussed in terms of the shapes and limits of these distributions and their geographical distribution. This chapter aims to interpret the data by knowledge of the regional geology, combined with the current understanding of the geological controls of thermal annealing of fission tracks in apatite and comparisons with patterns of data from other fission track studies, reviewed in Chapter 3.

Numerical annealing models constrained from laboratory timescale (less than 1 year) experiments, involving an extrapolation over 10^6 to 10^8 orders of magnitude in time provide a complimentary approach to the interpretation of apatite fission track data. Mathematical representations of fission track annealing are incorporated into computer simulations, providing predictive or data-driven models of thermal history (Laslett et al., 1987).

5.2. The annealing of fission tracks in surface exposed samples.

At temperatures greater than ~ 60 - 120°C over geological time (1 to 10 Myr), fission tracks in apatite become unstable and anneal. In samples cooling from temperatures >120°C, fission tracks accumulate whereas during the heating of samples into this temperature window, known as the partial annealing zone (PAZ), pre-existing tracks will shorten to a degree determined by the maximum temperature reached, resulting in erasure if these temperatures attain >120°C*. In general, the regional temperature field is primarily controlled by heat flow from depth.

Calculation of heat flow (units, mW m^{-2}) depends on a variety of factors including lithology, textural relationships, fracturing, porosity and fluid flow. In view of these complex factors, geothermal gradient has become a more routinely used concept, representing the mean value of

*Some annealing may occur at all temperatures (see Wagner and van den Haute, 1992).

change in crustal temperatures over a vertical distance. Geothermal gradient is related to heat flow by equation (5.1):

$$\text{Geothermal gradient} = \frac{\text{Heat flow}}{k} \qquad (5.1)$$

The constant, k is the thermal conductivity of rocks which commonly varies between 1 and 6 W $m^{-1}K^{-1}$ (typical values for uncompacted shales and low porosity quartzite respectively), depending upon lithological properties of particular rocks. On average, k approximates to 2-3 W $m^{-1}K^{-1}$ (Sclater et al., 1980) and these values can be used to estimate a mean crustal geothermal gradient. Although commonly used for fission track data interpretation, the geothermal gradient has little physical meaning being a mean estimation of heat flow variation based on mean properties of mean lithologies. The average geothermal gradient for the upper crust is generally assumed to be 30°C km^{-1} derived from an average crustal heat flow of 59 mW m^{-2} (Sclater et al., 1980). These values delineate an average depth for the apatite PAZ (60-120°C) of between 2 to 4 km. **Figure 5.1** summarises the variation in geothermal gradient in differing tectonic settings.

When constructing an informative thermal history from apatite fission track data, the shape of the track length distribution is the important key to understanding thermal perturbations, as each track length shortens to a length dictated by the maximum temperature attained since its formation. However, fission track data are initially interpreted in terms of temperatures. To convert these temperatures to estimates of burial and exhumation thicknesses requires inference of a geothermal gradient.

5.2.1 Cooling and exhumation of samples.

Radiometric dating methods have often been used to calculate cooling trajectories. The phenomena of closure temperature varying in different minerals (Dodson, 1973), whereby a mineral's radiometric clock will start after that mineral has cooled through a temperature (specific to the mineral and the radiogenic system) has been widely used to determine cooling rates and infer uplift rates (e.g. Jäger, 1973; Hurford, 1986). Closure temperature is also related to the rate of cooling (Wagner and van den Haute, 1992). Calculation of uplift by isotopic methods uses the simple relationship given in equation (5.2):

$$\text{rate of uplift} = \frac{\text{rate of cooling}}{\text{geothermal gradient}} \qquad (5.2)$$

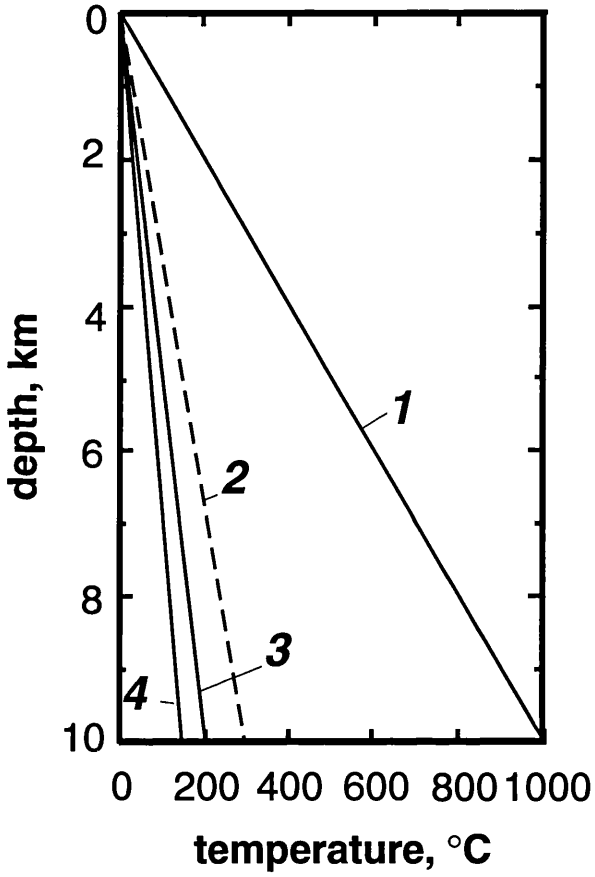

Fig. 5.1. Geothermal gradients calculated assuming a thermal conductivity of 2-3 W m-1 K-1. 1: geothermal gradient of 100°C km-1 for crust younger than 4 Ma, heat flow = 250 mW m-2; 2: Average crustal geothermal gradient of 30°C km-1; 3: geothermal gradient of 20°C km-1 for crust aged between 120 and 140 Ma, heat flow = 46 mW m-2; 4: geothermal gradient for cratonic regions of 15°C km-1, heat flow = <38 mW m-2 (graph compiled from data in Sclater et al., 1980).

This equation assumes that the geothermal gradient was constant throughout the duration of cooling. A cooling curve for a particular rock sample can be constructed by plotting apparent radiometric age against assumed closure temperature of the various dated mineral phases. **Figure 5.2** shows a hypothetical example of a cooling curve from a granite, involving Rb-Sr, K-Ar, zircon and apatite fission track methods. The curve is typical of a magmatic intrusive body, cooling rapidly to the temperature of its host rock, followed by slower, monotonic cooling caused by exhumation. The importance of cooling rate is highlighted in the interpretation of apatite fission track data. A fission track age may represent a monotonic cooling age (as in Fig. 5.2), but in such a case the undisturbed basement confined track length distribution (Gleadow et al., 1986b) would be expected. This is not always the case and in these circumstances the length distribution will provide information relating to the sample's sojourn in the PAZ. The low temperature sensitivity of apatite fission tracks allows for the detection of more complex scenarios at upper crustal levels, where sedimentation resulting in burial, or erosion resulting in exhumation are important geodynamic processes.

Denudation is the exhumation of a landscape as a product of physical and chemical erosion and is influenced by climatic, fluvial, aeolian or glacial surface processes. The resulting creation of topography accentuates the importance of the vertical movements of the Earth's crust which have resulted in precise definitions of the terminology used to define what, until recently, has been described simply as 'uplift' or 'uplift and erosion'.

The tectonically-induced, vertical movement of a landsurface, with respect to a specific datum (usually sea level) is known as *surface uplift*. When isostatic equilibrium is attained during denudation, the upward movement of the rock column with respect to a specific datum, again usually sea level, is termed *crustal uplift* (England and Molnar, 1990). **Figure 5.3** illustrates the principles of these concepts. Crustal uplift will equal surface uplift only if there is no denudation. If denudation does occur, then crustal uplift exceeds surface uplift. If crustal uplift rate is equal to the denudation rate, then there will be no surface uplift. However, in reality, crustal uplift often occurs at a lower rate than denudation and therefore surface elevation is generally reduced rather than increased. As illustrated in **Figure 5.4** it is generally crustal uplift that is important for the interpretation of apatite fission track data gathered from surface exposed samples.

The major, or at least the most readily assessed denudational process is fluvial. Rivers can carry eroded material in the form of sediment

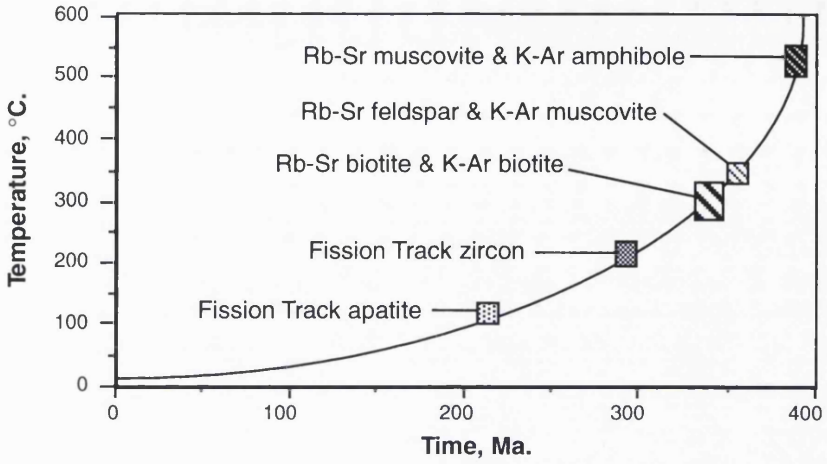

Fig. 5.2. A hypothetical cooling curve showing the closure temperatures for commonly used radiogenic systems (compiled from information in Harland et al., 1989).

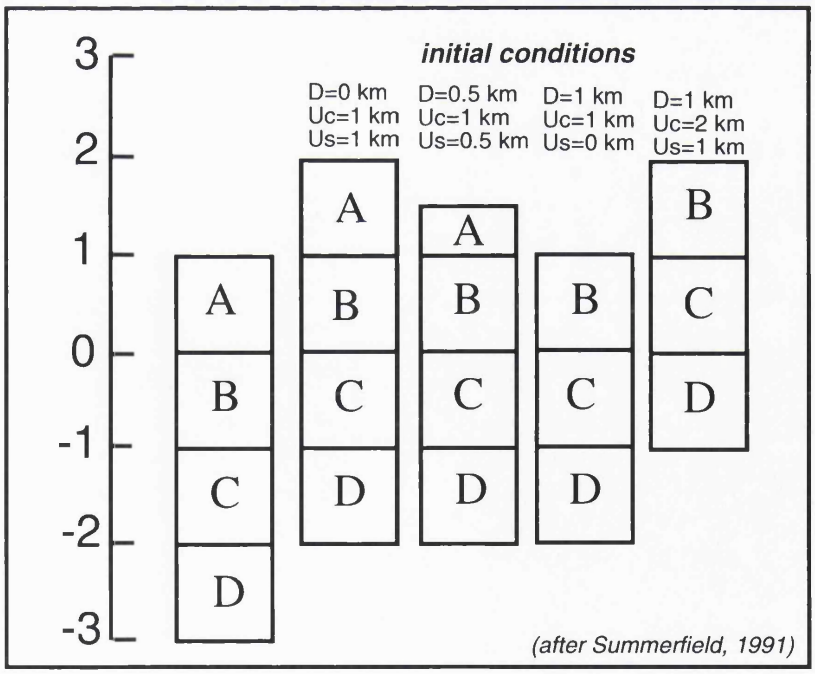

Fig. 5.3. The difference between surface uplift and crustal uplift. D is the depth of denudation, and Uc and Us are the amounts of crustal and surface uplift respectively. If local (Airy) isostasy is maintained, then denudation of a given amount will be accompanied by a crustal uplift of around 80% of the depth of denudation (after Summerfield, 1991).

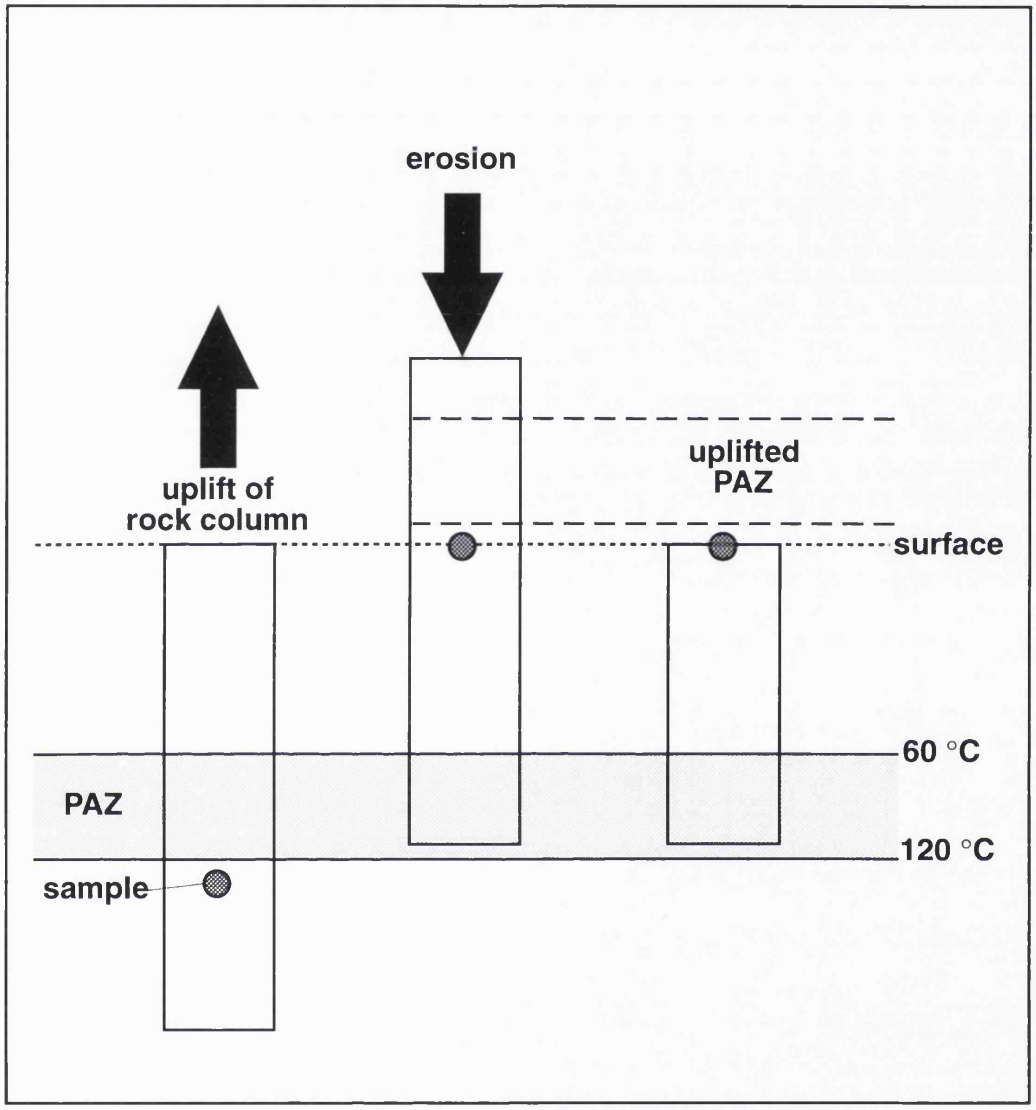

Fig. 5.4. A diagram to illustrate how a sample can be exhumed by crustal uplift, without any major changes in the elevation of the landsurface.

load or as dissolved material (solute load). From studies of Holocene river sediment transport systems an average lowering of the landsurface of 8 mm ka^{-1}* has been estimated (Summerfield, 1991).

Evidence of uplifted partial annealing zones, as in the work of Fitzgerald and co-workers (e.g. Fitzgerald and Gleadow, 1988; Fitzgerald et al., 1991; Foster and Gleadow, 1992; cf. Kamp et al., 1989 and R. W. Brown et al., 1990), shows a distinctive pattern in age distribution reflecting rates and timing of uplift. Such data are derived from analysis of apatite fission track samples collected from extensive vertical profiles in the Transantarctic Mountains and other regions with similar elevation. **Figure 5.5** shows an example of an uplifted PAZ from the Kukri Hills and Mount Doorly regions of the Transantarctic Mountains showing the characteristic dog-leg distribution of ages in relation to elevation. This type of fission track age distribution is comparable with that in boreholes. In surface exposed samples, they exist as the result of rapid exhumation of vertical sections of stable crust (Fitzgerald and Gleadow, 1990). Such regions require a very low rate of denudation for this situation to be preserved. For the most part denudation is a highly active process and the results of crustal uplift are more common. Therefore a more frequently observed situation exhibits a decrease of fission track age with an increase of local elevation (Zeitler et al., 1982).

5.2.2. Heating of samples.

Heating of a rock sample can occur as a result of igneous intrusive and extrusive activity, the result of tectonic activity inducing local temperature increase, as a result of burial and potentially as a result of the circulation of hydrothermal systems. All these situations can lead to the partial or total annealing of fission tracks in apatite and the appearance of reduced ages. Once again, the track length distribution is of primary importance in the interpretation of the data, but, with exception of burial, such resetting mechanisms are frequently on a local rather than regional scale.

5.2.2.1 Thermal effects of magmatic influence.

An obvious geological heat source is from primary magmatic activity. Early recognition of the thermal resetting of fission tracks in apatite was made by Hurford (1977a), on noticing that the Criffel-Dalbeattie granite of the Southern Uplands region of Scotland gave zircon and sphene fission

*mm ka^{-1} is the conventionaly used unit for present day denudation rates. For geological time periods, 1 mm ka^{-1} = 1 m Ma^{-1}.

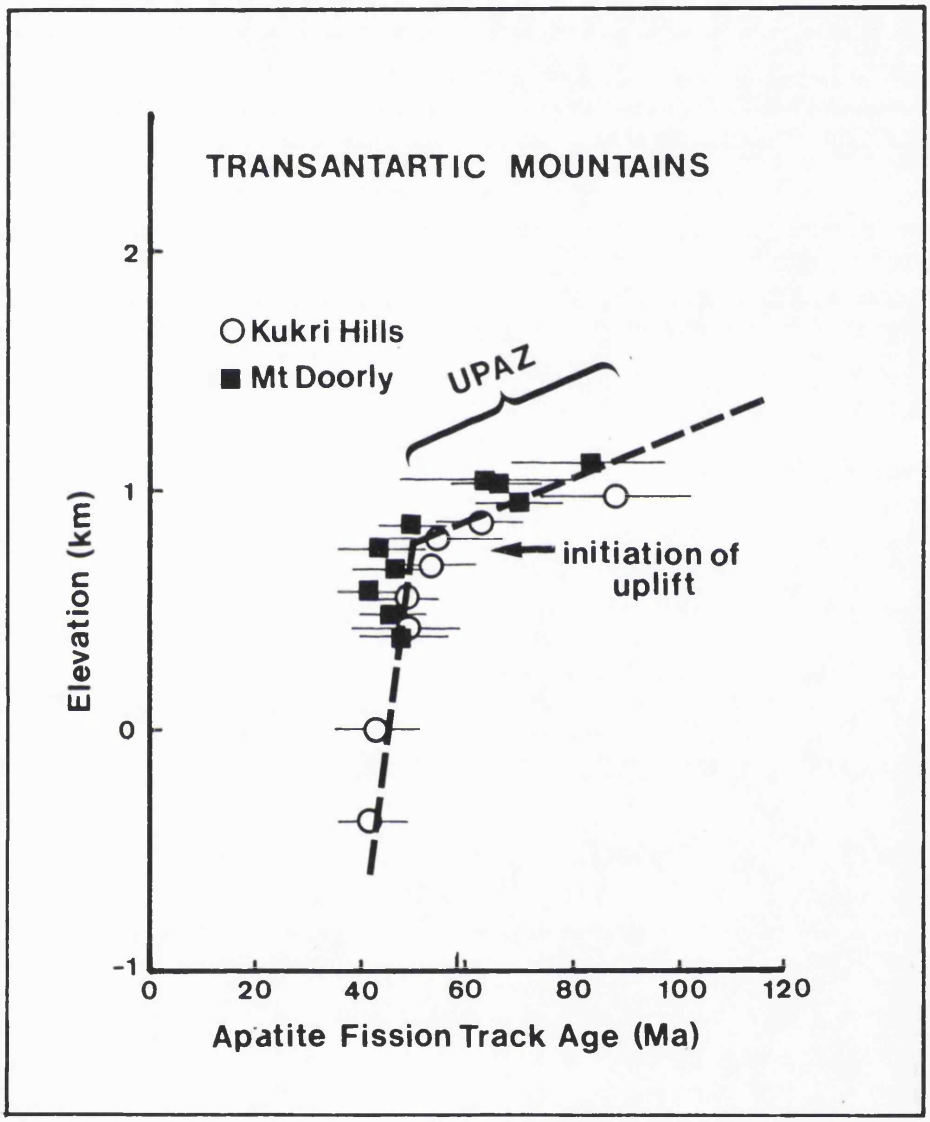

Fig. 5.5. Uplift history of the Transantarctic Mountains (after Fitzgerald et al., 1986). The graph shows a plot of apatite fission track age versus elevation for sample collected along transects in the Kukri Hills and Mount Doorly regions. The upper part of the profile represents an uplifted partial annealing zone. The break in slope of the graph at about 50 Ma represents the onset of uplift. The gradient of the lower slope denotes the average rate of uplift.

track ages concordant with intrusion ages calculated by other methods, but that apatite ages were considerably younger (Cretaceous) and one, collected adjacent to an early Tertiary dyke gave an age of 58 Ma. Because of their low annealing temperatures, fission tracks in apatite are sensitive to a larger thermal aureole around such a body, of greater extent than any petrological or textural transformations. The extent of this thermal zone is directly related to the size of the intrusion. Hence a metre-scale dyke will have a metre-scale thermal aureole. Accelerated heat flow as a result of igneous activity can be due to either intrusive or extrusive magmatism. Effects upon the local country rock adjacent to sills, dykes and extrusive material (particularly lavas and ignimbrites) are sometimes apparent as baked margins, extending normally a short distance away from the intrusion. Sills or dykes within sequences at depth will cause local perturbation in the geothermal gradient. The influence of an igneous sheet can produce an inverted geothermal gradient beneath it. Large igneous intrusions, like the late Variscan Cornubian Batholith of SW England also reveal the nature of such systems to act as a thermal conductor, thereby enhancing the local geothermal gradient. This effect is apparent only in the strata directly above the intrusion.

5.2.2.2 Heat flow due to crustal thinning.

As continental extension proceeds, the crust becomes progressively thinned. The McKenzie (1978) model of pure shear crustal extension **(Fig. 5.6)** is the simplest hypothesis to deal with both conceptually and mathematically, and is therefore taken as the starting point for the bulk of the extension, subsidence and thermal models used to represent the kinematics of rifting. At its simplest, assuming that the temperatures at the base and the top of the lithosphere are constant, the geothermal gradient will increase in proportion to crustal thinning, compressing the isotherms. Obviously, this is a local effect, restricted to the area of extended crust. Away from this region, the isotherms will resort back rapidly to their original spacing, where the crust has not been thinned. As rifting normally takes place in discrete regions, the effects of rifting are unlikely to be detected away from these zones, and consequently on the rift flanks themselves, these effects are negligible (Buck et al., 1988; Gallagher et al., 1993).

5.2.2.3 Thermal effects of hot fluids.

Resetting of fission tracks in apatites due to the presence of hydrothermal circulation is a questionable but probable mechanism (Green et al., 1993). The fluids in question are either hydrothermal, associated with

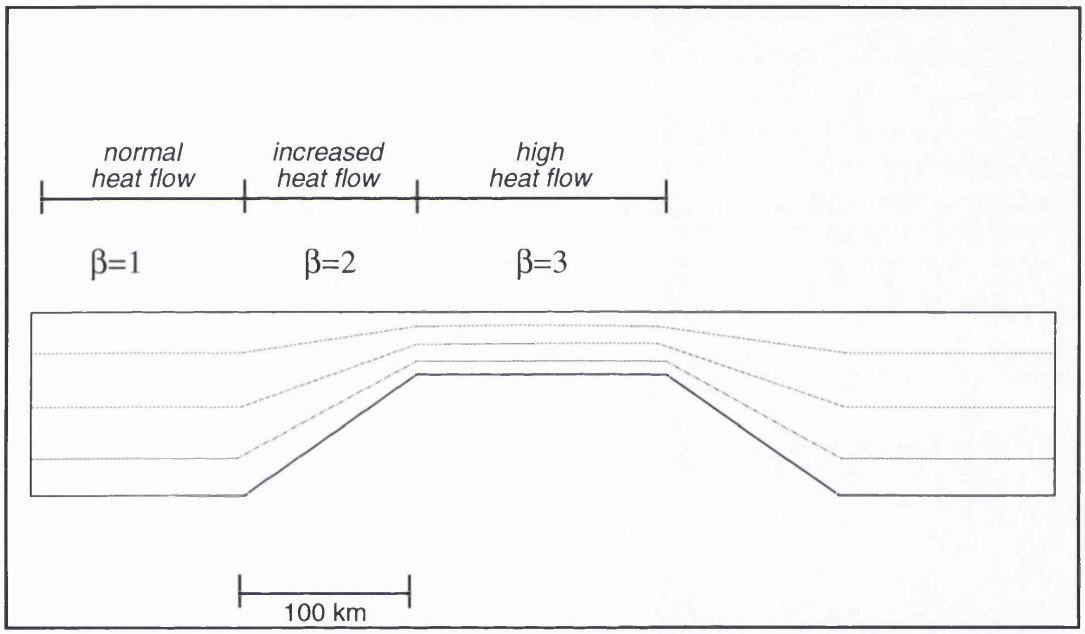

Fig. 5.6. As the crust is thinned by a factor β, the isotherms become compressed (after McKenzie, 1978). The heat flow decreases rapidly from the axis to the rift flanks.

local igneous activity or thermally heated meteoric waters. If the fluids are continually circulating and convecting they can be re-heated at depth. The temperatures attained by hot fluids and the length of time these temperatures are retained within the crust are not well constrained or understood. Summer and Verosub (1989) have made estimations that volcanically generated fluids can affect regions of up to 10,000 km^2, and they have been calculated to travel distances of around 330 km (Deming, 1993).

The presence of the near surface (i.e. < 1000 m) heated meteoric fluids is important to fission track analysis as these may have profound affects upon annealing in crustal regions much higher than the assumed PAZ. Many studies of fluid flow have been related to circulation in sedimentary basins. Hot circulating fluids must be thermally recharged or they will cool. The importance of gravitationally driven meteoric waters from the elevated basement complexes adjacent to sedimentary basins has been emphasised in several studies (e.g. Deming, 1993; Jessop and Majorowicz, 1993) where they have been found to increase significantly the geothermal gradient in localised regions. At present, fluid temperatures are estimated from crystallisation temperatures of mineral phases, and from measurements taken over time in boreholes. Consequently it is acknowledged that fluids attain temperatures sufficient to anneal fission tracks in apatite and therefore these could account for local anomalies in fission track datasets. These fluids must maintain annealing temperatures over geological time.

The importance of fluid flow to fission track analysis has been highlighted by Green et al. (1993) who have re-examined the data of Green (1986) and Lewis et al. (1992a), originally interpreted in terms of simple denudation. The appearance of early Tertiary palaeotemperature "highs" and "lows" in Northern England cannot be interpreted by uniform denudation alone **(Fig. 5.7)**.

Recently Holliday (1993) proposed that the thickness of eroded sediment estimated from fission track analysis in Green (1986) and Lewis et al. (1992) is twice as large as that calculated from sedimentological and stratigraphic estimates of sediment thickness. This discrepancy may be accounted for by the palaeogeothermal gradient being greater than the assumed 30°C km^{-1}, at around 53°C km^{-1} due to the low thermal conductivity of chalk, which is assumed to be the most probable overburden.

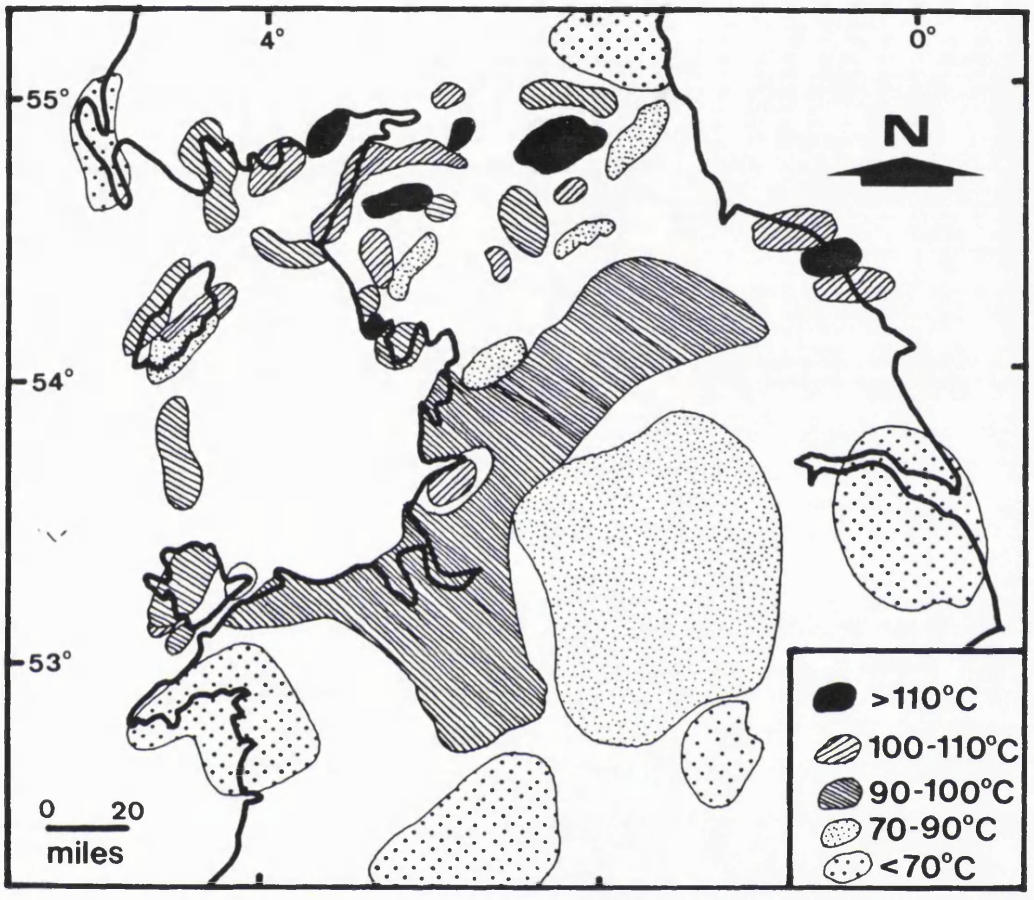

Fig. 5.7. A map of palaeotemperatures estimated from apatite fission track ages in northern England promoting the possibility of 'hotspots' formed by circulating hot fluid systems (Green et al., 1993).

5.3 Geological interpretation of the apatite fission track data from the Armorican and Hesperian Massifs.

The regional evolution of the area has been described in Chapters 2 and 3. The geological controls of the Bay of Biscay continental margins are, at their most rudimentary, the denudation of a Palaeozoic orogenic belt, formed at the end of the Carboniferous during the suturing of Pangaea, and its fragmentation during the Mesozoic breakup of the supercontinent. At present, there are negligible traces of Mesozoic and Cenozoic sediments exposed overlying the Armorican and Hesperian Massifs, although it is probable that they once existed and have subsequently been eroded. However, it is these eras that are represented by the fission track ages.

At the end of the Variscan Orogeny, the Armorican and Hesperian Massifs were deeply denuded. This took place during the Permian, the erosive surface possibly representing one similar to that revealed today. There are Permian terrestrial sediments onlapping upon the Variscan Basement around the Hesperian Massif and in the north-eastern part of the Armorican Massif. The apparent removal of these sediments from other regions of the massif suggests that further erosion of the basement has taken place since the Permian.

Such rapid denudation of mountain belts is not uncommon. Regions of high elevation endure erosion often at rates >1000 mm ka^{-1} (from solid and solute transport loads of the principal rivers draining from the Himalayas; Milliman and Meade, 1983). Erosion rates >5000 mm ka^{-1} have been recorded from the highest areas of the Southern Alps of New Zealand where local crustal uplift rates are ~7000 mm ka^{-1} (Selby, 1982). Erosion is a continually active process influenced primarily by elevation. Consequently mountain chains will suffer erosion during orogenic activity, and this will continue after the cessation of activity, until elevation is no longer sufficient to provide the potential for high denudation rates. England and Richardson (1980) believe that denudation can remove thicknesses of 60 km from mountain belts, most of this occurring during orogenic activity. Brown (1993) suggests from data published elsewhere (e.g. Jones and Brown, 1990; Dallmeyer and Brown, 1992) that there was rapid cooling/tectonic exhumation of Southern Brittany at rates of approximately 850 m Ma^{-1} maintained for 10 Myr towards the end of the Variscan Orogeny.

The oldest apatite fission track ages (230 -270 Ma) in this thesis are possibly representative of the initial erosion of the Variscan Mountains, seemingly representing monotonic cooling/unroofing of the basement. This is supported by the track length data where the distributions are of the

undisturbed basement-type (Gleadow et al., 1986b). These samples are all from the eastern parts of the Armorican Massif bordering the Bay of Biscay.

Towards the end of the Permian and during the lower Triassic, the region was rifted, locally in the Bay of Biscay and in the Western Approaches-English Channel region, and regionally in the whole of the Atlantic region. This would have induced enhanced heat flow in the rift zones from crustal thinning and associated volcanism, although thermal effects decay rapidly away from the rift axes (Gallagher et al., 1993). This effect was minimal in the Bay of Biscay region, as shown by the subsequent formation of non-volcanic passive margins (Bott, 1992) and also by the paucity of early Triassic (230 -250 Ma) apatite fission track ages along these rifted margins.

These periods of rifting from the Triassic to the Jurassic and beginning of seafloor spreading in the North Atlantic region during the middle Cretaceous were associated with great thicknesses of sedimentation in the North Atlantic region, especially in the rift basins. However, the Biscay and Galicia margins were starved and contain little sediment when compared with regions such as the Western Approaches Basins (e.g. Chapman, 1989). The Paris, Aquitaine, English Channel, Western Approaches, Asturian and Duero sedimentary basins onlap onto the Variscan Massifs, which have allegedly remained as upstanding blocks for much of their Mesozoic and Cenozoic history (Cogné, 1974). However, this does not necessarily mean that they have escaped sedimentary cover. Throughout Europe, the majority of the Variscan belt is today under sedimentary cover with only isolated blocks upstanding. Variscan rocks occur at the surface today either reactivated as part of the Alpine Orogeny (Alps and Pyrenées) or in the Massif Central, which has suffered copious Quaternary volcanism, on the flanks of the Rhine Graben (the Vosges and Schwarzwald), and on the western margins of Europe, as the Armorican, Hesperian and Cornubian Massifs. The sedimentary history of the west European Variscan Massifs and their importance as source regions for the basins is outlined in section 2.4.

In the Bay of Biscay region, all the apatite fission track data are derived from surface outcropping samples, situated on the rift flanks of the Bay. Therefore they are unlikely to have been influenced by the thermal effects of rifting and consequently the Mesozoic ages observed are most probably a record of burial and subsequent exhumation. The denudational processes were probably aided by an increase in elevation as a result of rift-related doming in the Upper Jurassic and Lower Cretaceous (Ziegler, 1990). The observation of clastic sediment thickness in the surrounding basins and

their provenance cannot be ignored. In the majority, the fission track ages represent a Jurassic to Cretaceous evolution which is presumably linked to these processes.

The post-Cretaceous evolution of the Armorican Massif is less well documented, although relicts of Tertiary transgressions are exposed in parts of the massif. Gentle deformation was incurred as a result of the Alpine orogenic phases. The surrounding offshore basins, particularly the Western Approaches and the English Channel underwent major inversion as a result of tectonism related to the early Alpine Orogenic phases and North Atlantic Opening. These events were unlikely to have been limited only to the basinal regions and probably affected the adjacent blocks, including the Armorican, Cornubian and Hesperian Massifs (see data of Lewis et al., 1992a). The Iberian Plate was tectonically active at this time, culminating in the Pyrenean collision. Guimerà (1984) reports two main compressive phases affecting the interior of the Iberian plate (Late Cretaceous to Lower Eocene and Oligocene), followed by a post orogenic end-Oligocene minor extensional regime. This tectonism is reflected in the Eocene ages in the Asturian Arc.

The possibility of hot fluid systems as a resetting mechanism is as ever, an unknown quantity. The area is structurally complex and highly mineralised, with numerous regional-scale thrusts and faults, many of which are deep seated, and all are capable of acting as conduits for fluids.

Recognition of resetting in fission track systems and the determination of the resetting time has been facilitated by use of the 'banana curve' **(Fig. 5.8).** where apparent age is plotted against mean track length. Green (1986) first used this with a range of apatite ages between 270 and 60 Ma on rock samples from Northern England. At that time the younger (~80 Ma) apparent apatite ages could not be ascribed to a known thermotectonic event. Green (1986) therefore proposed that the track length population formed broadly as two separate populations, an older and a younger, with different distributions related to the different apatite ages. This graph shows the variation of mean track length and standard deviation as plotted against apatite fission track age, and the 'banana' shaped curve is characteristic of gradual resetting of apatites and replacement of the 'old' population of tracks with a 'new' population.

The data presented in this thesis are presented in this fashion, enhanced with the overlay of data fields **(Fig 5.9).** Those samples with the oldest apparent ages and longer mean track lengths have seen no significant thermal perturbations since their formation, whereas those at the young age end of the graph have been affected by more recent activity. The middle

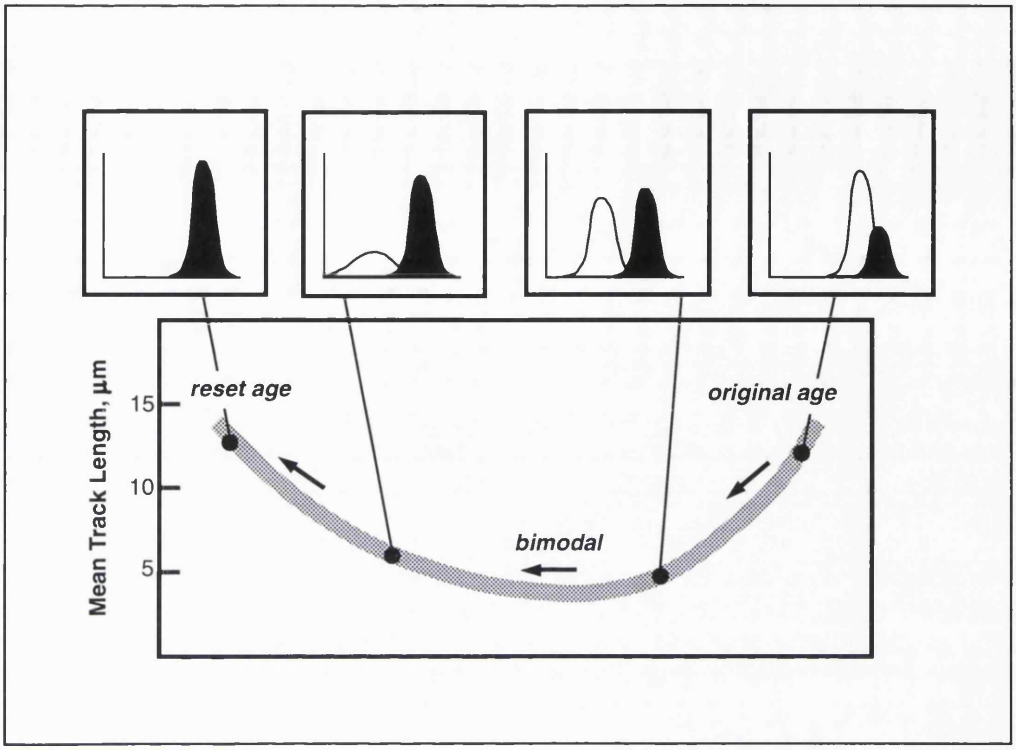

Fig. 5.8. An age resetting curve showing the relation ship of old (white) and new (black) populations of fission tracks to apatite fission track age when a sample has suffered partial to total annealing (after Green, 1986).

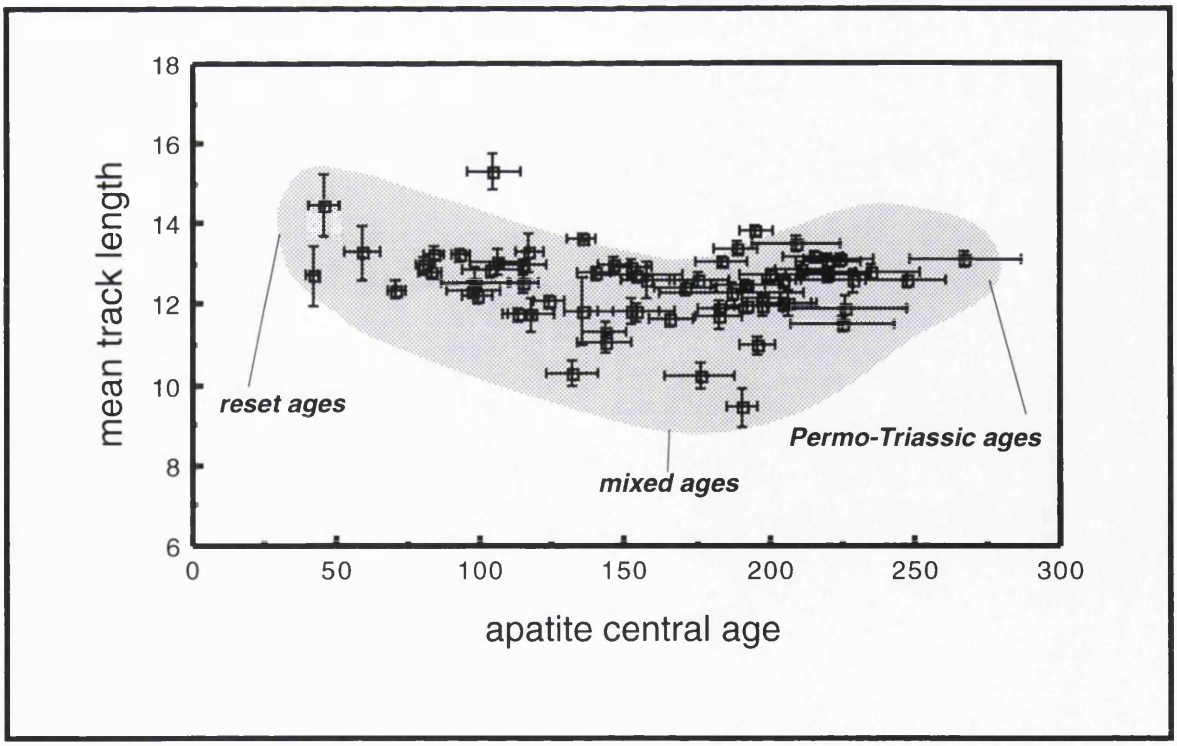

Fig. 5.9. The apatite fission track data for the Armorican and Hesperian Massifs, plotted on a 'banana plot', fission track age versus mean track length. The two fields on the plot are shaded.

region of the curve is composed of 'mixed ages' which possess a population of older confined track lengths inherited from the original post-Variscan cooling episode and newer population of tracks which have formed subsequently. This graph of fission track ages and length measurements from the Armorican and Hesperian Massifs is compared with a composite plot of other available apatite fission track data from other exposed Variscan Massifs **(Fig. 5.10)**, and the trends are very similar.

In summary, the fission track data in this thesis present a range in apatite fission track ages from the original Permian unroofing to those concurrent with early Tertiary convergence of the Iberian Plate on stable Europe. The data in this study contrasts with that of Green (1986) in that the resetting curve is flatter, there being no mean track lengths >14 μm (those that do exist in this data set are calculated from a small number of confined tracks and are relatively imprecise). In an attempt to further understand the data, computer modelling of plausible thermal histories is required, using predictive forward modelling and data-driven methods.

5.4 Modelling of the apatite fission track data of the samples from the Armorican and Hesperian Massifs.

The modelling program used to aid interpretation of the data in this thesis is 'Monte Trax', developed within the London Fission Track Research Group. It allows the input of temperature-time (T-t) points, either singly or with bounds, from which thermal history scenarios are constructed. There are two possible approaches to modelling the fission track data within this program. Firstly, *forward modelling* uses a single, user defined thermal history, for which the program predicts an age and length distribution for comparison with measured values. Secondly, *data-driven random simulation* modelling matches the observed data against age and length values produced from randomly selected T-t scenarios within loosely defined bounds to distinguish the better thermal history.

Monte Trax, like other modelling programs developed to aid in the interpretation of fission track data is based primarily upon what is understood of the annealing characteristics of fission tracks in apatite. A series of algorithms have been devised as a result of laboratory annealing experiments performed on apatites of different chemistries by various workers. The most commonly used algorithm is that of Laslett et al. (1987) based on the annealing characteristics of Durango Apatite. Other authors have derived algorithms for strontian apatite and other fluorapatites (Crowley et al., 1991; Carlson, 1990). As yet a model for the annealing of tracks in chlorapatites remains unpublished. None of the published

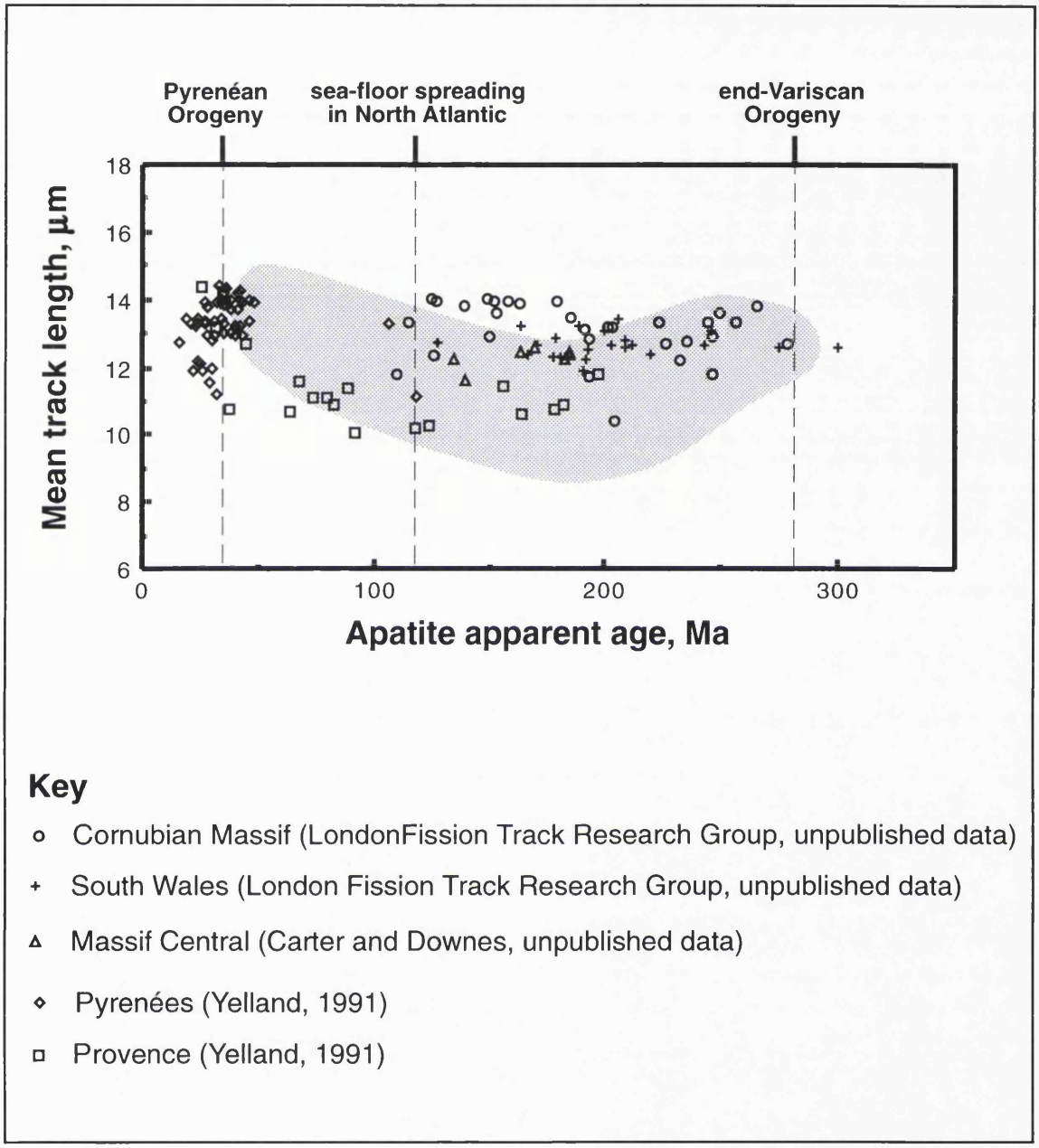

Fig. 5.10. Available fission track data from the exposed Variscan basement of western Europe, plotted as a banana curve. Major tectonic events are arbitrarily marked on the upper axis. the shaded area represents the field occupied by the data in this thesis.

alogorithms truly incorporate the possible variety of chemical compositions that may occur within the apatite population of a sample, especially with the possible ranges of compositions within sedimentary rocks. With such a proliferation of modelling algorithms, one must acknowledge that eincreased care should be taken when using them. It can become too easy to rate a model on its ability to match the observed data, and for it then to appear more reliable than others.

The Laslett et al. (1987) algorithm was chosen to model the data in this thesis, as the apatite chemistry of the samples is similar to that of Durango Apatite (this is further discussed in Chapter 8). This algorithm is currently the most widely used and accepted model although it underpredicts the annealing behaviour of chlorine-rich apatites. Other published algorithms model thermal history scenarios that do not substantially differ in their predictions from the Laslett et al., (1987) model.

5.4.1 Forward models.

In this study the Monte Trax modelling application was initially used in its simplest form to predict apatite fission track data from a specific thermal history. A series of T-t points were specified and a thermal history constructed between these points. As a preliminary examination of the data, these forward models were devised to ascertain those thermal history scenarios, in simplest terms of cooling and heating, which are plausible and those which can be immediately discarded. This approach is not rigorous, and so the fit of the predicted data to the observed data was assessed broadly and qualitatively using the following criteria. If the predicted data and observed data were within error, then the fit was good; if they were not, then the fit was poor and if the predicted track length distribution matched observed distribution then the fit was reasonable (but not perfect). The information entered into the modelling program assumes a Permo-Triassic surface palaeo-temperature of 20 ± 10°C. This is arrived at on the assumption that the Biscay region lay near the equator in an arid to semi-arid climate during the time of the Permian proposed maximum unroofing (Hay et al., 1981; Smith et al., 1981). The nine models are described below, lettered alphabetically (A-I) and illustrated on **Figure 5.11.**

• A. MONTE TRAX 1. The simplest hypothesis is to use the two known points in the sample's thermal history. The samples are, in the majority Palaeozoic crystalline rocks; all pre-existing tracks would have been totally annealed at temperatures >120°C (probably due to deep burial) at the end of the Variscan Orogeny. Accordingly, the first constrained point is at a temperature of 120°C at 300 Ma, all tracks forming prior to this would

have been already annealed. Monotonic steady state cooling to present day temperatures is then envisaged. This thermal history and the predicted fission track values are illustrated in **Figure 5.11a**. Although the predicted apparent age of 213 Ma is comparable with the older observed fission track ages from the Bay of Biscay region, the track length distribution is not. The predicted values are compatible with the undisturbed basement type distribution of Gleadow et al., (1986b), with a MTL of 13.6 μm, and σ of 2.0 μm.

•B. MONTE TRAX 2. As noted in Chapter 4, the appearance of few lengths >16 μm in the observed data is important in deciphering a thermal history. This phenomenon indicates that the newest tracks have formed under partial annealing temperatures. Therefore in model B the possibility of recent, rapid cooling bringing the samples out of the PAZ was tested using a third arbitrary T-t point in this model of 80°C at 10 Ma. **Figure 5.11b** shows that this model provides a reasonable fit to the observed track length distributions from the western Armorican Massif (MTL is 10.57 μm, σ is 1.85 μm). However, the predicted age is far too young for samples in this region, being 79 Ma. This is a better age-fit to samples from western Galicia.

•C. MONTE TRAX 3. The Variscan Massifs were denuded during the Permian, with a substantial part of the mountain belt removed (Smith et al., 1974), and terrestrial sediments lie above the unconformity. **Figure 5.11c** shows the results of incorporating this Permian unroofing, subsequent gradual reburial and exhumation, by adding a fourth T-t point of 20°C at 270 Ma. This provides a reasonable fit to the data, especially those from parts of the Armorican Massif, although the predicted age of 223 Ma is older than is frequently observed. The predicted MTL is 11.7 μm and σ is 1.03 μm.

•D. MONTE TRAX 4. The predicted thermal history in **Figure 5.11d** investigates the effect upon the fission track data of Permian unroofing and Cretaceous burial with a period of residence within the PAZ. The results are a poor fit to the observed data. The age (231 Ma), MTL (12.34 μm) and standard deviation (1.94 μm) show some similarity to the observed values, but the length distribution is bimodal and has too many lengths >16 ∝μ. The length distribution is the most diagnostic feature of the thermal history suffered by a rock sample and thus it is the most important predicted parameter to be fitted to the observed data.

•E. MONTE TRAX 5. Furthering the hypothesis of Monte Trax 4, the sample was taken to deeper regions of the PAZ, and its sojourn there was extended, until cooling between mid-Cretaceous and the present. The model predicts an undisturbed basement-type distribution (MTL is 13.34

μm, σ is 2.28 μm) with an age of 93 Ma **(Fig. 5.11e)**. This yields a poor fit to the observed data.

•F. MONTE TRAX 6. Upper Jurassic burial to the lower regions of the partial annealing zone, followed by gradual cooling, and then more rapid cooling gives a good average fit to the observed data **(Fig. 5.11f)**. The predicted age is 143 Ma, MTL is 11.75 μm and the σ is 1.89 μm.

•G. MONTE TRAX 7. This model tested Permian cooling, followed by burial to depths below the PAZ during the Mesozoic. This produced a reasonable fit of predicted age to samples from north-western Galicia (101 Ma), but the track length distribution is again an undisturbed basement type distribution **(Fig. 5.11g)** and not consistent with the observed data (MTL is 13.53 μm, s is 2.07 μm).

•H. MONTE TRAX 8. The possibility of Permian cooling followed by Upper Jurassic - Lower Cretaceous burial to lower regions of the PAZ, and then gradual cooling to the present day was tested **(Fig. 5.11h)**. Once again, although the age fit was good (190 Ma), the distribution was of the undisturbed basement-type (MTL is 12.71 μm, σ is 2.76 μm) and therefore a poor fit to the data.

•I. MONTE TRAX 9. A final model testing rapid exhumation in the Permian followed by little subsequent cooling provides a very poor fit to all parameters of the data, predicting an undisturbed volcanic-type distribution, and an end-Variscan age, 283 Ma. The MTL is 14.97 μm and σ is 1.13 μm **(Fig. 5.11i)**. This is the evolution apparently predicted for the Variscan Massifs during the Mesozoic (e.g. Ziegler, 1990), and published in many palaeogeographic reconstructions. The fission track data indicate that the Variscan Massifs were not landmasses throughout this time.

Having previously reasoned that the dominant mechanism of cooling of mountain belts subsequent to their formation is denudation, these preliminary forward models (summarised in Table 5.1) indicate that it is likely that the basement samples have undergone the following thermal history. A period of exhumation during the Permo-Trias, followed by burial, reaching maximum depth in the Jurassic and Cretaceous was succeeded by erosion of accumulated Mesozoic material, which lead to today's surface exposure. It would appear that the samples were not buried below the lower bounds of the PAZ. Models F and C provide the closest match the data.

The majority of the models, although providing reasonable fits to the age and mean track length values, have predicted track length distribution which are unlike the observed length distributions. In particular, the model thermal histories produce length histograms with

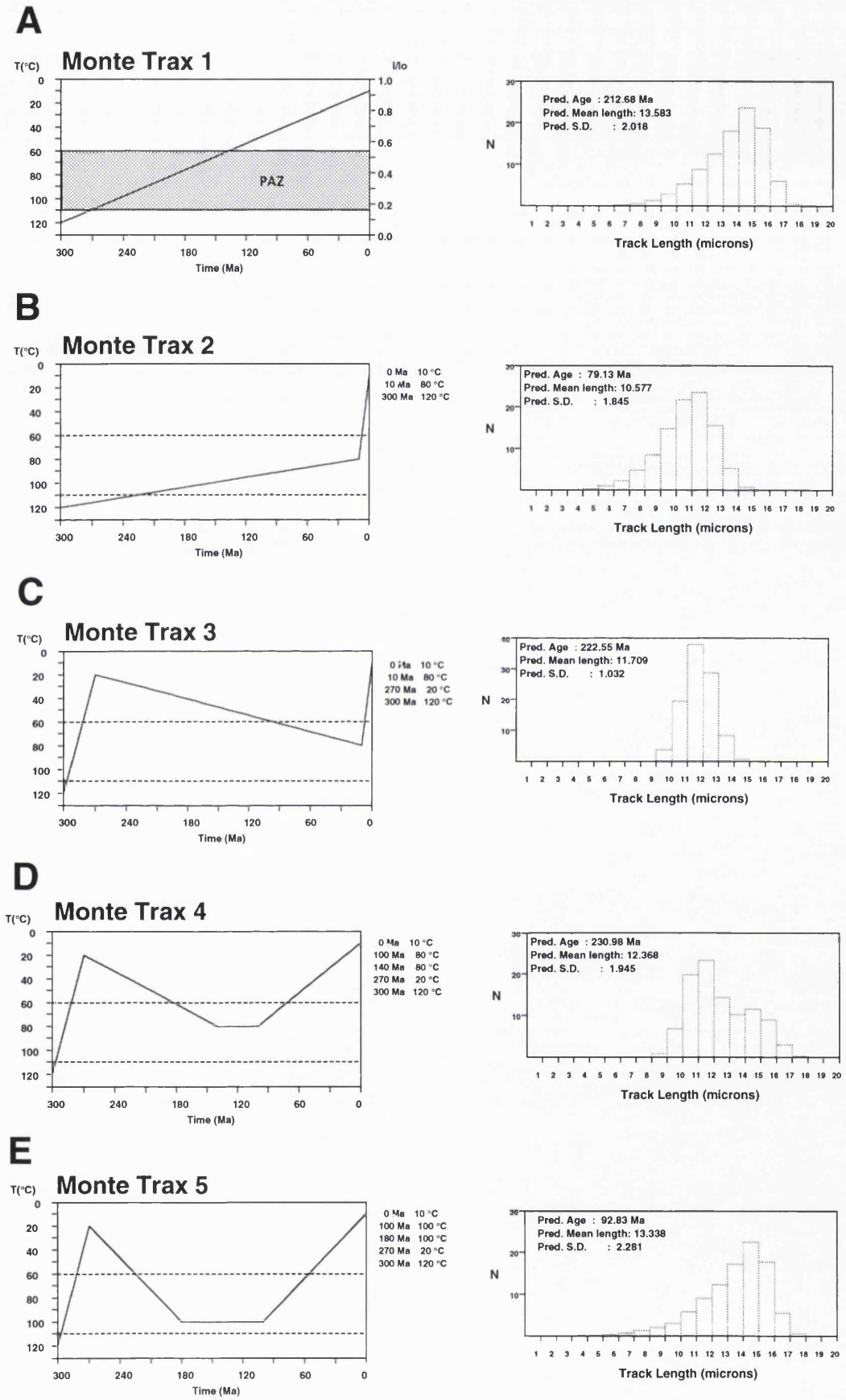

Fig. 5.11a-e. Preliminary forward models (A-E). A: slow, monotonic denudation (the PAZ is shaded for reference). B: slow denudation followed by recent, rapid denudation. C: rapid denudation during the Permian, followed by slow, monotonic burial during the Mesozoic and early Tertiary, and then late Tertiary to recent rapid exhumation. D: Rapid denudation during the Permian followed by Mesozoic burial to maximum temperatures of 80°C, followed by monotonic exhumation. E: As above, with maximum temperatures of 100°C, and a longer residence in the PAZ.

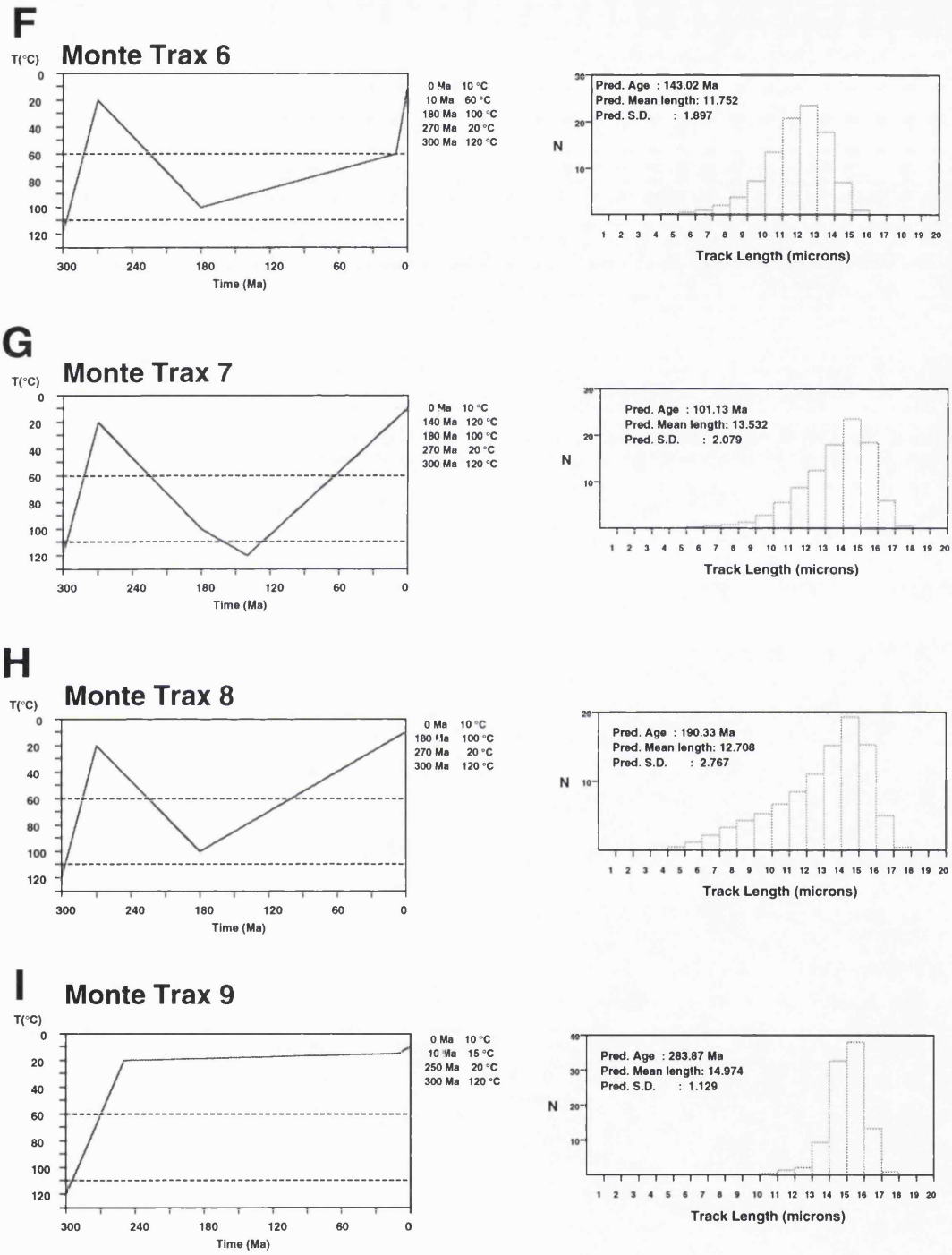

Fig. 5.11f-1. Preliminary forward models (F-I). F: rapid denudation during the Permian followed by Mesozoic burial to the lower regions of the PAZ and slow, monotonic denudation followed by rapid recent exhumation. G: rapid Permian denudation, followed by burial with maximum temperatures below the PAZ, and then monotonic exhumation to the present. H: As above but with, maximum temperatures in the PAZ. I: rapid Permian denudation, followed by extremely slow exhumation between the Permian and the present.

occasionally positive, rather than negative, skews. When compared to the observed data, the predicted length distributions have a relatively large component of tracks >16 μm.

Model	Qualitative data fit	Comments.
A	age: fits E. Armorican data. length distribution: no fit.	POOR
B	age: fits W. Galicia. length distribution: no fit.	POOR
C	age: fits E. Armorican data. length distribution: fits E. Armorican data.	REASONABLE
D	age: fits E. Armorican data. length distribution: no fit.	POOR
E	age: fits W. Galicia. length distribution: no fit.	POOR
F	age: fits N. Spain & W. Armorican data. length distribution: all data	GOOD
G	age: fits W. Galicia. length distribution: no fit.	POOR
H	age: W. Armorican data length distribution: no fit.	POOR
I	age: no fit. length distribution: no fit.	POOR

Table 5.1 A summary of the preliminary forward models and their fit to the observed fission track data.

5.4.2. Data-driven random simulations.

The parameters from which the simulations are calculated are entered in the form of a number of time-temperature (T-t) points with bounds, defining a box in T-t space. An example is shown in **Figure 5.12.** These time-temperature points are entered using known geological constraints and plausible assumptions, such as the timing of known unconformities and known tectonic events. Gross uncertainties in the geological record can be incorporated by using large bounds on the T-t points. The observed apatite fission track data are entered in the form of an age, a mean track length and a track length distribution standard deviation.

The Monte Trax application simulates a specified number of randomly selectedthermal history paths that pass through the allocated T-t boxes. Length and age parameters predicted by the simulation are

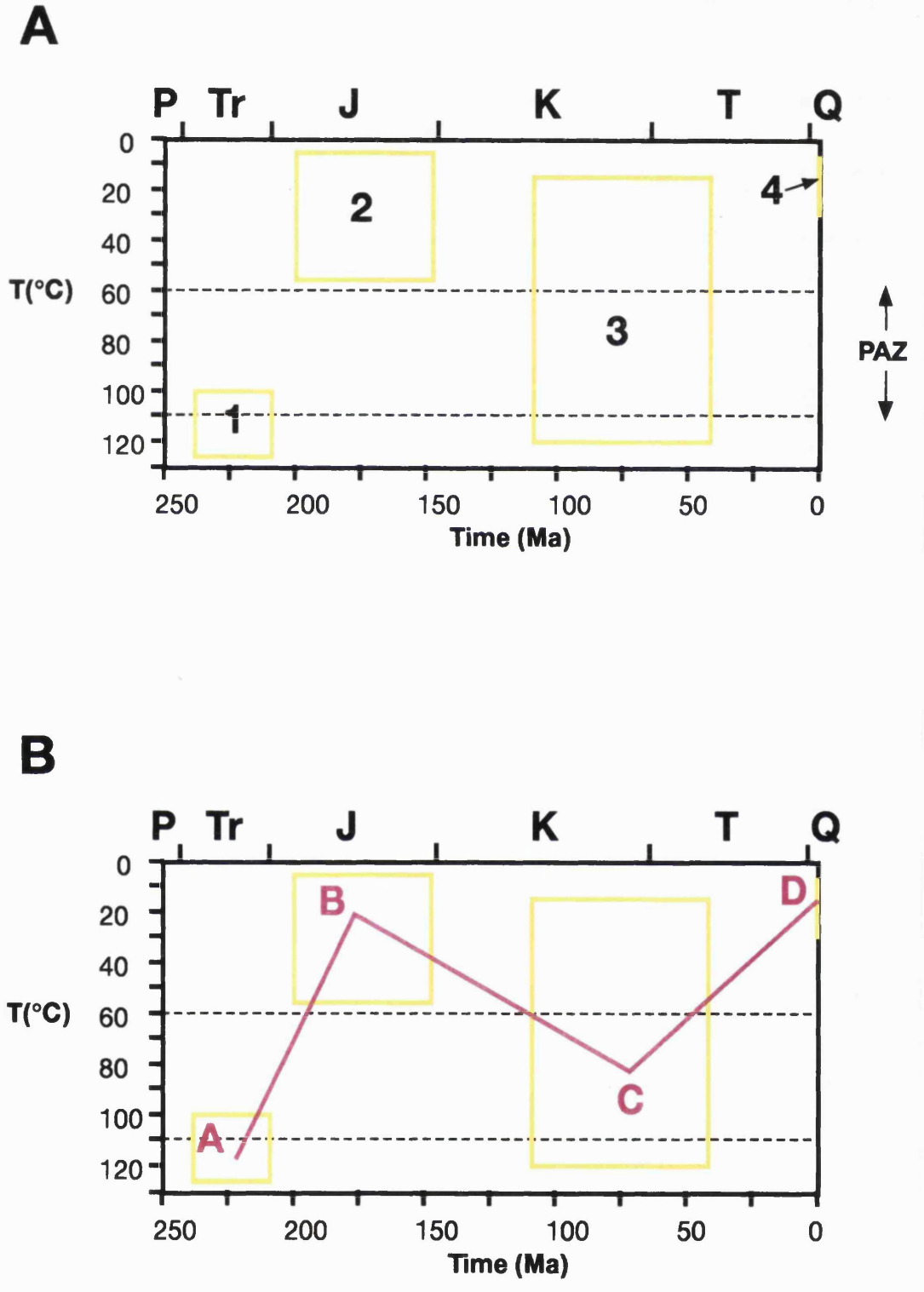

Fig. 5.12. a). A diagram illustrating the placing of time-temperature boxes (1-4) for data-driven simulations, with respect to geological time and temperatures. b). A thermal history scenario constructed to pass through the boxes.

statistically compared to the observed apatite fission track data, and sorted into the following categories: T-t paths that match the age and length data; T-t paths that match the age data alone; T-t paths that match the length data alone and T-t paths that fail both data sets. These can then be compared directly to the entered data. It is possible to return to the original input data and alter either the bounds, times or temperatures, and the plots will be recalculated. In this way the thermal history model can evolve.

The apatite fission track data in this thesis were modelled in all cases using a starting point near the end of the Variscan orogeny (at 300 ± 20 Ma) when all the samples can be safely assumed to have resided some depth in the crust, prior to cooling and unroofing. The temperature can be put at the lower limit of the partial annealing zone at 120±20°C. Therefore this time-temperature box has a small error, as it is a tightly constrained starting point. The next point is the established view that the Variscan massifs were unroofed during the Permian, and so logically a T-t box at near the end Permian (at 250 ± 50 Ma) can be plotted against a temperature of 20 ± 10°C. This temperature allows the sample to be at or close to the surface at this time. A greater temperature and larger bound are used in the early experiments (i.e. 60 ± 60°C) to cover the possibilities that the region was not exposed, and that it possibly lay within the PAZ.

The data are modelled using a single set of values representative of the regional spread of ages and lengths rather than specific, individual central ages. If individual central ages lie away from the regional spread, then they hold a case for further modelling of these specific samples. The age, length and standard deviation errors incorporated into the model should be large enough to encompass the spread of data around the chosen mean (e.g. 150±30 Ma). The same is true for the mean track length and standard deviation values.

The modelling of the data began with the simplest geological scenario and evolved to more complex thermal histories. Data from the English Channel margin has been included with that from the Bay of Biscay margins as the data from each region are within error of each other and on a broad scale probably underwent similar thermal histories.

5.4.3. Basement from the Variscan internal and mobile zones.

The following age and length values were input in the preliminary experiment, *slow cool 1*: Age: 220±20 Ma; MTL: 12.5±1.0 μm; SD: 1.5±0.5 μm. The aim of this modelling experiment and the second (*slow cool 2*) is to model the older ages in the region. The time temperature points for *slow cool 1* are in **Table 5.2.**

	Time	temp.
1	300±20	120±40
2	250±30	60±60
3	100±50	60±60
4	0	20±10

Table 5.2 T-t values with bounds for *slow cool 1.*

These data constrained a starting and a finishing point to relatively precise times and temperatures. The timing of T-t points 2 and 3 were constrained assuming Permo-Trias unroofing of the massif, and its Mesozoic breakup. These two middle points had maximum error on the temperature, from surface exposure to a depth below the PAZ. The result is that a large variety of T-t paths could be plotted, and the most feasible path selected. The 200 simulation runs are plotted in **Figure 5.13a**, and those runs that fit both the age and length data input are plotted on **Figure 5.13b**. The age and length fit data show two major trends. The first involves a gradual slow cooling of the sample being monotonically cooled above the PAZ. A second distinct trend shows the sample being rapidly cooled and unroofed during the Permian, then being buried to temperatures of ~80°C during the mid Cretaceous. This second group concurs with the accepted view that the Variscan Massifs were unroofed soon after the cessation of orogenic activity, and the observation that Permian sediments lie unconformably upon the massifs in many parts of the belt. These two trends are best illustrated in **Figures 5.13 c and d**. The best run (rank 1) shows a scenario depicting Permian cooling and denudation (although not necessarily brought to the surface). The 4^{th} ranked run shows a slow-cooling T-t path, with more rapid cooling beginning in the late Cretaceous. Both the 1^{st} and 4^{th} ranked runs have predicted track length distributions similar to the observed data, although they exhibit a minor positive skew. However, the mean track length and standard deviation provide a good fit to the observed values. The 4^{th} ranked run, a monotonic slow cooling scenario, although providing a reasonably good fit to the observed data should on geological grounds, be discounted.

Consequently, geological field observations coupled with the fit of the data to a Permian cooling-unroofing scenario, permitted the model to be further constrained by narrowing the temperature errors in T-t box 2. The revised T-t bounds for the second model, *slow cool 2* is in **Table 5.3**. The age and track length data entered were identical to those in *slow cool 1.*

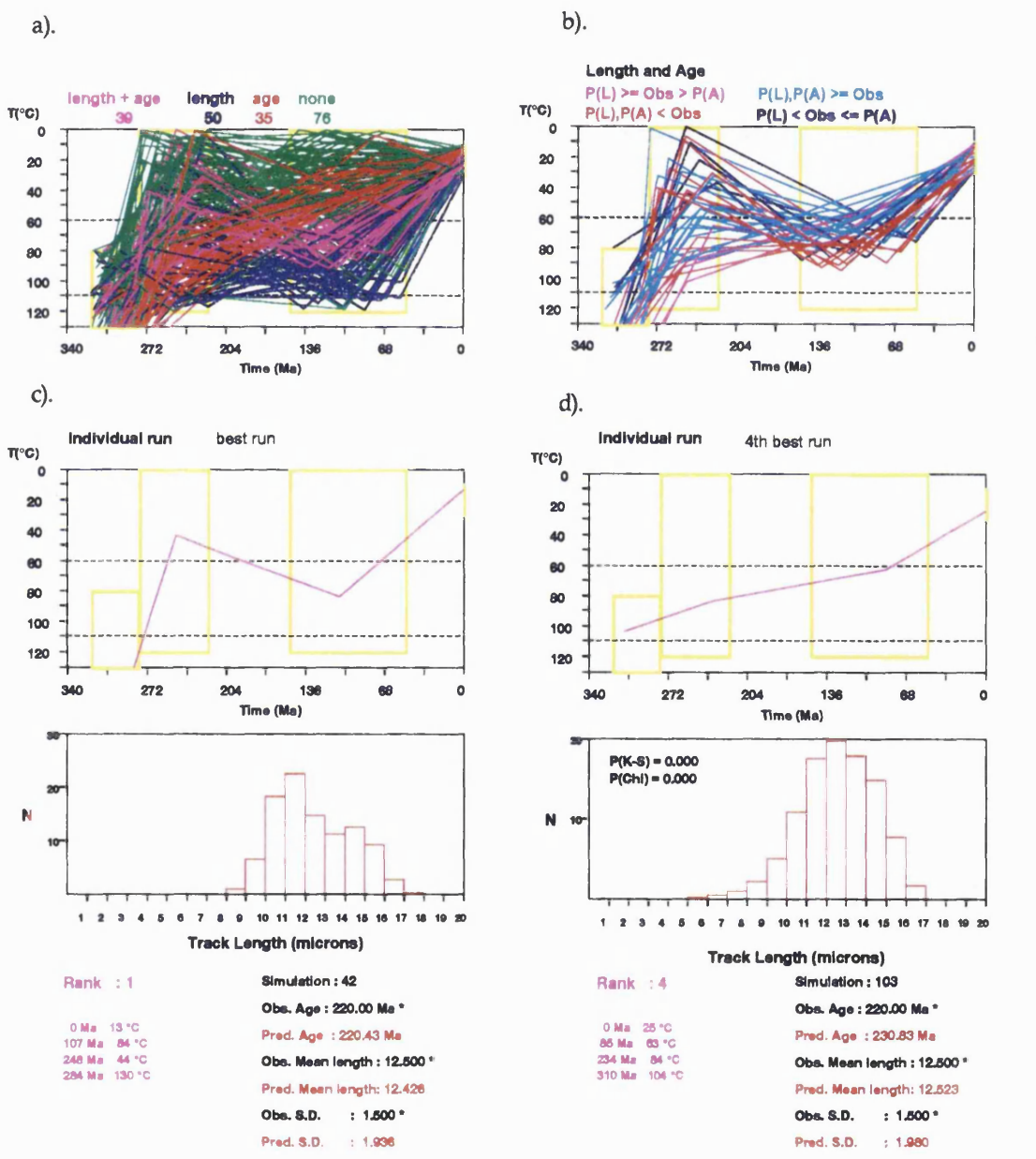

Fig. 5.13 a-d). Input data and simulations for the modelling experiment Slow Cool 1. In a). green is a failure, red fits age only, blue fits length only and pink fits length and age.

	Time	temp.
1	300±20	120±40
2	250±30	20±20
3	100±50	60±60
4	0	20±10

Table 5.3. T-t values with bounds for *slow cool 2*.

The 200 Monte Carlo simulations for *slow cool 2* are plotted in **Figure 5.14 a.** The 'failed' runs (those that do not fit the input age and length data, coloured green on the diagram) can clearly be seen to define the geological scenario whereby the Variscan Massifs remained at or near the surface as upstanding blocks since their unroofing during the Permian. All the other runs, i.e. those that fit age and length, age only and length only, all describe a thermal history that involves burial, possibly to depths where total annealing of fission tracks would take place, some time during the Cretaceous **(Fig. 5.14b)**. The best-fit run **(Fig. 5.14c)** predicts that maximum burial took place in the earliest Tertiary (64 Ma), although the length and age fitting plot shows that maximum burial may have occurred at any time in the defined time range.

A further series of modelling experiments were contrived to model the younger groups of ages witnessed on the Bay of Biscay continental margins. These experiments were labelled consecutively *young ages 1* to *young ages 5*. The first two experiments input the following age and length data: age: 160±30 Ma, MTL: 12.5±1.0 μm and SD 2.0±0.5 μm. These represent the bulk of Jurassic-lower Cretaceous ages measured for the samples, located in southern Armorica and northern Spain. The T-t bounds for *young ages 1* is shown in **Table 5.4.**

	Time	temp.
1	300±20	120±20
2	250±30	60±60
3	110±20	60±60
4	0	10±10

Table 5.4 T-t values with bounds for *young ages 1*.

The simulations in *young ages 1* assume a preliminary model identical to that of *slow cool 1* constraining only the time and temperature at the end Variscan. T-t boxes were placed around the Permo-Trias and at the climax of rifting and breakup activity in the Cretaceous. Temperatures were given maximum bounds at these points. Age and length fit simulations all predicted a thermal history involving monotonic uplift between 300 Ma and the present **(Fig. 5.15)**. This scenario is unlikely.

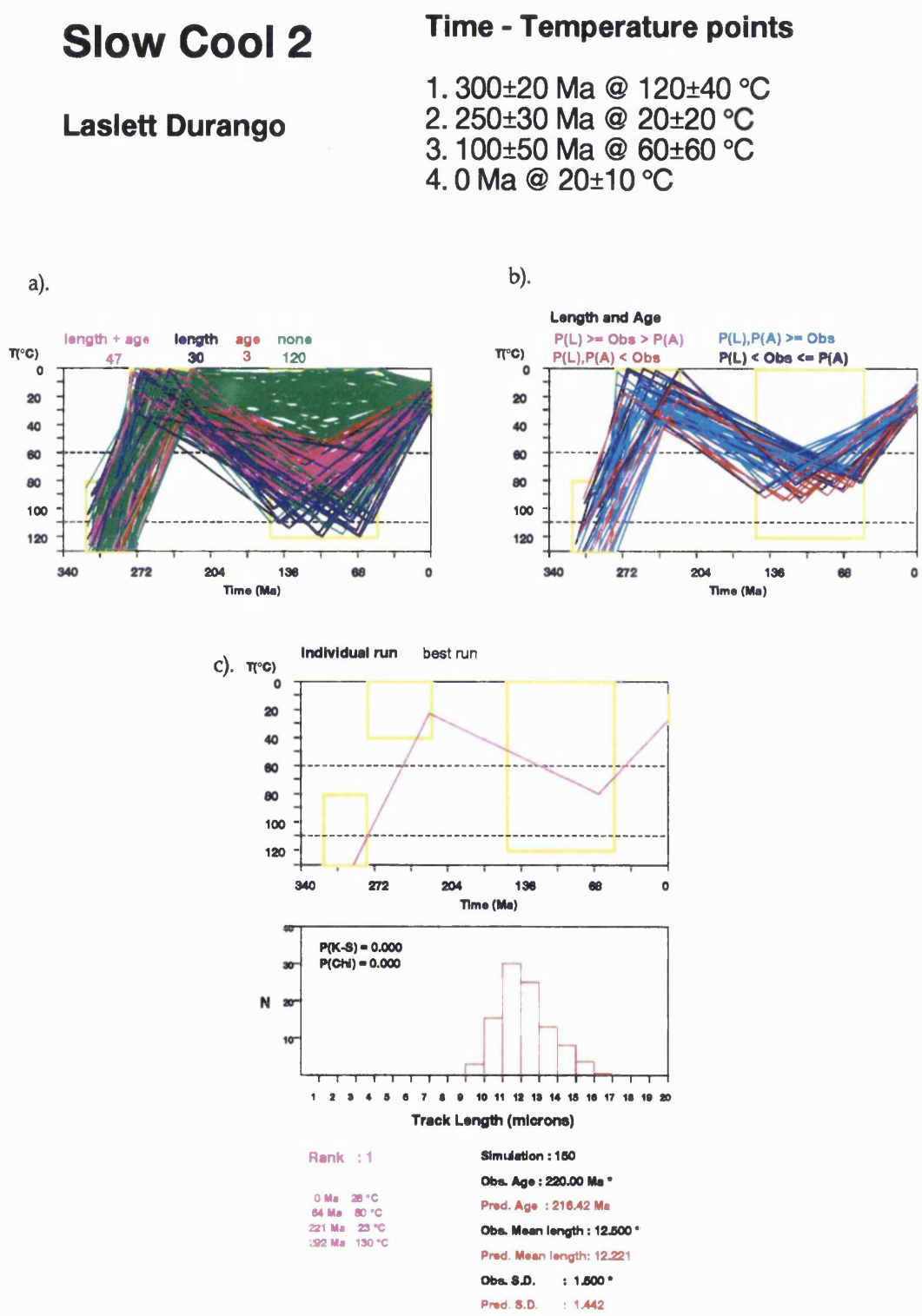

Fig. 5.14 a-c). Input data and simulations for the modelling experiment Slow Cool 2. In a). green is a failure, red fits age only, blue fits length only and pink fits length and age.

However, "age only fit" predictions fitted the familiar scenario of Permian unroofing, followed by Mesozoic (Cretaceous) burial to the lower regions of the PAZ. The track lengths predicted for these values were within the defined experimental uncertainties. The experiment *young ages 2* constrained the thermal history to unroofing during the Permian, and discarded the less feasible slow, monotonic cooling histories of *young ages 1*. The T-t box bounds are shown in **Table 5.5**.

	Time	**temp.**
1	300±20	120±40
2	250±30	30±30
3	110±20	60±60
4	0	10±10

Table 5.5 T-t values with bounds for *young ages 2*

Although no thermal history predicted both length and age values which fitted the measured data, as in *young ages 1* the ages fitted well, and the mean track lengths were not too dissimilar to the observed data. The predicted track length distributions have large standard deviations (around 3 μm) and approached bimodality, whereas the observed data had narrow distributions. The 2nd ranked run appeared to fitted the data better, although the predicted track length distribution had a strong negative skew, and very short lengths were present **(Fig. 5.16)**. The distribution is similar to that of an 'undisturbed basement' type (Gleadow et al, 1986b), possibly because the sample is predicted never to have attained temperatures less than ~ 50°C until the early Tertiary.

Young ages 3 incorporated a new set of age and length data to model the very youngest upper Cretaceous ages located in western Galicia. These were as follows; age: 95±20 Ma, MTL: 12.5±0.5 Ma and SD: 1.75±0.5 Ma. The T-t bounds are shown in **Table 5.6.** The thermal history in *young ages 3* showed a story comparable to that of *young ages 2*. A similar thermal history is postulated except that the model predicts a deeper burial, possibly to temperatures below the PAZ in the mid to upper Cretaceous.

	Time	**temp.**
1	300±20	120±40
2	250±30	30±30
3	110±20	60±60
4	0	10±10

Table 5.6. T-t values with bounds for "young ages 3"

Although these models yield predicted values which fit the fission track age data reasonably well, the predicted lengths fail to match the

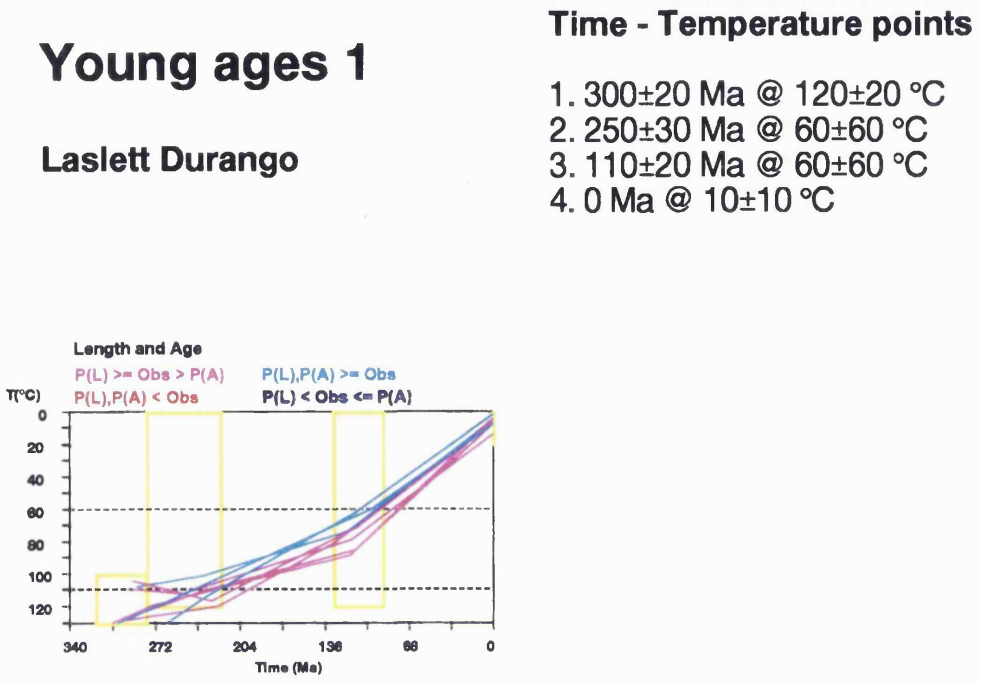

Fig. 5.15. Input data and length and age fit simulations for the modelling experiment Young ages 1.

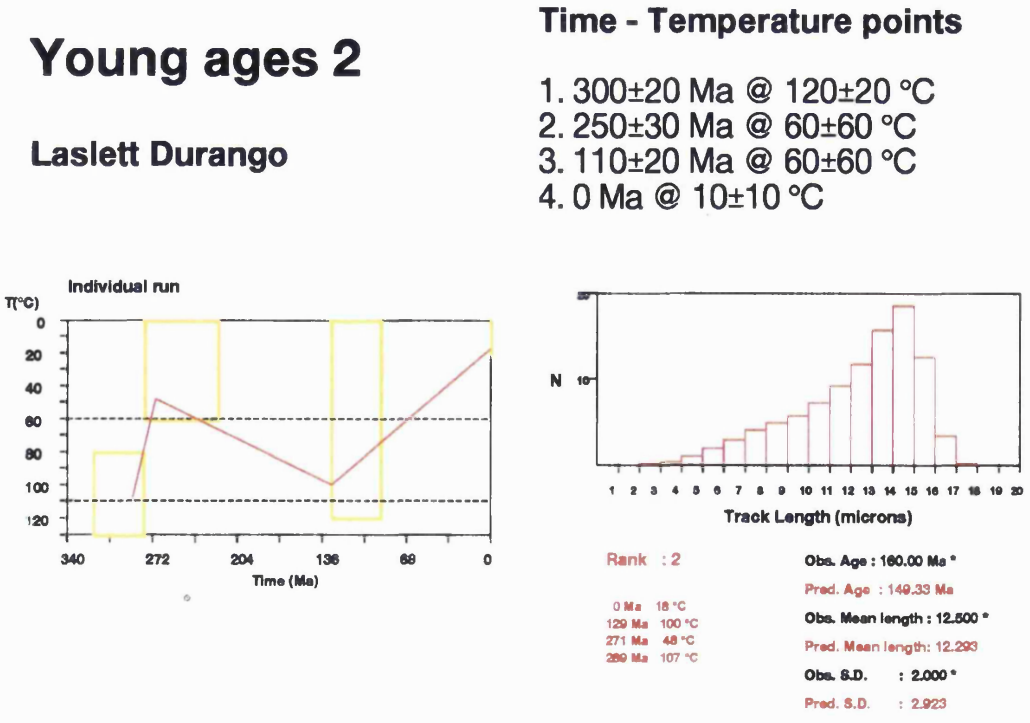

Fig. 5.16. Input data and 2nd best fit simulations for the modelling experiment Young ages 2.

observed length distributions. Each thermal history provides length distributions with >16 μm lengths (rare in the observed data) and often predict broad, bimodal distributions, particularly the case in the *young ages* series of models. Consequently a T-t scenario must be devised that excludes the appearance of long track lengths. A return to the preliminary forward models shows that, although perhaps less geologically viable at first view, the influence of elevated temperatures and/or burial persisting until the Miocene (Model F) predicted ages and lengths which match the observed data well. The model *recent uplift* was devised with the following T-t boxes **(Table 5.7)**, notably with the addition of a fifth time input at 10 Ma. The input age and track length data was: age: 160±30 Ma, length: 12±1 μm and 2±0.5 μm.

	Time	**temp.**
1	300±20	120±20
2	250±30	20±20
3	150±30	90±30
4	10±10	60±60
5	0	10±10

Table 5.7. T-t values with bounds for *recent uplift*.

All the T-t runs for *recent uplift* are plotted in **Figure 5.17.** The runs that failed to predict values which fit the observed data all remained at depth in the PAZ until the end of the Tertiary, and consequently any hypothesis implicating late Tertiary to Recent deep denudation of the massifs as a sole mechanism for the observed reduced ages must be discounted. The simulation runs that predicted values that matched the observed data all had the similar history of burial in the Jurassic to the lower regions of the PAZ, followed by slow, monotonic exhumation until the Miocene. Rapid denudation ensued between the Miocene and the present day. The best fit run and 2nd best fit both agree with the observed data precisely.

Attempts to model the anomalously young fission track age from the Armorican massif (VEND 16, 59 Ma) were abandoned because it was obviously not influenced by regional events alone, being surrounded by the oldest ages encountered. A possibility exists that this rock may have been reset by a localised geothermal system.

5.4.4. The Asturian Arc.

The anomalously young (Eocene) fission track ages obtained from the Asturian Arc were modelled in the series of experiments named *Asturia 1*, *Asturia 2* and *Asturia 3*. For all of these experiments the

following tightly constrained age length data were input: Age: 43±3 Ma, MTL: 12.5±0.5 μm and SD: 2.5±0.2 μm. Few horizontal confined tracks were present in these samples, and as a result the track length distributions are not conclusive.

The T-t data for *Asturia 1* are in **Table 5.8.** The thermal history T-t boxes are distinct from those used in the previous regions modelled. As one of the samples to yield an Eocene fission track age (SPA 38) is a Permo-Trias terrestrial sediment surface, or near surface exposure is assumed as a starting point. T-t box 2 puts large errors on the position of the sample during continental separation in the Aptian-Albian, and T-t box 3 does the same for the Eocene, prior to the Pyrenean collision.

	Time	**temp.**
1	250±30	20±20
2	115±20	60±60
3	40±10	60±60
4	0	10±10

Table 5.8. T-t values with bounds for *Asturia 1.*

Only two runs predicted age and length values which fitted the observed values in *Asturia 1* **(Fig. 5.18).** Both predicted a period of burial initiated in the mid-Cretaceous and continuing until cooling or unroofing at some time since the Eocene (37 Ma).

Asturia 2 modelled the effect of the entire region being buried at all time until recent times (i.e. the possibility of rapid burial soon after deposition) and the T-t points are shown in **Table 5.9.** In the *Asturia 2* Monte Carlo simulation, all the 200 runs predicted age and length values that failed to match the observed values, implying that this is an improbable scenario. The average run for this simulation gave a fission track age of 209.5 Ma with a MTL of 12.5 μm, SD 1.5 μm. Although the track length predictions are not unfeasible, the age is far too old.

	Time	**temp.**
1	250±30	60±60
2	115±20	60±60
3	40±10	60±20
4	0	10±10

Table 5.9 T-t values with bounds for *Asturia 2.*

Asturia 3 tested the scenario in which the sample had suffered no deep burial since the end of the Variscan orogeny, compatible with the accepted view. The T-t bounds are shown in Table 5.10 As with *Asturia 2*, all

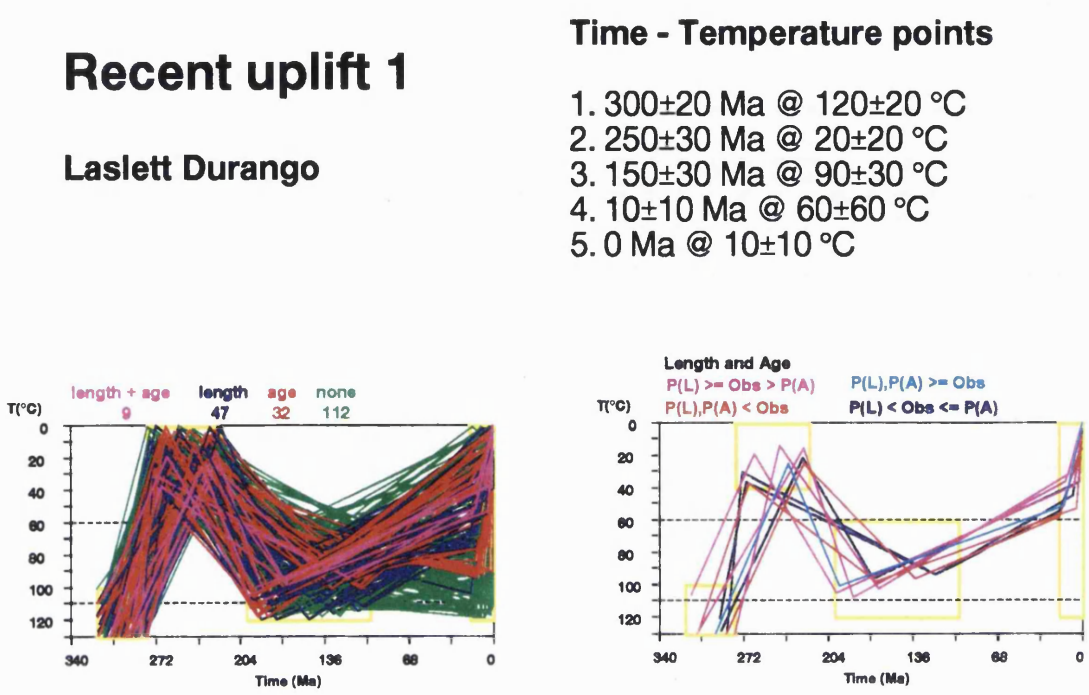

Fig. 5.17. Input data and length and age fit simulations for the modelling experiment recent uplift 1. Colours for all simulations plot is as in 5.14.

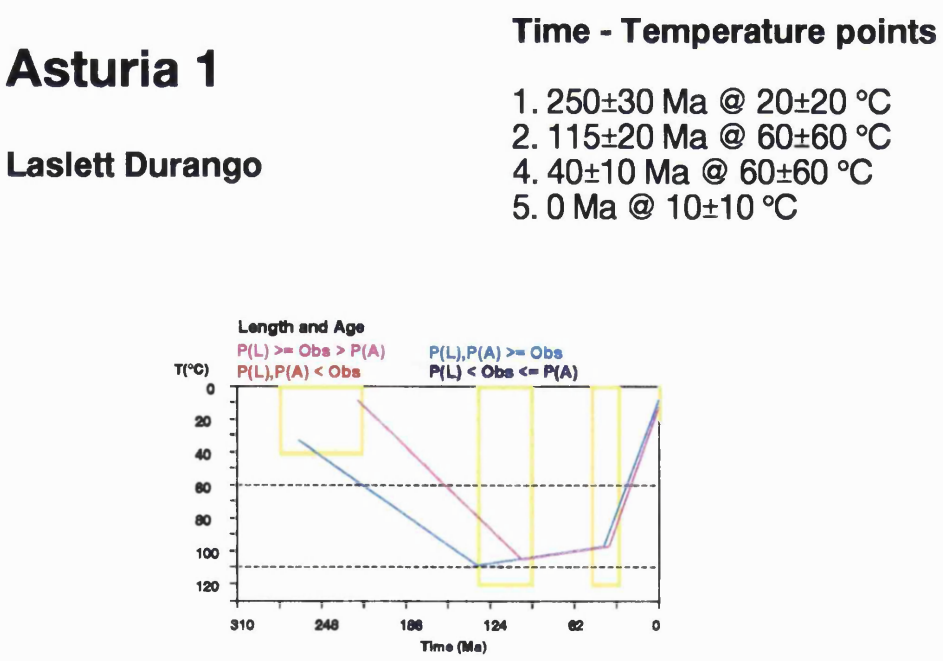

Fig. 5.18. Input data and length and age fit simulations for the modelling experiment Asturia 1.

200 simulations failed to predict the measured age and length values, again showing that this represents an unlikely scenario. The predicted age distribution cannot be confidently compared to observed data because the uranium density was too low to produce enough confined tracks with which to accumulate a sufficiently precise data set.

	Time	temp.
1	250±30	20±20
2	115±20	40±40
3	40±10	40±40
4	0	10±10

Table 5.10 T-t values with bounds for Asturia 3.

5.5 Summary and discussion.

The apatite fission track data presented in this thesis provide a new insight into the hitherto poorly understood post-Variscan evolution of the Armorican and Hesperian Massifs. Geological evidence complemented by computer modelling simulations provide a history of Permian unroofing, followed by burial during the Mesozoic and subsequent exhumation, revealing the massifs as observed at the present day.

The model *slow cool 1* predicted two possible scenarios both of which provided reasonably good fits to the data. The first involved a monotonic slow cooling scenario which should be discounted on a geological basis, as there is evidence that the Variscan belt was eroded down to a peneplain in the Lower Permian (Smith et al., 1974). The second scenario allowed the massifs to be exhumed in the Permian, and then buried during the Mesozoic, to be re-exhumed in the later Mesozoic and Tertiary.

Slow cool 2 constrained the model to fit a thermal history which involves a Permian exhumation, and the simulations predicted a situation wherein ensuing Mesozoic burial occurred to temperatures of approximately 90°C. Similar situations were predicted from the models devised to predict the appearance of the younger ages observed.

The model *recent uplift* was devised in an attempt to improve predictions of track length distributions to observed distributions. A situation similar to that predicted in the preliminary forward model F, predicted good fits to the observed age and length data. Consequently this appears to be the most likely thermal history for the evolution of the Variscan Massifs from the end of the Variscan Orogeny to the present day.

The relationship of the presented interpretation of the data to the known geology is as follows. Firstly, the fission track data accommodates deep denudation of the Armorican massif occurring during the Permian.

However, gradual monotonic cooling from the end-Carboniferous to the present can be discounted as an unviable thermal history. It is also unlikely that the rocks remained at the surface throughout the Mesozoic after initial exhumation during the Permo-Trias. The accepted view that the Armorican and Hesperian Massifs have remained as upstanding terrestrial blocks since the Permian is contested here as the apatite fission track data show clear evidence of burial during the Mesozoic. As a result of these modelling experiments, a proposed thermal history of the Armorican and Hesperian Massifs is illustrated in **Figure 5.19**. Assuming a geothermal gradient of 30°C km^{-1}, Permian exhumation was followed by burial to depths of 3 to 3.5 km (90-100°C), attaining these maximum depths in the mid Jurassic. This was followed by gradual exhumation during the Upper Jurassic to mid Miocene to the upper limit of the PAZ (60°C) at a rate of ~12 m Ma^{-1}. During the late Miocene, the rate of uplift apparently increased significantly to rates approaching ~130 m Ma^{-1}.

The anomalously young Eocene ages determined in the Asturian Arc have proved more complicated to explain. However, the models predict that the innermost Asturian Arc has undergone burial to the lower regions of the PAZ (but not to resetting temperatures) and has only been exhumed since the Neogene. Alternatively, these young ages could exist as a result of resetting by hot fluids moving along the many faults, fractures and thrusts of this region. This view is supported by the remagnetisation data of Schott and Peres (1987). Such fluids were possibly generated due to Pyrenean collision. Although not readily explicable, a strong case can be made for the influence of hot fluids on the anomalously young age of VEND 16, existing as it does in the region where the oldest ages are found.

The geographical relationships of the data show a generalised trend of increasing age away from the North Atlantic rift axis and are apparently unrelated, save in their obvious spatial distribution, to the rifting and opening of the Bay of Biscay. The data further uphold the passive nature of this particular rift when compared to major continental breakup, such as that of the Atlantic Ocean.

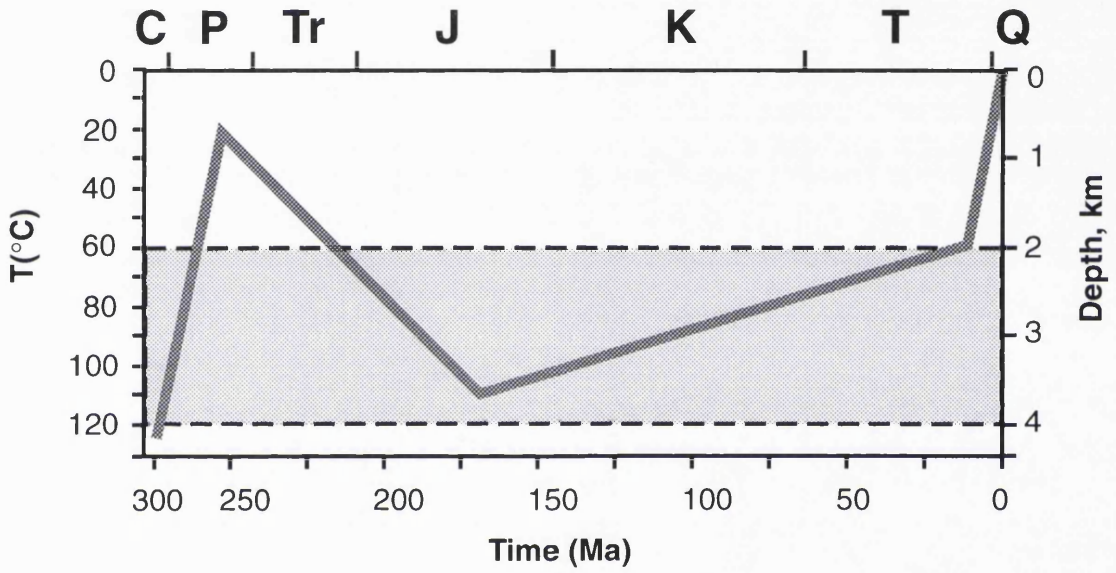

Fig. 5.19. The proposed regional thermal history of the continental margins of the Bay of Biscay deduced from geological controls and data-driven computer modelling.

Chapter 6.

The Mesozoic and Cenozoic evolution of the Western European Variscan Massifs: dynamic versus quiescent geological environments.

6.1 The apatite fission track data from the continental margins of the Bay of Biscay.

Apatite fission track analyses of rock samples from the Armorican Massif of western France and the Hesperian Massif of north-western Spain have revealed and clarified the hitherto poorly understood post-Variscan evolution of the region. In this chapter, comparisons of these data are made with available fission track data from other Variscan massifs, and from similar tectonic environments.

The apatite fission track data from the Bay of Biscay dispute some previously held concepts pertaining to palaeogeographic reconstructions for the region during the Mesozoic. In this chapter, tentative palaeogeographic maps are constructed to illustrate the major points.

The results of the fission track data reveal a range in ages from ~70 Ma in westernmost Galicia, increasing eastwards to ~270 Ma in Vendée. The geological interpretation of the apatite fission track data from the region was determined primarily from the currently accepted regional geological evolution and data-driven computer modelling. The stratigraphic evidence indicates that the region underwent deep denudation during the Permian, and that terrestrial Permo-Triassic sediments were deposited upon the peneplained massifs is upheld by the work in this thesis. However, the apatite fission track analysis predicts that, assuming a geothermal gradient of 30°C km^{-1}, rapid burial of the region ensued during the Early Mesozoic, with maximum burial to depths of 3 to 3.5 km during the Early-Mid Jurassic (Bajocian-Bathonian). Accelerated denudation during the Upper Jurassic to mid Miocene removed ~2 km of overburden at average rates of ~12 m Ma^{-1}. Rapid denudation at very high rates of ~130 m Ma^{-1} are proposed to have occurred since the Miocene, revealing the present landsurface.

6.2 A new palaeogeography for the Mesozoic of west-central Europe.

Palaeogeographic reconstruction requires a multidisciplinary approach. Maps are compiled dominantly from knowledge of

sedimentology, stratigraphy, palaeontology and plate tectonics. Many Mesozoic palaeogeographic maps are based upon the linking of faunal provinces between existing sedimentary rocks in surviving basins, and little credit is given to regions that have no Mesozoic sedimentation.

Apatite fission track data from the Armorican and Hesperian Massifs presented in this thesis provide conclusions similar to those drawn from other fission track data (e.g. the British Isles) where kilometre-scale burial and subsequent exhumation have played a major and hitherto unknown role (Green, 1986; Lewis et al., 1992a). The currently held theory published recently in Palaeogeographic atlases (cf. Ziegler, 1990, Cope et al., 1992), that the Armorican and Hesperian Massifs have remained upstanding blocks is contested by the interpretation of the fission track data. A series of new palaeogeographic maps from the Lower Permian to the end-Cretaceous is presented here based on information from already published work, and the apatite fission track data presented here. The sedimentological and stratigraphic information on the presented maps are from Ziegler's (1990) Geological Atlas of Western and Central Europe, this being the most recent, available compilation of data on a regional scale. This atlas includes little information for north-west Iberia. Consequently the palaeogeographic data for this region is compiled from the geological maps and other published sources. Information on sea-level variation is from Vail et al., (1977).

6.2.1 Permian to Triassic palaeogeography (280-208 Ma).

Published Permian and Triassic palaeogeographic reconstructions show a degree of affinity with the interpretation of the fission track data from the Bay of Biscay. During this time the European climate was warm and arid to semi-arid (Hay et al., 1981), and the suturing of Pangaea caused a retreat of shelf seas. The Hercynian (including the Variscan) Mountain belt was of high to moderate relief during this time although the topography was progressively lowered substantially during these periods. The newly uplifted mountain belt would have probably behaved as an orographic feature separating arid and semi-arid climates. Denudation of the mountains produced kilometre-scale fluvial and lacustrine sedimentation in the developing rift basins (Bay of Biscay, Western Approaches) and conglomerates and similar deposits within intermontane basins **(Fig. 6.1.)**. It is likely that such deposits would have been far more widespread than represented upon Ziegler's (1990) reconstructions from the Early Permian to Late Triassic, and would have initiated burial of the Massifs. During the upper Triassic **(Fig. 6.2.)**, restricted marine conditions developed in the Bay

Fig. 6.0. A key to the Palaeogeographic maps in Chapter 6

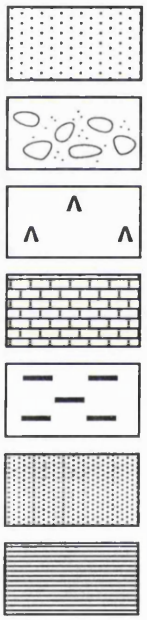

N.B. The symbols represent regional depositional environments rather than distinct lithofacies

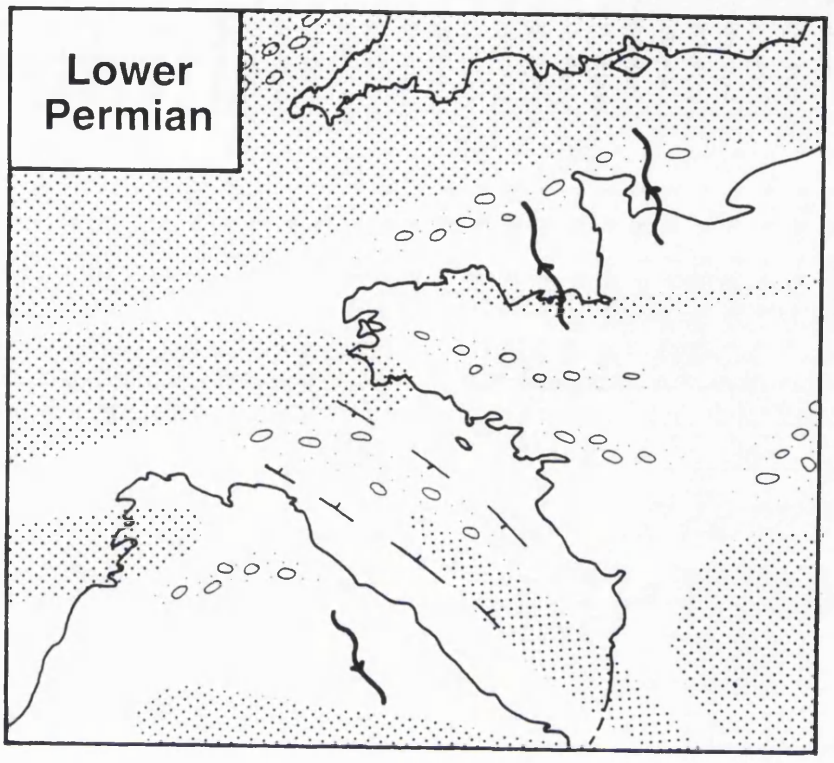

Fig. 6.1. Lower Permian palaeogeographic map (after Ziegler, 1990; Warrington and Ivimey-Cook, 1992).

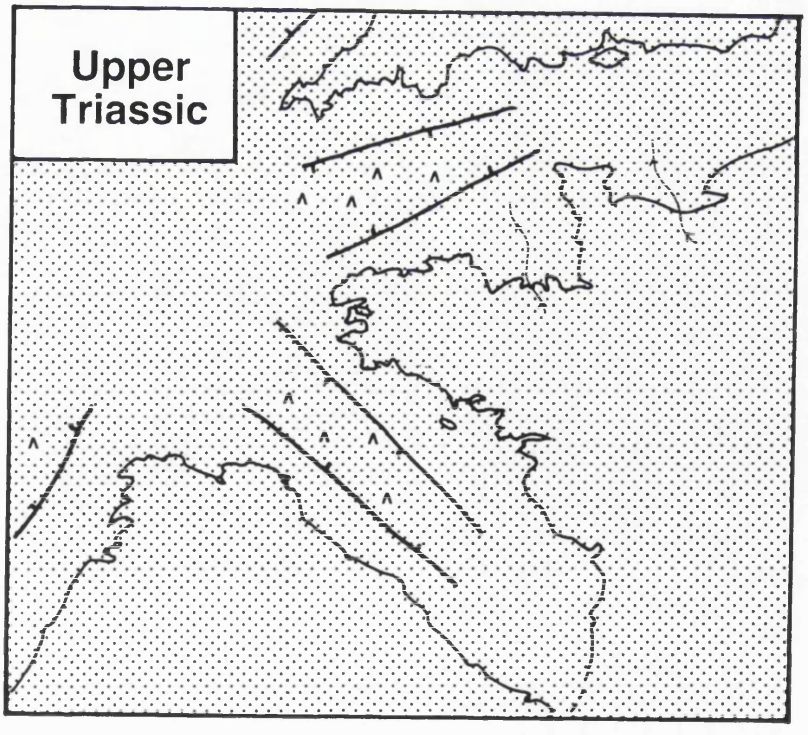

Fig. 6.2. Upper Triassic palaeogeographic map (after Ziegler, 1990; Warrington and Ivimey-Cook, 1992).

of Biscay represented by the formation of evaporites. The shorelines of the Armorican and Cornubian Massifs are poorly defined during this time (Warrington and Ivimey-Cook, 1992).

6.2.2 Rhaetian - Hettangian palaeogeography (210-204 Ma).

During the earliest Jurassic, marine environments were dominant over the region. The major clastic source regions at this time were the Cornubian and London-Brabant Massifs. The London-Brabant Massif, a Caledonian landmass trending NE-SW to the north of the Armorican Massif, developed marginal clastic deposits and fed sediments into the North Sea Basin. The Cornubian, Armorican and Hesperian Massifs in contrast were not important as source regions (Ziegler, 1990; Bradshaw et al., 1992). The thermal constraints imposed by the fission track analyses indicate that at this time the Armorican and Hesperian Massifs were undergoing active sedimentation and undergoing burial. In view of the regional evolution, it is feasible that they were partly, if not totally submerged, which allowed the deposition of carbonates and other shallow marine sediments, similar to those found in the Paris, Western Approaches and Bay of Biscay **(Fig. 6.3.)**.

6.2.3 Sinemurian - Aalenian palaeogeography (204-174 Ma).

Sinemurian to Toarcian was the time of a transgression; sea-levels later subsided during the Aalenian. Shallow marine sedimentation laying down carbonates and organic-rich shales, prevailed during the Early Jurassic. The Armorican Massif became more prominent as a source region providing limited clastic supply to the basins on the north-eastern and north-western margins. However, this does not necessary imply that it was a large area of land exposed above sea-level, and the Cornubian massif was also possibly partly submerged (Bradshaw et al., 1992) There is no evidence of clastic supply from the Hesperian Massif into the Bay of Biscay or Atlantic regions at this time. Sediments were fed southwards into the Duero Basin from the Hesperian Massif (Julivert et al., 1981) during this time **(Fig. 6.4)**.

6.2.4 Bajocian - Oxfordian palaeogeography (174-155 Ma).

A gradual transgression continued during the Bajocian and Bathonian. Sedimentation was restricted dominantly to thick carbonate deposits as marine waters deepened. Once again the Variscan massifs were not important source regions. Fringing reefs are located on the eastern margin of the Armorican Massif (Ziegler, 1990), which implies that some land was emergent, but by no means was this necessarily Palaeozoic

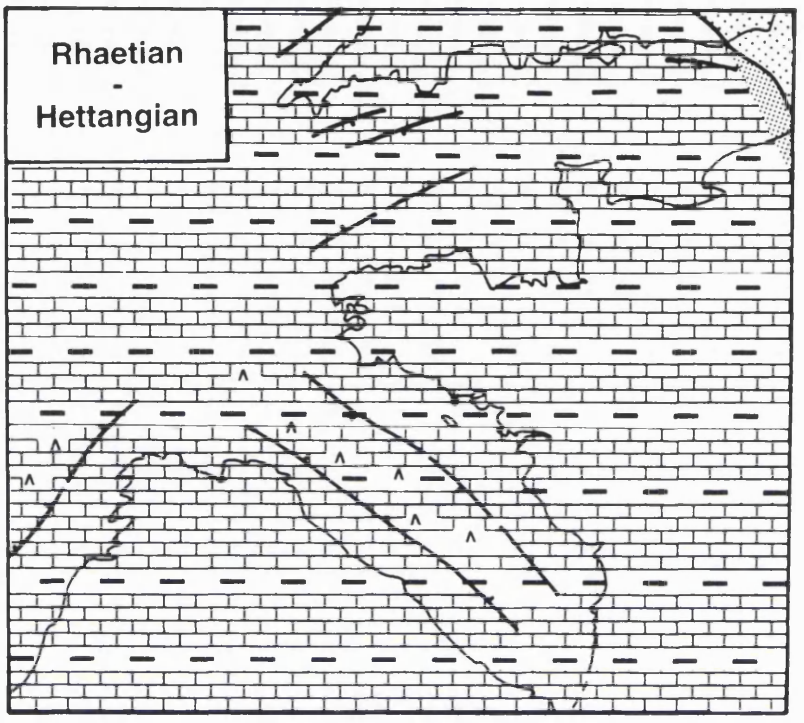

Fig. 6.3. Rhaetian-Hettangian palaeogeographic map (after Ziegler, 1990; Bradshaw et al., 1992).

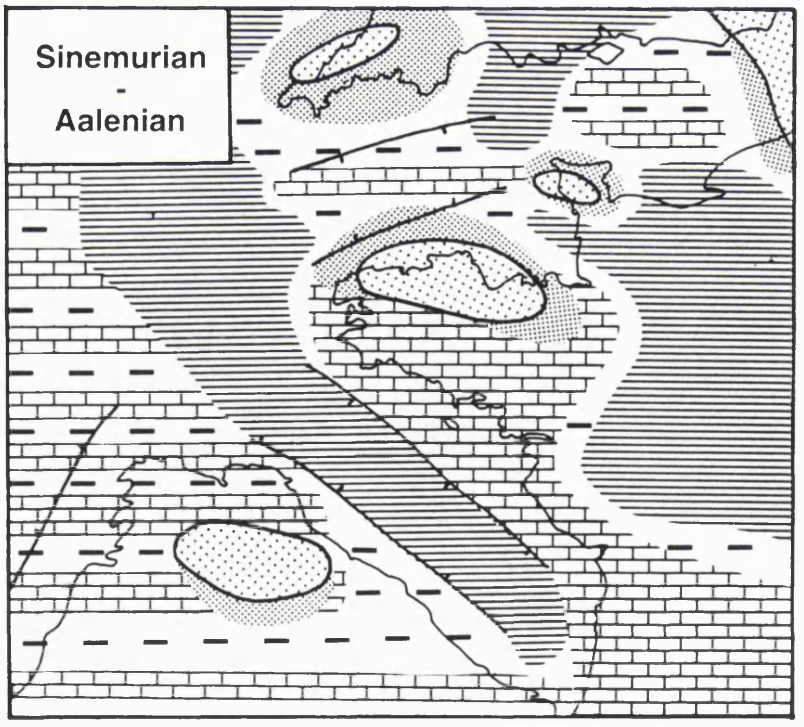

Fig. 6.4. Sinemurian-Aalenian palaeogeographic map (after Julivert et al., 1981; Ziegler, 1990; Bradshaw et al., 1992).

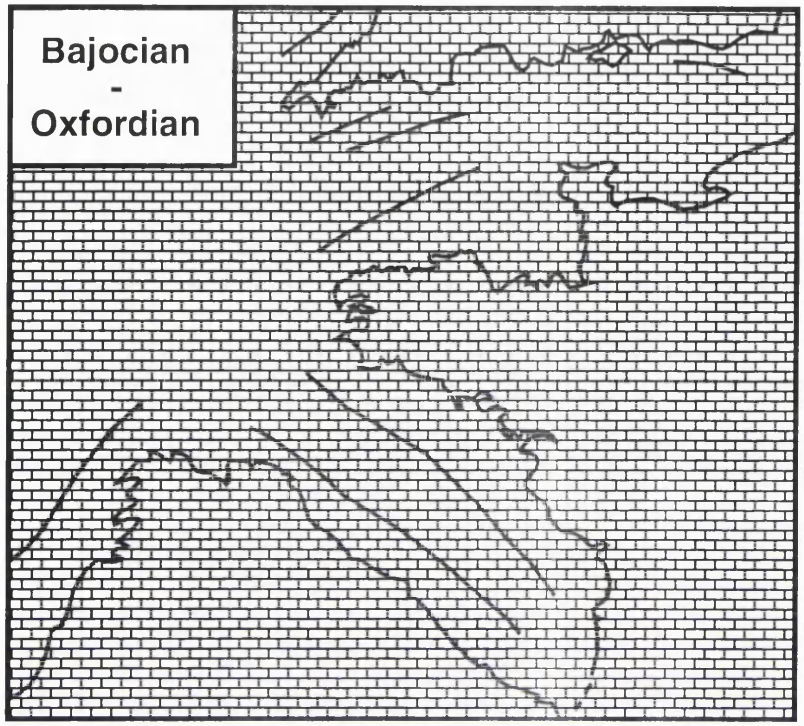

Fig. 6.4a. Bajocian-Oxfordian palaeogeographic map (after Ziegler, 1990; Bradshaw et al, 1992).

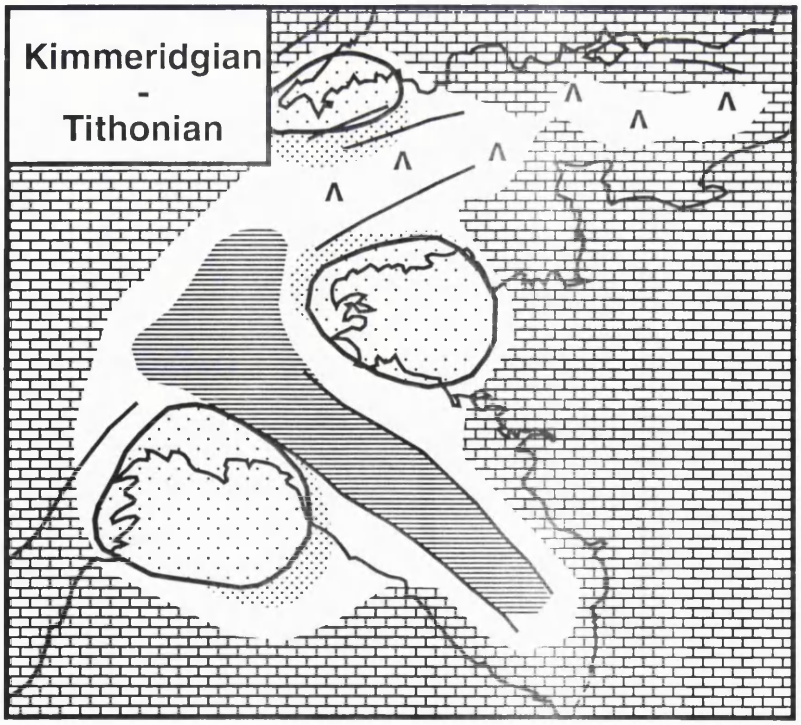

Fig. 6.4b. Kimmeridgian-Tithonian palaeogeographic map (after Ziegler, 1990; Bradshaw et al, 1992).

basement. Also the appearance of Fullers Earths at this time in The English Channel region suggests the emergence of volcanic edifices, possibly located on the Cornubian Massifs (Bradshaw et al., 1992). It is during this time that the apatite fission track data predict maximum burial, and this correlates with the regional transgressive environment.

6.2.5 Kimmeridgian - Tithonian palaeogeography (155-146 Ma).

Sea-level remained high until the Mid Kimmeridgian, with regression occurring during the later Kimmeridgian to Tithonian. By this time the rift dome associated with the formation of the Bay of Biscay was beginning to form and the Armorican, Cornubian and Hesperian Massifs around the Biscay triple junction began to be uplifted and became emergent. Consequently they were of renewed importance as source regions, supplying sediment into the Western Approaches and Cantabrian Basins. Evaporites formed in the Western Approaches and English Channel basins. The Armorican and Hesperian Massifs were source regions for limited marginal clastic sedimentary rocks. Meanwhile waters deepened substantially in the Biscay rift zone and deeper marine shales and turbidites (derived from the Hesperian Massif) were deposited.

6.2.6 Berriasian - Barremian palaeogeography (146-125 Ma).

The Biscay rift dome attained its maximum extent immediately prior to the onset of seafloor spreading in the Bay of Biscay and the Galicia Banks-Flemish Cap regions. The Armorican, Hesperian and Cornubian Massifs became emergent and sedimentation was limited to terrestrially derived fluvio-deltaic sediments deposited into the Western Approaches, English Channel (Hancock and Rawson, 1992), Paris and Cantabrian Basins (Ziegler, 1990, Julivert et al., 1981). Shallow to deep marine sedimentation continued in the Bay of Biscay rift. The Lower Cretaceous was a time of clastic-dominated sedimentation patterns in all regions **(Fig. 6.5)**.

6.2.7 Aptian - Albian (125-97 Ma).

Sea-floor spreading in the Bay of Biscay began in the Aptian-Albian, with the initiation of subsidence in the rift dome and consequent further reduction in land areas. The sedimentation was shallow marine and dominantly sandstones and shales; initially, all the massifs were important source regions. By the late Albian the land areas were decreasing (Hancock and Rawson, 1992). Deeper marine carbonates were deposited on the Armorican and North Spanish shelves, and deep water conditions prevailed in the widening Bay of Biscay. Sands and carbonates were

deposited in the subsiding Cantabrian Basin, sourced from the Iberian Meseta (Gabaldón-López, et al., 1989), in the Duero basin deposition was of a similar style (Julivert et al., 1981).

6.2.8 Cenomanian - Maastrichtian palaeogeography (97-65 Ma).

The Upper Cretaceous was a time of a general increase in global sea-level, with an associated reduction of clastic supply. Shallow marine conditions prevailed and this was accompanied by the deposition of carbonates. In northern Europe, the chalk seas deepened attaining maximum transgression during the Campanian. At this time, the Armorican (and possibly Cornubian) landmasses once again became submerged (Hancock, 1987, Hancock and Rawson, 1992). The Hesperian massif was probably emergent, as a result of Pyrenéan convergence. The Spanish Cantabrian, Duero and Ebro Basins were separate sedimentary environments. The Armorican and Hesperian Massifs shed carbonate sands and bioclastics (Gabaldón-López et al., 1989; Julivert et al., 1981). Deepest waters in the Campanian laid down limestones and marls. Sea-level subsided regionally during the Maastrichtian.

The fission track data do not provide any further interpretations or conclusions to the evolution of this region during the Late Cretaceous. However the palaeogeographic overview provides further resolution to the constructed thermal history. The major transgressive events were a time of sedimentation of thick chalk deposits throughout the North Sea - English Channel region. It is therefore probable that there was sedimentation in the region of the Armorican and Cornubian Massifs, if not in the Hesperian Massif. Therefore a second period of burial affected at least parts of the region after the opening of the Bay of Biscay.

6.2.9 Tertiary and Quaternary palaeogeography.

The fission track data do not dispute the published palaeogeographic reconstructions for the Tertiary. Western Europe underwent rapid inversion and became emergent primarily due to Alpine compression and the opening North Atlantic Ocean. As a consequence, thicknesses of clastic sediments were deposited in all the offshore basins (Ziegler, 1990; Murray, 1992), and into northern part of the Duero Basin, sourcing the Hesperian Massif (Julivert et al., 1981). Having had most of the accumulated Mesozoic sediments removed, minor transgressions spread onto the denuded Armorican Massif. A global cooling event in the late Cenozoic, detected from stable isotope data **(Fig. 6.6)**, would have had the effect of increasing glaciation, storms and disrupting vegetation, humidity

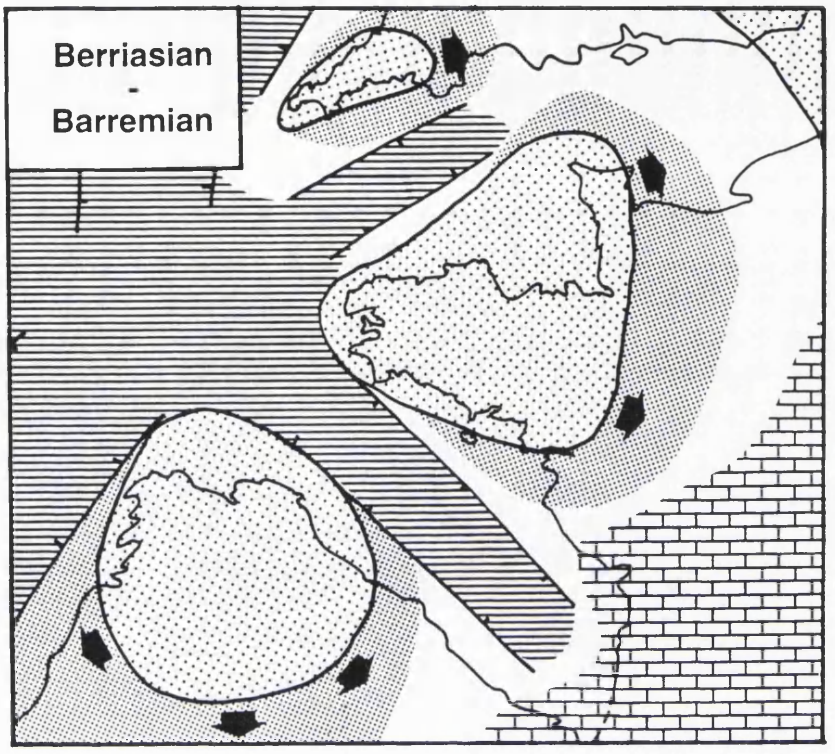

Fig. 6.5. Berriasian-Barremian palaeogeographic map (after Julivert et al., 1981; Ziegler, 1990; Hancock and Rawson, 1992).

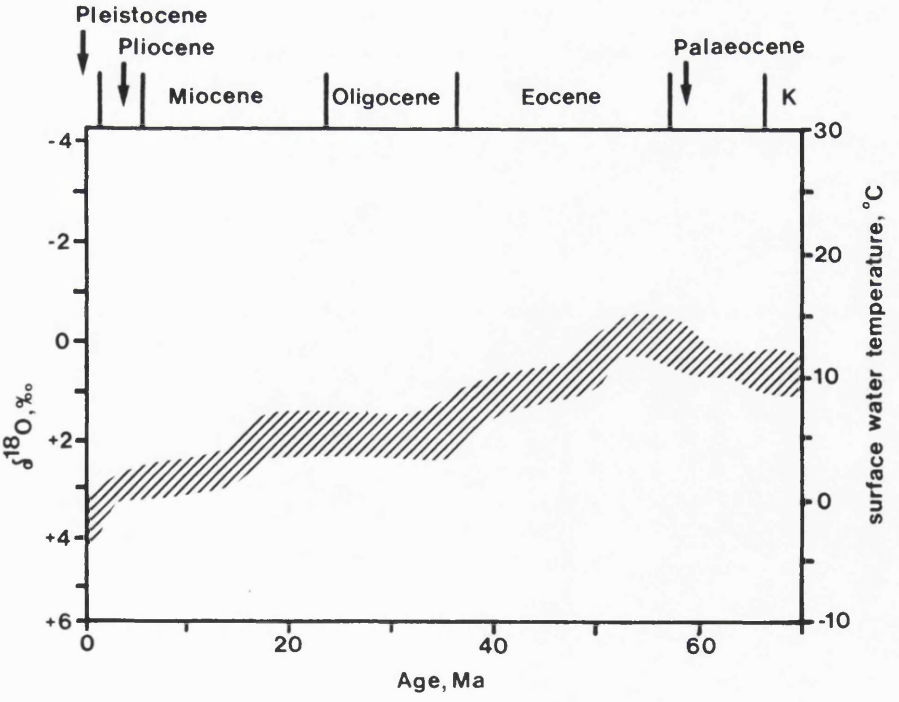

Fig. 6.6. Oxygen isotope records and inferred temperatures for the past 70 Myr, from ocean deep waters in the South Atlantic. Ocean deep waters are formed at high latitudes, therefore this curve can represent the isotope composition of high latitude surface waters. Prominent global cooling events occurred in the Mid Eocene, the Early Oligocene, the Mid Miocene and the Plio-Pleistocene (after Molnar and England, 1990).

and precipitation patterns. All of these events may have significantly increased denudation rates (Molnar and England, 1990). The region became totally emergent during the Pleistocene. Further denudation occurred during the Quaternary due to the glaciations, the Cantabrian Mountains were particularly affected.

6.3 Discussion and implications.

An important point drawn from this chapter is that examination of the palaeogeographic reconstructions for the Mesozoic enables further refinements to the thermal history proposed in the previous chapter (see Fig. 5.19). During the Upper Cretaceous, the chalk seas were well developed in Northern France, the British Isles and the North Sea, and reached maximum transgression in the Campanian. Thicknesses of c. 500-1000 m of chalk are at present preserved in basin areas (Hancock, 1987). This is probably not representative of the true thickness, the top of the chalk providing a prominent unconformity in the North Sea and adjacent regions. The Armorican and Cornubian Massifs were undoubtedly submerged during the Campanian, and probably underwent chalk sedimentation, therefore a second burial episode during the Campanian maximum transgression is proposed to accommodate this. According to the thermal history derived in Chapter 5, this period was a time of monotonic exhumation. Consequently further modelling is required to assess whether the fission track data are consistent with this refined scenario.

6.4. Modelling a second phase of burial.

The revised thermal history was tested by running a forward model to examine whether or not the fission track data would fit this hypothesis. The results of the modelling are illustrated in **Figure 6. 7**. The predicted fission track data resemble those observed from the Armorican Massif, in terms of track length distribution and apparent age. Two data-driven random simulations modelled the thermal history, both using the same constraining time-temperature points, but two separate suites of input fission track data. The first tested the Campanian model against the fission track data from the Armorican Massif. The T-t data and input fission track parameters, as well as the thermal history scenarios predicted that matched observed age and lengths are illustrated on **Figure 6.8** There were 13 fits to age and length data in this particular set of simulations. The 10 best runs predicted fission track ages between 153 and 188 Ma. These ages and their associated length distributions since they are from the western Armorican Massif imply that this thermal history is applicable to this region. The

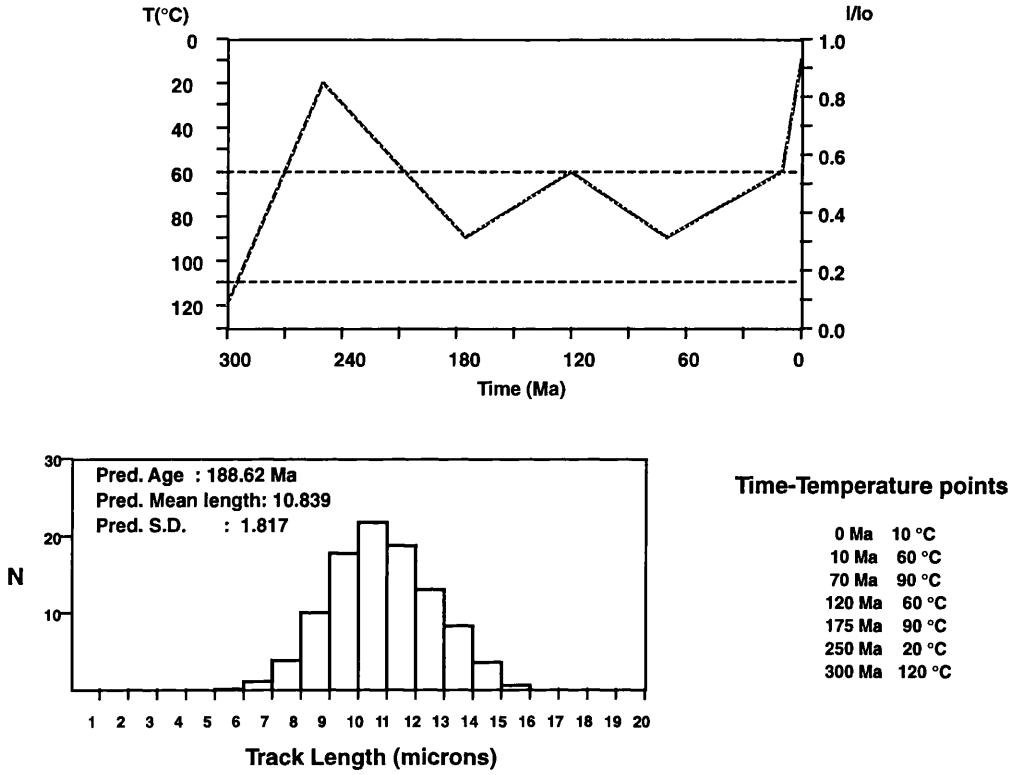

Fig . 6.7. The forward model used to predict an apatite fission track age and length distribution for a thermal history involving burial of the sample during maximum transgression during the Campanian.

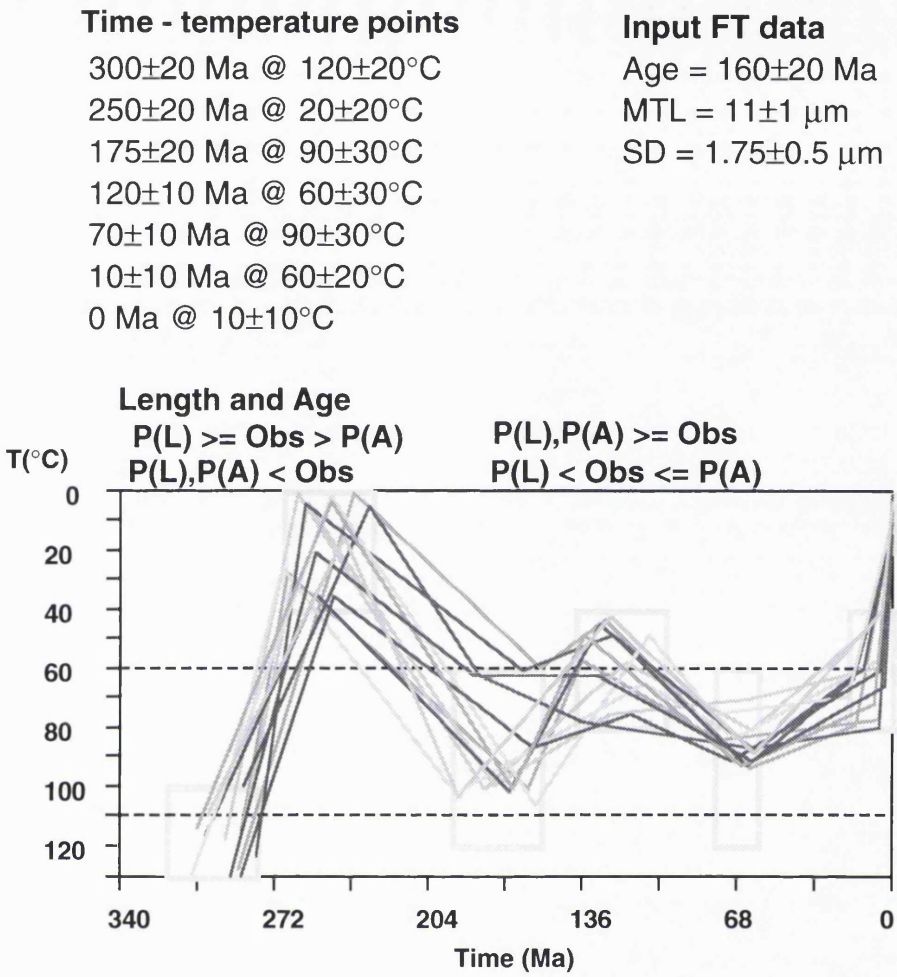

Fig. 6.8. The length and age fits for the data-driven thermal history model testing the hypothesis of a second Upper Cretaceous burial. The fission track data input were designed to model the data from the Armorican Massif.

model suggests that this second burial of the Armorican Massif attained maximum temperatures of ~80-90°C. It is a reasonable assumption that the overburden was chalk, therefore a geothermal gradient for compacted chalk of 53°C km^{-1} (Holliday, 1993) is used to estimate depths of burial. The resulting value of >2 km burial is compatible with the thicknesses of chalk preserved in sedimentary basins (Hancock, 1987).

The modelling experiment was repeated using fission track age and length parameters representative of those observed in western Galicia: age, 90±20 Ma, MTL, 12±1 μm and σ, 1.75±0.5 μm. Seafloor spreading in Bay of Biscay had practically ceased by this time, and the Hesperian Massif was separate from the Armorican Massif. Importantly, it was undergoing different sedimentation patterns. The model provided no matches to the observed age and length data and it can therefore be considered as unviable in this region.

6.5. Summary.

Whilst contributing to palaeographic knowledge of the regions presently surrounding the Bay of Biscay, the reconstructions in sections 6.2.1 to 6.2.9 also provide further refinements of the Late Cretaceous thermal history for the Armorican Massif, and indicate that its geological evolution during this time was distinct from that of the Hesperian Massif.

Published regional (Ziegler, 1990; Cope et al., 1992) differ from the reconstructions proposed in this chapter in that they portray the western European Variscan Massifs as remaining as emerged land since the end of the Variscan orogeny, undergoing only minor marine incursions. The fission track data observed in the Armorican and Hesperian Massifs represent a thermal history involving burial during the Mesozoic, and therefore suggest that this is not the case. Submersion of, and associated sedimentation on these Massifs is proposed during the Middle to Upper Jurassic to allow burial to temperatures estimated from interpretation of the fission track data.

However, the Upper Cretaceous (Campanian) transgressions provide evidence in the Armorican Massif of chalk sedimentation. This otherwise unaccounted for period of burial was forward modelled and the results showed that it was a viable refinement to the final model proposed in Fig. 5.19. Data-driven simulation experiments constrained that Campanian burial occurred in the Armorican Massif but did not affect the Hesperian Massif.

The revised thermal history is illustrated in **Figure 6.9.** Following maximum heating to temperatures of ~100°C (equating to a burial depth of

3-3.5 km, assuming a geothermal gradient of 30 °C km^{-1}), cooling caused by exhumation proceeded during the Upper Jurassic, in response to the formation of the Biscay Rift Dome. Approximately 1.5 km of chalk were deposited on the Armorican Massif during the Upper Cretaceous and subsequently removed during the Tertiary and Quaternary. The thermal history for the last 60 Myr is similar to that proposed in Chapter 5.

The predicted thermal history for the Hesperian Massif remains unaltered from that proposed in Chapter 5. There is no evidence either stratigraphically or from the fission track data that it has been buried since the Mid Jurassic.

ADDENDUM

Further explanation regarding heat flow in areas of thinned crust should be added to the interpretation of the fission track data. The effects of a variation in geothermal gradient and the proximity of the rift flanks is described below with respect to the temperatures involved in apatite fission track analysis. Cochran (1983) estimates that during rifting a transient thermal elevation of the rift flanks will arise creating an elevation of ~500 m on these flanks. This thermally elevated rift flank will decay spatially and temporally with a time constant of 60 Ma. Hiscott (1989) proposed from Atlantic margin basin stratigraphy that a "rift dome" was in evidence around the Biscay Triple Junction during the Late Jurassic and Early Cretaceous. This edifice probably represented the type of structure modelled by Cochran (1983), rather than a large rift dome of the type associated with a mantle plume. An elevation of 500 m on the Armorican and North Spanish rift flanks is appropriate to produce the erosion on a scale predicted by the apatite fission track analysis over a period equivalent to the time constant (see page 185)

The rift flanks will have suffered enhanced heat flow from lateral transfer of heat from the rift zone. From Cochran's model, the heat flow on the rift flank is elevated by ~30% relative to an averaged continental crustal heat flow ~59 mW m^{-2} (Sclater et al, 1980). Broadly speaking this is equivalent to a geothermal gradient of between 40 and 27 °C km^{-1} assuming a thermal conductivity of 2 - 3 W m^{-1} K^{-1}. If the geothermal gradient was at 40 °C km^{-1} this would decrease the depth to the sampled horizon by ~1 km to 2.0 - 2.5 km rather than 3.0 - 3.5 km (predicted using a geothermal gradient of 30 °C km^{-1}) during the Mid to Late Jurassic. This in turn would decrease the amount of subsequent erosion by a similar amount. However, even if the geothermal gradient was > 40°C km^{-1}, denudation in the order of ~2 km would be required to expose rocks with apatite fission track ages and track length distributions comparable to those observed in the samples from the Armorican and Hesperian Massifs (see figure below).

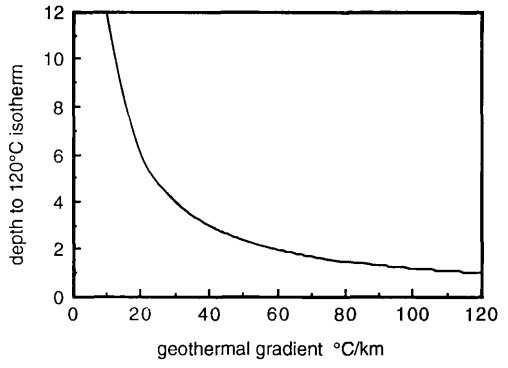

The figure above shows the relationship between the geothermal gradient and the depth to the 120°C isotherm (the base of the PAZ).

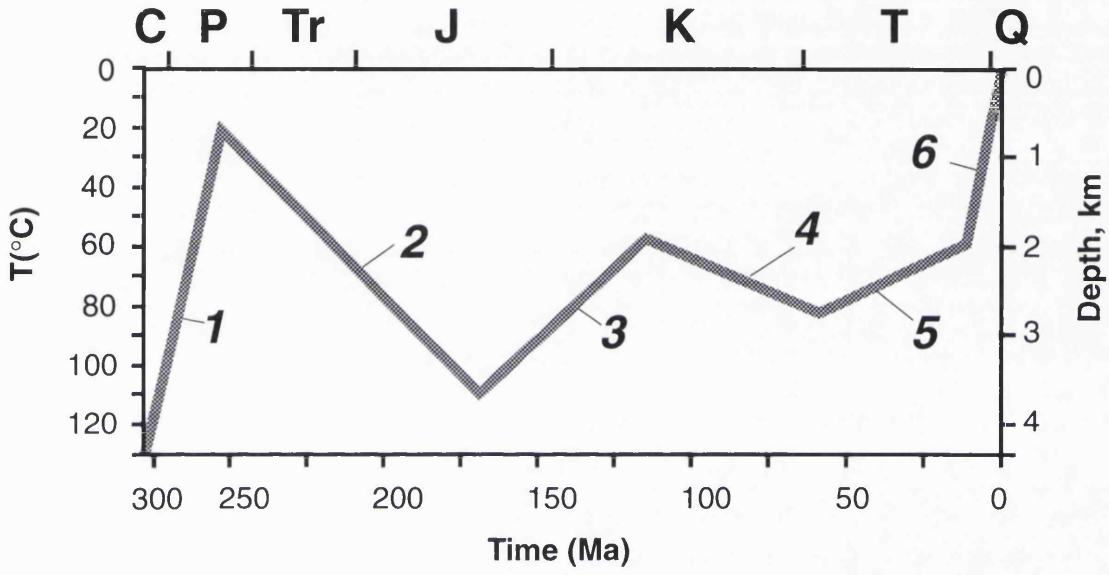

Fig. 6.9. The thermal evolution of the Western European Variscan Massifs. 1. rapid post-orogenic uplift, leading to exhumation of the Variscan basement during the Permian. 2. Early Mesozoic burial of the basement by sedimentary overburden. Maximum burial occurring in the Early-Mid Jurassic. 3. Partial exhumation of the buried massifs associated with crustal upwarping, leading to the formation of the Biscay Rift Dome in the Lower Cretaceous. 4. A second burial associated with the subsidence of rift dome and sedimentation associated with high sea-levels during the later Cretaceous. 5. Early Tertiary crustal uplift and denudation. 6. Accelerated denudation associated with late Tertiary global cooling, Alpine compression and Quaternary glaciations.

Chapter 7

The influence of paragenesis and crystal structure on the formation and fading of fission tracks in apatite.

7.1 Introduction.

Apatite is the most abundant phosphate mineral and is present as an accessory in most rock types. Although it occurs as a primary igneous and metamorphic mineral, it also forms authigenically as sedimentary phosphate deposits. Apatite is also the compositional material of bone and teeth, and consequently will enter the fossil record from this route as well. The general chemical formula of apatite is $Ca_5 (PO_4)_3$ (OH, F, Cl), but is prone to many substitutions into the lattice for the calcium and phosphate groups as well as for the anions (Latil, 1975).

Apatite is the most important mineral used in fission track analysis, primarily because it is geologically ubiquitous and contains sufficient uranium. Apatite annealing behaviour has been studied in far greater detail than in any other mineral, and as a result it has been observed that apatite crystal chemistry may have profound effects upon the annealing behaviour of fission tracks (Green et al., 1986). This is an important issue and is a current stumbling block in the precise interpretation of apatite fission track analyses. It is because of this compositional control that the crystal chemistries of the dated grain populations should be known, especially in samples of sedimentary rocks where the apatite crystals are likely to have been derived from several provenance areas. This present research has been motivated by a poor understanding of the actual effects of change in chemistry upon fission track annnealing.

The variation in apatite crystal chemistry is primarily determined by the geochemical environment in which it originally formed. These chemical changes can have significant effects in apatites on the crystallographic scale and further, on the morphology and behaviour of fission damage within the crystal lattice.

7.2 The geological occurrence of apatite species.

Apatite occurs dominantly as an accessory mineral in many igneous and metamorphic rocks and, due to their high specific gravity (3.1 - 3.35 g cm^{-3}) and their resistance to weathering, apatites are often incorporated into the sedimentary rock record as detrital minerals.

Authigenic sedimentary apatite is usually cryptocrystalline 'collophane' (carbonate hydroxyl fluorapatite, often called 'limonite'), in which the Ca_3OH group has, in part, substituted for the PO_4 group. Phosphorites deposits, derived from coprolites and bone material, are particularly rich in sedimentary apatite and represent a valuable economic source for phosphate extraction. Only 20% of the worlds economic phosphates come from igneous apatite, often associated with iron deposits, whereas ~75% of world production come from sedimentary phosphorites, the remaining few % being derived from bird and bat guano (Cathcart, 1991). Despite the importance of these authigenic sedimentary deposits, their lack of sufficient uranium and cryptocrystalline structure renders them unusable for fission track analysis, and they can consequently be disregarded.

Primary igneous apatites comprise ~0.1-1% of granitic and other acid rocks **(Fig. 7.1)**, their abundance diminishes drastically in basic rocks. Carbonatites are particularly apatite-rich, often occurring in percentages equivalent to the major rock forming minerals. Locally up to 96% apatite occurs in apatite-diopside-phlogopite rocks (i.e. phoscorite) associated with highly alkaline magmatism.

The substitutions of fluorine, chlorine and hydroxyl anions within apatite is dependent on the relative abundance of these three anions in the original melt, the temperature at which the phases crystallised and their interaction with already crystallised apatites. If all three anions are present in the melt, fluorapatite is the most likely mineral to form (Ekström, 1973; Latil and Maury, 1977). In high temperature melts, hydroxylapatites and chlorapatites have a greater likelihood of forming. In many cases, apatites exhibit compositional zoning both for trace and major elements **(Fig, 7.2)**.

Although fluorapatites are the most abundant species, most contain varying amounts of chlorine. Stormer and Carmichael (1971) and Whitney and Stormer (1985), report that of all igneous rocks, calc-alkaline-dacitic rocks such as the Fish Canyon and Bishop Tuffs tend to have often about 1 weight percent chlorine in the apatites. There is further evidence of large variation between the fluorapatite and chlorapatite end members within layered basic intrusions such as the Bushveld Complex (Boudreau et al., 1986). Here the cumulus apatites are fluorapatites, the non-cumulus apatites contain F-OH-Cl, interstitial and vein apatites are chlorapatites. The formation of the latter phase is probably due to interference of chlorine-rich fluids (Boudreau et al., 1986).

Extrusive igneous rocks tend to be of a more homogenous apatite composition than plutonic apatites as a consequence of rapid crystallisation

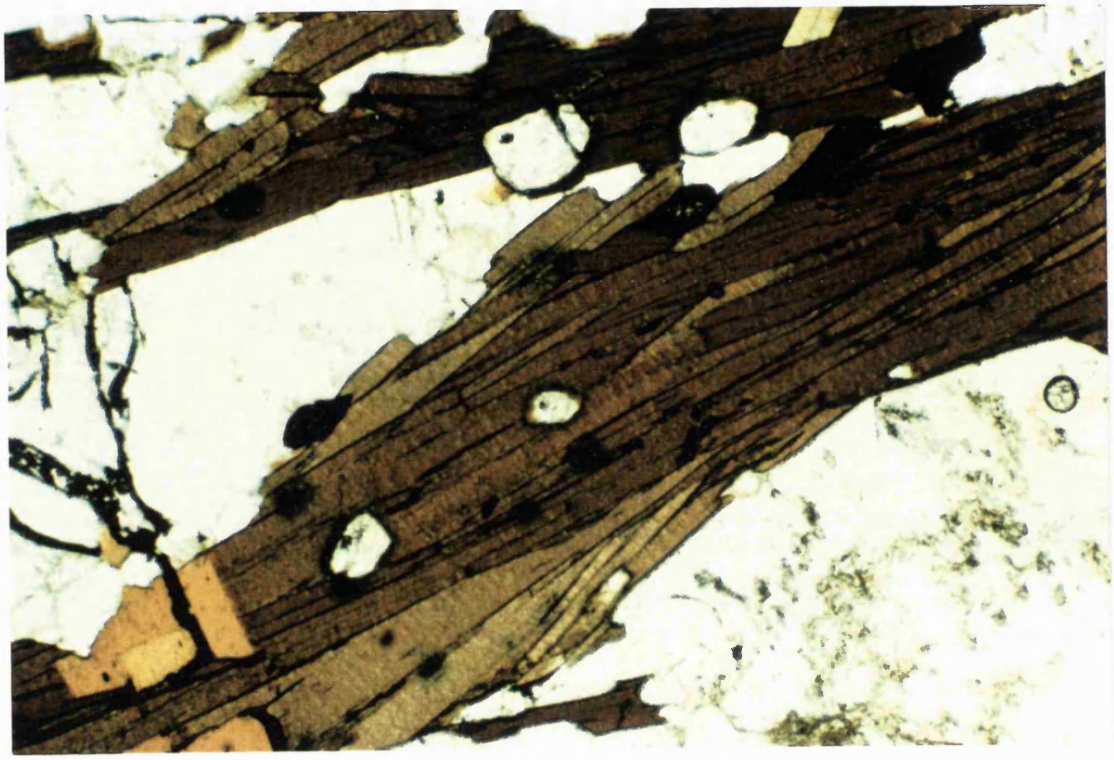

Fig. 7.1. Photomicrograph of apatites in a migmatised granite from Southern Brittany (x 10)

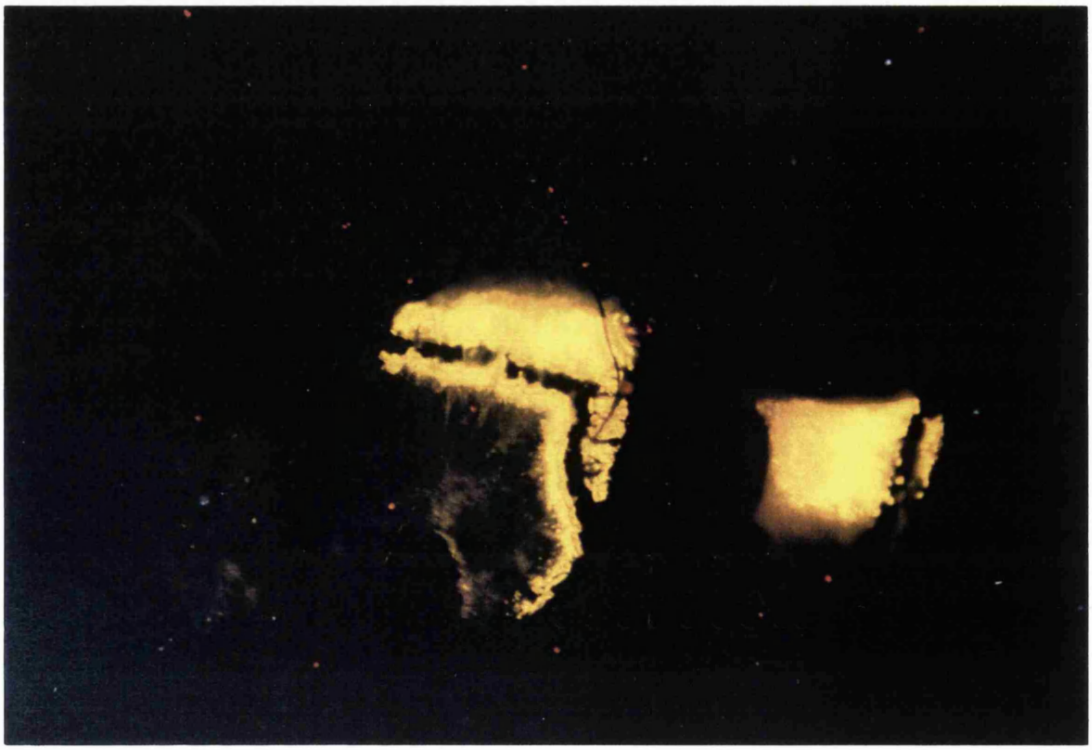

Fig. 7.2. Photomicrograph showing trace element zoning in apatites, from Turf Pits Mine, Yorkshire, revealed by cathodoluminescence.

in a geologically instantaneous cooling episode. However, apatite phenocrysts which crystallised prior to eruption or even during an earlier eruption can easily become incorporated into a lava or ash during explosive volcanism.

In igneous systems, chlorine is expelled from degassing magmas, along with other volatiles (water and carbon dioxide) as the melt rises (Metrich and Rutherford, 1992) and as a result it is a common constituent of geological fluids. Thus mineral deposits surrounding fumaroles are often chlorine-rich. In silicic melts, chlorine will be concentrated in the water rich vapour above the melt (Webster and Holloway, 1988). As a consequence the chlorine depleted melt will lead to the formation of fluorapatites in the magma, whereas chlorapatites are more common in hydrothermal systems where trace elements are often transported as chlorine-metal complexes (Webster, 1992). Single apatite crystals are known to reach enormous sizes (~1 m) in hydrothermal veins in parts of Norway and Canada.

All apatite species are common in thermally and regionally metamorphosed rocks. Chlorapatites are common in metasomatised calc-silicate rocks and impure limestones, often in association with phlogopite and scapolite. During metamorphism, minor substitutions may occur, but apatites are not readily altered if the bulk rock chemistry remains the same. However, metasomatic rocks can contain unusual apatite compositions, due to the influence of volatile rich fluids.

Under the right circumstances, i.e. contact metamorphism, hydrothermal or meteoric alteration, where F-ions are likely to be transported, it is likely that chlorapatite and hydroxylapatite will trend to fluorapatite by replacement of the ions within the lattice. Fluorine will incorporate itself into the lattice with decreasing temperature (Latil, 1975), whereas the incorporation of chlorine depends upon an elevated temperature (600-700°C) as well as a high pH and high ion activity of Cl^- in the fluid phase (Ekström, 1972).

Detrital apatites occurring in sediments are obviously governed in chemistry and paragenesis entirely by their primary source rock. A sediment may have been reworked and have several different source rocks and so the resulting apatite populations may be of extremely varied chemistry.

7.3 The crystallographic structure of apatite.

The crystallographic structure of apatite was originally determined independently by Mehmel (1930) and Naray-Szabo (1930). Further refinements on the structure were made by Beevers and McIntyre

(1946), Subsequent redefinements have been made with the increase in crystallographic knowledge and analytical technology.

Apatites, in the majority, fall into the hexagonal crystallographic system and have a spatial group P^6_3/m. Due to structural variations caused by the varying sizes of the substituting anions, chlorapatites and hydroxylapatites are monoclinic and have a space group P^2_1/b (Prener, 1967). The crystals are often hexagonal prismatic (**Fig. 7.3**). On a crystallographic scale, the unit cell in plan view is a parallelogram having two equal edges at 120° to each other and a third which is perpendicular to these **(Fig. 7.4)**. There are three axes of vertical symmetry; i) hexagonal screw axes; ii) 3-fold rotation axes and iii) 2-fold screw axes. Along the type i. axes, each placed a distance of 0.5 the c-axis apart. These Ca atoms are bonded to oxygen atoms, three in the same plane as the calcium, and three in between each Ca atom. The O atoms in the same plane as the Ca atoms are alternately raised or lowered and form the orthophosphate (PO_4) tetrahedra. There are three different bond lengths associated with the PO_4 tetrahedra. These are defined as P-O_I, P-O_{II} and P-O_{III} (Naray-Szabo, 1930; Mehmel, 1930), distinguished by their differing bond lengths of 1.82Å, 1.49Å and 1.60Å respectively. The P atoms also occur in planes, positioned approximately half-way between the Ca atoms **(Fig. 7.5)**.

The entire structure has a hexagonal network, like a honeycomb, with channels parallel to the c-axis passing through the structure. The walls of these channels are lined with oxygen atoms, arranged such that there are six "caves" along the unit length, into which fit three Ca atoms, each fitting half way into each cave. Consequently, there are two different sites occupied by the Ca atoms. Those that lie along the 3-fold rotation axes are known as Ca(I) types and those in the caves as Ca(II). These Ca(II) cations form the apices of equilateral triangles, perpendicular to the A_6 helixes.

The fluorine, chlorine or hydroxyl groups are situated between the planes of Ca(II) atoms. These planes are located at 0.25 and 0.75 the length of the unit cell, and are offset from each other by a rotation of 60° along the axis perpendicular to them. In fluorapatite, the fluorine lies at the intersection of the plane with the helicoidal axis. For chlorapatite, there are two possible positions for the Cl^- ions, 1.2 Å either above or below the calcium plane (Hughes et al., 1989). Consequently, there are two possible positions in which the Cl^- ions can exist within the lattice. The OH^- group is sited at 0.35Å above or below the plane, therefore like the chlorine, there are two possible sites which it can occupy **(Fig. 7.6)**.

The dimensions of the apatite unit cell have been measured by various authors using X-ray powder diffraction techniques, the results are

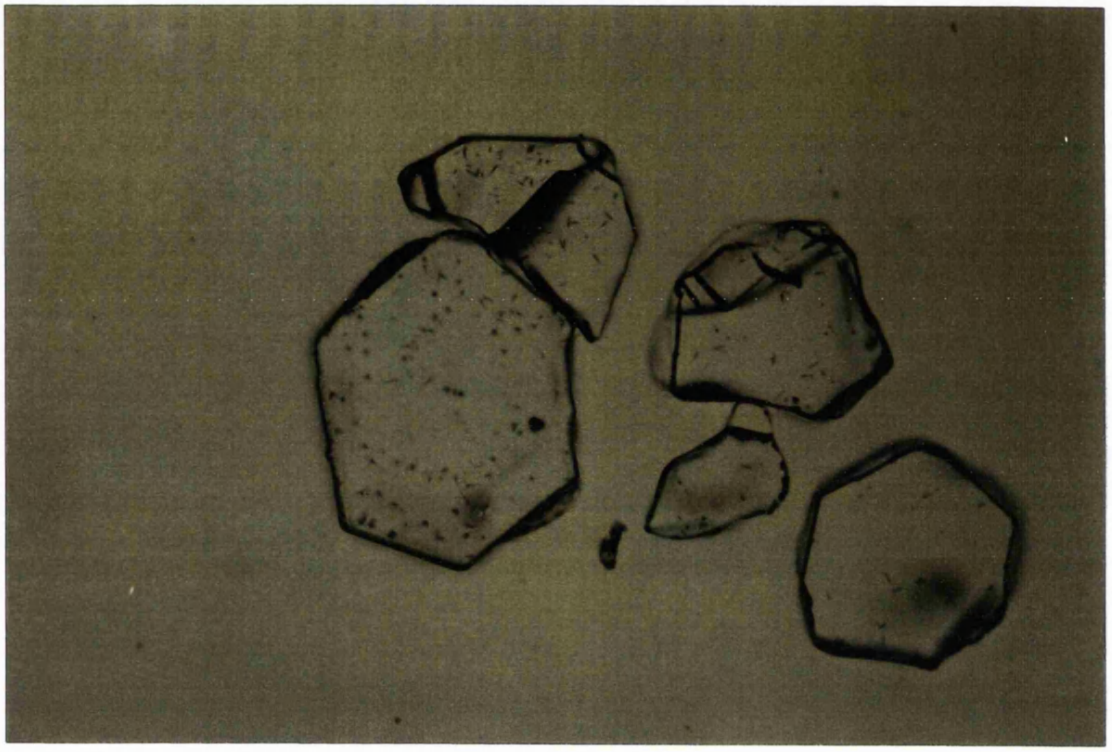

Fig. 7.3. Hexagonal basal sections of apatite crystals (250 x)

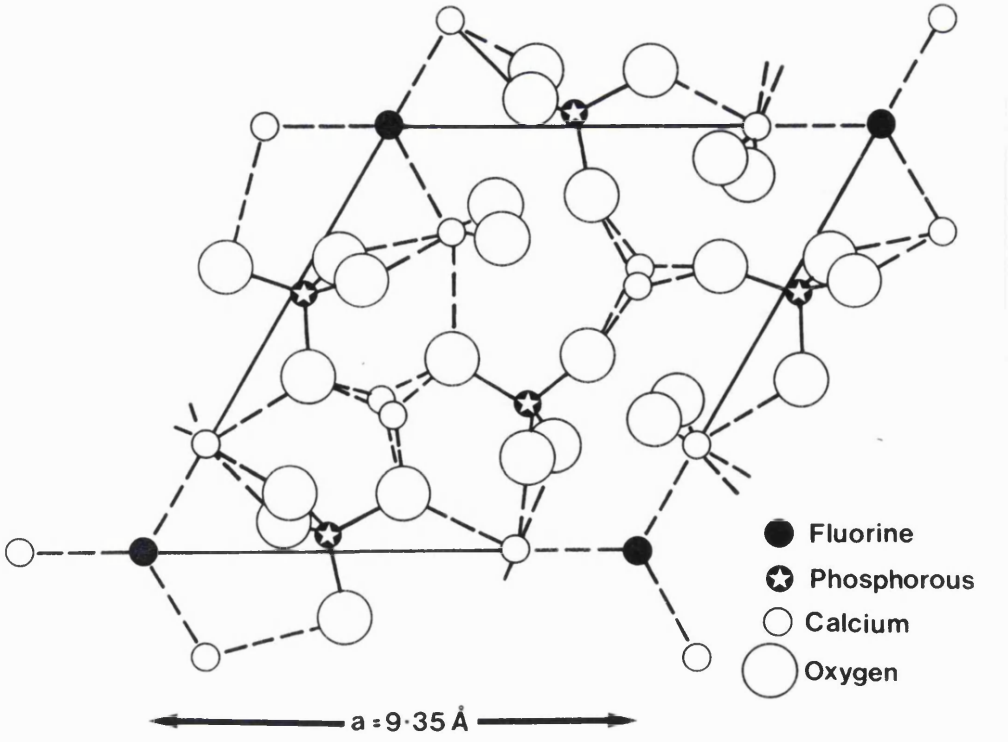

Fig. 7.4. Apatite unit cell (after Mackie et al., 1972).

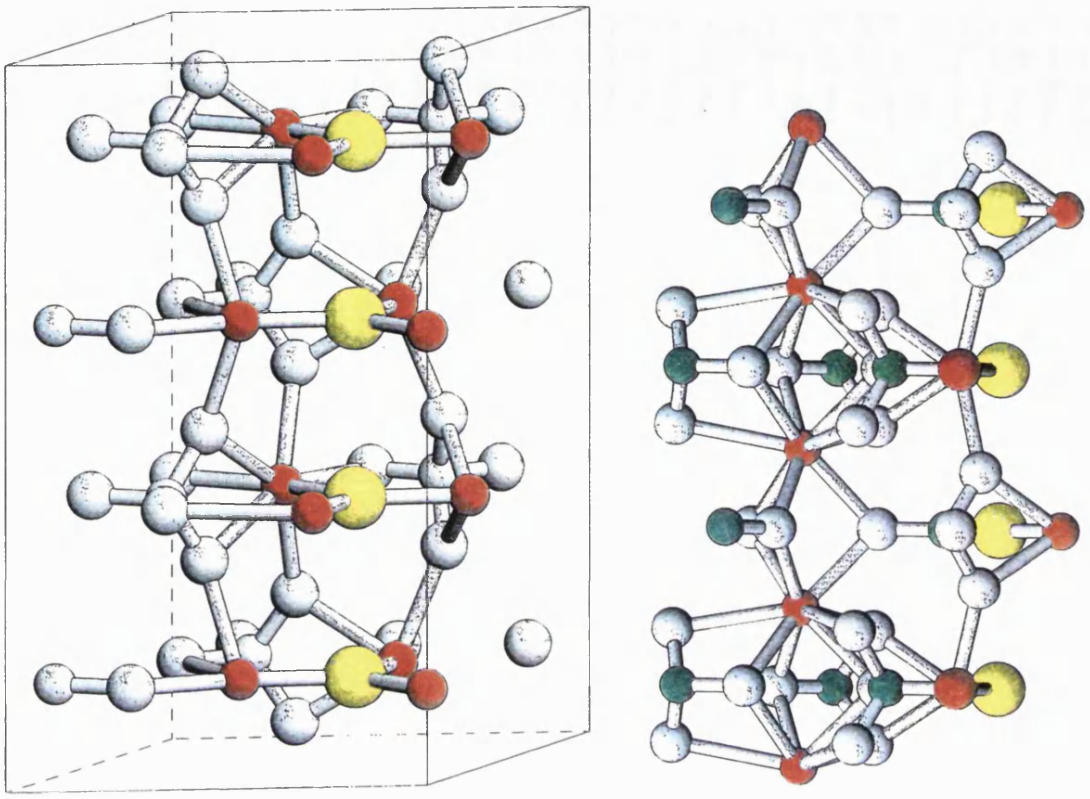

Fig. 7.5. View perpendicular to unit cell (Beevers and MacIntyre, 1946). In both digrams, yellow atoms, fluorine; red atoms, calcium; green atoms, phosphorous; white atoms, oxygen. A). shows fluorine chains surrounded by Ca_{II}. B). shows PO_4 tetrahedra and Ca_I polyhedra on the left, and part of the fluorine-Ca_{II} on the right.

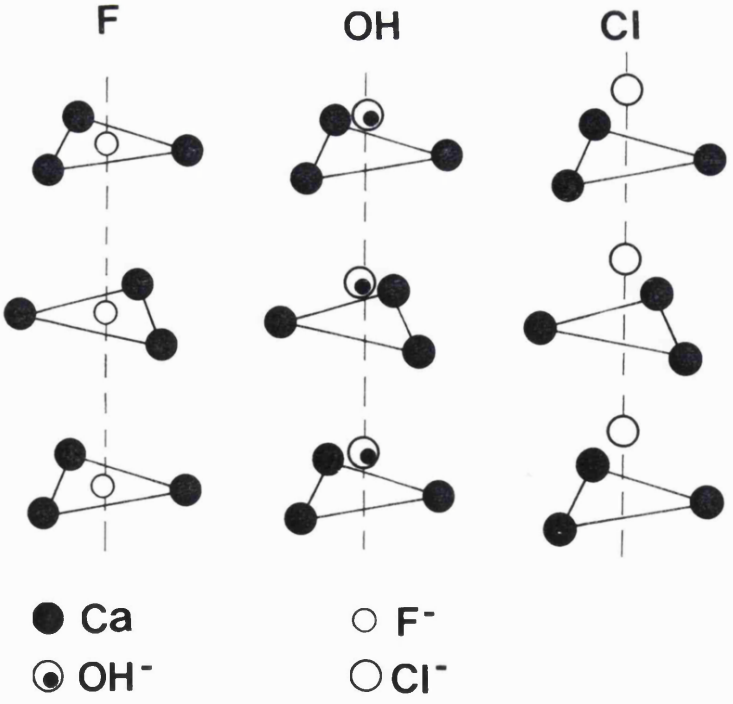

Fig. 7.6. Variation in the positioning of fluorine, chlorine and hydroxyl ions in apatite (Latil, 1975).

summarised in **Table 7.1**. The chlorapatite end-member has the largest unit cell dimensions, and fluorapatite the smallest. The differences are fundamentally due to the different sites of the F^-, Cl^- and OH^- ions within the lattice. Besides the distortion of the lengths of the unit cell, the effects of the different positions of the anions propagates throughout the structure of the lattice, slightly deforming the Ca (I) O_9 polyhedra and the PO_4 tetrahedra in terms of the cation bond lengths and polyhedra orientations. However this deformation is minimal. The Ca(II)O_5 (F, Cl, OH) (O) polyhedron is much more noticeably affected, the Ca(II)-X (where X = F, Cl or OH) bond length is substantially different for each anion substitution (Hughes et al., 1989).

a Å	c	Species	Author
9.37	6.88	F	Naray-Szabo (1930)
9.391	6.878	F (Durango)	Young et al. (1969)
9.398	6.878	F	Hughes et al. (1989)
9.42	6.94	OH	Larsen et al. (1952)
9.418	6.875	OH	Hughes et al. (1989)
9.432	6.881	OH	Kay et al. (1964)
9.598	6.776	Cl	Hughes et al. (1989)
9.413	6.882	F - Cl - O	Young et al. (1969)
9.41	6.91	Sr - F	Larsen et al. (1952)
9.76	7.21	Sr - OH	Larsen et al. (1952)

Table 7.1 Apatite unit cell dimensions.

The atomic arrangements of hexagonal fluorapatite and monoclinc chlorapatite and hydroxylapatite do tend to suggest that the end members are immiscible in solid solution. However, structural adjustments do take place which enable continuous solid solutions to occur. These adjustments may be accommodated in three ways; i) major shifts in the column anion positions compared to those of the end members, ii) reduction in symmetry from hexagonal to monoclinic in chlorapatites and hydroxylapatites, and/or iii) reordering of anions within individual columns but disordering of columns throughout the apatite structure (Hughes et al., 1989). In fact the differences between the two structures is relatively minor, and chlorapatites have been referred to as having pseudo-monoclinic symmetry (Prener, 1967).

7.4. Fission Tracks in Apatite.

7.4.1 The formation of fission tracks.

It is the presence of uranium occurring as a trace element in apatite that allows the mineral to act as a geochronometer. The uranium atom probably substitutes isomorphously into the calcium site (Altschuler, et al., 1958), and is almost always present at 10-100 ppm.

Uranium and thorium are the only naturally occurring, radioactive elements to undergo spontaneous fission as a decay mechanism. Price and Walker (1963) defined those particles capable of forming tracks as those having masses greater than 3 (amu) and energies greater than 100 MeV. Uranium is known to have some twelve isotopes, the three most common naturally occurring isotopes in order of abundance are ^{238}U (>99%), ^{235}U (0.71%) and ^{234}U (trace amounts). Only one uranium atom in every two million decays by fission, and 95 % of those fission decays are likely to be derived from ^{238}U. When fission occurs, the uranium atom will divide into two roughly equal sized particles, plus a few stray electrons and neutrons. Fission tracks in a solid are the linear areas of defects* formed by the splitting atom as each particle moves away from the other at an angle of 180°, propelled by the release of considerable kinetic energy (3.3×10^{-11} J). The 'Ion Spike Explosion' model (Fleischer et al., 1965) best accounts for the observed end products of fission decay within a crystalline solid. The model involves ionization along the path of the fission fragment, which in turn causes an unstable, cylindrical region of charged ions, repelling each other and pushing into the interstitial regions in the lattice **(Fig. 7.7)**. Durrani and Bull (1987) outlined a three stage mechanism for track formation in a crystalline solid. A primary physico-chemical stage envisions the fission fragments losing much of their energy by small collisions with the lattice, which eventually retards the fragments. Initially, the fragments carry a high positive charge, but become neutralised as they attract electrons from other ions. A final, direct collision of a fragment with atoms at the end of the track will probably lead to a chain of displacements. A second physico-chemical stage occurs as the system retains its equilibrium, through the ionised particles undergoing secondary reactions. Finally the ions and free radicals react, producing the end products of the radiation. The nature of the resulting fission damage depends on the mass and charge of the atom undergoing fission and the geometry and lattice characteristics of the crystal in which it occurs.

---

* Here a defect is defined as a vacancy or an atom occurring in an interstitial position.

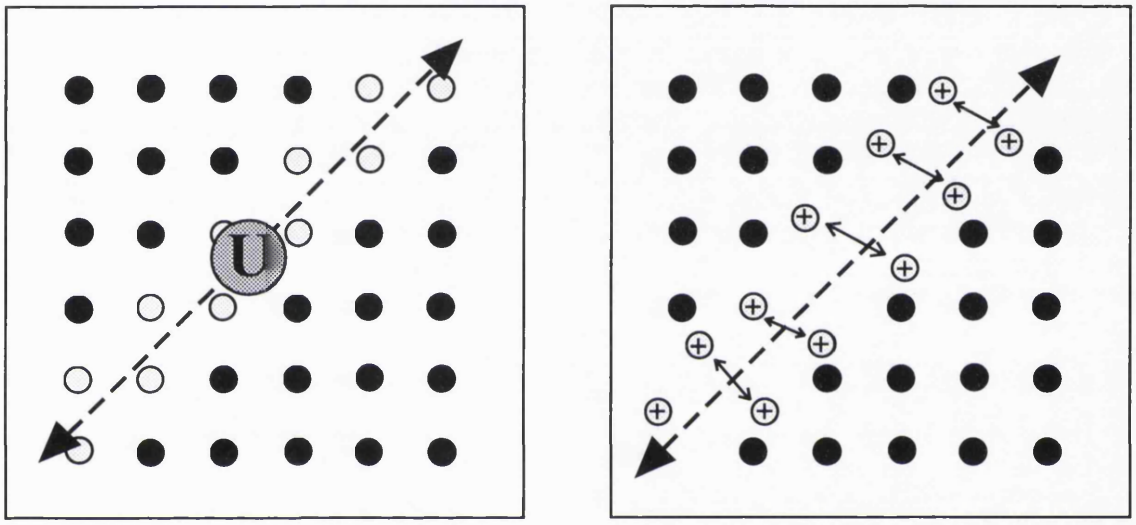

Fig. 7.7. The ion explosion spike mechanism (after Fleischer et al., 1965)

7.4.2 Track morphology.

The observation of fission tracks under an optical microscope first requires the fission damage to be revealed through chemical etching in an appropriate solvent which is for apatite, nitric acid. Latent (unetched) tracks can only be viewed under Transmission Electron Microscopy (TEM) and are known in apatite to have a maximum diameter of ~50 Å and a length of ~16 μm. However, most observations of track geometry have to date been made on etched samples **(Fig. 7.8)**. Importantly, fission tracks are distinguished from other defects that may be present in crystals on the following criteria (Fleischer and Price, 1964b).

- they form line defects of limited length (i.e. < 20μm)
- they are straight
- they exhibit no preferred orientation

Fission tracks within an apatite crystal exist as randomly oriented, roughly cylindrical, linear chains of defects in the crystal lattice. Carlson (1990) has postulated a model describing the geometrical characteristics of a fission track and how it may become annealed. Although Carlson's model has little basis in observation, it postulates that the distribution of defects across the diameter of the track can be assumed to be approximately Gaussian, and the length of the track approximates to a parallel-sided cylindrical central section 11 μm in length, with a taper zone existing for about 2.5 μm at each end **(Fig. 7.9)**. More recently latent tracks have been studied by Paul and Fitzgerald (1992). Observation by TEM of the morphology of thermal neutron induced fission tracks from ^{235}U revealed that at high magnifications (500, 000 x), the lengths of the tracks appear to have a 'pseudosinusoidal' morphology, the wavelength equal to the track diameter, and the cross section reflects the crystal symmetry, being hexagonal rather than circular.

As described in section 7.2.1 above, the orientation of the chains of Ca(I) atoms, parallel to the c-axis are strong and well bonded, whilst the atoms arranged perpendicular to the c-axis have a weaker attraction. This atomic arrangement affects fission track morphology. The mean track length (MTL) parallel to the c-axis is longer than that perpendicular to it (Green, et al., 1986; Carlson, 1990; Donelick, 1991). Paul and Fitzgerald's (1992) TEM observations show that tracks have a diameter of 9 nm parallel to the c-axis and only 5 nm perpendicular to it. Donelick's (1991) experiments revealed that the variation of MTL between c-axis parallel and c-axis perpendicular sections is predictable (within limitations) and can be plotted in the form of radii of an ellipse, the shortest radius correlating to the MTL perpendicular to c, and the longest to the MTL parallel to c **(Fig.**

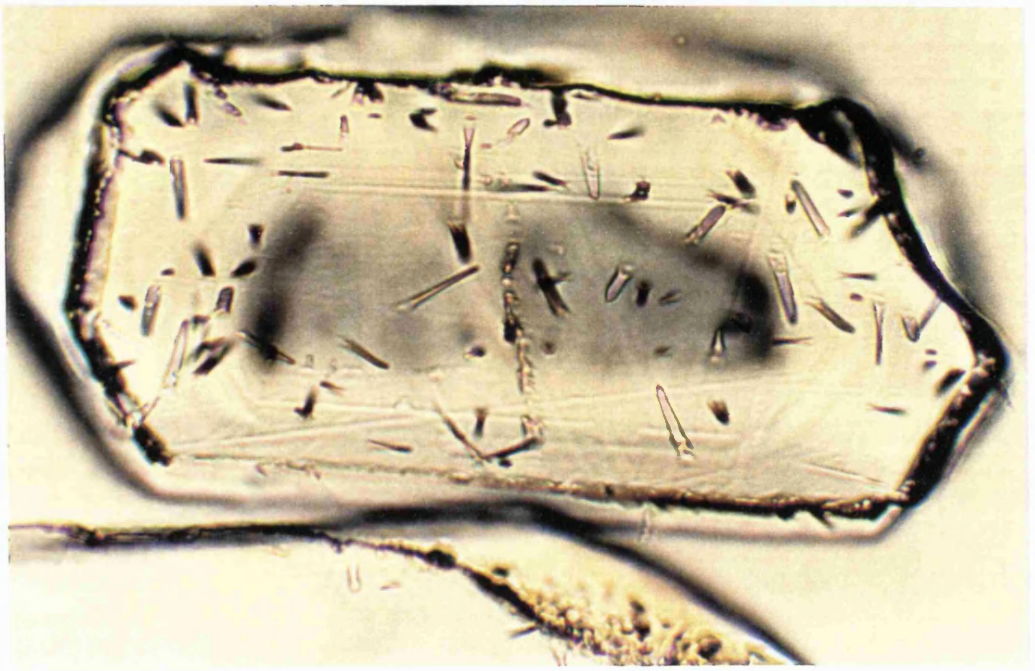

Fig. 7.8. Etched fission tracks in an apatite crystal.

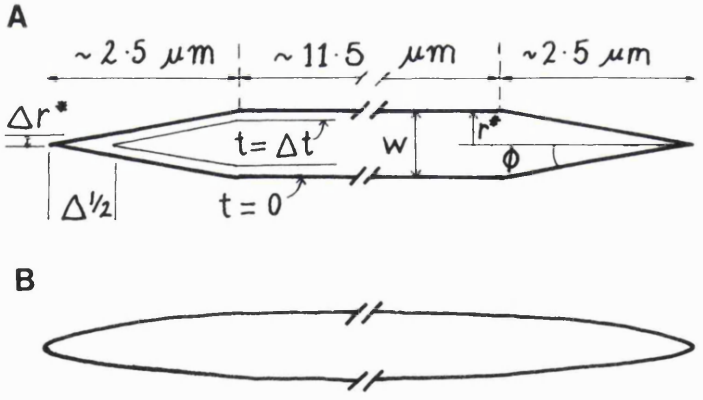

Fig. 7. 9. Geometry of fission tracks associated with the process of annealing (a) a cylindrical zone of disruption ~ 11 μm long, with a width, w, of a few tens of Å, is terminated by two conical tips, each ~2.5 μm in length. The radius of this region is r*. An annealing episode of duration Δt produces a decrease in radius Δr*, and a decrease in length of Δl/2 at each end. The ratio of these decrements is tan φ, where φ is the angle of taper. (b) is an alternative representation where the radius of the disrupted zone decreases monotonically and in a non-linear fashion from the axial centre to the tips of the tracks. Such a geometry gives equivalent predictions, within experimental error to those produced in (a) when modelled mathematically. However, the maths are less complex and cumbersome for scenario (a). After Carlson (1990).

7.10). A possible explanation for this is that a track forming perpendicular to the Ca(I) axes will find it harder to disrupt the strong bond configurations than one that forms parallel to these helicoidal axes (Donelick, 1991). Paul and Fitzgerald (1992) account for their measured discrepancies in length to be due to a greater rebound and relaxation of the crystal structure in response to the greater energy needed to disrupt it significantly in the formation of a fission track.

7.4.3 The annealing of fission tracks in apatite and the influence of crystal chemistry.

The phenomena of the gradual shrinking (annealing) of latent fission damage when subjected to an increase in temperature was first recognised by Fleischer et al. (1965). Subsequently, considerable research has been focused on apatites, both in the laboratory and in naturally occurring situations (i.e. subsurface samples). Laboratory annealing experiments under either isothermal or isochronal conditions, have been conducted upon tracks induced in totally annealed apatite samples over maximum periods of 1 yr, at temperatures of several hundred °C. The results of these experiments are conventionally displayed in the form of an Arrhenius plot (Fleischer et al., 1965; Green et al., 1985). In principal, the annealing experiments examine the reduction in track density, ρ, or length, l, compared with the original density, ρ_0, or length, l_0. An Arrhenius plot allows inverse temperature versus log time for the experiments to be plotted, and the points representing equal track densities at these times and temperatures fall along straight lines, which can then be simply extrapolated to geological timescales. An example is shown in **Figure 7.11.** In this example, the equal degrees of track reduction fall along parallel lines. This is typical for monocompositional single crystals (such as Durango); frequently, fanning Arrhenius plots arise **(Fig. 7.12)** when analyses are made on aliquots of apatites extracted from rocks, where a variation in composition may be present to cause this distortion (see below; Green et al, 1985).

Green et al., (1986) examined the annealing of induced fission tracks in Durango apatite, ascertaining that the primary factors controlling annealing behaviour are the anisotropy of the crystal and the chemical composition of the apatite. As mentioned in the previous section, there is a variation of track length with angle to the c-axis and this, in turn, affects the rate of annealing. Those tracks parallel to the c-axis are more resistant to the effects of heat than those at a higher angle to it. The appearance of chlorine

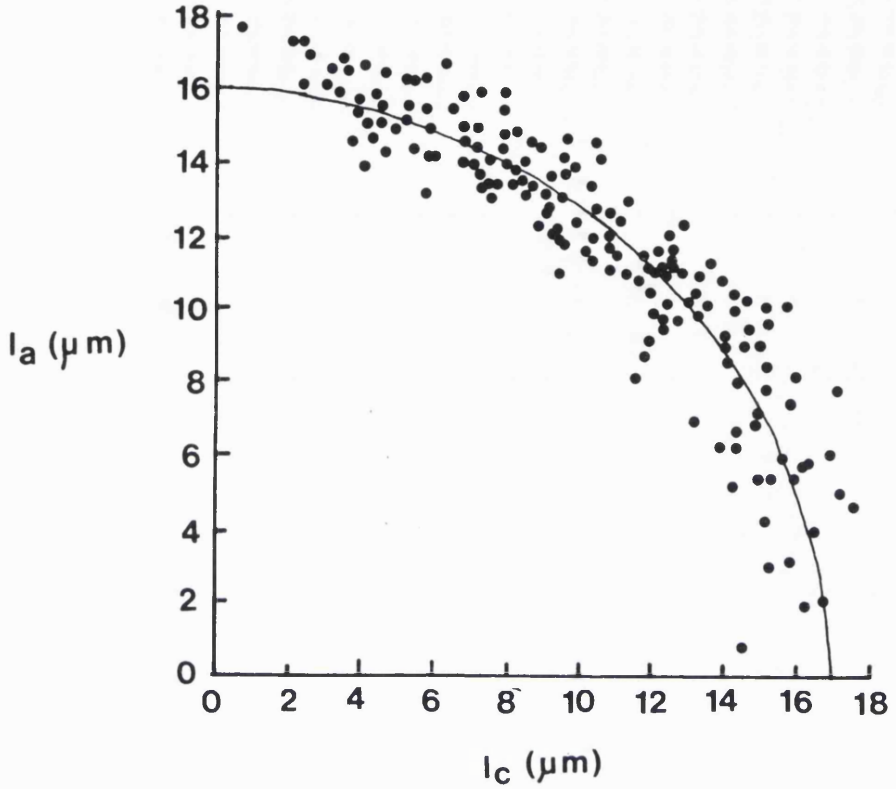

Fig. 7.10. Polar plots (after Donelick, 1991) of confined track lengths. Each data point represents a single pair of length angle measurements (li, θi). Track length is measured as along a radius connecting the origin and the data point. The angle between the azimuth of the track and the c-axis is that between the radius and the horizontal axis.

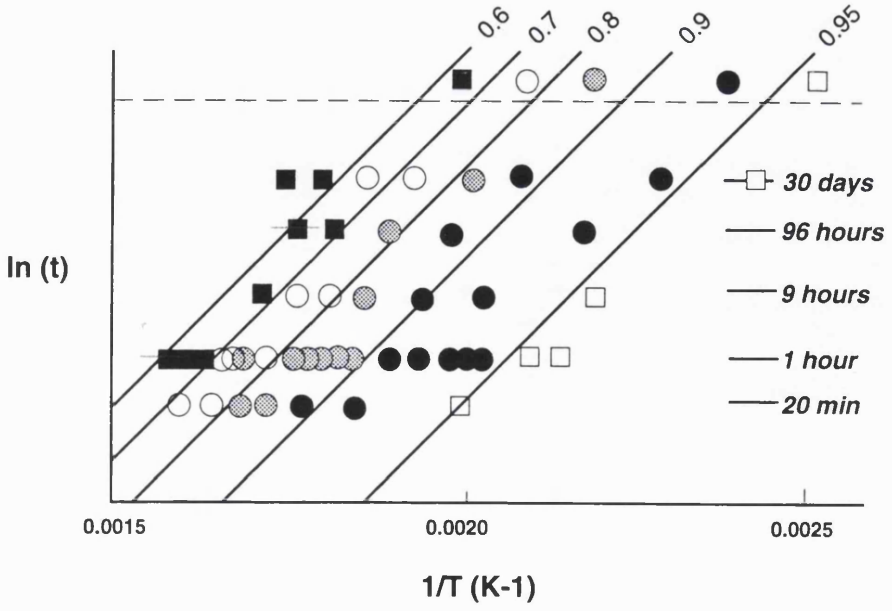

Fig. 7.11. Arrhenius plot with parallel lines of equal degrees of track length reduction during annealing in Durango apatite (after Green et al., 1985).

within the crystal is also responsible for a resistance to annealing, and this will be dealt with in further detail in the following section.

Two physical stages in the process of annealing have been recognised (Green et al., 1986; Carlson, 1990). In a first stage, the taper zone of Carlson (1990) disappears aided by radial shrinkage as the track shortens inwards from both ends, then having reached about two-thirds of its original length it disappears more rapidly, again by a combination of shortening and radial shrinkage. This stage has been observed to be accompanied by the appearance of unetchable gaps in the track. The breaking up of latent tracks has also been witnessed by Paul and Fitzgerald (1992) on exposure of induced tracks in a sample to electron bombardment (radiolytic annealing). The entire process appears to be a diffusive one as the disrupted atoms reposition themselves within the structure when subjected to an increase in temperature **(Fig. 7.13)**.

The importance to fission track analysis of fluorine-chlorine substitutions was highlighted by Green et al. (1986). In laboratory annealing experiments using samples of almost pure chlorapatite from Snarum in Norway, temperatures that were sufficient to erase totally, all the tracks in samples of Durango apatite (i.e. 370° C for 1 hour) did not remove tracks of lengths up to 15 μm. It was evident that the fluorine and chlorine content of apatite is apparently a key factor in the differential annealing rates of fission tracks (Green et al., 1986). This conclusion was promoted after analysing downhole samples from the Otway Basin, Victoria, Australia, where the range in compositions of the annealed grains were apparently an influence on the ages **(Fig. 7.14)**. Near end-member fluorapatites (~ 0.05 weight per cent chlorine) from Otway boreholes are totally annealed at downhole temperatures ~ 95°C (Green et al., 1986). In summary, fluorapatites anneal at ~ 95°C over an assumed geological heating period of 10 - 40 Ma. However, apatites containing 1.4 wt % chlorine begin to show resistance to track length annealing at these temperatures. Apatites containing 2.0 wt % chlorine are not totally annealed until 125°C.

From these temperature constraints, a spread in single grain ages influenced by differing grain chemistries will only be apparent if the sample has undergone certain types of thermal histories (Tingate, 1990). Assuming that there was an appropriate compositional spread in the sample, the single grain ages would reveal it if the rock had been heated to ~ 95°C, and then cooled ~ 25°C, or if the rock had simply cooled from a high temperature (> 125°C). In this case, the chlorine-rich apatites in the sample would begin to retain new formed tracks at higher temperatures. Samples with a spread in

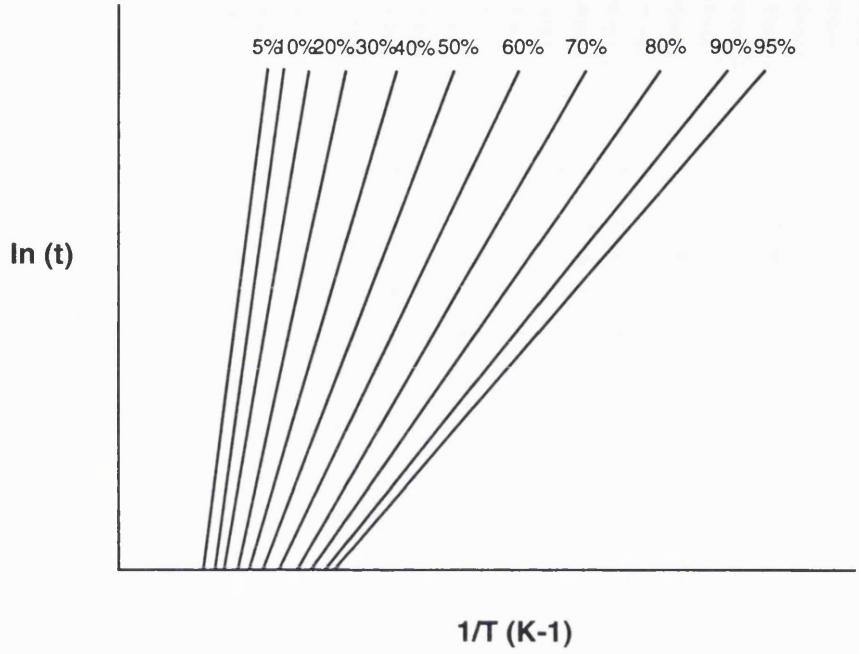

Fig. 7.12. A cartoon depicting a fanning Arrhenius diagram of the type plotted by Wagner (1972) for the annealing of aliquots of Libyan desert glass. Per cent degree of annealing is marked along the top.

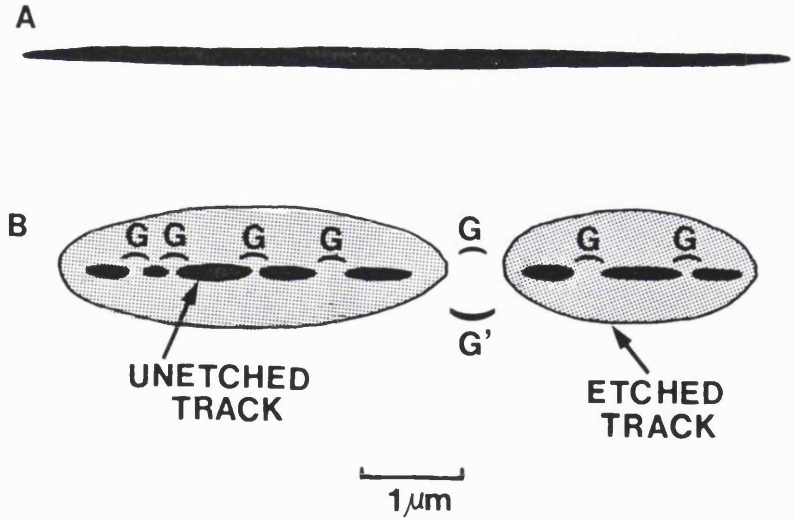

Fig. 7.13. Morphology of latent fission tracks in apatite (a) before and (b) after the onset of annealing (after Paul and Fitzgerald, 1992) as observed using TEM. Small gap zones appear in the unetched track during annealing. These regions are often but not always obliterated by annealing.

apatite composition which cool rapidly from high temperatures before residing at moderate temperatures (~ 50°C) then cooling to ~20°C, would not reveal a compositional spread of ages as initially all the tracks would have formed below annealing temperatures.

Before conclusions are immediately arrived at assuming a different chlorine composition to account for anomalous single grain ages, it must be remembered that there may be other reasons for a spread. If a sample has suffered little or no annealing, a spread may be directly attributable to the ages of the provenance regions regardless of compositions. Another factor influencing single grain age variation could be a human one; sample contamination or analytical mistakes could account for the odd single grain age.

Chlorapatites are often noticeable in etched samples because they have, in comparison with fluorapatites, enlarged etch pits **(Fig. 7.15)**. It is another important characteristic of chlorapatites to have a greater bulk etch rate than fluorapatites.

That chlorine is the only element substituting into apatite affecting the annealing kinetics of fission tracks is assumed, but has not been rigorously tested. The ability of apatite to enable substitutions to occur by many trace elements for most positions cannot be ignored. Few other common substitutions in the lattice have been studied under experimental conditions. Crowley et al. (1991) compared the behaviour of fluorapatite with strontian apatite and found the annealing characteristics of each to be identical. Finally, there may well be other factors as yet unknown that dictate annealing, for example substitution by other elements besides chlorine. Although there is evidence that this is not so (i. e. the discriminant analyses of Seiber, 1986), all the possibilities have not been fully explored.

7.4 Summary.

The fundamental controls upon the chemistry of apatites derive ultimately from the genesis of igneous and metamorphic rocks, and are dictated by the geochemical environment in which they were first formed. The majority of magmatic apatites are likely to be fluorapatites, and the chemistry of apatites within an intrusion is unlikely to vary significantly from one grain to another. Chlorapatites and hydroxylapatites are more common in metasomatic and hydrothermal environments. However, these species are comparatively rare. A mixed population of apatite chemistries may occur in an crystalline rock, but these occur only in relatively uncommon situations.

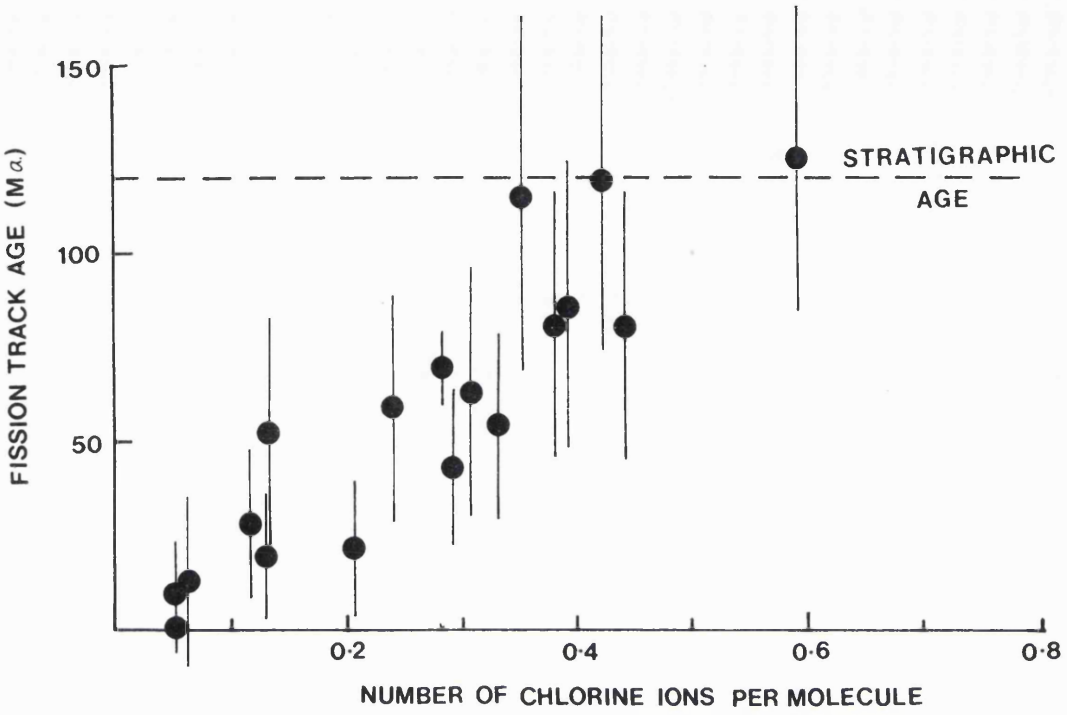

Fig. 7.14. The relationship between track retention (indicated by fission track age) and chlorine content of individual grains from an Otway Group sandstone borehole sample at 2595 m and 92°C. The composition of Durango apatite is included for reference (after Green et al., 1986).

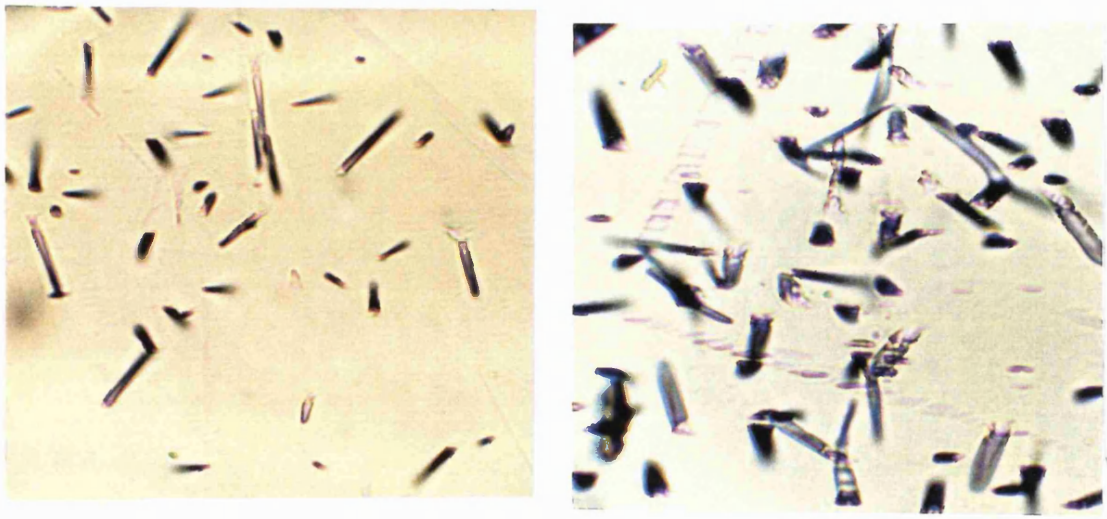

Fig. 7.15. Comparison of etch pits in fluorapatites and chlorapatites. Both photomicrographs are taken at the same magnification (625 x), but the chlorapatite (A) has far larger etch pits than the fluorapatite (B). Both samples were etched under the same conditions.

Distinguishing chlorapatites from fluorapatites is an important consideration for workers in apatite fission track analysis. In several laboratory annealing experiments and from geological situations, fission tracks in chlorapatites have been observed to be far more resistant to annealing than those in fluorapatites. Tracks in chlorapatites may be totally annealed at 120 - 130°C rather than in the region of 95°C for fluorapatite. Although relatively rare, the appearance of chlorapatites can be important when interpreting certain thermal histories, and apatite composition should be determined, especially when analysing clastic sedimentary rocks.

Chapter 8

Infrared microspectroscopy as applied to apatites for fission track analysis.

8.1 Introduction.

At elevated temperatures, the relationship between the sensitivity of fission track annealing in apatite and chlorine contained in the structure has been shown to be the dominant factor in influencing variation in single grain ages of a sample. Fission tracks in chlorine-rich apatites are more resistant to annealing and will ultimately yield older ages than those in the more common fluorine-rich apatites. An important advance in fission track methodology will be made if a method of directly comparing chlorine content of individual apatite crystals with their fission track age is devised.

The aim of this project is to investigate the possibilities of infrared (IR) microspectroscopy as an efficient method for evaluating the fluorine or chlorine component of apatites used in fission track analysis. Is it possible to relate an apatite fission track single grain age directly to fluorine and/or chlorine content? Specimens of apatites of varying F and Cl contents have been acquired to develop the technique and to test this hypothesis.

In previous studies linking chemical composition with apatite fission track annealing, anomalously old single grain ages have been attributed to the presence of chlorine-rich apatites. In most cases, assessments of compositional spread within a sample have been made using electron microprobe analyses of a separate aliquot from that which was subjected to fission track analysis. This method has several distinct disadvantages. Firstly, although the electron microprobe gives reliable and quantitative analyses, many of the low atomic number elements that occur in apatite (i.e. fluorine, hydroxyl, carbon) have very low detection limits, due primarily to absorption of their characteristic wavelength X-rays within the measuring system. Secondly, during routine fission track analysis approximately twenty apatite grains are counted to calculate the apparent age. To obtain a precise assessment of the possible compositional spread within a sample, a large number of grains would need to be microprobed. This is a laborious process, requiring increase in analysis time and is further compounded by the careful sample preparation needed for electron microprobe work (see Appendix 1) and the damage to the grains that this type of analysis incurs. Although this damage may be small, it would

destroy fission tracks and render any future fission track analysis of the sample impossible.

The possibilities of IR microspectroscopy are examined, as a non destructive, rapid analytical technique. As IR microspectroscopy is not routinely used as a quantitative technique, it is necessary to form a calibration between the IR wavenumber and a quantitative measure of fluorine and chlorine composition. For these experiments a set of samples was acquired for analysis and their fluorine chlorine contents assessed using an electron microprobe. The aim is to provide a relationship between the probe analyses and the IR spectra from which a calibration may be devised. The results are used to assess the capabilities of the IR technique for use as a routine chemical composition determination technique for apatites used in fission track analysis.

The rudiments of the theory of reflection IR microspectroscopy and its application to apatites are described in the following section. More detailed explanations of vibrational spectroscopy including both IR and the complimentary technique of Raman spectroscopy, and their applications to mineralogy are described in detail in McMillan (1985) and McMillan and Hofmeister (1988).

8.2 Infrared microspectroscopy of apatites.

8.2.1. Vibrations of crystals and the interaction with IR light.

Infrared is the region of the electromagnetic spectrum with frequency, v (*in vacuo*), in the range 10^{12} to 10^{14} cps and wavelength, λ, in the range 10^{6} to $4x10^{4}$ Å. In this work, the vibrational energies of IR radiation are given in wavenumbers ($1/\lambda$ cm^{-1}), which is standard notation; the range of IR radiation in wavenumbers is 100 - 4000 cm^{-1}. Vibrational energies of molecules and minerals are in the IR region (Kieffer and Navrotsky, 1985).

Infrared spectroscopy is the measurement of the interaction of electromagnetic radiation with molecular bonds. A molecule can be regarded at its simplest form as two atoms, of masses, m_1 and m_2, joined by a bond, which behaves in a manner analogous to a spring. The length of this spring in equilibrium is r_o. The movement of the system can be described as obeying Hooke's Law (Equation 8.1).

$$F = -k \Delta r \qquad (8.1)$$

Where F is the restoring force proportional to m_1 and m_2, k is the force constant of the spring, expressing its resistance to extension or compression.

As a rule, the stronger the molecular bond, the greater the force constant. Δr is the change in length from r_o as the spring is either extended or compressed. This simple vibrational behaviour is the called the classical harmonic oscillator (McMillan, 1985). Although not entirely appropriate for describing the complexities of vibrational behaviour of atoms within a crystal and the effects of the interactions of electromagnetic radiation, it is a useful starting point for visualising the concept.

When a quantum of light, a photon, enters a crystal, it is retarded, and is termed a polariton. As a molecule within a crystal is forced to vibrate by the interaction of this polariton, it is influenced by its neighbouring atoms. This sets up a chain-reaction of vibrations through the crystal which resemble waves, known as lattice vibrations. In analogy to light, a quantum of lattice vibration is called a phonon **(Fig. 8.1)**. The total number of possible vibrations in a crystal is 3n, where n is the number of atoms in the unit cell. The remaining 3n-3 modes are vibrational modes observed by IR or Raman (the complimentary method) spectroscopy. For a lattice vibration to interact with IR light, the wavelengths must be similar. As the unit cell-edges of most crystals are in the region of 10 to 100 Å long, only long wavelength lattice vibrations will interact with the wavelength of IR light.
Lattice waves have either transverse or longitudinal motion, that is they cause atomic displacements respectively perpendicular or parallel to the direction of propagation. Both wave forms have optic vibrational modes, producing a transverse optic (TO) mode and the longitudinal optic (LO) mode **(Fig. 8.2)**.

8.2.2. Reflectance IR spectra.

An IR beam incident on the surface of a crystal is partly reflected, transmitted and absorbed, whilst the crystal emits radiation **(Fig. 8.3).** Kirchoff's Law (Equation 8.2) expresses the behaviour of an IR beam incident on the surface of a crystal, where T, A, R and κ are respectively the coefficients of transmission, absorption, reflection and emission, as functions of the frequency of the radiation, v.

$$T(v) = 1 - A(v) - R(v) - \kappa(v) \qquad (8.2)$$

In the ideal case where there is only reflection and transmission of the beam, and no component of absorption, the Fresnel Formula (8.3) gives the reflectivity of the crystal at normal incidence.

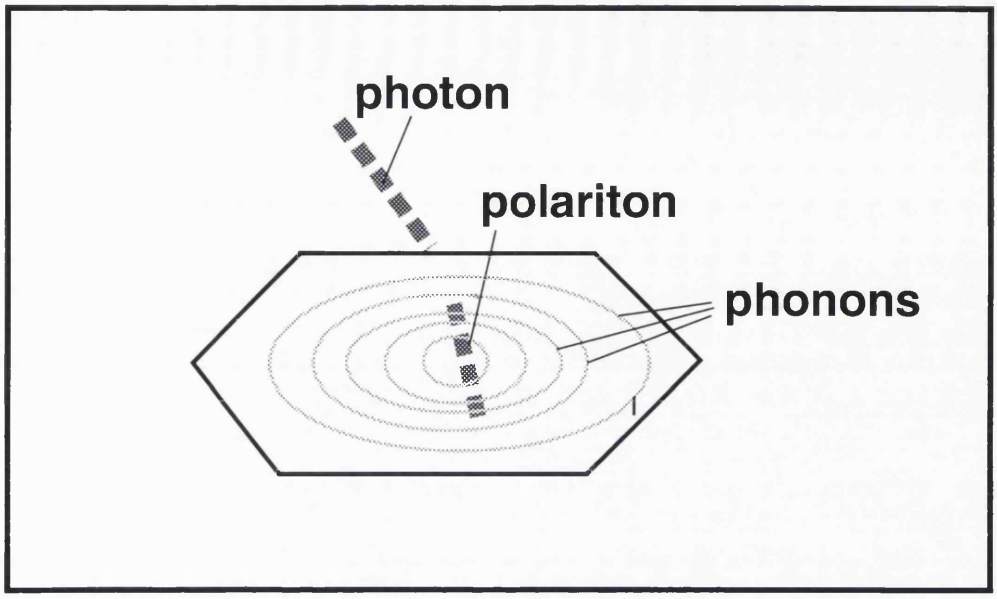

Fig. 8.1. A photon of light enters a crystal and becomes retarded, as a polariton. The interaction of the polariton with the crystal causes lattice waves to propagate through the crystal producing phonons.

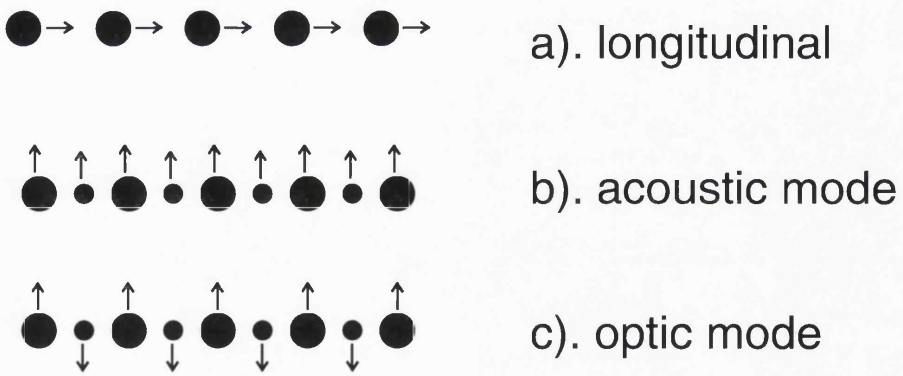

Fig. 8.2. a). Illustrates a longitudinal lattice vibrational mode in a monatomic chain of atoms. b). The acoustic modes; for any crystal, there are three lattice vibrational modes where all the atoms in the unit cell move in phase in the same direction. c). When atoms move in opposing directions, these motions can generate a changing dipole moment and hence interact with light. These are the optic modes.

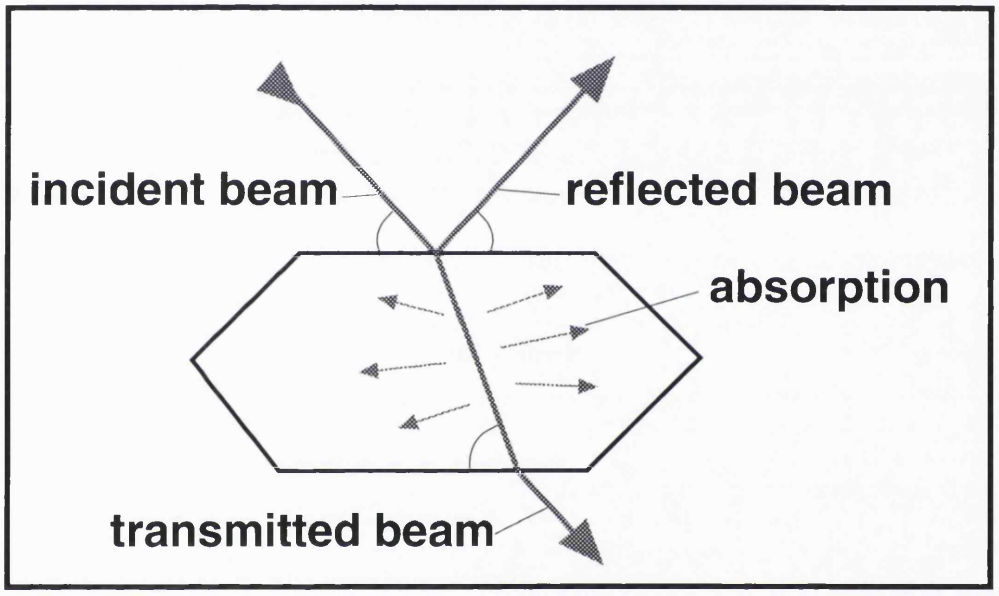

Fig. 8.3. An incident beam of light can be transmitted, reflected or absorbed by a crystal.

$$R = \frac{(n-1)^2}{(n+1)^2} \tag{8.3}$$

Where refractive index, n, is defined as:

$$n = \frac{c}{v} \tag{8.4}$$

c is the speed of light *in vacuo*, and v is the velocity of the propagation of the electromagnetic radiation within the crystal. The dielectric constant, ε, also dependent on refractive index was defined by Frölich (1958) as:

$$\varepsilon = n^2 \tag{8.5}$$

Once incident on the crystal, the polariton's velocity, v, in the crystal is affected by the precise nature of its interaction with the crystal. However it is primarily dependent on the wavelength of the light, and as a result, n and ε will vary with wavelength. This behaviour, in an ideal situation, is illustrated in **Figure 8.4a.** As the frequency of the light approaches that of a vibrational mode of a crystal, v_o, a phonon is created by the polariton forcing the nuclear displacements of the transverse normal vibrational modes of the lattice. As the polariton becomes retarded reaching the frequency of the phonon, n and ε increase asymptotically towards infinity. At this point the crystal becomes totally reflecting (R = 1) as no light can propagate through the crystal. On the high frequency side of this resonance, ε returns from infinity, crossing the ε = 0 axis at the frequency of the longitudinal vibrational lattice mode, v_L. Hence, the LO frequency of a crystal can be determined from IR reflectance spectra.

In the case of a real crystal (Fig. 8.4b.), light is absorbed due to dissipation of energy due to anharmonic processes. This is known as dielectric loss. Absorption is accounted for by the refractive index and the dielectric constant become complex. The dielectric loss function ε″(v) has its maximum at the TO frequency. Total reflection cannot occur (due to the absorbed component) and the resulting reflectivity is expressed in Equation 8.6, where n has real and imaginary parts, n = n′ + *i*n″:

$$R = \frac{(n'-1)^2+(n'')^2}{(n'+1)^2+(n'')^2} \tag{8.6}$$

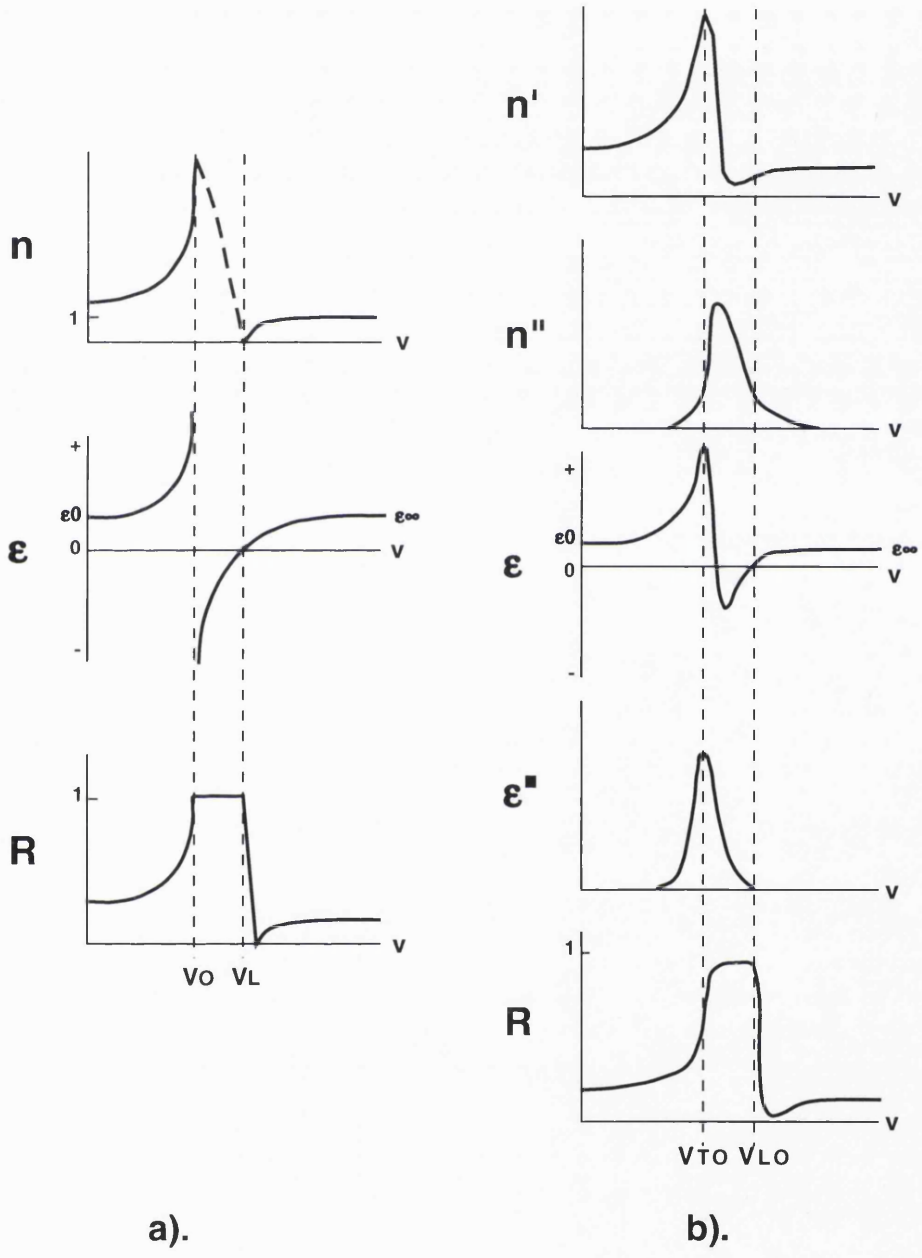

Fig. 8.4a. n(ν), ε(ν) and R(ν) curves for an ideal, non-absorbing crystal. The dielectric constant, ε, and the refractive index, n, go to positive infinity at the IR resonant frequency,VO, which is also at the frequency of the transverse lattice mode. The ε(ν) curve crosses the axis ε=0 at the frequency of the corresponding longitudinal mode, VL. The refractive index is undefined, and the infrared reflectance = 1 between VO and VL. b). A 'real' case with infrared absorption through anharmonic processes. The refractive index and dielectric constant are now both complex. The imaginary part of the dielectric constan, ε"(ν) shows a maximum at the TO frequency, VTO, VLO is defined from the point at which the real part, ε'(ν), crosses the frequency axis. The reflectivity curve does not rise perfectly to R=1 and there may be some structure in the 'forbidden' region of VO to VL (after McMillan and Hofmeister, 1988).

Because of the occurrence of TO and LO modes in each peak of a spectrum, IR reflection peaks can be relatively broad. The TO and LO wavenumbers, from Figure 8.4b can be estimated from the half peak-height intensities **(Fig. 8.5)**.

8.2.3. IR microspectroscopy of apatites.

Apatites with general chemical formula, $Ca_5(PO_4)_3(F, Cl, OH)$ are characterised by the presence of PO_4 tetrahedral groups. An individual PO_4 tetrahedral group has 9 degrees of vibrational freedom (i.e. $15\text{-}3_{rotational}\text{-}3_{acoustic}$). In the apatite crystal, four of these modes are IR active, and are shown in **Figure 8.6**. These are a) the symmetric P–O stretching frequency, ν_1=980 cm^{-1}; b) the symmetric P–O bend, ν_2=363 cm^{-1}; c) the triply degenerate antisymmetric P–O stretch, ν_3=1082 cm^{-1} and d) the triply degenerate antisymmetric P–O bend, ν_4=515 cm^{-1}. When reflectance IR is used not all the bands are detected. However, the ν_3 is always present whatever the section analysed (Kislovsky and Knubovets, 1968).

The lengths and orientations of the P–O bonds are affected by the positioning of the F^- or Cl^- anions within the lattice, because of the differences in the electrostatic forces exerted by each anion cause identifiable distortions of the PO_4 tetrahedra. However, the effects of these substitutions upon the orthophosphate tetrahedra are minimal in comparison to those suffered by the calcium polyhedra (Hughes, et al., 1989), but they are sufficient to be sensitive to IR spectroscopy. Accordingly, ν_1 varies between the species, appearing at 969 cm^{-1} for pure fluorapatite and at 960 cm^{-1} for pure chlorapatite. In both crystal structures the phosphate ion appears in the same orientation relative to the trigonal calcium plane. The symmetric stretching frequency of the phosphate ion increases with the repulsive forces exerted on the P–O bond by the anions. These forces are highest for the fluorine ion and lowest for the chlorine ion (Stutman et al., 1965). The differences are small because they are somewhat compensated for by the strong positive force exerted by the trigonal calcium plane. The ν_3 and ν_4 bands are broad, and are therefore not so easily resolved (Stutman et al., 1965). The usual bands are from ~1050 cm^{-1} to 1125 cm^{-1}. This variation is most likely to be associated with the three different P–O bonds, $P\text{–}O_I$, $P\text{–}O_{II}$ and $P\text{–}O_{III}$. Kislovsky and Knubovets (1968) have shown that these bond lengths can be assigned the wavenumbers 1050 cm^{-1}, 1100 cm^{-1} and 1125 cm^{-1} respectively, the oscillation frequency decreasing with increasing bond length. This is the ν_3 vibrational mode. Infrared reflection spectra are sensitive to isomorphous substitutions within the crystal lattice, making it possible to detect variations in the fluorapatite-chlorapatite solid solution

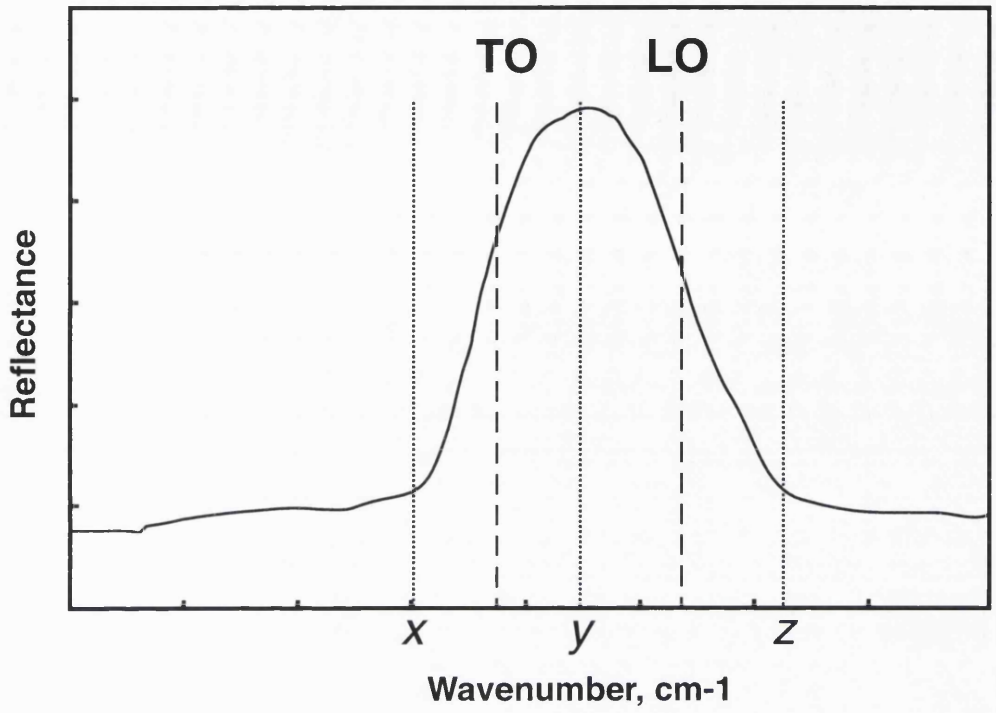

Fig. 8.5. An example of a peak in an infrared reflection spectrum. The transverse optic (TO) and longitudinal optic (LO) wavenumbers are calculated by measurements of the baseline on each side of the peak, and the position of the peak itself at x, y and z wavenumbers. The TO and LO wavenumbers are situated at 1/2 the peak height, hence TO = x-(x-y)/2 and LO = y-(y-z)/2.

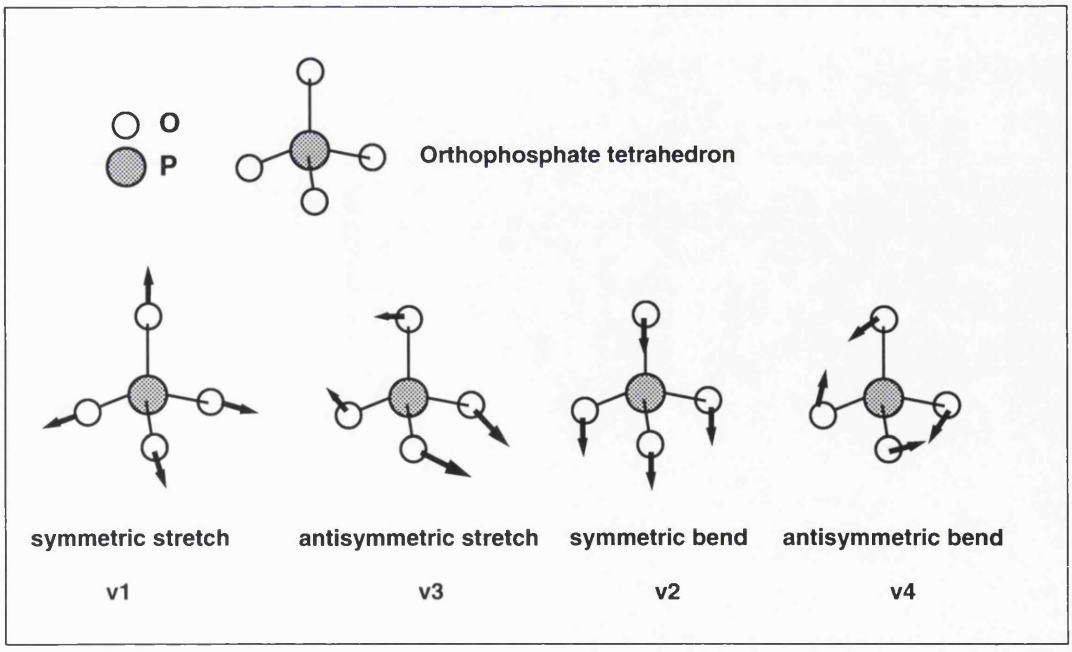

Fig. 8.6. The diagram illustrates the vibrational modes of the orthophosphate molecule. These modes are modified in an actual crystal.

(Kislovsky and Knubovets, 1968; Stutman et al., 1965; Adler 1964). The O_{III} is the only oxygen to be in direct contact with the fluorine or chlorine anion. The intensity of the P–O_{III} band decreases as F is partially replaced by OH, and is absent in the pure OH end-member. Noticeable variations in the ν_4 mode occur as F is substituted for by OH, giving a peak at 600 cm^{-1} where one would have been previously absent (Kislovsky and Knubovets, 1968).

In apatites where there has been substitution for the Ca^{2+} ion, for instance by rare earth elements or strontium, the intensity of the ν_3 band increases, and shifts by two or three wavenumbers towards the high frequency region. These variations can be explained by the substitution of trace elements with a 3+ charge for the Ca^{2+}, making the bond more ionic, which increases in the intensity of the spectral band for that region (Kislovsky and Knubovets, 1968).

8.3. Development of IR microspectroscopy as a technique for the analysis of apatite chemistries for fission track analysis.

In order to provide quantitative analyses of fluorine and chlorine in apatite using IR microspectroscopy, a method of calibration must be devised. Electron microprobe analyses of the fluorine and chlorine contents of a set of apatites were made, prior to them being analysed by IR microspectroscopy. A calibration between the two could therefore be used to determine the fluorine and chlorine content of apatites.

8.3.1. The apatite data set.

The microprobe analyses were carried out on a collection of apatites provided by the British Museum Department of Mineralogy, Geotrack™ International, and personal donations. Fission track laboratory age standards were also used (Durango, Fish Canyon Tuff and Mount Dromedary apatites). The collection of apatites are dominantly derived from pegmatitic and ore-bearing formations, although there are apatites from other geological environments. Museum samples are by their very nature unusual in some way, be it compositional, or otherwise. There is therefore an automatic bias towards this unusual character within the samples. The compositional range of these samples is not an accurate representation of those occurring in nature, where it is known that the bulk of apatites occur as accessory minerals in igneous rocks and have a chemical composition very similar to that of the Durango apatite (Seiber, 1986). A brief description of the apatites used in the IR and microprobe analyses is contained in Appendix 3.

8.3.2. Electron microprobe analyses.

All chemical analyses were carried out on the electron microprobe facility at the Open University, except for GUN-F which was analysed by Kevin Crowley at the University of Oklahoma.

At the Open University, the chemical analyses were carried out on a Cambridge Instruments M9 Electron Microprobe, using an accelerating voltage of 20 kV with an absorbed current of 3.05×10^4 amps with the Faraday cage in. The count time for each element was 30 seconds. The analyses were for fluorine and chlorine only, and these counts were calibrated using 'BMP' (an apatite from Wilberforce, Ontario, provided by the British Museum) as a standard for fluorine, and 'ACL' (a synthetic potassium chloride grown in the geochemistry laboratory at the Open University) as a standard for chlorine.

The final counts were converted from apparent percentage element to weight percentage element using four samples that are well characterised by chemical analyses and have been used as standards for microprobe analyses of apatites in other works (Seiber, 1986; Yelland, 1991). They are apatite from the Renfrew pegmatite in Canada; Durango apatite from Cerro de Mercado, Mexico; 'PFG-201', a pegmatitic fluorapatite (of unknown origin) and 'Chlorapatite F' from a pegmatite in Southern Norway. The electron microprobe results are summarised in **Figure 8.7.**

8.3.3. IR analysis of the apatite samples.

Most of the techniques used for determining the IR spectra of materials involve passing the radiation given off by a source beam through, or reflected from, a sample and then comparing it to an unattenuated reference beam. The technique of FTIR spectroscopy allows all the frequencies of a broad region of IR energy to be measured simultaneously. Recording and calculating such a measurement (called an interferogram) is difficult to interpret since the intensities of all the frequencies of energy are summed together. Fourier transformation is used to convert the interferogram into a spectrum. Two interferograms, one each for the sample and the reference (unattenuated) beam must be recorded, transformed and ratio-ed to produce the spectrum used for chemical analyses. The FTIR system used in this study is the Bruker IFS 45 spectrometer with a Bruker IR microscope. This system is capable of operating with transmitted or reflected light and IR **(Fig 8.8 and Fig 8.9).**

The addition of the microscope makes it possible to work with small sample sizes, giving measurement areas of approximately 20-150 μm diameter. The spectral range is from 600 - 4800 cm^{-1}. The detector is a

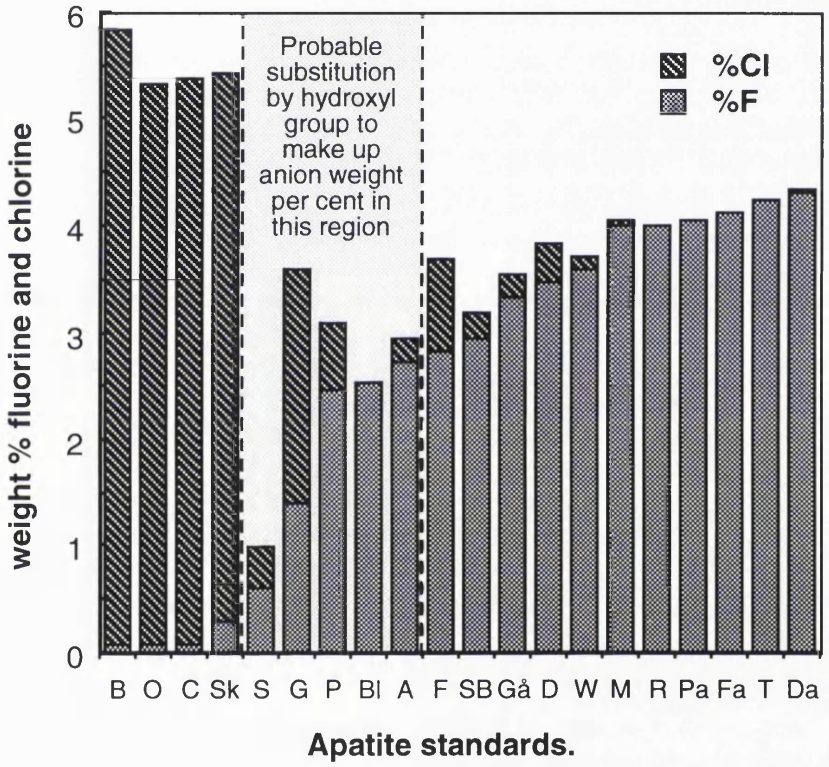

Fig. 8.7. The fluorine and chlorine compositions of the apatite standards, plotted in the form of a bar chart. The abbreviations for the crystals are in Table 8.1.

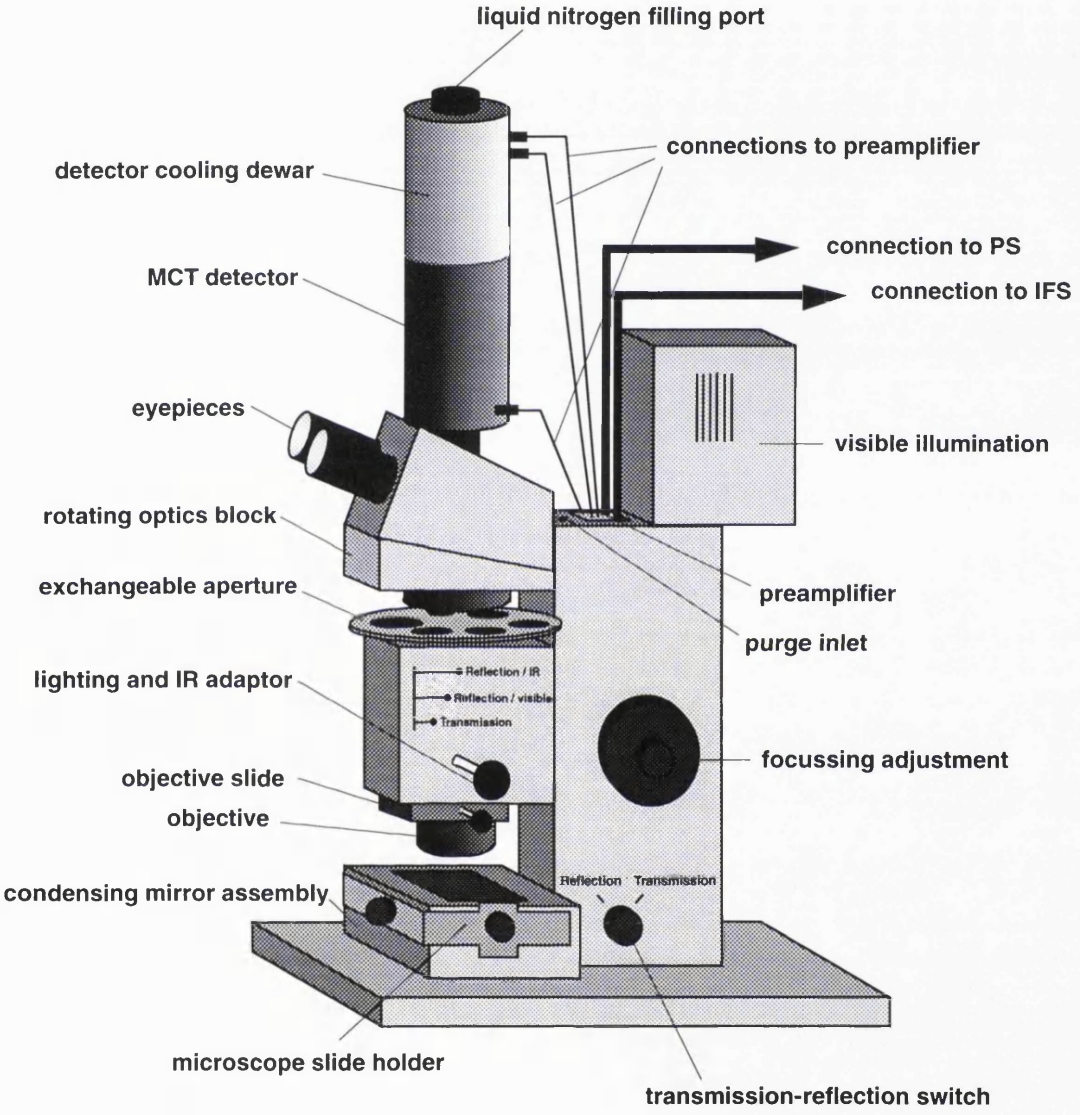

Fig. 8.8. The Bruker IFS 45 IR microscope used for the analyses in this thesis.

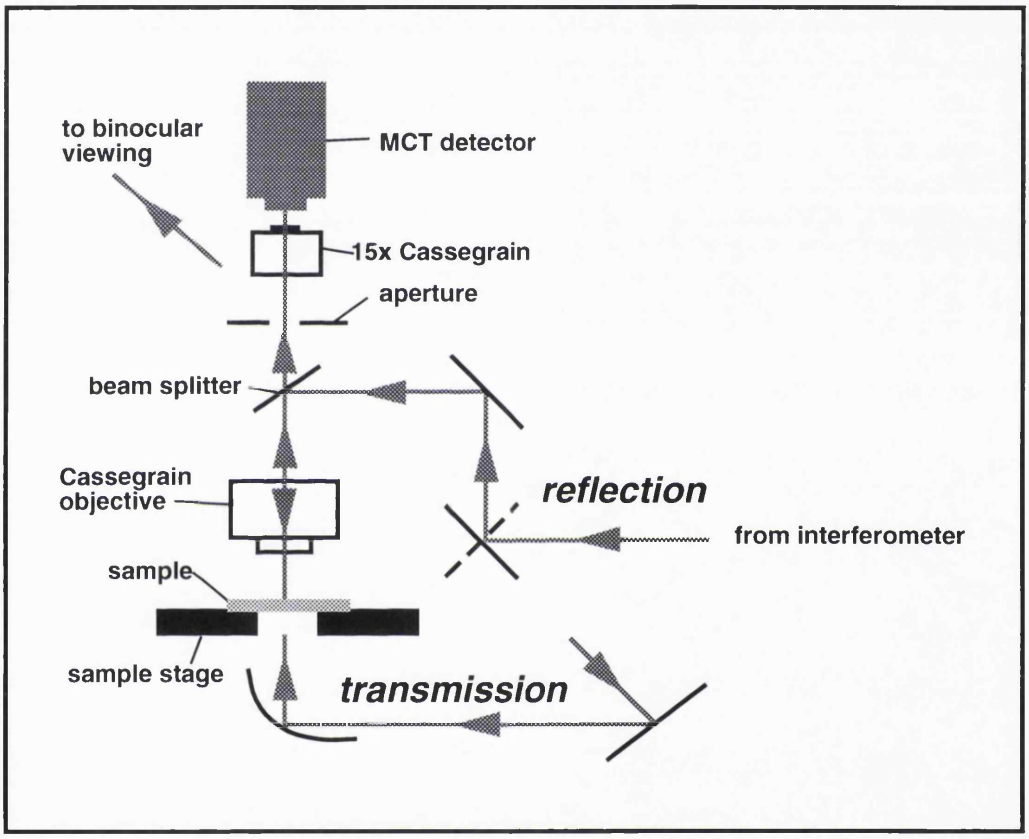

Fig. 8.9. The optic arrangement of the Bruker IFS 45 IR microscope used in these analyses.

medium range, liquid nitrogen cooled Mercury-Cadmium-Telluride (MCT) detector. Samples are open to the air (corrected for using a background sample), giving ease of specimen manipulation.

The IR microscope has an optical adaptation for aligning the sample. The optics block may then be rotated away, allowing the Helium-Neon (He-Ne) IR laser beam to pass. The depth of focus for both the optics and the beam is identical.

The 20 apatite 'standard' samples were analysed using both transmittance and reflectance FTIR microspectroscopy. A typical IR spectrum of apatite obtained in transmittance mode is shown in **Figure 8.10.** The transmittance spectra of the crystals were acquired using individual apatite grains placed on a KBr disc. Although more vibrational modes of apatite are revealed in transmission spectra, this method is not practical as an analytical technique for apatites used in fission track analysis, as the sample preparation is totally incompatible with that for fission track methods. Analysis of fission track apatites by transmittance IR involves the preparation of two separate aliquots, and this is precisely the mode of sample analysis that this work is trying to avoid.

8.3.4. Reflectance IR microspectroscopy of the apatite samples.

The reflectance IR spectrum of apatites differs from the transmittance spectra in that it has a singular 'double peak' in the region 1100 - 1050 cm^{-1} **(Fig. 8.11)**. These peaks represent the PO_4 ν_1 and ν_3 bands, although ν_1 at 980 cm^{-1} is rarely detected, small shoulders can occur at this point. The dominant band is the ν_3, P-O antisymmetric stretching vibration. The spectra were recorded in the region 900 - 1300 cm^{-1} to focus on this double peak. No other peaks were seen in the spectra. In fission track analysis, only the c-axis parallel (prismatic) face is used in calculating ages and measuring track lengths, and consequently only this orientation is used for the IR analyses. The OH^- peak (when present, expected at approximately 3600 cm^{-1}) is not detected in this plane.

The IR wavenumber was recorded for peak **a**, trough **b** and peak **c** on each spectrum for five crystals from each of the 20 apatite standards **(Fig. 8.12)**. The double peak represents two peaks, and the trough **b** is only a feature of the spectrum in that it forms the intersection between these two frequencies **(Fig. 8.13)**. The trough **b** equates approximately to the LO frequency of peak **a**. The IR wavenumbers collected for the apatite standards is displayed on **Table 8.1.** Measurement of the wavenumber of the two PO_4 peaks (**a** and **c**) and the trough (**b**) between them shows that there is a clear shift towards decreasing wavenumber as the specimen becomes more

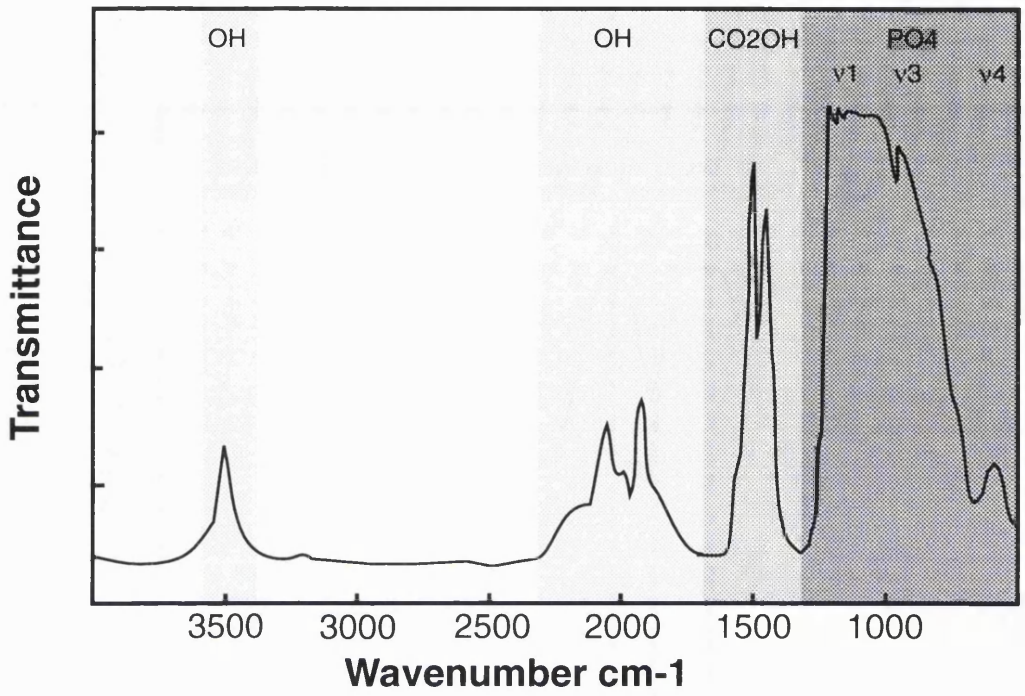

Fig. 8.10. A transmittance IR spectra of apatite. This spectrum reveals several identifiable, characteristic peaks, four major peaks can be seen, occurring broadly in the regions of 3500 cm-1, 2000 cm-1, 1500 cm-1 and 1000 cm-1. The 3500 cm-1 and 2000 cm-1 peaks can be assigned to the vibrations of the OH- group and the 1000 - 600 cm-1 to those of the orthophosphate v1, v3 and v4 modes. The peak at 1500 cm-1 is less well defined or described, it is often very small and not always present. It can be assigned to a partial substitution within the lattice by CO_2-OH for the orthophosphate tetrahedra forming carbonate-apatite (Ross, 1974).

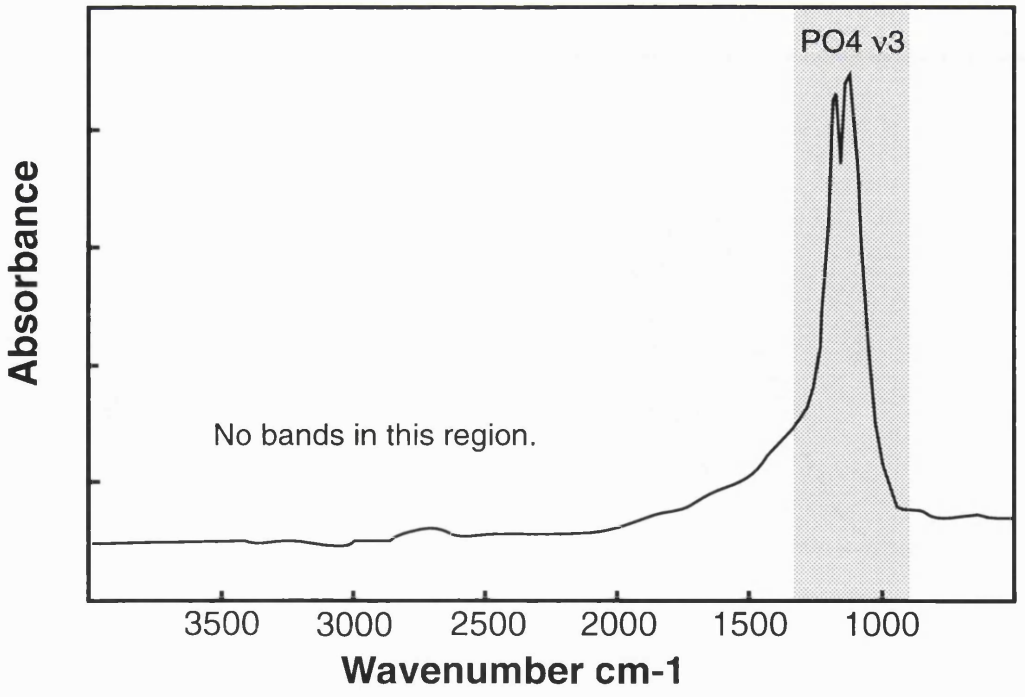

Fig. 8.11. Complete refelectance spectra of apatite, showing the orthophosphate double peak at around 1100 cm-1.

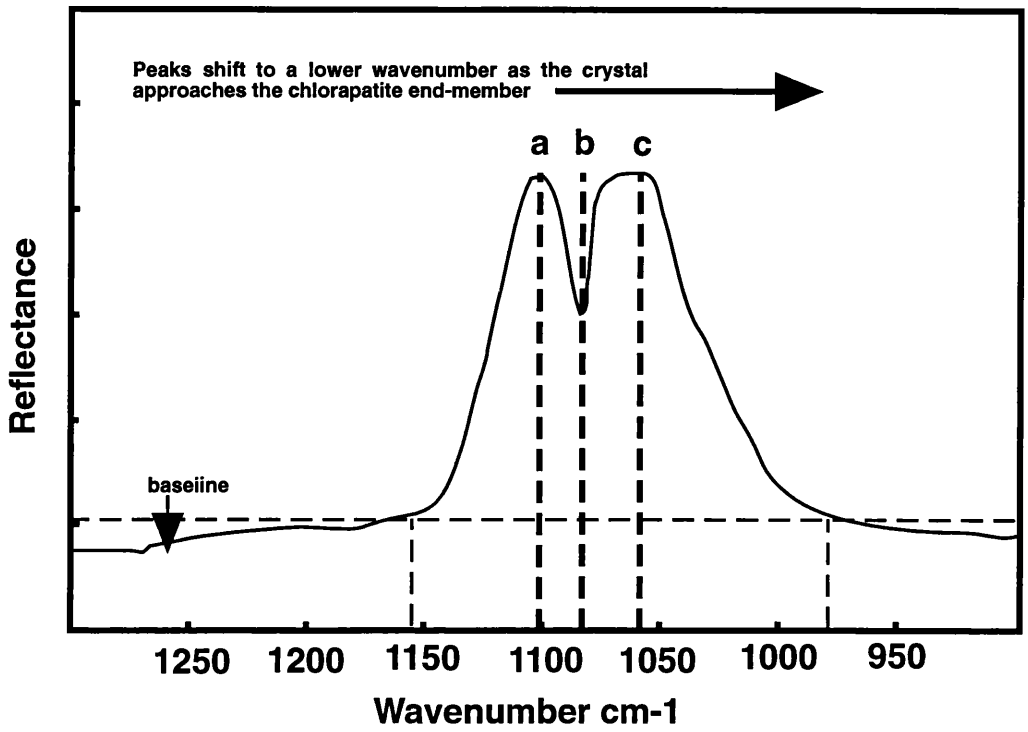

Fig. 8.12. Reflectance spectra between 950 and 1250 cm-1, showing the position of peaks **a** and **c** and the trough **b**, and the direction of shift of the peaks with the addition of chlorine to the apatite. The peak and trough wavenumbers are measured at the positions of the vertical dashed lines.

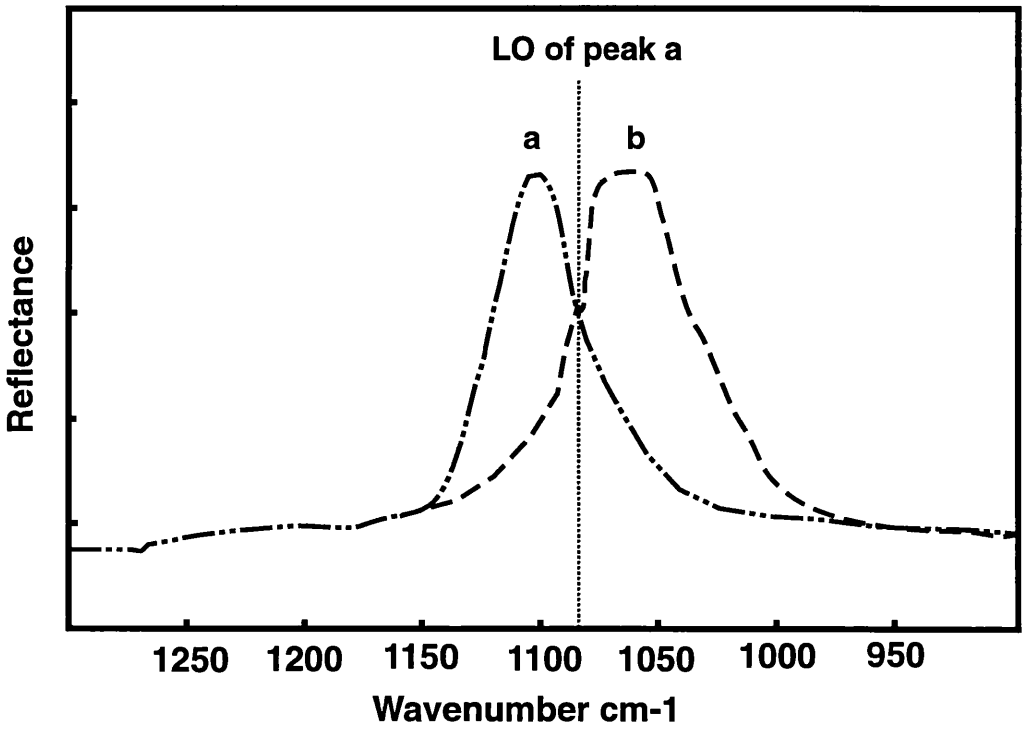

Fig. 8.13. The diagram illustrates how the 'double peak' actually represents two peaks, with the intermediate trough corresponding to the LO mode of peak **a**.

Table 8.1. The apatite standards used for analysis in this thesis, with their corresponding fluorine and chlorine contents and IR wavenumbers for the peaks **a** and **c**, and the trough **b**.

Abbreviation	Sample	Species	Locality	%F	%Cl	IR peak wavenumbers cm^{-1}		
						a	b	c
SB	South Burgess	F	Ontario, Canada	2.94	0.23	1103±0.01	1084±0.01	1063±1
S	Snarum	F	Buskerud, Norway	0.60	0.39	1098±1	1082±0.01	1055±1
B	Bamble	Cl	Telemark, Norway	0.08	5.74	1095±0.01	1074±0.01	1055±1
A	Arendal	F	Aust-Agder, Norway	2.73	0.22	1104±0.01	1083±0.01	1067±1
Sk	Skaaland Mine	Cl	Aust-Agder, Norway	0.29	5.14	1098±0.01	1074±0.01	1055±1
Gå	Gållivare	F	Norrbotten, Sweden	3.32	0.23	1105±0.01	1086±0.01	1062±1
W	Wakefield	F	Quebec, Canada	3.60	0.10	1110±0.01	1085±0.01	1066±1
Fa	Faraday	F	Ontario, Canada	4.11	0.00	1103±0.01	1086±0.01	1063±1
Da	Dandarragan	F	Western Australia	4.32	0.01	1093±0.01	1088±0.01	1049±1
D	Durango	F	Cerro de Mercado, Mexico	3.47	0.37	1104±0.01	1085±0.01	1062±1
O	Ødegårdens Verk	Cl	Telemark, Norway	0.08	5.24	1094±0.01	1074±0.01	1053±1
Pa	Panasqueira Mine	F	Beira Baixa, Portugal	4.06	0.00	1103±0.01	1086±0.01	1065±1
Bl	Bluestone Quarry	F	Massachussetts, USA	2.52	0.00	1103±0.01	1085±0.01	1063±1
T	Turf Pits Mine	F	Yorkshire, UK	4.25	0.00	1098±0.01	1088±0.01	1053±1
R	Renfrew	F	Ontario, Canada	4.01	0.00	1104±0.01	1087±0.01	1066±1
C	Chlorapatite-F	Cl	Aust-Agder, Norway	0.08	5.30	1095±0.01	1073±0.01	1050±1
P	PFG 201	F	unknown	2.46	0.63	1101±0.01	1084±0.01	1062±1
F	Fish Canyon Tuff	F	Colorado, USA	2.81	0.87	1099±0.01	1083±0.01	1061±1
M	Mt. Dromedary	F	Tilba Tilba, NSW, Australia	4.00	0.04	1103±0.01	1086±0.01	1061±1
G	Gun-F	Cl-F	Utah, USA	1.39	2.20	1101±0.01	1080±0.01	1060±1

enriched in chlorine. This important phenomenon allows reflectance IR to be a practical method of detecting the compositional changes across the fluorapatite-chlorapatite solid solution.

The y-axis values represent the reflectance, and this varies with respect to the orientation of the crystal and its degree of reflectivity. Apatites in which fission tracks are etched must pass certain criteria for selection for age calculation and track length measuring purposes. They must be aligned parallel to the crystallographic c-axis, and well polished. The crystal must be relatively free of inclusions or the tracks would be totally obscured, rendering precise counting difficult. Those crystals which perform badly with IR for having poor reflection would normally not be used for fission track analysis and can be legitimately discarded. Measurements of the reflectance at each of two control points (at 1250 and 950 cm^{-1} respectively) indicate the differing values of this shift. Measurements were taken on crystals of known crystallographic orientation (i.e. basal and c-axis parallel sections). These tests were performed on samples of Durango, Fish Canyon Tuff and Mount Dromedary apatites with the fission tracks etched. For basal sections of apatite, the fission tracks are etched as large, hexagonal pyramidal pits, whereas on c-axis parallel sections, the etch pits of the tracks are aligned parallel to each other and to the c-axis.

Sections can occasionally be determined from their shape; in euhedral crystals of apatite, basal sections are hexagonal, and c-axis parallel sections are often rectangular. The spectra produced by IR analysis show no change in peak wavenumber for either section. Therefore it can be concluded that crystal orientation does not affect the wavenumber of the peaks. However, the y-axis co-ordinates are highly variable, and the ratio of the highest intensity to lowest intensity in the band peaks (i.e. **b/c**) gives constant values **(Table 8.2)**. The differences between the ratios of **b/c** for each section are significant enough to enable rapid identification of crystallographic orientation if necessary.

8.4. Calibration.

Using reflectance IR, the experiments demonstrated that there is a decrease in IR wavenumber of the peaks as the apatite chemistry approaches the chlorapatite end-member. Calibration graphs plot the electron microprobe analyses of the chlorine and fluorine contents of the apatites set against the wavenumber of **a**, **b** and **c** on the IR spectra for the apatite standards. The spectra collected for the crystals showed that the results produced by the FTIR technique are reproducible, with a precision of 1 cm^{-1}. The IR wavenumbers of the apatite standards have an approximately linear

relationship with respect to wt % fluorine and chlorine **(Figs. 8.14)**. There is an anomalous spread of the data points when the composition approaches the pure fluorapatite end-member. This unexpected decrease in wavenumber is apparent in the plots for **a** and **c**, but not in the plot for **b**. An explanation to account for this behaviour is a response to structural adjustments creating the 'true' hexagonal crystallographic group (chlorapatites are monoclinic). The trough **b**, which closely approximates the LO frequency of peak **a** remains a more reliable value.

	Basal section	**c-axis parallel section.**
	b / c	**b / c**
Durango.	0.46	0.67
	0.47	0.59
	0.47	0.57
	0.44	
	0.48	
Average	0.46	0.61
Fish Canyon Tuff.	0.45	0.79
	0.45	0.79
	0.45	0.68
Average	0.45	0.75
Mount Dromedary.	0.47	0.71
	0.42	0.65
	0.48	0.73
Average	0.46	0.67

Table 8.2 The ratios of IR wavenumber of **b**: **c** for fission track age standards.

The most distant point from the line of plot **b** is Snarum apatite. Although in this study, this sample is assigned to a fluorapatite species, it is probably hydroxyl-rich. This conclusion is arrived at by the relatively small amount of combined fluorine and chlorine in the sample. Another component is needed to complete the anion quota of the crystal, and the most probable candidate is the hydroxyl (OH^-) group. Although this example cannot be ignored, hydroxylapatites have been shown to be relatively rare in nature (Seiber, 1986). From **Figure 8.7.**, there are other apatites which probably contain the hydroxyl group, however in these the OH^- component is not large enough to cause significant deviation from the line.

The linear nature of the relationship between trough **b** and the wt % fluorine and chlorine (shown in Fig. 14) make this curve the obvious choice for use towards compositional estimation. **Figure 8.15** shows the

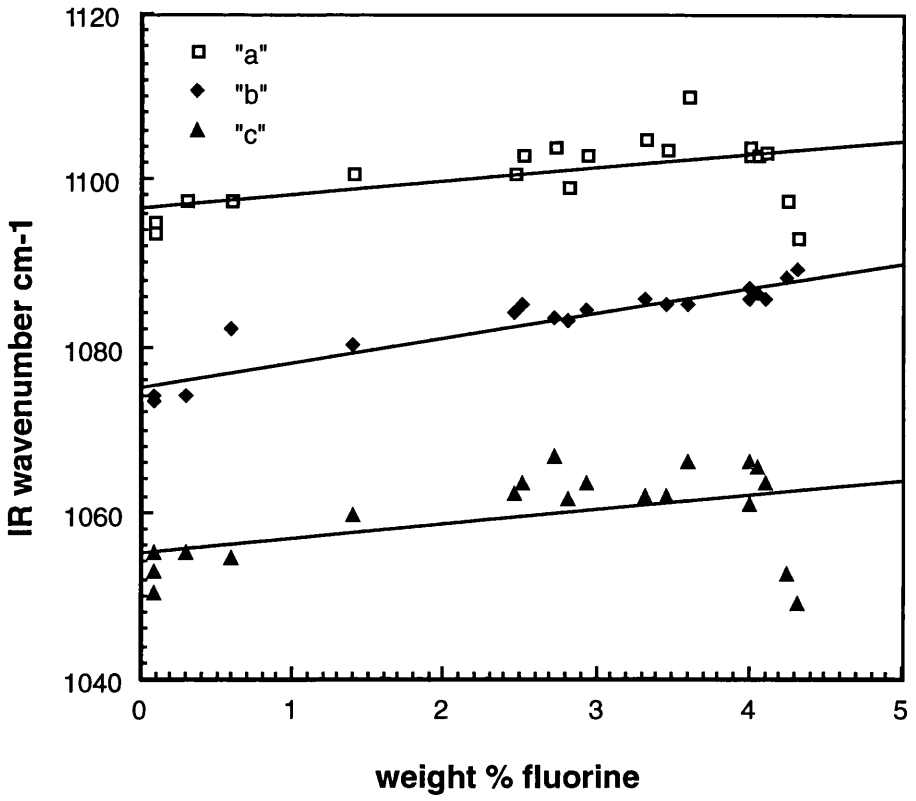

Fig. 8.14a. The IR wavenumbers for the peaks a, b and c, plotted against the fluorine contents of the apatite standards.

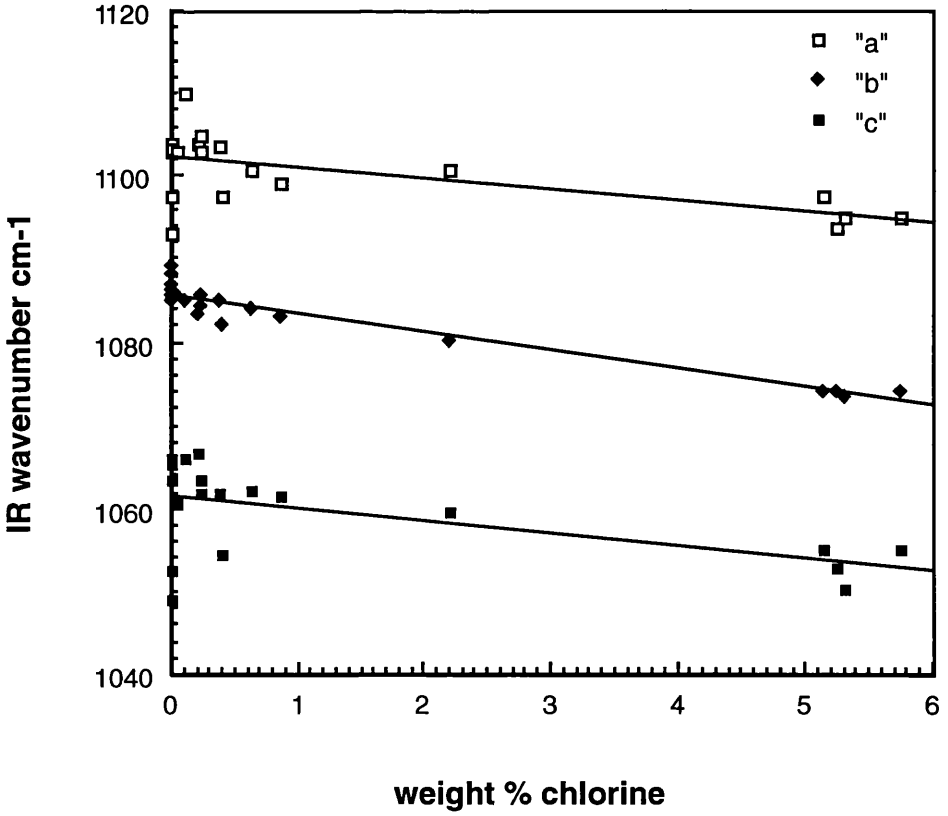

Fig. 8.14b. The IR wavenumbers for the peaks a, b and c, plotted against the chlorine contents of the apatite standards.

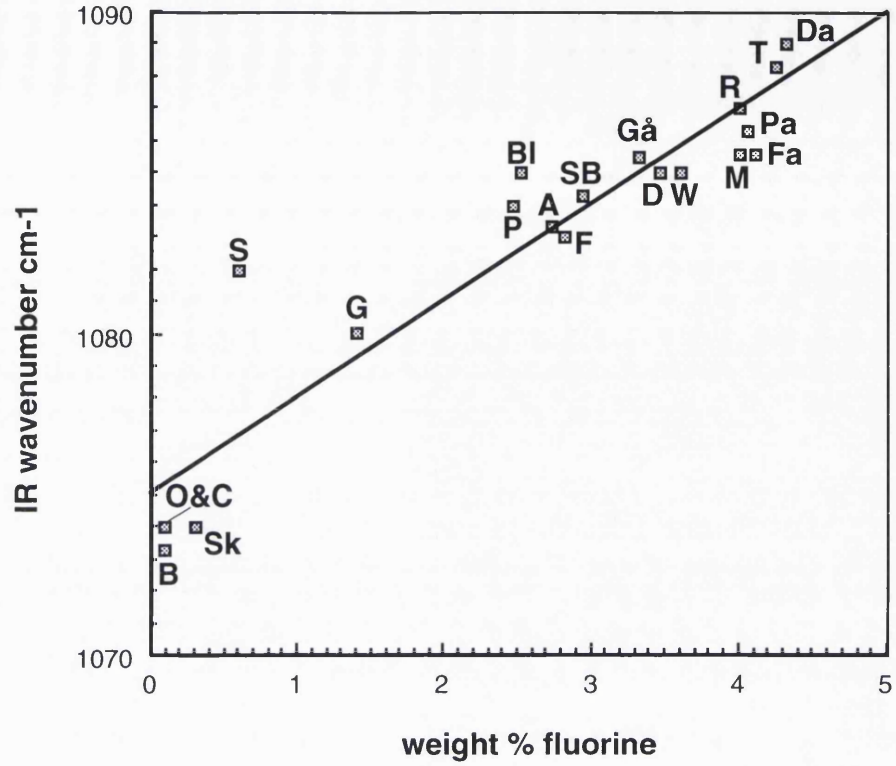

Fig. 8.15a. The IR wavenumber for the trough b, plotted against the fluorine contents of the apatite standards. The abbreviations are in Table 8.1.

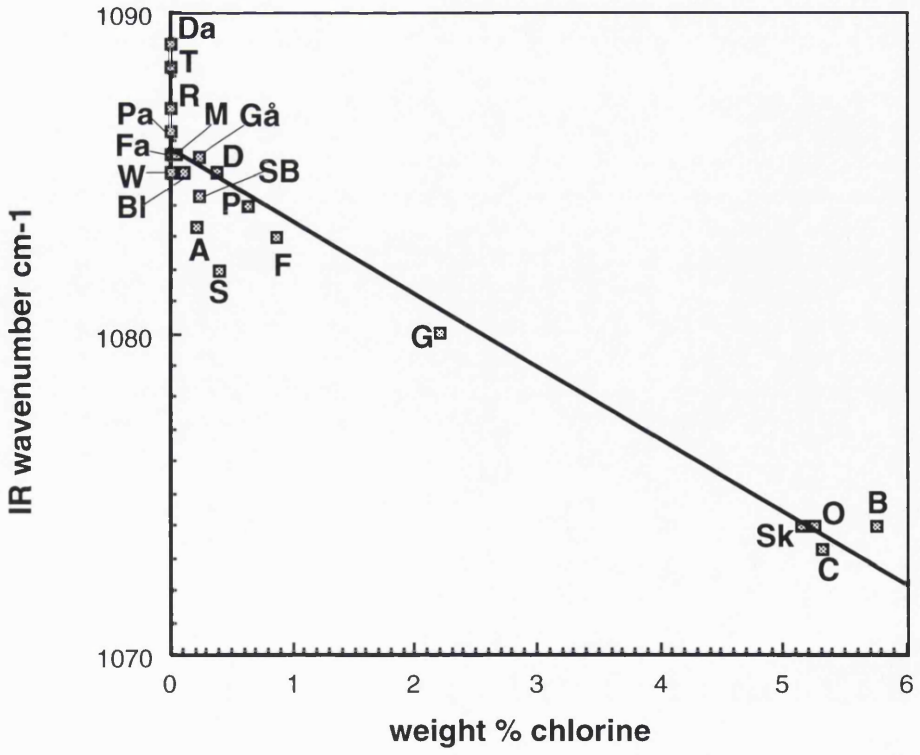

Fig. 8.15b. The IR wavenumber for the trough b, plotted against the chlorine contents of the apatite standards.

more precise plots of the trough wavenumber versus fluorine and chlorine composition for each of the analysed apatite standards.

For the graph of wt % fluorine (x) versus IR wavenumber (y), the equation of the straight line is

$$y = 1075.10 + 2.9935\,x \qquad R^2=0.88 \qquad (8.7)$$

For the graph of wt % chlorine versus IR wavenumber, the equation of the straight line is

$$y = 1085.70 - 2.2526\,x \qquad R^2=0.93 \qquad (8.8)$$

From observation of the IR wavenumber, it is simple to solve these equations for the wt % fluorine or chlorine.

8.5. Testing the technique on fission track samples.

The experimental and technical work outlined above has culminated in a semi-quantitative analytical technique for the determination of fluorine and chlorine content of apatite. It is important now that these preliminary results should be assessed to test the application using samples already dated by fission track analysis that show anomalous single grain ages. Speculations as to the possible variety of chemical compositions of the samples may be made from purely observational characteristics of the apatite crystals, coupled with prior geological knowledge. Some assumptions on the diversity of provenance may be made from observations of the crystal morphology and some pointers towards the chemistry ascertained by the size of the etch pits of the fission tracks (see Fig. 7.15).

The samples analysed for varying fluorine and chlorine contents included selected samples from the Armorican Massif, discussed in the earlier part of this thesis. Two other apatite fission track samples known to show anomalous single grain ages were also analysed.

8.5.1. Experimental procedure.

Because it is necessary to analyse the individual crystals upon which fission track ages were calculated, they have to be relocated on the grain mounts for the purpose of IR microspectroscopy. The sample grain mounts were photographed onto colour print film at magnification of 5x and then pieced together to form a photomosaic of the grain mount **(Fig. 8.16)**. The original grains on which single grain ages were calculated were

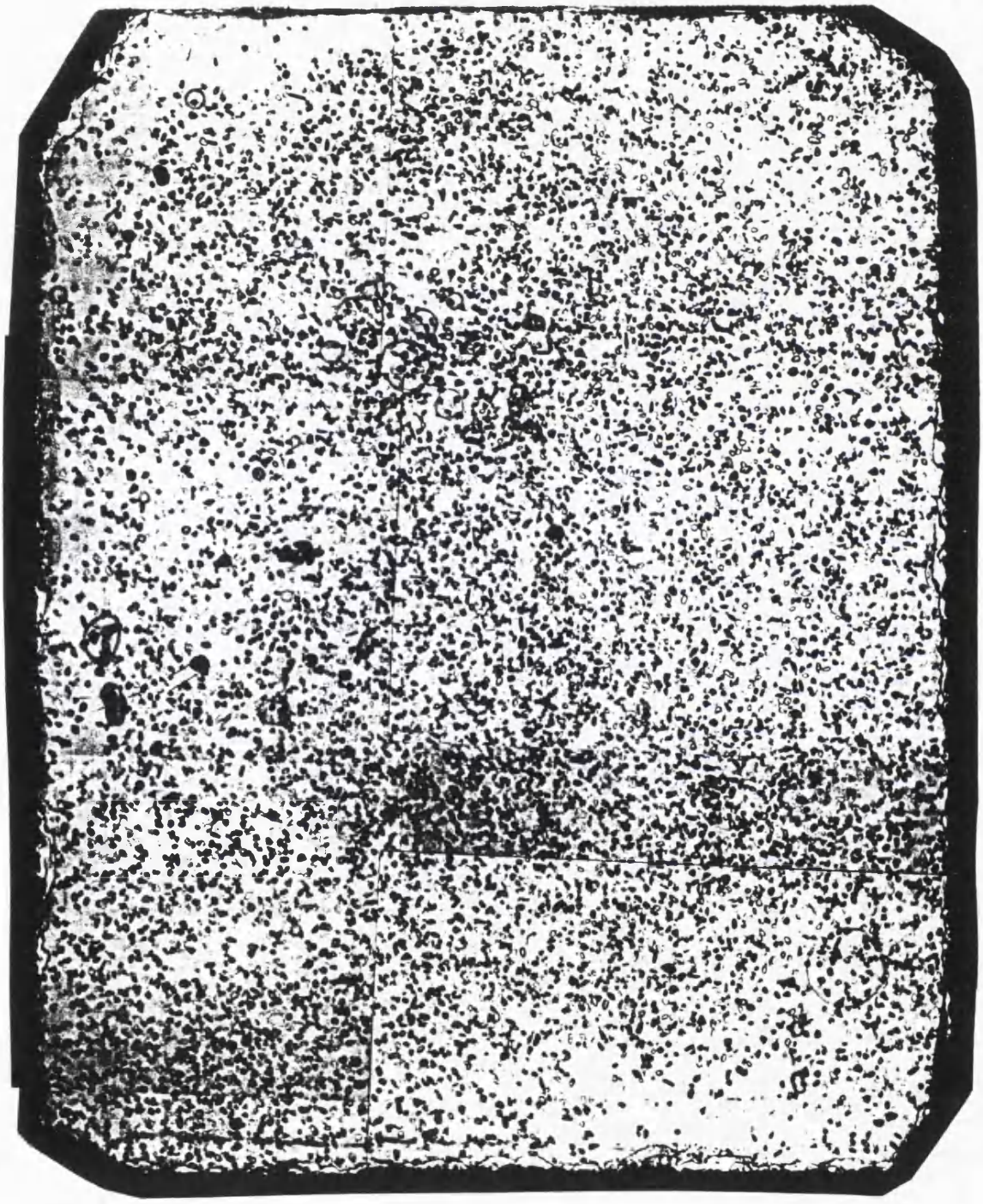

Fig. 8.16. A photomosaic of a grain mount as used for apatite fission track samples and FTIR microspectroscopy. Other species of mineral grains are present. The mount is on a piece of glass of area ~ 1 cm^2.

relocated and marked with flags denoting the order of calculation. Occasionally problems were encountered with relocation of the grains due to loss of alignment of the stage since the crystals were originally subjected to fission track analysis. This problem would not normally occur if this technique were to become routine, as crystals would be marked at the time of age calculation. Another problem encountered was that the crystals were of poor reflectance, or much pitted due to the etching of anomalously high numbers of defects or fission tracks and consequently an IR measurement could not be taken or was too poor to allow recognition of the peaks. Each crystal was analysed and the position of the peaks on the spectrum recorded. The position of the central trough **b** was then compared with the single grain age calculated for that crystal.

8.5.1.1. Samples from the Armorican Massif.

The following samples were analysed; VEND 9 (granite), VEND 10 (biotite-sillimanite gneiss), VEND 17 (metasediment), NOR 1 (granodiorite), NOR 9 (dolerite) and BRET 14 (granite). The single grain ages for each sample and the corresponding position of the IR inter-peak trough 'b' are shown on **Table 8.3.**

The IR spectra of these samples were remarkably consistent. The wavenumber for the central trough **b** varied between 1085 and 1087 cm^{-1} for all the samples except VEND 10, where two grains recorded a wavenumber of 1083 cm^{-1}. This equates to a chemistry of ~3.06 - 4.29 (±1) wt % fluorine and negligible chlorine (>0.31 wt %). This is the same chemical variation that would be expected within an aliquot of Durango apatite, demonstrating consistency in chemistry within the igneous rocks analysed.

8.5.1.2. TX-19a Central North Sea.

The sample from the Sole Pit inversion axis in the east Central North Sea is from well 48/7a-9, collected from an interval of 5030 - 5270 ft and at a downhole temperature of ~ 50°C, having undergone previous residence in the partial annealing zone. Apatite fission track analysis produced a central age of 79±7 Ma (relative error 29.17 %) against a stratigraphic age of 242 Ma. Two single grain ages were anomalously old **(Fig. 8.17)**, with ages approaching the stratigraphic age (209±121 Ma and 230±71 Ma; Alún O'Brien, pers. comm.).

The results of the FTIR analyses on each apatite crystal showed a direct correlation with the older ages and the lowest values for trough **b**.

Table 8.3. Samples used for apatite fission track analysis and tested for variation in single grain age using IR microspectroscopy. Single grain age errors are compiled in Table 4.3.

	BRET 14			NOR 1			NOR 9			VEND 9			VEND 10			VEND 17	
xtl	SGA	IR	xtl	SGA	IR	xtl	SGA	IR	xtl	SGA	IR	xtl	SGA	IR	xtl	SGA	IR
1	151.59	1087±0.01	1	143.48	1085±0.01	1	165.39	1085±0.01	1	177.78	1087±0.01	1	244.91	1087±0.01	1	41.08	1087±0.01
2	153.76	1085±0.01	2	254.80	1087±0.01	2	518.68	1085±0.01	2	233.56	1087±0.01	2	346.14	not located	2	122.46	1085±0.01
3	103.07	1085±0.01	3	246.28	1087±0.01	3	566.49	1085±0.01	3	266.56	1087±0.01	3	305.16	1083±0.01	3	242.64	1085±0.01
4	138.01	1087±0.01	4	112.08	1085±0.01	4	282.39	1087±0.01	4	176.73	1087±0.01	4	281.27	1083±0.01	4	325.45	1085±0.01
5	195.43	1087±0.01	5	168.17	1087±0.01	5	289.47	1085±0.01	5	283.98	1087±0.01	5	266.68	not located	5	155.46	1087±0.01
6	186.28	1087±0.01	6	110.44	1087±0.01	6	309.65	1085±0.01	6	167.82	1087±0.01	6	266.36	1085±0.01	6	122.46	1087±0.01
7	134.93	1087±0.01	7	239.81	1087±0.01	7	161.65	1085±0.01	7	215.03	1087±0.01	7	266.87	1085±0.01	7	122.46	not located
8	193.15	1085±0.01	8	223.62	1087±0.01	8	304.35	1085±0.01	8	218.65	1087±0.01	8	185.25	1085±0.01	8	234.42	not located
9	146.67	1087±0.01	9	286.05	1087±0.01	9	164.28	1085±0.01	9	197.20	1085±0.01	9	348.41	1085±0.01	9	242.64	not located
10	134.97	1085±0.01	10	140.10	1087±0.01	10	229.76	1085±0.01	10	203.57	1087±0.01				10	141.58	not located
11	191.90	1087±0.01	11	197.92	1085±0.01	11	175.24	1085±0.01	11	222.58	1087±0.01				11	144.20	not located
12	189.33	1087±0.01	12	207.10	1087±0.01	12	271.75	1085±0.01	12	231.11	1087±0.01				12	242.64	not located
13	169.12	1087±0.01	13	232.84	1085±0.01	13	191.65	1085±0.01	13	300.69	1085±0.01						
14	206.35	1085±0.01	14	249.93	1087±0.01	14	233.92	1085±0.01	14	207.57	1087±0.01						
15	146.47	1085±0.01	15	173.58	1085±0.01	15	259.69	1083±0.01	15	205.79	1087±0.01						
16	224.75	1087±0.01	16	195.73	1085±0.01	16	217.91	1087±0.01	16	165.24	1087±0.01						
17	217.55	1087±0.01	17	179.62	1087±0.01	17	264.35	1085±0.01	17	215.28	1087±0.01						
18	180.34	1087±0.01	18	178.53	1087±0.01	18	213.25	1085±0.01	18	206.21	1085±0.01						
19	155.27	1087±0.01	19	175.09	1087±0.01	19	208.08	1085±0.01	19	152.40	not located						
20	187.40	1085±0.01				20	242.12	1087±0.01									

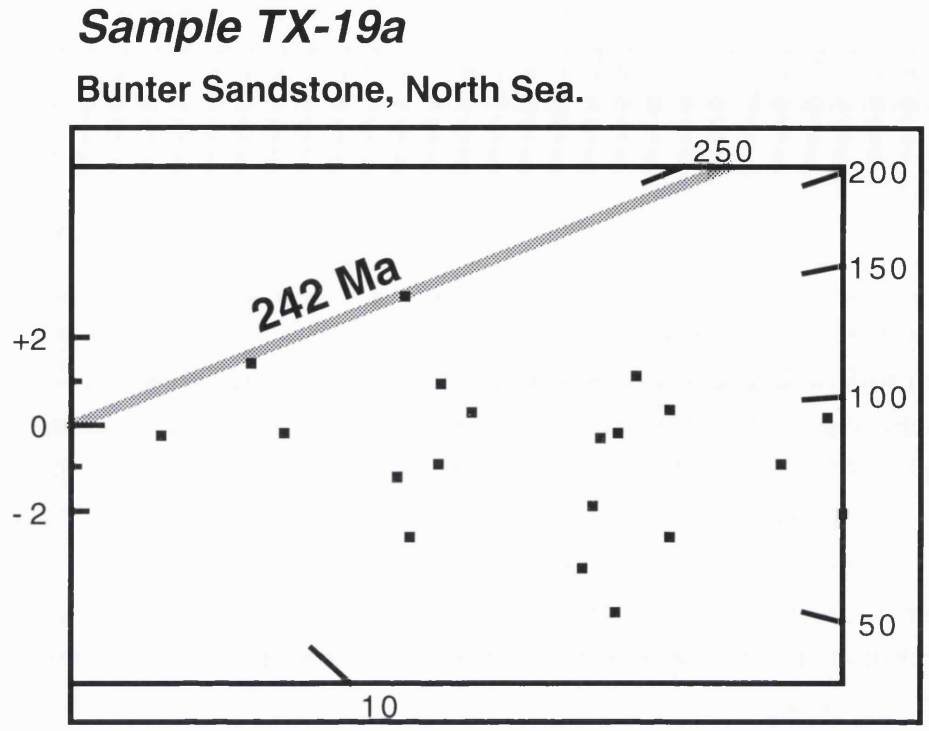

Fig. 8.17. Radial plots of apatite fission track single grain ages from the Triassic of the North Sea, sample TX-19a.

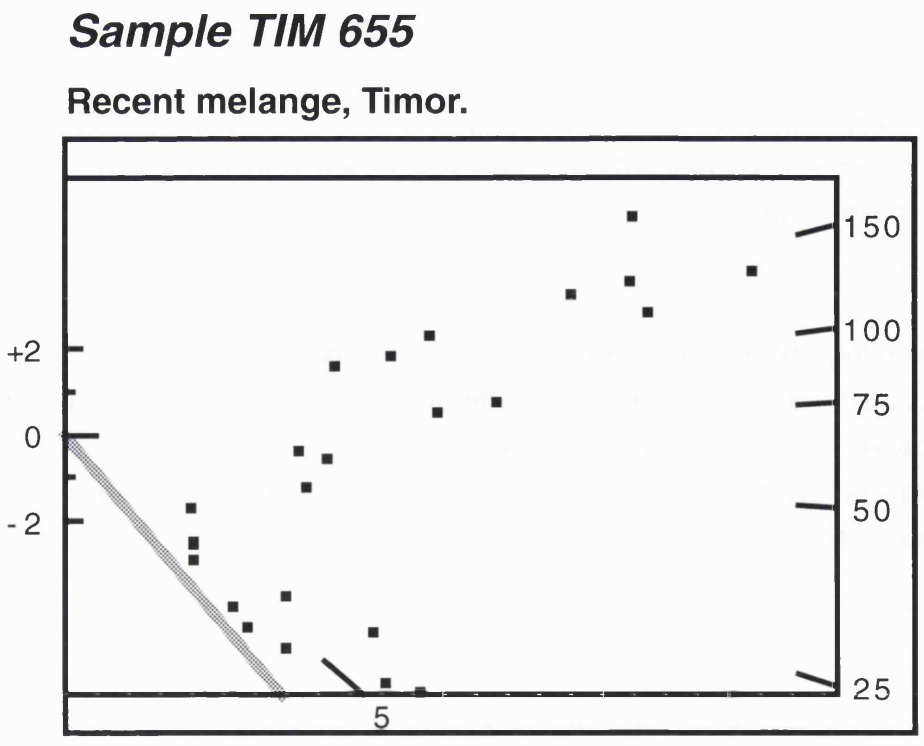

Fig. 8.18. Radial plots of apatite fission track single grain ages from a recent melange from Timor, sample TIM 655. The stratigraphic age of the samples is denoted by the grey, solid line

In the case of this sample, this is a highly conclusive result that an increase in chlorine will affect the annealing kinetics of fission tracks in apatite.

8.5.1.3. TIM 655 East Timor.

This is a surface outcropping sample from a recent melange complex in East Timor. The exact lithology and geological setting are unknown. The radial plot shows a well-defined bimodal distribution of single grain ages **(Fig. 8.18)**. This distribution was originally interpreted as two separate provenance area ages rather than a result of partial annealing (A. Carter pers. comm.). No correlation between fission track age and fluorine or chlorine composition was detected. However a considerable range in apatite composition was apparent in the sample. The IR wavenumbers for trough **b** range between 1078 and 1087 cm^{-1}. This indicates a spread within the sample from pure chlorapatite to Durango apatite-type composition.

The apatite single grain ages of sample TX-19 and TIM 655 were plotted versus their corresponding IR wavenumber for trough **b.** The anomalously old single grains plot conspicuously at the lowest wavenumbers **(Fig. 8.19)**. Apart from these grains, the others analysed grains had fluorine and chlorine contents similar to that of Durango Apatite, or with a higher fluorine content than Durango Apatite. Within these two groups there is no clear evidence that these two groups of composition (the high fluorine group and the Durango-type group) have any correlation to the degree of partial annealing, and hence variation in single grain ages. They would be indistinguishable within the sample as they both contain ages within the same ranges.

It appears that there is a 'critical value' of chlorine above which fission tracks have increased stability and resistance to temperature. From Figure 8.19, we can assume that the level of significance for an apatite containing negligible hydroxyl group is at or below 1083 cm^{-1} wavenumbers, which provides a corresponding chlorine content of 0.8 wt % for this critical value.

8.6. Conclusions.

FTIR microspectroscopy is a technique from which a semi-quantitative chemical composition analyses for fluorine and chlorine content can be completed on apatite samples used for fission track analysis.

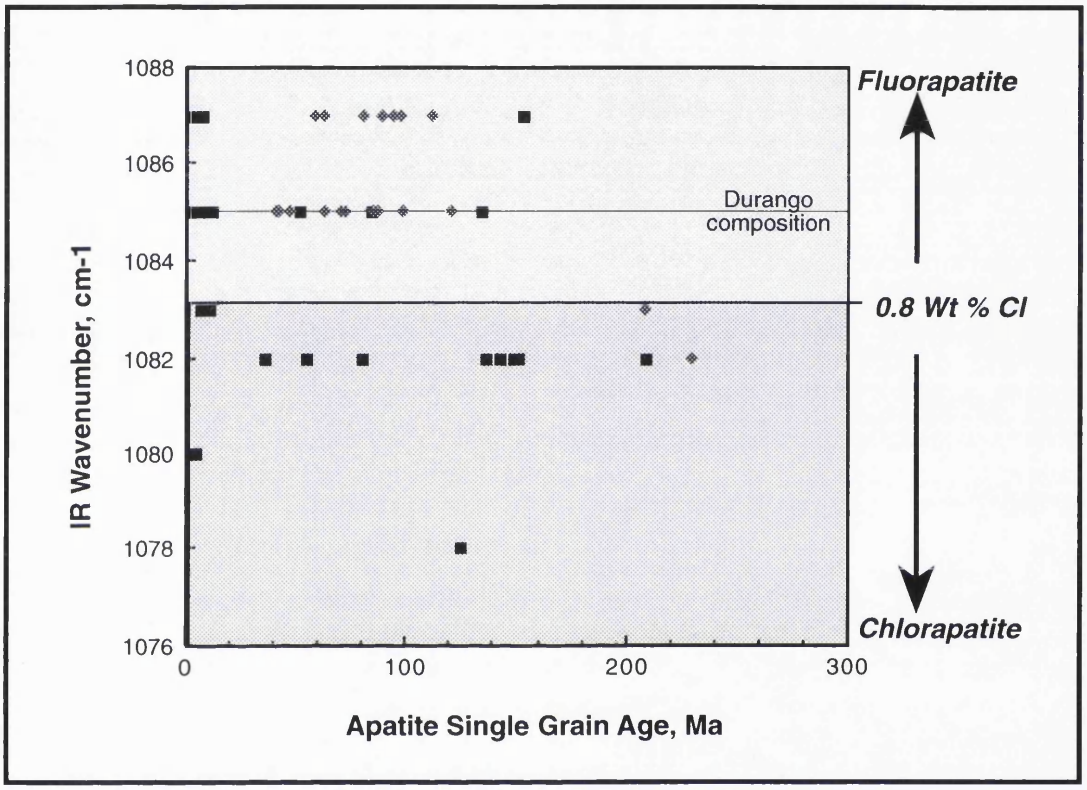

Fig. 8.19. A Plot of IR wavenumber v. single grain age for the Timor sample, TIM 655 (black squares) and the Sole Pit sample, TX-19a (grey diamonds). Note that the two oldest Sole Pit samples are the richest in Cl. There is no correlation between age and composition in the Timor sample. The spread here must be due to composition.

As a diagnostic tool for the chemical analysis of apatites for fission track analysis, transmittance IR spectroscopy is not particularly useful as the technique is most suited to large, well-formed crystals or the use of powders dispersed in KBr (Tuddenham and Lyon, 1960; Russell, 1974). Fission track analysis uses crystal 'grains' of approximately 50 μm diameter, mounted on microscope slides and these are totally unsuitable for transmittance IR.

In contrast reflectance IR is an ideal technique for the compositional determination of apatites because it is directly applicable to the prepared grain mounts used in fission track analysis. IR analyses can be made on the individual crystals on which fission track single grain ages were measured, *in situ* on the grain mount. This allows a direct correlation between apparent fission track age and chlorine (or fluorine) content to be made. This is an important advance within the methodology of apatite fission track analysis. A limitation of the technique is the present inability to detect or compensate for the hydroxyl component that may be present in apatites.

The experiments conducted on apatite fission track samples from the Armorican Massif revealed that the compositional spread encountered in these samples was not significant, and that they had compositional range similar to that of Durango apatite. Furthermore, in relation to the data interpretation in Chapter 5, this proves that the Laslett et al. (1987) annealing algorithm was an accurate choice for modelling these data.

The appearance of chlorine in apatite increases the resistance to the annealing of the fission tracks is corroborated by these results, although it is not apparent from this set of experiments that this relationship is linear. There appears to be a critical amount of chlorine (~0.8 wt %) within the crystal above which the tracks develop a greater resistance to annealing.

If these assumptions are true, it is not so much the chemistry that affects the annealing behaviour as the adjustments to the crystal structure caused by the substitution of large ions such as chlorine. The pure chlorapatite end member belongs to the monoclinic rather than the hexagonal crystal system (Mackie et al., 1972). This change in anisotropy may have a greater bearing on annealing than the substitution of chlorine alone. If this is true, then any ion of a similar size substituting in critical amounts will likewise affect annealing.

Chapter 9

Epilogue.

9.1. Apatite fission track analysis of the continental margins of the Bay of Biscay: a summary of conclusions.

A reconnaissance collection of samples from the Variscan Basement of western France and north-western Spain have been subjected to apatite fission track analysis, yielding new insights into the Mesozoic evolution of the region. Although the lithologies sampled were primarily Proterozoic and Palaeozoic crystalline rocks, the fission track data indicate that they had been affected by more recent thermotectonic episodes, associated mainly with rifting and eventual continental breakup in the Bay of Biscay and the North Atlantic Ocean.

Coming from the rift-flanks, the samples, although unlikely to have been directly affected by the tectonics and accelerated heat flow associated with rifting and breakup, have been profoundly affected by the geomorphological processes associated with this tectonic environment: namely, a rift dome uplift, which created an elevated region which became a sedimentary source for the surrounding basins.

The fission track data were first interpreted using the regional geological constraints preserved in the stratigraphic record and computer modelling techniques incorporating algorithms derived from annealing experiments on fission tracks in apatite. This indicated that the Armorican and Hesperian Massifs underwent burial to temperatures of ~100-120°C during the Lower to Middle Jurassic, attaining maximum temperatures at c. 170 Ma. These maximum temperatures can be equated to maximum burial depths of 3-3.5 km, assuming a geothermal gradient of 30 °C km^{-1}. The timing of this maximum burial was just prior to the formation of the Biscay Rift Dome which attained a maximum elevation in the Lower Cretaceous before the onset of seafloor spreading in the Aptian-Albian.

The interpretations of the fission track data obviously have profound implications for the regional palaeogeographic evolution, revising estimates of sediment thickness and distribution. Furthermore, examination of palaeogeographic reconstructions has also indicated that high sea levels during the later Cretaceous suggest a second episode of post-Permian burial. However, this Campanian burial is only apparent in the Armorican Massif, which is well within the province of chalk deposition; it is proposed that ~1500 m of chalk were deposited on the Armorican Massif during this time. Subsequent erosion of the Armorican Massif between the

Maastrichtian and the present, occurred as part of the emergence of Europe, driven by the Alpine orogeny. An acceleration in denudation rates during the last 10 Ma, was possibly influenced by Upper Tertiary global cooling episodes and, more recently, by Quaternary glaciations.

The post-breakup evolution of the Hesperian Massif differs from that of the Armorican Massif in that it does not appear to have suffered burial during the Campanian. The thermal history proposed for this region envisages Mid-Jurassic maximum burial, with subsequent exhumation of the Massif until the upper Cretaceous at average rates of ~12 m Myr^{-1}. This was followed by more rapid exhumation as in the Armorican Massif, commencing in the Miocene at rates of ~130 m Myr^{-1}.

9.2. Determination of fluorine and chlorine contents of apatites using FTIR microspectroscopy.

The major conclusion derived from Chapter 8 is that reflectance infrared microspectroscopy is an ideal technique for providing a semi-quantitative evaluation of the fluorine and chlorine contents of apatites used for fission track analysis. Importantly, the method can be readily applied to the individual apatite grains upon which fission track ages have been determined, giving a direct correlation between apatite single grain age and chemical composition. The technique is rapid in comparison to electron microprobe analysis, non-destructive and requires no further sample preparation. All these advantages contribute to making it an advantageous, routine method for this type of analysis.

It is proposed that the relationship of resistance to track annealing with the increase in chlorine content is not linear, because it is impossible to distinguish separate age groups corresponding to composition from the single grain age spreads in analysed samples. However, evidence that chlorine content above a critical value (> 0.8 wt % in the crystal) would begin to cause a resistance to annealing is apparent from the examination of single grain compositions and corresponding fission track ages. It is postulated from these data that the annealing of fission tracks in apatite is affected by the substitution of large anions causing an alteration in crystal structure, initiating a change from hexagonal to monoclinic symmetry, rather than as a consequence of the chemical nature of the substituting ion.

9.3. Future work.

9.3.1. Furthering understanding of the thermotectonic evolution of Western Europe.

There is plenty of scope for continuing apatite fission track analysis in onshore and offshore western Europe. This thesis has studied the evolution of the onshore sections of the Bay of Biscay passive margins. Extension of this work to samples from the Armorican Shelf, the Western Approaches, English Channel, North Spanish Margin and Galicia Basins would provide a complementary study for the offshore evolution of the region.

In continental Europe, it would be useful to apply the technique of apatite fission track analysis to model the behaviour of other massifs that have been regarded as land during much of the Mesozoic and Cenozoic; for example the London Brabant and Massif Central. At present only limited fission track data have been determined in these regions. Collaboration with other disciplines (i.e. sedimentology, stratigraphy and palaeontology) would provide further constraints on the palaeogeographic reconstructions.

9.3.2. The annealing of fission tracks in apatite and its relationship to crystal chemistry (or structure?).

The scope for further work examining the annealing of fission tracks in apatite is immense. On a crystallographic scale it would be of great value to examine the relationships of the fission tracks, as defects, to apatite crystal structure, further equating this with the established annealing properties, perhaps with the aid of synthetically grown, uranium-doped crystals. The effects of other substitutions into the lattice either into the anion site or into other ion sites, for example the Ca_I site should be further investigated, and this would require a series of precisely defined annealing experiments. Comparisons with the thermal stability of other crystal defects would provide a more rigorous analogy with the behaviour of fission tracks within a crystal.

The infrared microspectroscopy of apatites used for fission track analysis would become more efficient if the system were automated. This would considerably speed determination of individual apatite grain chemistries, removing the time used in searching for the necessary crystals on photomosaic maps.

These apatite fission track studies have resulted in a new understanding of the geological evolution of Western-most Europe and the

development of a novel methodology for determining the relative abundance of chlorine and fluorine in apatites. This latter advancement provides a tool for the rigorous interpretation of single grain age spreads with respect to apatite chemistry, an aspect which, to date, has generally been neglected.

References

Adler, H. H., 1964, Infra-red spectra of phosphate minerals; Symmetry and substitution effects in the pyromorphite series. *Am. Min.* 49, 1002-1015

Allen, P., 1981, Pursuit of Wealden models. *J. Geol. Soc. Lond.*, 138, 375-437.

Alonso, J. L., 1989, Fold reactivation involving angular unconformable sequences; theoretical analysis and natural examples from the Cantabrian Zone (Northwest Spain)., *Tectonophysics*, 170, 57-77.

Alonso, J. L., Marcos, A. and Pulgar, J. A., 1991, Persistent basement wrenching as controlling mechanism of Variscan thin-skinned thrusting and sedimentation, Cantabrian Mountains, Spain: comment. *Tectonophysics*, 194, 171-176.

Altschuler, Z. S., Clarke, R. S. and Young, E. J., 1958, Geochemistry of uranium in apatite and phosphorite. *USGS. Prof. paper*, 314-D

Åmli, R., 1975, Mineralogy and rare earth geochemistry of apatite and xenotime from the Gloserheia Granite Pegmatite, Froland, Southern Norway. *Am. Min.* 60, 607-620.

Andrews, D. J. and Sleep, N. H., 1974, Numerical modelling of tectonic flow behind island arcs. *Geophys. J. R. Ast. Soc.*, 38, 237-251.

Andriessen, P. A. M., 1990, Anomalous fission track apatite ages of the Precambrian basement in the Hunnedalen region, South-western Norway. *Nucl. Tracks Radiat. Meas.* 17, 285-291.

Andriessen, P. A. M. and Bos, A., 1986, Post-Caledonian thermal evolution and crustal uplift in the Eidford area, western Norway., *Norsk Geol. Tidss.*, 66, 243-250.

Argand, E. 1924, la tectonique de l'Asie. Proc. XIII Intern. Congress, Brussels, 171-372.

Arthaud, F. and Matte, P., 1975, Les décrochements tardi-hercyniens du sud ouest de l'Europe. Géometrie et essai de reconstitution des conditions de la deformation. *Tectonophysics*, 25, 139-171.

Autran, A. and Cogné, J., 1980, La zone interne du domaine varisque dans l'Ouest de la France et le développement de l'orogène varisque., 26^{me} Congrès Geol. Intern., Paris, 90-11.

Autran, A., Barriere, M., Bonin, B., Didier, J., Fluck, P., Fourcade, S., Giraud, P., Jonin, J., Lameyre, J., Orsini, J-B., Vivier, G., 1980, Les granitoïdes de France. in "Evolutions geologique de la France.", *Mém. BRGM*, 107, 51-97.

Auvray, B. and Martin, H., 1982, Excursion dans le Nord du Massif Armoricain (Domaines Mancellien and Domnonéen), Université de Rennes, Institut de Géologie.

Auvray, B, Charlot, R. and Vidal, P., 1980a, Données nouvelles sur le Protérozique inférieur du domaine nord-Armoricain (France): âge et signification. *Can. J. Earth Sci.* 17, 532-538.

Auvray, B., Mace, J., Vidal, P. and Van der Voo, R., 1980b, Rb-Sr dating of the Plouezec volcanics, N. Brittany; implications for the age of red-beds (Series-Rouges) in the northern Armorican Massif., *J. Geol. Soc. Lond.*, 137, 207-210.

Bacon, M. and Gray, F., 1970, A gravity survey in the eastern part of the Bay of Biscay. *Earth & Planet. Sci. Letts.*, 10, 101-105.

Bacon, M., Gray, F. and Matthews, D. H., 1969, Crustal structure studies in the Bay of Biscay. *Earth & Planet. Sci. Letts.*, 6, 377-385.

Bale, P. and Brun, J. P., 1986, Late Precambrian thrust and wrench zones in northern Brittany (France)., *J. Struct. Geol.*, 11, 391-405.

Barber, A. J. and Max, M. D., 1979, A new look at the Mona Complex (Anglesey, North Wales). *J. Geol. Soc. Lond.*, 136, 407-432.

Barbier, F., Le Pichon, X. and Duvergé, J., 1986, Structure profond de la marge nord-Gascogne, Implications sur le mécanisme de rifting et de formation de la marge continentale, *Bull. Cent. Recherches et Explor. Prod. Elf Aquitaine*, 10(1), 105-121

Bard, J. P., Burg, J. P., Matte, P. and Ribeiro, A., 1980, La Chaîne hercynienne d'Europe occidentale en termes de tectonique des plaques., in 'Géologie de l'Europe' Ed. Cogné, J. and Slansky, M., *Mém. BRGM* 108, 233-246.

Barrière, M., Cogné, J. and Vidal, P., 1971, La trondhjemite de Douarnenez: une intrusion magmatique ordovicienne dans les schistes cristallins du sud-Finistérre. *C. R. Acad. Sci. Paris.* 273, 1556-1559.

Bastida, F., Marcos, A., Marquínez, J., Martinez-Catalan, J. R., Perez-Estaun, A. and Pulgar, J. A., 1984, La Coruña (1), Mapa Geologico d'España 1:200,000 scale, I. G. M. E., Madrid.

Bastida, F., Martinez-Catalan, J. R., Pulgar, J. A., 1986, Structural, metamorphic and magmatic history of the Mondoñedo nappe (Hercynian belt, NW Spain). *J. Struct. Geol.*, 8, 415-430.

Beevers, C. A., and McIntyre, D. B., 1946, The atomic structure of fluorapatite and its relation to that of tooth and bone material. *Min. Mag.*, 27, 254-257.

Bernard-Griffiths, J., Cantagrel, J-M. and Duthou, J-L., 1977, Radiometric evidence for an Acadian tectonometamorphic event in the Western Massif Central, France. *Conts Min. Pet.*, 61, 199-212.

Berthé, D., Choukroune, P. and Jegouzo, P., 1979, Orthogneiss, mylonite and non coaxial deformation of granites: the example of the South Armorican Shear Zone. *J. Struct. Geol.*, 1, 31-42.

Bertrand, L, 1921, les anciennes mers de la France et leur depots. Flammarion. Paris.

Bhatnagar, V. M., 1967, IR Spectra of fluorapatite and fluorchlorapatite. *Experentia*, 23, 10-12.

Bigazzi, G., 1981, The problem of the decay constant λ_f of ^{238}U., *Nucl. Tracks.*, 5, 35-44.

Bland, A. M., 1984, Field relations within the south-west Jersey Granite complex. *Proc. Ussh. Soc.*, 6, 54-69.

Boillot, G., 1984, Some remarks on the continental margins in the Aquitaine and French Pyrenées., *Geol. Mag.*, 121, 407-412.

Boillot, G., Dupeuble, P. A. and Malod, J., 1979, Subduction and tectonics on the continental margin off northern Spain., Marine Geology, 32, 53-70.

Boillot, G., Mougenot, D., Girardeau, J. and Winterer, E. L., 1989, Rifting processes on the West Galicia Margin, Spain., in: 'Extensional tectonics and stratigraphy of the North Atlantic margins.' *AAPG Mem.* 46, 363-377.

Bosworth, W., 1985, Geometry of propagating rifts., *Nature*, 316, 625-627.

Bott, M. H. P., 1992, Passive margins and their subsidence., *J. Geol. Soc. Lond.*, 149, 805-812.

Boudreau, A. E., Mathez, E. A. and McCallum, I. S., 1986, Halogen geochemistry of the Stillwater and Bushveld complexes: Evidence for transport of the platinum-group elements by Cl-rich fluids. *J. Pet.*, 27, 967-986.

Bradshaw, M. J., Cope, J. C. W., Crips, D. W., Donovan, D. T., Howarth, M. K., Rawson, P. F., West, I. M. and Wimbledon, W. A., 1992, Jurassic. in: Cope, J. C. W., Ingham, J. K. and Rawson, P. F. (Eds.) Atlas of Palaeogeography and Lithofacies. Geological Society, London, Memoir 13., 107-129.

Braun, J. and Beaumont, C., 1989, Contrasting styles of lithospheric extension : implications for differences between the basin and range province and rifted continental margins., 'Extensional tectonics and stratigraphy of the North Atlantic margins.' *AAPG Mem.* 46, 53-79.

BRGM, ELF-Re, ESSO-REP, SNPA, 1974, Géologie du bassin d'Aquitaine. Orléans, BRGM.

Brown, M., 1993, P-T-t evolution of orogenic belts and the causes of regional metamorphism. *J. Geol. Soc. Lond.*, 150, 227-241.

Brown, M., Power, G. M., Topley, C. G. and D'Lemos, R. S., 1990, Cadomian magmatism in the North Armoricain Massif. in. D'Lemos, R. S., Strachan, R. A. and Topley, C. G. (Eds.) The Cadomian Orogeny. *Geol. Soc. Spec. Pub.*, 51, 181-213.

Brown, R. W., Rust, D. J., Summerfield, M. A., Gleadow, A. J. W. and De Wit, M. C. J., 1990, An early Cretaceous phase of accelerated erosion on the south western margin of Africa: evidence from apatite fission track analysis and the offshore sedimentary record. *Nucl. Tracks.*, 17, 339-350.

Brun, J-P. and Burg, J-P., 1982, Combined thrusting and wrenching in the Ibero Armorican Arc: a corner effect during continental collision. *Earth & Planet. Sci. Letts.*, 61, 319-322.

Brun, J-P and Choukroune, P., 1983, Normal faulting, block tilting and décollement in a stretched crust, *Tectonics*, 2, 345-356.

Buck, W. R., Martinez, F., Steckler, M. S. and Cochran, J. R., 1988, Thermal consequences of lithospheric extension: pure and simple shear. *Tectonics*, 7, 213-234.

Bugge, J. A. W., 1978, Norway. in Mineral deposits of Europe. in: H. U. Bowie, A. Kvalheim, A. and Haslam, H. W. (Eds.),Volume 1: Northwest Europe., The Institution of Mining and Metallurgy, The Mineralogical Society.

Bullard, E. C., Everett, J. and Gilbert Smith, A., 1965, A symposium on continental drift. *Phil. Trans. Roy. Soc. Lond.*, Ser. A, 258, 41-51.

Burke, K., 1977, Aulacogens and continental breakup., *Ann. Rev. Ear. Plan. Sci.*, 5, 371-396.

Cabanis, B., 1974, La tectonogenèse hercynienne dans la région de Morlaix et sa signification à l' échelle du nord-ouest de la Bretagne. *Bull. Soc. Géol. France.*, (7), 16, 230-237.

Cabanis, B., 1980, Les événements hercyniens dans le nord-est de la Bretagne (Pays de Léon et Bassin de Morlaix)., abstract, in: R. A. Roach, Conference Report, Structure and tectonic evolution of the Armorican Massif., *J. Geol. Soc. Lond.*, 137, 211-216.

Calvez, J. Y. and Vidal, P. H., 1978, Two billion year old relics in the Hercynian belt of Western Europe. *Conts. Min. Pet.*, 65, 395-399.

Cande, S. C. and Kristofferson, Y., 1977, Late Cretaceous magnetic anomalies in the North Atlantic., *Earth & Planet. Sci. Letts.*, 35, 215-224.

Capdevila, R. and Floor, P., 1980, Les differents types de granites hercyniens et leur distributions dans le nord ouest de l'Espagne. *Bol. Geol. Min.*, LXXXI-II-III, 215-225.

Capdevila, R. and Vialette, Y., 1970, Estimation radiometrique de l'âge de la deuxieme phase tectonique hercynienne en Galice moyenne (Nord-Ouest de l'Espagne). *C. R. Acad. Sci., Paris*, Serie D., 270, 2527-2530.

Carey, S. W., 1958, A tectonic approach to continental drift. Symposium on Continental drift, University of Tasmania, Hobart. 177-355.

Carlson, W. D., 1990, Mechanisms and kinetics of apatite fission track analysis. *Am. Min.*, 75, 1120-1139.

Cathcart, J. B., 1991, Phosphate deposits of the United States-discovery and development; Economic geology and outlook for the future. in: Gluskoter H. J., Rice D. D. & Taylor R. B. (Eds.), The Geology of North America vol. P-2 Economic Geology. The Geological Society of America., 153-164.

Chadwick, R. A., Evans, D. J. and Smith, N. J. P., 1992, Permo-Triassic rifting in southern Britain. Permian and Triassic rifting in NW Europe, Abstracts, 21-22 October 1992, The Geological Society of London.

Chapman, T. J., 1989, Permian to Cretaceous structural evolution of the Western Approaches Basin (Melville sub-basin), U.K., in: M. A. Cooper and G. D. Williams (Eds.), Inversion tectonics., *Geol. Soc. Lond. Spec. Pub.* 44, 177-200.

Chauval, J. J. and Mansuy, C., 1981, Micropalaeontology du Proterozoique du Massif Armoricain (France). *Precamb. Res.*, 15, 25-42.

Choukroune, P. and Mattauer, M., 1978, Tectonique des plaques et Pyrenées: sur la fonctiennement de la faille transformante nord-pyrenéenne; comparison avec des modèles actuels. *Bull. Soc. Géol. France.*, 7, 689-700.

Cloetingh, S. A. P. L., Wortel, M. J. R. and Vlaar, N. J., 1982, Evolution of passive continental margins and initiation of subduction zones. *Nature*, 297, 139-142.

Cogné, J., 1964, Esquisse tectonique de la région comprise entre la Baie de St Brieuc et la Baie de Mont St Michel., *Bull. Soc. Belg. Géol. Pal. Hydro.*, 23, 222-227.

Cogné, J., 1974, Le Massif Armorican. in 'Géologie de la France, vol. 1; vieux massifs et grands bassins sédimentaires.', Ed. J. Debelmas, Doin, Paris. 105-161.

Cogné, J. and Peaucat, J. J., 1973, Une étape magmatique nouvelle dans l'evolution hercynienne sud-Armoricain; le granite orthogneissique de Pors-Poulhan en Baie d'Audierne (Finistérre sud). *C. R. Acad. Sci. Paris.*, 277, 2601-2604.

Cogné, J. and Wright, A. E., 1980, L' Orogène Cadomien., in 'Géologie de l'Europe' Ed. Cogné, J. and Slansky, M., *Mém. BRGM* 108, 29-55.

Cope, J. C. W., Ingham, J. K. and Rawson, P. F. (Eds.), 1992, Atlas of Palaeogeography and Lithofacies. Geological Society London, Memoir 13.

Coward, M., 1992, The Permo-Triassic: an overview of regional tectonics. Permian and Triassic rifting in NW Europe, Abstracts, 21-22 October 1992, The Geological Society of London.

Coward, M., Harvey, M. and Ruffell, A., 1992, Tectonic evolution of Plymouth Bay and adjacent English Channel. Permian and Triassic rifting in NW Europe, Abstracts, 21-22 October 1992, The Geological Society of London.

Cox, A., 1980, Rotation of microplates in western North America. In; Strangway, D. W. (ed.) The Continental crust and its mineral deposits. *Geol. Ass. Can., Spec. Pap.*, 20, 305-321.

Crowley, K. D., Cameron, M. and Schaeffer, R. L., 1991, Experimental studies of annealing of etched fission tracks in fluorapatite. *Geochim. Cosmochim. Acta.*, 55, 1449-1465.

D'Lemos, R. S., Strachan, R. A. and Topley, C. G., 1990, The Cadomian Orogeny in the North Armoricain Massif: a brief review. in. D'Lemos, R. S., Strachan, R. A. and Topley, C. G. (Eds.) The Cadomian Orogeny. *Geol. Soc. Spec. Pub.*, 51, 3-12.

Dallmeyer, R. D. and Brown, M., 1992, Rapid Variscan (c. 300 Ma) exhumation of Eo-Variscan (c. 400 Ma) metamorphic rocks from South Brittany, France: 40Ar/39Ar age data and tectonic implications. Geol. Soc. Am. Annual Meeting, Cincinnati, Ohio. Abstracts with program, 24, A236.

Darbyshire, D. P. F. and Shepherd, T. J., 1985, Chronology of granite magmatism and associated mineralization, SW England., *J. Geol. Soc. Lond.*, 142, 1159-1177.

de Charpal, O., Montadert, L., Guennoc, P. and Roberts, D. G., 1978, Rifting, crustal attenuation and subsidence in the Bay of Biscay. *Nature*, 275, 706-711.

Deming, D., 1993, Estimates of permeability on a basin scale from observations of terrestrial heat flow in a sedimentary basin, north slope of Alaska. in: J. Parnell, A. H. Ruffell and N. R. Moles (Eds.), Geofluids '93 Extended Abstracts, 88-91.

den Tex, E. and Floor, P., 1971, A synopsis of the geology of Western Galicia., In. Histoire Structurale de Golfe de Gascoigne, *Pub. Institut Français Pét., Collections Coll. Sém.*, 22, I.3.

Denis, E. and Dabbard, M. P., 1988, Sandstone petrography and geochemistry of late Proterozoic sediments of the Armorican Massif (France) - a key to basin development during the Cadomian orogeny. *Precamb. Res.*, 42, 189-206.

Derégnaucourt, D. and Boillot, G., 1982, Nouvelle carte structurale du Golfe du Gascoigne. *C. R. Acad. Sci. Paris.*, 294, 219-222.

Deutsch, S. and Chauris, L., 1965, Age de quelques formations cristallophyllienes et granitiques de Pays de Léon (Finistérre). *C. R. Acad. Sci. Paris.*, 260, 615-617.

Dodson, M. H., 1973, Closure temperature in cooling geochronological and petrological systems. *Conts. Min. Pet..*, 40, 259-274.

Donelick, R. A., 1991, Crystallographic orientation dependence of mean etchable fission track length in apatite: an empirical model and experimental observations. *Am. Min.*, 76, 83-91.

Doré, A. G., 1992, Synoptic palaeogeography of the Northeast Atlantic Seaway: late Permian to Cretaceous. in: J. Parnell (Ed.) Basins on the Atlantic Seaboard: Petroleum Geology, Sedimentology and Basin Evolution. *Geol. Soc. Spec. Pub.* 62, 421-446.

Doré, F., Juignet, P., Larsonneur, C., Pareyn, C. and Rioult, M., 1978, Guides Géologiques Régionaux; Normandie. Masson, Paris.

Dott, R. H. and Batten, R. L., 1976, Evolution of the Earth., McGraw Hill Inc., 503 pp.

Douglas, R. J. W. (Ed.), 1968, Geology and economic minerals of Canada. Geological Survey of Canada. 838 pp.

Dunham, K. C., 1952, Fluorspar. Memoir of the Geological Survey Special Publication on the Mineral Resources of Great Britain. Vol. 4, 143 pp.

Dunham, K. C., 1974, Epigenetic minerals. in: Rayner D. H. & Hemingway J. E. (Eds.), The geology and mineral resources of Yorkshire , *Yorks. Geol. Soc.*, 293-309.

Durand, S. and Lardeux, H., 1985, Guides Géologiques Régionaux; Bretagne. Masson, Paris.

Durrani, I. R. and Bull, R. K., 1987, Solid state nuclear track detection (principles, methods and applications)., Pergamon Press, Oxford.

Ekström, T. K., 1972, Coexisting scapolite and plagioclase from two iron formations in Northern Sweden., *Lithos*, 5, 175-185.

Ekström, T. K., 1973, Synthetic and natural chlorine bearing apatite. *Conts. Min. Pet.*, 38, 329-338.

Enay, R. and Mangold, C., 1982, Dynamique biogéographique d'évolution des faunes d'Ammonites au Jurassique. *Bull. Soc. Géol. France.*, 7, 1025-1046.

Engel, W. and Franke, W., 1983, Flysch sedimentation: its relations to tectonism in the European Variscides. In: Martin, H. and Eder, W. (Eds.) Intracontinental foldbelts: case studies in the Variscan Belt of Europe and the Damara Orogen of Namibia, Springer Verlag, Berlin. 267-288.

England, P. C. and Molnar, P., 1990, Surface uplift, uplift of rocks and exhumation of rocks. *Geology*, 18, 1173-1177.

England, P. C. and Richardson, S. W., 1980, Erosion and age dependence of continental heat flow. *Geophys. Jour. Roy. astr. Soc.*, 62, 421-437.

Ewing, J., Burkle, L. H., Saito, T. and Poppe, H., 1971, Geophysical and geological studies of Cantabria Seamount and its environs. in: Histoire Structurale du Golfe de Gascoigne. Editions Technip, Paris. 12.1-12.14.

Fisher, R. B. and Ring, C. E., 1957, Quantitative infra-red analysis of apatite mixtures. *Anal. Chem.* 29, 431-434

Fitzgerald, P. G. and Gleadow, A. J. W., 1988, Fission track geochronology, tectonics and structure of the Transantarctic Mountains in Northern Victoria Land, Antarctica., *Chem. Geol. (Iso. Geosci. Sect.).*, 73, 169-198.

Fitzgerald, P. G. and Gleadow, A. J. W., 1990, New approaches in fission track geochronology as a tectonic tool: examples from the Transantarctic Mountains., *Nucl. Tracks.*, 17, 351-357.

Fitzgerald, P. G., Sandiford, M., Barrett, P. J. and Gleadow, A. J. W., 1986, Asymmetric extension associated with uplift and subsidence in the Transantarctic Mountains and the Ross Embayment. *Earth & Planet. Sci. Letts.*, 81, 67-78.

Fitzgerald, P. G., Fryxell, J. E. and Wernicke, B. P., 1991, Miocene crustal extension and uplift in south-eastern Nevada: constraints from fission track analysis. *Geology*, 19, 1013-1016.

Fleischer, R. L. and Price, P. B. ,1964a, Decay constant for the spontaneous fission of ^{238}U., Phys. *Rev.*, 133, B63-B64.

Fleischer, R. L. and Price, P. B. ,1964b, Techniques for geological dating of minerals by chemical etching of fission fragment tracks. *Geochim. Cosmochim. Acta.*, 28, 1705-1714.

Fleischer, R. L., Price, P. B. and Walker, R. M., 1965, Effects of temperature, pressure and ionisation on the formation and stability of fission tracks in minerals and glasses. *J. Geophys. Res.*, 70, 1497-1582.

Fleischer, R. L., Price, P. B. and Walker, R. M., 1969, Nuclear tracks in solids., *Sci. Am.*, 220, 30-39.

Foster, D. A. and Gleadow, A. J. W., 1992, The morphotectonic evolution of rift-margin mountains in central Kenya: constraints from apatite fission track thermochronology. *Earth & Planet. Sci. Letts.*, 113, 157-171.

Foulger, G. R., Jahn, C. H., Seeber, G., Einarsson, P., Julian, B. R. and Heki, K., 1992, Post-rift stress relaxation at the divergent plate boundary in Northeast Iceland., *Nature*, 358, 488-490.

Frölich, H., 1958, Theory of dielectrics. Dielectric constant and dielectric loss. Oxford, University Press.

Gabaldón-López, V., Olivé-Davo, A., Ramirez-Merino, J. I., Alvaro-López, M., Ramirez-del-Pozo, J. and Aguilar-Tomás, M., 1989, Bermeo-Bilbao (5 & 12)., Mapa Geologico d'España 1:200,000 scale, I. G. M. E., Madrid.

Gabilly, J., 1978, Guides Géologiques Régionaux; Poitou-Vendée-Charentes. Masson, Paris.

Galbraith, R. F., 1990, The radial plot: graphical assessment of spread in ages. *Nucl. Tracks.* 17, 207-214.

Galbraith, R. F., 1992, Statistical models for mixed ages., 7th International Workshop on Fission Track Thermochronology, Abstracts with Programs, Philadelphia, July, 1992.

Gallagher, K., Hawkesworth, C. J. and Mantovani, M. S. M., 1993, The denudation history of the onshore continental margin of SE Brazil inferred from fission track data. submitted to *J. Geophys. Res.*

Garcia-Mondéjar, J., 1989, Strike-slip subsidence of the Basque-Cantabrian Basin of northern Spain and its relationship to the Aptian-Albian opening of the Bay of Biscay., in: 'Extensional tectonics and stratigraphy of the North Atlantic margins.' *AAPG Mem.* 46, 395-409.

Garwin, L. J., 1985, Fission track dating and tectonics in the eastern Pyrenées., Unpublished PhD thesis, University of Cambridge.

Gibbons, W., 1990., Transcurrent ductile shear zones and the dispersal of the Avalon superterrane. in. D'Lemos, R. S., Strachan, R. A. and Topley, C. G. (Eds.) The Cadomian Orogeny. *Geol. Soc. Spec. Pub.*, 51, 407-423.

Gibbons, W. and Horak, J., 1990, Contrasting metamorphic terranes in Northwest Wales. in. D'Lemos, R. S., Strachan, R. A. and Topley, C. G. (Eds.) The Cadomian Orogeny. *Geol. Soc. Spec. Pub.*, 51, 315-329.

Gilchrist, A. R. and Summerfield, M. A., 1990, Differential denudation and flexural isostasy in formation of rifted margin upwarps., *Nature*, 346, 739-742.

Ginzburg, A., Whitmarsh, R. B., Roberts, D. G., Montadert, L., Camus, A. and Avedik, F., 1985, The deep seismic structure of the northern continental margin of the Bay of Biscay., *Ann. Geophys.*, 3, 499-510.

Gleadow, A. J. W. and Brooks, C. K., 1979, Fission track dating thermal histories and tectonics of igneous intrusions of East Greenland. *Conts. Min. Pet.*, 71, 45-60.

Gleadow, A. J. W. and Fitzgerald, P. G., 1987, Uplift history and structure of the Transantarctic Mountains: new evidence from fission track dating of basement apatites in the Dry Valleys area, Southern Victoria Land. *Earth & Planet. Sci. Letts.*, 82, 1-14.

Gleadow, A. J. W. and Lovering, J. F., 1977, Geometry factor for external detectors in fission track dating. *Nucl. Track Detects.*, 1, 99-106.

Gleadow, A. J. W., Duddy, I. R., Green, P. F. and Hegarty, K. A., 1986a, Fission track lengths in the apatite annealing zone and the interpretation of mixed ages. *Earth & Planet. Sci. Letts.*, 78, 245-254.

Gleadow, A. J. W., Duddy, I. R., Green, P. F. and Lovering J. F., 1986b, Confined fission track lengths in apatite: A diagnostic tool for thermal history analysis. *Conts. Min. Pet..*, 94, 405-415.

Gonzalez-Lodeiro, F., Hernandez-Urroz, J., Martinez-Catalan, J. R., Naval-Balbin, A., Ortega-Girones, E. and DePablo-Macia, J. G., 1984, Santiago de Compostela (7), Mapa Geologico d'España 1:200,000 scale, I. G. M. E., Madrid.

Graviou, P., Peaucat, J. J., Auvray, B. and Vidal, P., 1988, The Cadomian Orogeny in the Northern Armorican Massif: petrological and geochronological constraints on a geodynamical model. *Hercynica*, IV, 1, 1-13.

Green, P. F., 1985, Comparison of zeta calibration baselines for fission track dating of apatite, zircon and sphene. *Chem. Geol.*, 58, 1-22.

Green, P. F., 1986, On the thermo-tectonic evolution of northern England: Evidence from fission track analysis. *Geol. Mag.*, 123, 493-506.

Green, P. F., Duddy, I. R., Gleadow, A. J. W. and Tingate, P. R., 1985, Fission Track annealing in apatite: Track length measurements and the form of the Arrhenius plot. *Nucl. Tracks.* 10, 323-328.

Green, P. F., Duddy, I. R., Gleadow, A. J. W., Tingate, P. R. and Laslett, G. M., 1986, Thermal annealing of fission tracks in apatite; 1. A qualitative description. *Chem. Geol.*, 59, 237-253.

Green, P. F., Duddy, I. R. and Bray, R. J., 1993, Early Tertiary heating in Northwest England: fluids or burial (or both?). in: J. Parnell, A. H. Ruffell and N. R. Moles (Eds.) Geofluids '93 Extended Abstracts, 119-123.

Grimaud, S., Boillot, G., Collette, B. J., Mauffret, A., Miles, P. R. and Roberts, D. B., 1982, Western extension of the Iberian-European plate boundary during the Early Cenozoic (Pyrenean) convergence: a new model. *Mar. Geol.*, 45, 63-77.

Guerrot, C. and Peaucat, J. J., 1990, First evidence for Archaean rocks and early Proterozoic high grade metamorphism within the west European Hercynian belt: the Bay of Biscay granulites. *Geol. Soc. Aust. Abstracts*, 27, 42.

Guimerà, J., 1984, Palaeogene evolution of deformation in the northeastern Iberian Peninsula., *Geol. Mag.*, 121, 413-420.

Hancock, J. M., 1987, Chalk in the North Sea., in: JAPEC course notes 54.

Hancock, J. M. and Rawson, P. F., 1992, Cretaceous. in: Cope, J. C. W., Ingham, J. K. and Rawson, P. F. (Eds) Atlas of Palaeogeography and Lithofacies. Geological Society, London, Memoir 13., 131-139.

Hanmer, S. K., Le Corre, C. and Berthé, D., 1982, The role of Hercynian granites in the deformation and metamorphism of Brioverian and Palaeozoic rocks of Central Brittany. *J. Geol. Soc. Lond.*, 139, 85-93.

Hansen, K., 1988, Preliminary report of fission track studies in the Jameson Land Basin, East Greenland., *Rapp. Grønlands geol. Unders.*, 140, 85-89.

Harland, W. B., Armstrong, R. L., Cox, A. V., Craig, L. E., Smith, A. G., and Smith, D, G., 1989, A Geologic Time Scale. Cambridge University Press.

Hay, W. W., Barron, E. J., Sloan, J. L. and Southam, 1981, Continental drift and the global pattern of sedimentation. *Geol. Runds.*, 70, 302-315.

Hendriks, M., Jamieson, R. A., Willet, S. D. and Zentilli, M., 1993, Burial and exhumation of the Long Range Inlier and surroundings, Western Newfoundland: results of an apatite fission track study. submitted to *Can. J. Earth Sci.*

Hiscott, R. N., Wilson, R. C. L., Gradstein, F. M., Pujalte, V., García-Mondéjar, Boudreau, R. R. and Wishart, H. A., 1989, Comparative stratigraphy and subsidence history of Mesozoic rift basins of North Atlantic., in: 'Extensional tectonics and stratigraphy of the North Atlantic margins.' *AAPG Mem.* 46., 74, 60-67.

Holliday, D. W., 1993, Mesozoic cover over northern England: interpretation of apatite fission track data. *J. Geol. Soc. Lond.* 150, 657-660.

Hughes, J. M., Cameron, M. and Crowley, K. D., 1989, Structural variations in natural F, OH and Cl apatites. *Am. Min.*, 74, 870-876.

Hurford, A. J., 1977a, Fission track dates from two Galloway granites, Scotland., *Geol. Mag.*, 114, 299-304.

Hurford, A. J., 1977b, A preliminary fission track dating survey of Caledonian 'newer and last granites' from the highlands of Scotland. *Scot. J. Geol.*, 3, 271-284.

Hurford, A. J., 1990, Standardisation of fission track dating calibration: recommendation by the Fission Track Working Group of the I. U. G. S. Subcommission on Geochronology. *Chem. Geol.*, 80, 171 - 178.

Hurford, A. J. and Carter, A., 1991, The role of fission track dating in discrimination of provenance. in: Morton, A. C., Todd, S. P. and Haughton, P. D. W. (Eds.), Developments in sedimentary provenance studies. *Geol. Soc. Spec. Pub.* 57, 67-78.

Hurford, A. J. and Green, P. F., 1982, A users guide to fission track dating calibration. *Earth & Planet. Sci. Letts.*, 59, 343-354.

Hurford, A. J. and Green, P. F., 1983, The zeta age calibration of fission track dating. *Chem. Geol.*, 1, 285-317.

Hurford, A. J. and Hammerschmidt,., 1985, $^{40}Ar/^{39}Ar$ and K/Ar dating of the Bishop and Fish Canyon tuffs: calibration ages for fission track dating standards. *Chem. Geol.*, 58, 23-32.

Jaffey, A. H., Flynn, K. F., Glendenin, L. E., Bently, W. C. and Essling, A. M., 1971, Precision measurements of the half-lives and specific activities of ^{235}U and ^{238}U. *Phys. Rev.*, 4, 1889-1906.

Jäger, E., 1977, The evolution of the central and western European Continent. in La Chaîn Varisque de Europe Moyenne et occidentale. *Coll. int. Cent. natn. Rech. scient.*, 243, 227-239.

Jessop, A. M. and Majorowicz, J. A., 1993, Heat flow from the basement of the Western Canada Sedimentary Basin and its redistribution in the sedimentary succession. in: J. Parnell, A. H. Ruffell and N. R. Moles (Eds.), Geofluids '93 Extended Abstracts, 92-95.

Johnson, R. J. and van der Voo, R., 1990, Pre-folding magnetization reconfirmed for the late Ordovician-Early Silurian Dunn Point Volcanics, Nova Scotia. *Tectonophysics*, 178, 193-205.

Johnsson, M. J., 1986, Distribution of maximum burial temperatures across the Northern Appalachian Basin and implications for Carboniferous sedimentation patterns., *Geology*, 14, 384-387.

Jones, D. L., Howell, D. G., Coney, P. J. and Monger, J. W. H., 1983., Recognition, character and analysis of tectonostratigraphic terranes in western North America. in: Hashimoto, M. & Uyeda, S. (Eds.) Accretion tectonics in the circum-Pacific regions, *Terra Scientific, Tokyo*, 21-35.

Jones, K. A. and Brown, M., 1990, High-temperature 'clockwise' P-t paths and melting in the development of regional migmatites, an example from southern Brittany, France. *J. Met. Geol.*, 8, 551-578.

Jonin, M. and Vidal, P., 1975, Etude geochronologique des granitoids de Mancellia, Massif Armoricain, France. *Can. J. Earth Sci.*, 12, 920-927.

Julivert, M., 1971, L'evolution structurale de l'arc asturien. In. Histoire Structurale de Golfe de Gascoigne, *Pub. Institut Français Pét., Collections Coll. Sém.*, 22, I.2.

Julivert, M., Fontboté, J. M., Ribeiro, A. and Condé, L., 1974, Mapa tectonico de la Península Ibérica y Baleares, 1 : 1 000 000 scale. I.G.M.E., Madrid.

Julivert, M., Martinez, F. J. and Ribeiro, A., 1980, The Iberian segment of the European Hercynian foldbelt., *Mém. BRGM* 108, 132-158.

Julivert, M., Truyols, J. and Garcia-Alcalde, J., 1981, Mieres (10), Mapa Geologico d'España 1:200,000 scale, I. G. M. E., Madrid.

Kamp, P. J. J., Green, P. F. G. and White, S. T., 1989, Fission track analysis reveals character of collision tectonics in New Zealand. *Tectonics*, 8, 169-195.

Kay, M. I., Young, R. A. and Posner, A. S., 1964, Crystal structure of hydroxylapatite. *Nature*, 204, 1050-1052.

Kearey, P. and Vine, F. J., 1990., Global tectonics. Blackwell Scientific Publications. 302 pp.

Kelley, S. H. and Duncan, I. J., 1986, Late Cretaceous to middle Tertiary tectonic history of the northern Rio Grande Rift, New Mexico., *J. Geophys. Res.*, 91, 6246-6262.

Kieffer, S. W. and Navrotsky, A., 1985, Chapter 1, Scientific perspective. in: Microscopic to Macroscopic, *Min. Soc. Am. Reviews in mineralogy*, 14, 1-9.

Kislovsky, K. D. and Knubovets, R. G., 1968, Sensitivity of infra-red spectra of single apatite crystals to isomorphism., *Doklady Akad. Sci. USSR Earth Sci. Sect.*, 179, 138-141. (Transl. 79, 1432-1435.)

Knutsen, C. Peacor, D. R. and Kelly, W. C., 1985, Luminescence, colour and fission track zoning in apatite crystals of the Panasqueira tin-tungsten deposit, Beira-Baixa, Portugal. ?????

Kohn, B. P. and Eyal, M., 1981, History of the crystalline basement of Sinai and its relation to opening of the Red Sea as revealed by fission track dating of apatites. *Earth & Planet. Sci. Letts.*, 52, 129-141.

Kossmat, F., 1927, Gliederung des variszichen Gebirgsbaues. *Abh. sächs. geol. Landesampts*, 1, 39 pp.

Kowallis, B. J., Christiansen, E. H., Crowley, K. D., Naeser, C. W., Miller, D. S. and Deino, A. L., 1992, Possible secondary age standard from altered volcanic ash beds in the middle Jurassic Carmel Formation , southwest Utah. 7th International Workshop on Fission Track Thermochronology Abstracts, 93.

Kuijper, R. P., 1979, U-Pb systematics and the petrogenetic evolution of infracrustal rocks in the Palaeozoic basement of western Galicia (NW Spain). Verh. Nr. 5, ZWO laboratorium voor Isotopen-Geology, Amsterdam, 1-110.

Lakatos, S. and Miller, D. S., 1983, Fission track analysis of apatite and zircon defines a burial of 4 to 7 km for lowermost Upper Devonian, Catskill Mountains, New York. *Geology*, 11, 103-104.

Lameyre J. and Autran, A., 1980, Les granitoïdes de France., in: "Evolutions geologique de la France.", *Mém. BRGM*, 107, 52-97.

Landes, K. K., 1938, Origin of the Quebec phlogopite-apatite deposits., *Am. Min.* 23, 359-390.

Larsen, E. S. Fletcher, M. H. and Cisney, E. A., 1952, Strontian apatite. *Am. Min.* 37, 656-658.

Laslett, G. M., Green, P. F., Duddy, I. R. and Gleadow, A. J. W., 1987, Thermal annealing of fission tracks in apatite; 2. A quantitative analysis. *Chem. Geol.*, 65, 1-13.

Latil, C., 1975, Contribution a l'étude des substitutions F^-, Cl^-, OH^- dans l'apatite. Application aux apatites des Granites Caledoniens d'Ecosse. Unpublished PhD thesis, Université de Pierre et Marie Curie, Paris.

Latil C. and Maury, R., 1977., Contribution a l'étude des échanges d'ion OH-, Cl- et F- et leur fixation dans les apatites hydrothermales. *Bull. Soc. Français Min. Crist.*, 100, 246.

Laughton. A. S. and Berggren, W. A., 1971, Deep sea drilling in the Bay of Biscay, symposium on the structural history of the Bay of Biscay. In. Histoire Structurale de Golfe de Gascoigne, *Pub. Institut Français Pét., Collections Coll. Sém.*, 22, VI.1-1 - 4.

Le Pichon, X., Sibuet, J. C. and Francheteau, J., 1977, The fit of the continents around the North Atlantic Ocean. *Tectonophysics*, 38, 169-209.

Leeder, M. R., 1982, Upper Palaeozoic basins of the British Isles - Caledonian inheritance versus Hercynian plate margin processes., *J. Geol. Soc. Lond.*, 139, 479-491.

Lees, G. J., 1990, The geochemical character of late Cadomian extensional magmatism in Jersey, Channel Islands. in. D'Lemos, R. S., Strachan, R. A. and Topley, C. G. (Eds.) The Cadomian Orogeny. *Geol. Soc. Spec. Pub.*, 51, 273-291.

Lefort, J-P., 1979, Iberian-Armorican arc and Hercynian orogeny in western Europe. *Geology*, 7, 384-388.

Lefort, J-P. and Ségoufin, J.,1978, Etude géologique de quelques structures magnétiques reconnues dans le socle péri-armoricain. *Bull. Soc. Géol. France.* 7, (20), 185-192.

Lepvrier, C. and Martínez-García, E., 1990, Fault development and stress evolution of the post-Hercynian Asturian Basin (Asturias and Cantabria, northwestern Spain). *Tectonophysics*, 184, 345-356.

Leutwein, F., Chauris, L., Sonet, J and Zimmerman, J. L., 1969, Etudes géochronologiques et géotectoniques dans le Nord-Finistère (Massif Armoricain). *Sciences de la Terre*, 4, 329-358.

Leutwein, F., Power, G., Roach, R. A. and Sonet, J., 1973, Quelques résultats obtenus des roches d'age précambrien du Cotentin. *C. R. Acad. Sci. Paris.*, 2121-2124.

Lewis, C. L. E., Green, P. F. G., Carter, A. and Hurford, A. J., 1992a, Elevated K/T palaeotemperatures throughout Northwest England: three kilometres of Tertiary erosion? *Earth & Planet. Sci. Letts.*, 112, 131-145.

Lewis, C. L. E., Carter, A. and Hurford, A. J., 1992b, Low temperature effects of the Skye Tertiary intrusion on Mesozoic sediments in the Sea of Hebrides Basin. in: J. Parnell (ed.) Basins on he Atlantic Seaboard: petroleum geology, sedimentology and basin evolution. *Geol. Soc. Spec. Pub.*, 62, 175-188.

Lister, G. S., Etheridge, M. A. and Symonds, P. A., 1991, Detachment models for formation of passive continental margins. *Tectonics*, 10, 1038-1064.

Mackie, P. E., Elliot, J. C. and Young, R. A., 1972, Monoclinic structure of synthetic $Ca_5(PO_4)_3$ Cl, chlorapatite., *Acta Cryst.*, B28, 1840-1848.

Maksaev, V., Gardeweg, M., Ramirez, C. F. and Zentilli, M., 1988, Fission track dating of El Laco and Incahuasi magnetite bodies in the high plateau of the Antofagasta region., V Chilean Geological Congress, vol.1, B1-B23.

Malod, J. A. and Mauffret, A., 1990, Iberian Plate motions during the Mesozoic., *Tectonophysics*, 184, 261-278.

Mareschal, J. C., 1983, Mechanisms of uplift preceding rifting., *Tectonophysics*, 94, 51-66.

Marshak, S., 1988, Kinematics of orocline and arc formation in thin skinned orogens., *Tectonics*, 7, 73-86.

Martinez-García, E., 1993, Late Hercynian evolution of the North Iberian Margin., in: BRGM Document 219., Abstracts, Late Orogenic Extension in Mountain Belts; March 1993, Montpellier. 135.

Masson, D. G. and Miles, P. R., 1984, Mesozoic sea-floor spreading between Iberia, Europe and North America. *Mar. Geol.*, 56, 279-287.

Masson, D. G. and Parson, L. M., 1983, Eocene deformation on the continental margin SW of the British Isles., *J. Geol. Soc. Lond.*, 140, 913-920.

Matte, P., 1986, La châine varisque parmi les châines palaéozoïque péri-atlantiques, modèle d'évolution et position des grands blocs continetaux au Permo-Carbonifère. *Bull. Soc. Géol. France.*, 8, 9-24.

Matte, P., 1991, Accretionary history and crustal evolution of the Variscan belt in Western Europe. *Tectonophysics*, 196, 309-337.

Matte, P. & Burg, J. P., 1981, Sutures, thrusts and nappes in the Variscan Arc of western Europe: plate tectonic implications., in: Thrust and nappe tectonics, *Geol. Soc. Spec. Pub.* 9, 353-358.

Matte, P. and Ribeiro, A., 1975, Forme et orientation de l' ellipsoïde de déformation dans la virgation hercynienne de Galice. Relations avec le plissement et hypothèses sur la genèse de l' arc ibéro-armoricain. *C. R. Acad. Sci. Paris.*, 280D, 2825-2828.

Matthews, S. C., 1984, Northern margins of the Variscides in the North Atlantic region: comments on the tectonic context of the problem. in Variscan Tectonics of the North Atlantic region, Ed. Hutton, D. H. W. and Sanderson, D. J. *Geol. Soc. Spec. Pub.* 14, , 71-85.

McCulloch, A., 1993, *Mar. Pet. Geol.*, in press.

McDougall, I. and Wellmam, P., 1976, Potassium-argon dates on some Cainozoic rocks from northeastern New South Wales. *J. Geol. Soc. Aust.*, 14, 225-234.

McDowell, F. W. and Keizer, R. P., 1977, Timing of mid-Tertiary volcanism in the Sierra Madre Occidental between Durango City and Mazatlan, Mexico. *Geol. Soc. Am. Bull.*, 88, 1479-1487.

McKenzie, D. P., 1978, Some remarks on the development of sedimentary basins. *Earth & Planet. Sci. Letts.*, 40, 25-32.

McKerrow, W. S. and Scotese, C. R. (Eds), 1990, Palaeozoic Palaeogeography and Biogeography. Geological Society, London, Memoir. 12, 435 pp.

McMillan, P. F., 1985, Chapter 2, Vibrational spectroscopy in the mineral sciences. in: Microscopic to Macroscopic, *Min. Soc. Am. Reviews in mineralogy*, 14, 9-63.

McMillan, P. F. and Hofmeister, A. M., 1988, Chapter 4, Infrared and Raman spectroscopy. in: Spectroscopic Methods in Mineralogy, *Min. Soc. Am. Reviews in mineralogy*, 18, 99-159.

McWhae, J. R. H., Playford, P. E., Lindner, A. W., Glenister, B. F. and Balme, B. E., 1958, The Stratigraphy of Western Australia. Melbourne University Press, 161 pp.

Mégnien, C., 1980a, Tectonogenèse du Bassin de Paris: étapes de l'évolution du bassin. *Bull. Soc. Géol. France.*, 7, 669-680.

Mégnien, C. (Ed), 1980b, Synthèse géologique du bassin de Paris. *Mém. BRGM* 102, vol. 2, Atlas.

Mehmel, M., 1930, Über die Struktur des Apatits. *Zeits. Kristal.*, 75, 323-331.

Metrich, N. and Rutherford, M. J., 1992, Experimental study of chlorine behaviour in hydrous silicic melts., *Geochim. Cosmochim. Acta.*, 56, 607-616.

Miller, D. S. and Duddy, I. R., 1989, Early Cretaceous uplift and erosion of the northern Appalachian Basin, New York, based on apatite fission track analysis. *Earth & Planet. Sci. Letts.*, 93, 35-49.

Miller, D. S. and Lakatos, S., 1983, Uplift rate of the Adirondack Anorthosite measured by fission track analysis of apatite., *Geology*, 11, 284-286.

Milliman, J. D. and Meade, R. H., 1983, World-wide delivery of river sediment to the oceans. *J. Geol.*, 91, 1-21.

Molnar, P. and England, P. C., 1990, Late Cenozoic uplift of mountain ranges and global climate change: chicken or egg? *Nature*, 346, 29-34.

Molnar, P. and Tapponier, P., 1975, Cenozoic tectonics of Asia; effects of a continental collision. *Science*, 189, 419-426.

Montadert, L. and Roberts, D, G,. 1976, Glomar Challenger sails on Leg 48. *Geotimes*, December, 19-23.

Montadert, L., Damotte, B., Delteil, J. R., Valéry, P. and Winnock, E., 1971, Structure géologique de la marge continentale septentrionale du Golfe de Gascogne (Bretagne et entrées de la Manche). In. Histoire Structurale de Golfe de Gascoigne, *Pub. Inst. Français Pét., Collections Coll. Sém.*, 22, III.2-1 - 22.

Montadert, L., Roberts, D. G., Auffret, E. A., Bock, W., DuPeuble, P. A., Hailwood, E. A., Harrison, W., Kagami, H., Lumsden, D. N., Muller, C. Schnikter, D., Thompson, R. W., Thompson, T. L. and Timofeev, P. P., 1977, Rifting and subsidence on passive continental margins in the North East Atlantic., *Nature*, 268, 305-309.

Montadert, L, de Charpal, O., Roberts, D., Guennoc, P. and Sibuet, J. C., 1979, Northeast Atlantic passive continental margins: rifting and subsidence processes. in: M. Talwani, W. Hay and W. B. F. Ryan (Eds.) Deep drilling results in the Atlantic Ocean; Continental margin and palaeoenvironment, Maurice Ewing Series, 3, 154-186.

Moore, M. E., Gleadow, A. J. W. and Lovering, J. F., 1986, Thermal evolution of rifted continental margins: new evidence from fission tracks in basement apatites from southeastern Australia., *Earth & Planet. Sci. Letts.*, 78, 255-270.

Morton, R., 1960, The Ødegården phosphate deposit. in Mineral occurrences in southern Norway; guide to excursions A15 and C12., H. Neuman (ed.), International Geological Congress XXI, Norden.

Murphy, J. B., Keppie, J. D., Dostal, J. and Hynes, A. J., 1990., The geochemistry and petrology of the late Precambrian Georgeville Group: a volcanic arc-rift succession in the Avalon terrane of Nova Scotia. in. D'Lemos, R. S., Strachan, R. A. and Topley, C. G. (Eds.) The Cadomian Orogeny. *Geol. Soc. Spec. Pub.*, 51, 383-395.

Murray, J. W., 1992, Palaeogene and Neogene. in: Cope, J. C. W., Ingham, J. K. and Rawson, P. F. (Eds) Atlas of Palaeogeography and Lithofacies. Geological Society, London, Memoir 13., 141-148.

Naeser, C. W., Izett, G. A. and Obradovich, J. D., 1980, Fission track and K/Ar ages of natural glasses. *USGS Bull.*, 1489, 31pp.

Nance, R. D., 1990., Late Precambrian-Early Palaeozoic evolution of part of the Avalon Terrane in southern New Brunswick, Canada. in. D'Lemos, R. S., Strachan, R. A. and Topley, C. G. (eds.) The Cadomian Orogeny. *Geol. Soc. Spec. Pub.*, 51, 363-383.

Naray-Szabo, S., 1930, "The structure of apatite(CaF)$Ca_4(PO_4)_3$." *Zeits. Kristall.*, 75, 387-398.

Nijman, W. and Savage, R. F., 1989, Persistent basement wrenching as controlling mechanism of Variscan thin-skinned thrusting and sedimentation, Cantabrian Mountains, Spain., *Tectonophysics*, 169, 281-302.

Nijman, W. and Savage, R. F., 1991, Persistent basement wrenching as controlling mechanism of Variscan thin-skinned thrusting and sedimentation, Cantabrian Mountains, Spain: reply., *Tectonophysics*, 194, 177-182.

Omar, G. I., Kohn, B. P., Lutz, T. M., Faul, H., 1987, The cooling history of Silurian to Cretaceous alkaline ring complexes, south eastern desert, Egypt as revealed by fission track analysis. *Earth & Planet. Sci. Letts.*, 83, 94-108.

Parnell, J., Anderson, T. B. and Ruffell, A. H., 1992, Basement influence on the geometry of Permo-Triassic basins in the north-west British Isles. Permian and Triassic rifting in NW Europe, Abstracts, 21-22 October 1992, The Geological Society of London.

Paul, T. A. and Fitzgerald, P. G., 1992, Transmission electron microscopic investigation of fission tracks in fluorapatite., *Am. Min.*, 77, 336-344.

Pauley, J., 1990, Sedimentology, structural evolution and tectonic setting of the Late Precambrian Longmyndian Supergroup of the Welsh Borderland, UK. in. D'Lemos, R. S., Strachan, R. A. and Topley, C. G. (Eds.) The Cadomian Orogeny. *Geol. Soc. Spec. Pub.*, 51, 341-353.

Peaucat, J. J., 1986, Behaviour of Rb-Sr whole rock and U-Pb zircon systems during partial melting as shown in migmatitic gneisses from the St. Malo Massif, NE Brittany, France. *J. Geol. Soc. Lond.*, 143, 875-885.

Pelhâte, A. and Mirouse, R., 1980, Formations sédimentares synorogénique de France: quelques exemples relatifs au cycle varisque. in: "Evolutions geologique de la France.", *Mém. BRGM*, 107, 194-200.

Pello, J., Julivert, M. and Marcos, A., 1981, Aviles (2), Mapa Geologico d'España 1:200,000 scale, I. G. M. E., Madrid.

Perez-Estaún, A., Bastida, F., Alonso, J. L., Marquínez, J., Aller, J., Alvarez-Marrón, J., Marcos, A. and Pulgar, J. A., 1988, A thin skinned tectonics model for an arcuate fold and thrust belt: The Cantabrian Zone (Variscan Ibero-Armorican arc.). *Tectonics*, 7, 517-537.

Perez-Estaún, A., Martinez-Catalán, J. R. and Bastida, F., 1991, Crustal thickening and deformation in the footwall to the suture of the Variscan belt of northwest Spain. *Tectonophysics*, 191, 243-253.

Pigram, C. J. and Davies, H. L., 1987., Terranes and the accretion history of the New Guinea orogen. *B. M. R. J. Austral. geol. geophys.* 10, 193-211.

Pitman, W. C. and Talwani, M., 1972, Seafloor spreading in the North Atlantic., *Bull. Geol. Soc. Am.*, 83, 619-646.

Playford, P. E., Cope, R. N., Cockbain, A. E., Low, G. H. and Lowry, D. C., 1975, The geology of Western Australia. Geological Survey of Western Australia, Memoir 2, 223-432.

Power, G. M., Brewer, T. S. Gibbons, W. and Brown, M., 1990, Later Precambrian foliated plutonic complexes of the Channel Islands and La Hague: Early Cadomian plutonism. in. D'Lemos, R. S., Strachan, R. A. and Topley, C. G. (Eds.) The Cadomian Orogeny. *Geol. Soc. Spec. Pub.*, 51, 215-229.

Prener, J. S., 1967, The growth and crystallographic properties of calcium fluor- and chlorapatite crystals., *J. Electrochem. Soc: Solid State Science*, 114, 77-83.

Price, P. B. and Walker, R. M., 1963, Fossil tracks of charged particles in mica and the age of minerals. J. Geophys. Res.., 68, 4847-4862.

Priem, H. N. A., Boelrijk, N. A. I. M., Verschure, R. H., Hebeda, E. H. and Verdurmen, E. A. T., 1970, Dating events of acid plutonism through the Palaeozoic of the western Iberian peninsula., *Ecl. Geol. Helvet.*, 63, 255-274.

Quesada, C., 1990, Precambrian successions in SW Iberia: their relationship to 'Cadomian' orogenic events. in. D'Lemos, R. S., Strachan, R. A. and Topley, C. G. (Eds.) The Cadomian Orogeny. *Geol. Soc. Spec. Pub.*, 51, 353-363.

Quesada, C., 1991, Geological constraints on the Palaeozoic tectonic evolution of tectonostratigraphic terranes in the Iberian Massif. *Tectonophysics*, 185, 225-245.

Rast, N., 1988, Variscan-Alleghanian Orogen., in: W. Manspeizer (ed.), Triassic-Jurassic rifting: continental breakup and the origin of the Atlantic ocean passive margins. Part A., Developments in Geotectonics, 22.

Raven, J. G. M. and Van der Pluijm, B. A., 1986, Metamorphic fluids and transtension in the Cantabrian Mountains of northern Spain: an application of the conodont colour alteration index. *J. Geol. Soc. Lond.*, 123, 673-681.

Ravenhurst, C., Donelick, R, Zentilli, M., Reynolds, P. and Beaumont, C., 1990, A fission track pilot study of the thermal effects of rifting on the onshore Nova Scotian margin, Canada., *Nucl. Tracks.*, 17, 373-378.

Ribeiro, A., Pereira, E. and Iglesias, M., 1991a, Flake tectonics in the northwest Iberian Variscides. *Tectonophysics*, (Abstract).

Ribeiro, A., Quesada, C. and Dallmeyer, R. D., 1991b, Tectonostratigraphic terranes and the geodynamic evolution of the Iberian foldbelt. *Tectonophysics*, (Abstract).

Ries, A. C., 1978, The opening of the Bay of Biscay - a review., *Ear. Sci. Rev.*, 14, 35-63.

Ries, A. C., 1979, Variscan metamorphism and K-Ar dates in the Variscan fold belt of S Brittany and NW Spain. *J. Geol. Soc. Lond.*, 136, 89-103.

Roach, R. A., Lees, G. J. and Shufflebotham, M. M., 1990, Brioverian volcanism and Cadomian tectonics, Baie de St Brieuc, Brittany: stages in the evolution of a late Precambrian basin. in. D'Lemos, R. S., Strachan, R. A. and Topley, C. G. (Eds.) The Cadomian Orogeny. *Geol. Soc. Spec. Pub.*, 51, 41-67.

Roden, M. K., 1991, Apatite fission track thermochronology of the Southern Appalachian Basin: Maryland, West Virginia and Virginia., *J. Geol.*, 99, 41-53.

Roden, M. K. and Miller, D. S., 1989, Apatite fission track thermochronology of the Pennsylvania Appalachian Basin. *Geomorphology*, 2, 39-51.

Rohrman, M., van der Beek, P. A. and Andriessen, P. A. M., 1992, The Mesozoic to Cenozoic thermal history of South Norway as revealed by apatite fission track analysis (AFTA) and thermal modelling studies.

Rosenfeld, U., 1978, Beitrag zur Paläogeographie des Mesozoikums in Westphalen. *N. Jb. Geol. Paläont. Abh.*, 156, 132-155.

Ross, S. D., 1974, Phosphates and other oxy-anions of group V. in: Farmer, V.C. (Ed.), The infrared spectra of minerals; Mineralogical Society Monagraph 4 .

Russell, J. D., 1974, Instrumentation and techniques. in: Farmer, V.C. (Ed.), The infrared spectra of minerals; Mineralogical Society Monagraph 4 .

Rutherford, E. H. and Soddy, F., 1902, The cause and nature of radioactivity., *Phil. Mag.*, ser. 6, 4, 370-396 & 569-585.

Ryan, W. B. F. and Hsü, K. J., 1971, Deep sea drilling on Gorringe Bank and it's relevance to the Bay of Biscay problem. In. Histoire Structurale de Golfe de Gascoigne, *Pub. Institut Français Pét., Collections Coll. Sém.*, 22.

Schott, J. J. and Peres, A., 1987, Palaeomagnetism of Permo-Triassic Redbeds from the Asturias and Cantabric Chain (Northern Spain): evidence for strong lower Tertiary remagnetizations. *Tectonophysics*, 140, 179-191.

Sclater, J. G., Jaupart, C. and Galson, D., 1980, The heat flow through oceanic and continental crust and the heat loss of the earth., *Revs. Geophys. Space Phys.*, 18, 269-311.

Seiber, K. G., 1986, Structure of the Lower Cretaceous sediments - Fish Creek area, Victoria, and the compositional variations in apatites. Unpublished Honours Thesis, University of Melbourne.

Selby, M. J., 1982, Hillslope materials and processes, Oxford University Press, p. 237.

Shackleton, R. M., Ries, A. C. and Coward, M. P., 1982, An interpretation of the Variscan structures in SW England., *J. Geol. Soc. Lond.*, 139, 533-541.

Shufflebotham, M. M. and Roach, R. A., 1985, A review of the geological relationships between the Brioverian Supergroup and Palaeozoic red beds around the Baie de St Brieuc, Brittany, in the light of illite crystallinity studies. *Proc. Ussher Soc.*, 6, 196-204.

Sibuet, J-C., 1973, South Armorican Shear Zone and continental fit before the opening of the Bay of Biscay. *Earth & Planet. Sci. Letts.*, 18, 153-157.

Sibuet, J. C., 1989, Palaeoconstraints during rifting of the Northeast Atlantic Passive Margins., *J. Geophys. Res.*, 94, 7265-7277.

Sibuet, J. C., 1992, New constraints on the formation of the non-volcanic continental Galicia-Flemish Cap conjugate margins., *J. Geol. Soc. Lond.*, 149, 829-840.

Sibuet, J-C. and Collette, B. J., 1991, Triple Junctions of Bay of Biscay and North Atlantic: new constraints on the kinematic evolution. *Geology*, 19, 522-525.

Skogseid, J. and Edholm, O., 1988, Early Cainozoic evolution of the Norwegian volcanic passive margin and the formation of marginal highs. in: Morton A. C. and Parson L. M. (Eds.), Early Tertiary Volcanism and the Opening of the NE Atlantic, *Geol. Soc. Spec. Pub.*, 39, 49-56

Smith, A. G., Hurley, A. M. and Briden, J. C., 1981, Phanerozoic paleocontinental world maps., Cambridge Earth Science Series, Cambridge University Press. 102 pp.

Smith, D. B., Brunstrom, R. G. W., Manning, P. I., Simpson, S. and Shotton, F. W., 1974, A correlation of Permian rocks in the British Isles., *Geol. Soc. Spec. Rep.* 5, 45 pp.

Soper, N. J., Webb, B. C. and Woodcock, N. H., 1987, Late Caledonian (Acadian) transpression in north-west England: timing, geometry and geotectonic significance. *Proc. Yorks. Geol. Soc.*, 46, 175-192.

Spadavecchia, A. and Hahn, B., 1967, Die Rotation-Skanner und einige Anwendungen. *Helv. Phys. Acta.*, 40, 1063-1079.

Srivastava, S. P. and Verhoef, J., 1992, Evolution of Mesozoic sedimentary basins around the North Central Atlantic: a preliminary plate kinematic solution. in: J. Parnell (ed) Basins on the Atlantic Seaboard: Petroleum Geology, Sedimentology and Basin Evolution. *Geol. Soc. Spec. Pub.* 62, 397-420.

Srivastava, S. P., Roest, W. R., Kovacs, L. C., Oakley, G., Levesque, S., Verhoef, J. and Macnab, R., 1990a, Motion of Iberia since the late Jurassic: results from detailed aeromagnetic measurements in the Newfoundland basin. *Tectonophysics*, 184, 229-260.

Srivastava, S. P., Schouten, H., Roest, W. R., Klitgourd, K. D., Kovacs, L. C., Verhoef, J. and Macnab, R., 1990b, Iberian plate kinematics: a jumping plate boundary between Eurasia and Africa. *Nature*, 344, 756-759.

Steckler, M. S., Omar, G. I., Karner, G. D. and Kohn, B. P., 1993, Pattern of hydrothermal circulation within the Newark Basin from fission track analysis. *Geology.*, 21, 735-738.

Steiger, R. H. and Jäger, E., 1977. Subcommission on Geochronology: convention on the use of decay constants in geo- and cosmochronology. *Earth & Planet. Sci. Letts.*, 30, 50-56.

Steven, T. A., Mehnert, H. H. and Obradovich, J. D., 1967, Age of volcanic activity in the San Juan Mountains, Colorado. *U S G S Prof. Pap.*, 575-D, D47-D55.

Stormer, J. C. and Carmichael, I. S. E., 1971, Fluorine - hydroxyl exchange in apatite and biotite: A potential geothermometer. *Conts. Min. Pet.*, 31, 127-131.

Strachan, R. A. and Roach, R. A., 1990, Tectonic evolution of the Cadomian belt in North Brittany. in. D'Lemos, R. S., Strachan, R. A. and Topley, C. G. (Eds.) The Cadomian Orogeny. *Geol. Soc. Spec. Pub.*, 51, 133-150.

Stutman, J. M., Termine, J. D. and Posner, A. S., 1965, Vibrational spectra and structure of the phosphate ion in some calcium phosphates. Transactions of the New York Academy of *Science.* 27, 669-675.

Suarez, O., Ruiz, F., Galan, J. and Vargas, I., 1978, Edades Rb-Sr de granitoides del occidente de Asturias (NW de España). *Trab. Geol.*, 10, 437-442.

Sullivan, K. D., 1983, The Newfoundland Basin: ocean-continent boundary and seafloor spreading history., *Earth & Planet. Sci. Letts.*, 62, 321-339.

Summer, N. S. and Verosub, K. L., 1989, a low temperature hydrothermal maturation mechanism for sedimentary basins associated with volcanic rocks. in. P.A. Price (ed.), Origin and evolution of sedimentary basins and their economic potential. *Am. Geophys. Union Geophys. Monograph* 48, 129-136.

Summerfield, M. A., 1991, Global Geomorphology; an introduction to the study of landforms. Longman, UK. 537 pp.

Tapponier, P. and Molnar, P., 1976, Slip line field theory and continental tectonics., *Nature*, 264, 319-324.

Tapponier, P. and Molnar, P., 1977, Rigid plastic indentation: the origin of syntaxis in the Himalayan belt. in Himalaya. *Sciences de la Terre.*, 268, 431-432.

Thommeret, M., Boillot, G. and Sibuet, J. C., 1988, Structural map of the Galicia Margin., in: Boillot, G., Winterer, E. L., Meyer, A. W. (Eds.), Proc. ODP, Scientific Results: College Station, Texas, 103, 31-36.

Tingate, P. R. 1990, Apatite fission track studies from the Amadeus Basin, Central Australia., Unpublished PhD thesis, University of Melbourne.

Treloar, P. J. and Strachan R. A., 1990, Cadomian strike-slip tectonics in NE Brittany. in. D'Lemos, R. S., Strachan, R. A. and Topley, C. G. (Eds.) The Cadomian Orogeny. *Geol. Soc. Spec. Pub.*, 51, 151-168.

Tuddenham, W. M. and Lyon, R.J.P., 1960, Infrared techniques in the identification and measurement of minerals. *Anal. Chem.*, 32, 1630-1634

Vail, P. R., Mitchum, R. M. and Thompson, S., 1977, Seismic stratigraphy and global changes of sea level: Part 4. global cycles of relative changes of sea level. *Mem. Ass. Pet. Geol.*, 26, 83-97.

Van der Voo, R., 1967, The rotation of Spain: Palaeomagnetic evidence from the Spanish Meseta. *Palaegeogr., Palaeoclimatol., Palaeoecol.*, 3, 393-416.

Van der Voo, R., 1969, Palaeomagnetic evidence for the rotation of the Iberian Peninsula. *Tectonophysics*, 7, 5-56.

Van Dongen, P. G., 1967, The rotation of Spain: Palaeomagnetic evidence from the eastern Pyrenées. *Palaegeogr., Palaeoclimatol., Palaeoecol.*, 3, 417-432.

van Calsteren, P. W. C., 1977, A mantle plume model interpretation for the Palaeozoic geology of Galicia with emphasis on the Cabo Ortegal area (NW Spain). *Proc. Kon. Ned. Akad. Wetensch.*, series B, 80, 156-168.

van den Haute, P., 1977, Apatite fission track dating of Precambrian intrusive rocks from the southern Rogaland (south-western-Norway). *Bull. Soc. Belge. Geol.*, 86, 97-110.

Vauchez, A., Maillet, D. and Sougy, J., 1987, Strain and deformation mechanisms in the Variscan nappes of Vendée, South Brittany, France. *J. Struct. Geol.*, 9, 31-40.

Verhoef, J. and Srivastava, S. P., 1989, Correlation of sedimentary basins across the North Atlantic as obtained from gravity and magnetic data, and its relation to the early evolution

of the North Atlantic., in: 'Extensional tectonics and stratigraphy of the North Atlantic margins.' *AAPG Mem.* 46, 131-147.

Vidal, P., 1973, Premieres données géochronologique sur les granites Hercyniens du sud du Massif Armoricain. *Bull. Soc. Géol. France*, 15, 239-245.

Vidal, P., 1980, L'évolution polyorogénique du Massif Armoricain: rapport de la geochronology et de la strontium. *Mém. Soc. Géol. Mineral. Bret.* 21.

Vidal, P., Deutsch, S., Martineau, F. and Cogné, J., 1974, Nouvelles données radiometriques en Baie de St Brieuc. Le probleme d'un socle ante-Cadomian nord-Armoricain., *C. R. Acad. Sci. Paris.*, 279, 631-634

Wagner, G. A., 1972, Spaltspurenalter von Mineralen und natürlichen Gläsern: eine Ubersicht., *Fortschr. Min.*, 49, 114-145.

Wagner, G. A. and van den Haute, P., 1992, Fission-track dating., Kluwer Academic Press. 285 pp.

Warrington, G. and Ivimey-Cook, H. C., 1992, Triassic. in: Cope, J. C. W., Ingham, J. K. and Rawson, P. F. (Eds) Atlas of Palaeogeography and Lithofacies. Geological Society, London, Memoir 13., 97-106.

Watts, M. J. and Williams, G. D., 1979, Fault rocks as indicators of progressive shear deformation in the Guingamp region, Brittany. *J. Struct. Geol.*, 1, 323-332.

Weber, K., 1984, Variscan events: early Palaeozoic continental rift metamorphism and late Palaeozoic crustal shortening. *Geol. Soc. Spec. Pub.* 14, Variscan Tectonics of the North Atlantic region, Ed. Hutton, D. H. W. and Sanderson, D. J., 3-22

Webster, J. D., 1992, fluid-melt interactions involving Cl-rich granites: experimental study from 2 to 8 kbar. *Geochim. Cosmochim. Acta.*, 56, 659-678.

Webster, J. D. and Holloway, J. R., 1988, Experimental constraints on the partitioning of Cl between Topaz-rhyolite melt and H_2O and $H_2O + CO_2$ fluids: new implications for granitic differentiation and ore deposition., *Geochim. Cosmochim. Acta*, 52, 2091-2105.

Weissel, J. K. and Karner, G. D., 1989, Flexural uplift of rift flanks due to mechanical unloading of the lithosphere during extension., *J. Geophys. Res.*, 94, 13,919-13,950.

Went, D. and Andrews, M., 1990, Post-Cadomian erosion, deposition and basin development in the Channel Islands and Northern Brittany., in. D'Lemos, R. S., Strachan, R. A. and Topley, C. G. (Eds.) The Cadomian Orogeny. *Geol. Soc. Spec. Pub.*, 51, 293-304.

Wernicke, B., 1985, Uniform sense normal simple shear of the continental lithosphere. *Can. J. Earth Sci.*, 22, 108-125.

White, R. S., 1988, A hot-spot model for Early Tertiary volcanism in the N Atlantic. in: Morton, A. C. and Parson L. M. (Eds.), Early Tertiary Volcanism and the Opening of the NE Atlantic, *Geol. Soc. Spec. Pub.*, 39, 3-15.

White, R. S. and McKenzie, D. P., 1989, Magmatism at rift zones: the generation of volcanic continental margins and flood basalts., *J. Geophys. Res.*, 94, 7685-7730.

White, R. S., Spence, G. D, Fowler, S. R., McKenzie, D. P, Westbrook, G. K. and Bowen, A. N., 1987, Magmatism at rifted continental margins. *Nature*, 330, 439-444.

Whitney, J. A. and Stormer, J. C., 1985, Mineralogy, Petrology and magmatic conditions from the Fish Canyon Tuff, Central San Juan Volcanic Field, Colorado., *J. Pet.*, 26, 726-762.

Williams, C. A., 1975, Seafloor spreading in the Bay of Biscay and its relationship to the North Atlantic., *Earth & Planet. Sci. Letts.*, 24, 440-456.

Williams, I. S., Tetley, N. W., Compston, W. and McDougall, I., 1982, A comparison of K-Ar and Rb-Sr ages of rapidly cooled igneous rocks: two points in the Palaeozoic timescale re-evaluated. *J. Geol. Soc. Lond.*, 139, 557-568.

Wilson, R. C. L., Hiscott, R. N., Willis, M. G. and Gradstein, F. M., 1989, The Lusitanian Basin of West-Central Portugal: Mesozoic and Tertiary tectonic stratigraphic and subsidence history. in: 'Extensional tectonics and stratigraphy of the North Atlantic margins.' *AAPG Mem.* 46, 341-361

Windley, B. F., 1986, The evolving continents. John Wiley and sons, ltd. 399 pp.

Wintsch, R. P. and Lefort, J. P., 1984, A clockwise rotation of Variscan strain orientation in SE New England and regional implications. in Variscan Tectonics of the North Atlantic region, Ed. Hutton, D. H. W. and Sanderson, D. J.*Geol. Soc. Spec. Pub.* 14, , 245-252.

Wright, A. E., 1976, Alternating subduction direction and the evolution of the Atlantic Caledonides. *Nature*, 264, 156-160.

Yelland, A. J., 1991, Thermo-tectonics of the Pyrenées and Provence from fission track studies. Unpublished PhD, thesis, Birkbeck College, University of London.

Young, E. J., Myers, A. T., Munson, E. L. and Conklin, N. M.,1969, Mineralogy and geochemistry of flourapatite from Cerro de Mercado, Durango, Mexico. *USGS Prof. Pap.* 650-D, D84-D93.

Zeigler, P. A., 1989, Evolution of Laurussia - a study in late Palaeozoic plate tectonics. Kluwer Academic Publishers London, 102 pp.

Zeigler, P. A., 1990, Geological atlas of Western and Central Europe., Shell Internationale Petroleum Maatschappij B. V. 232pp.

Zeitler, P. K., Tahirkheli, R. A. K., Naeser, C. W. and Johnson, N. M., 1982, Unroofing history of a suture zone in the Himalaya of Pakistan by means of fission track annealing ages. *Earth & Planet. Sci. Letts.*, 57, 227-240.

Appendix 1

Sample preparation.

A1.1 Extraction of apatites from rock samples and reduction of pure crystals to a suitably sized fraction.

NB. specific gravity of bromoform is 2.89, and that for di-iodomethane is 3.35.

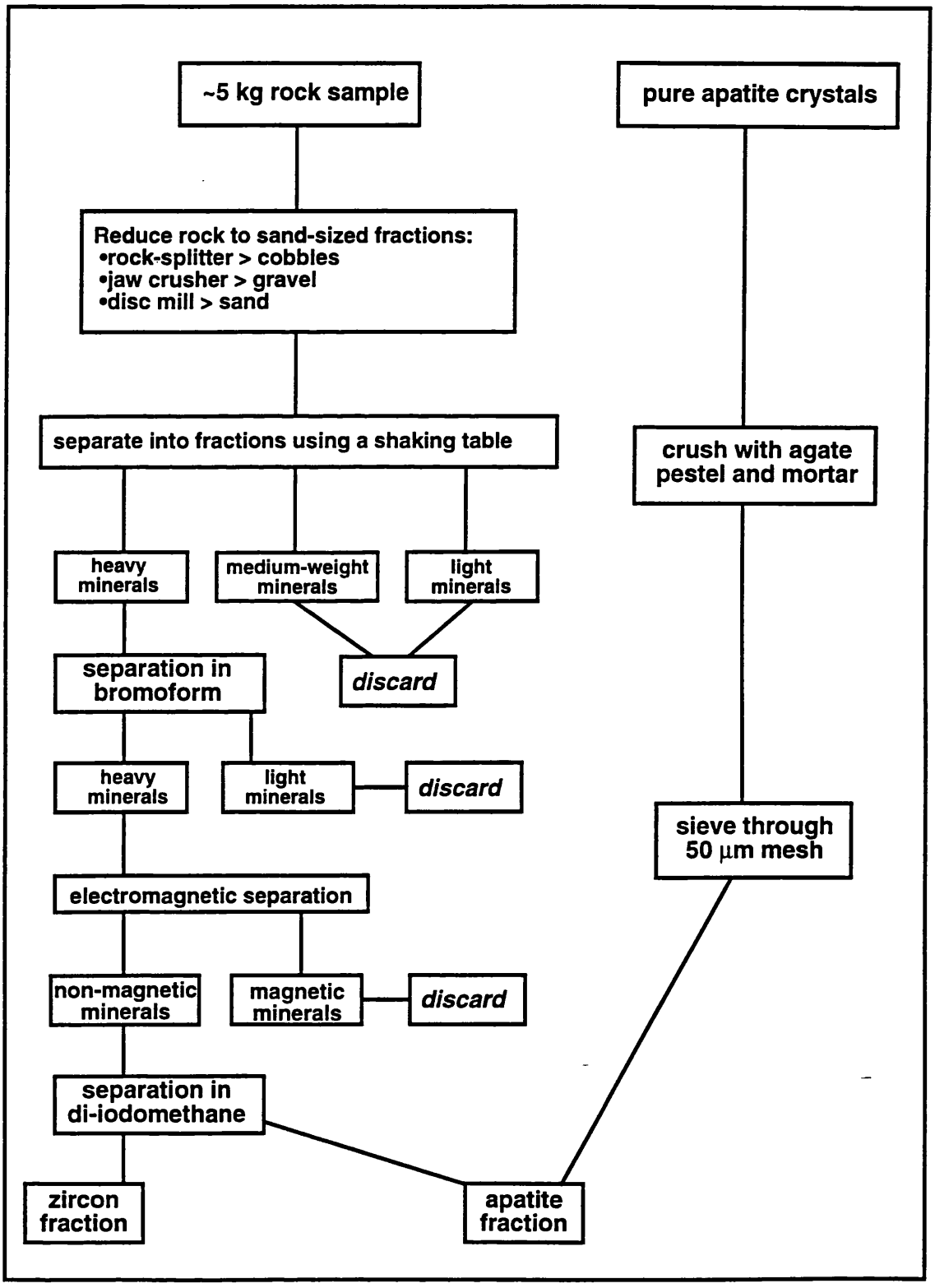

A1.2 Preparation of apatites for fission track analysis, IR microspectroscopy and electron microprobe analysis.

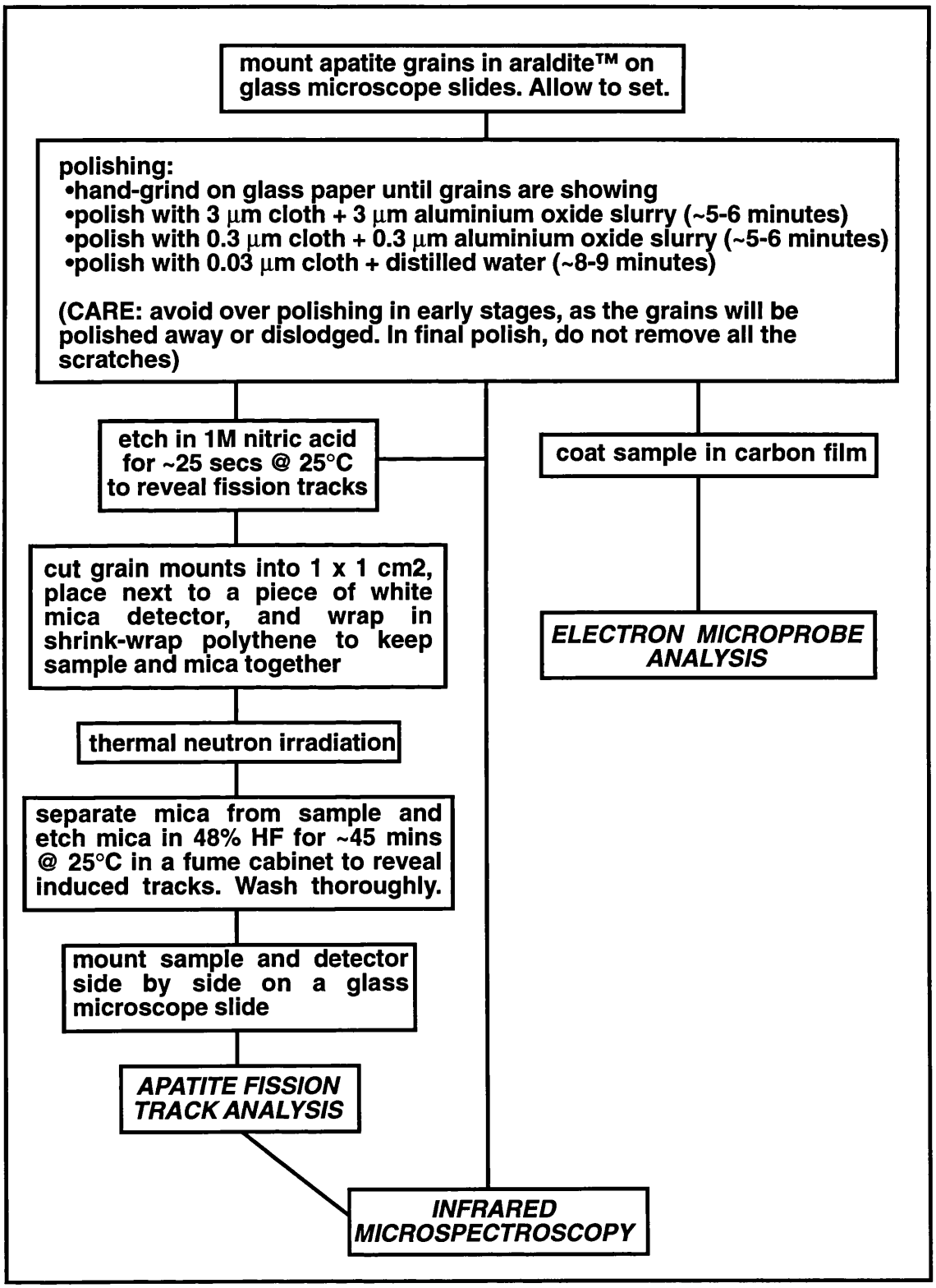

A1.3 Etching of fission tracks in apatite.

The rate of etching of fission tracks in apatite is greater than the bulk etch rate of the crystal (which in turn varies between crystallographic orientations). Once placed in an etchant, tracks become enlarged concentrically rather than by increasing the length (overetched tracks will develop a flattened end revealing that etching at the termination of a track is a far slower process). Three phases of track revelation are witnessed during etching. In the first phase, few tracks are revealed. This is followed by a phase where tracks are rapidly revealed, then finally a phase where a 'plateau' is reached, and no new tracks are formed (Wagner and van den Haute, 1992). Ideally, tracks should have a 'knife-blade' or 'dagger' shape as described by Gleadow (1981). As etching of the fission tracks is also accompanied by gradual removal of the crystal surface, if etching is prolonged, the polishing scratches on the crystal surface will be removed and eventually the number of fission tracks will decrease, as those at a high angle to the crystal surface will be removed. Consequently an optimum etching time is reached just after the plateau is attained.

The fission tracks in the apatites analysed in this study were revealed using 5M HNO_3, with an optimum etch time of between 23 - 26 seconds at room temperature. On removal from the etchant the sample slides are immediately placed under cold, running water to remove all traces of the etchant, and examined under the microscope. If over-etching of the apatites has occurred, they must be discarded and the process repeated with a fresh aliquot of the sample. Therefore it is sensible to remove samples for checking earlier rather than later, and then if necessary, they can be further etched.

Chlorapatite has a greater bulk etch rate than fluorapatite. A consequence of this is that etch pits in chlorapatite are slightly enlarged with respect to those in fluorapatite. Although this phenomena is recognised it has yet to be refined for use as a quantitative or semi-quantiative means for determining the chlorine content of the crystal (Donelick, 1992, *unpublished presentation at 7th International Fission Track Workshop, Philadelphia*).

A1.4 The zeta personal calibration factor.

A table showing the calculation of the zeta personal calibration factor and its standard deviation as used for the calculation of fission track ages in this thesis is presented in the table overleaf (table A1.4). The zeta values are calculated from age standards as described on pages 106 and 110.

Table A1.4. Zeta values calculated since November 1989 as used for the fission track age analyses presented in this thesis.

Date	Standard	N°. xtls?	Zeta	Error (±1σ)	pd/cm^2	ps/pi	Average	Std. Dev.
6-Nov-89	Durango	18	329.89	17.27	1742000	0.11		
16-Nov-89	Durango	18	320.44	17.15	1252000	0.1569		
29-Nov-89	FCT	20	268.72	21.23	1742000	0.119		
30-Nov-89	FCT	20	428.40	31.72	1746000	0.0748		
1-Dec-89	Durango	18	381.11	21.47	1214000	0.1361		
4-Dec-89	Durango	9	370.58	27.39	1116000	0.1522		
5-Dec-89	FCT	20	319.30	18.53	1265000	0.1384		
6-Dec-89	FCT	20	387.00	29.09	1141000	0.1266		
7-Dec-89	FCT	18	454.32	36.38	1214000	0.1014		
13-Dec-89	FCT	19	358.84	21.54	1214000	0.1284		
13-Dec-89	Mt. Drom.	18	398.27	25.53	1746000	0.0286		
15-Dec-89	Mt. Drom.	18	342.47	15.61	1746000	0.3327		
1-Jan-89	Durango	18	381.11	21.47	1214000	0.1361		
5-Jan-90	Mt. Drom.	20	346.78	28.64	1214000	0.473		
17-Jan-90	Mt. Drom.	18	357.14	16.55	1558000	0.3575		
26-Jan-90	FCT	18	289.43	15.70	1719000	0.1124		
29-Jan-90	Mt. Drom.	18	362.52	26.75	1613000	0.3406		
13-Mar-90	FCT	18	348.56	35.65	1382000	0.116		
28-Mar-90	FCT	18	346.84	21.88	1468000	0.1098		
19-Aug-90	Mt. Drom	18	353.39	26.18	1317000	0.427	357.26	6.34

i). rs and ri are respectively the density of spontaneous and the density of induced fission tracks occurring in the crystal. rd is the density of induced tracks in the dosimeter.

Appendix 2

Geological descriptions of the apatite yielding samples collected from the continental margins of the Bay of Biscay.

In France, samples were collected using information Durand and Lardeux (1985), Doré et al. (1978), Gabilly (1978) and Auvray and Martin (1982). The Spanish samples were collected using the information in the 1:200,000 IGME geological maps and their accompanying field guides (Bastida et al., 1984; Gonzalez-Lodeiro et al., 1984; Julivert et al., 1981 and Pello et al., 1981). Unless otherwise referenced, the information contained in these descriptions is from the above sources.

A2.1. Samples from Brittany.

Samples were collected during June, 1990. No grid references are available, the IGN serie verte (1 : 100 000) maps are recommended.

BRET 1. Brignognan Plage.

Granite de Brignognan.

This massif extends from Roscoff to Kerlouan, and was sampled at the type area of Brignognan, where it outcrops on the beach as large, weathered boulders and tors. Here it has a coarse grainsize (2-5 mm) with large phenocrysts of K-feldspar (2-3 cm), although at the margins of the intrusion it becomes much finer. At the western margins it carries xenoliths of the Plouguerneau migmatites. It is cut by a large number of aplitic and tourmaline-pegmatite veins, which are particularly well exposed on the coast between St-Pol-de-Léon and Roscoff. Emplaced during the lower Carboniferous, at around 345 Ma (Lameyre and Autran, 1980).

BRET 2-3. St Michel, Argenton.

Migmatites de Plouguerneau.

BRET 2 was collected from the beach directly below the chapel at the end of the D 32 road. At Argenton, the sample was from the northern side of the cove, accessed from the D 27.

At both St Michel and Argenton the migmatites look very much like granites, although they show a faint foliation in the alignment of some minerals. The rocks are rich in mica, the dominant minerals are bi-mu-qtz-pl and perthite. There is also accessory apatite in relative abundance and a small amount of chiastolite. Both are Cadomian relicts.

BRET 4. Plage Phare de Trezien.

Granite de St Renan.

The Granite de St Renan was sampled on the southern end of the cove, approximately 15 m from the slipway.

The granite de St Renan forms part of the St-Renan-Kersaint Massif which extends from the Ile-de-Molène to Plouvorn. The other component of the massif being the Granite de Kersaint. These two are largely differentiated by grainsize, the Kersaint being a coarse grained rock which outcrops in the east of the massif. The sampled unit was the Granite de St Renan, which is a fine grained leucocratic rock with which are associated a number of metalliferous ores, namely cassiterite, wolframite and scheelite. On the beach at Trézien, the rock is very pale but contains lenses of tourmaline, several centimetres across. In thin section, these minerals are dark green in colour and corroded.

At this locality, the stoped margins of the granite within the migmatites is exposed but in detail it is very complex, as the granite itself has become partly migmatised in areas.

The granite is Variscan; Rb-Sr and K-Ar radiometric ages have been obtained of between 352 and 331 Ma (Cogné and Peaucat, 1973; Deutsch and Chauris, 1965).

BRET 6. Pointe St Mathieu.

Micaschistes du Conquet.

The sample comes from rock outcrops below the D 85 approximately 0.5 km north of the end of the headland.

These schists do have a well developed schistosity with good segregation of minerals. The quartz and feldspar often are in lenses between the micas. The minerals are bi-mu-pl-qtz with abundant apatite and zircon, the latter as inclusions in the biotite. They are probably part of the Brioverian Supergroup, and therefore Upper Proterozoic age.

BRET 8. Tréboul.

Granite de Douarnenez.

The sample was collected from a small outcrop on the northern side of the supermarket car park in the village. This is on the D 7, just west of the harbour.

It is a granite with some foliation, there is a good alignment of the micas. The mineralogy is qtz-pl-bi-mu-Kfeld, with some myrmekitic texture. Accessory zircon, apatite and rare sphene exist. Possibly part of the

Granite de Douarnenez, and therefore possibly the same age (450 Ma, see below).

BRET 9. Pointe de Beuzec.
Granite de Douarnenez.

The granite was sampled from the cliffs on the Pointe, directly below the car park. The Granite de Douarnenez is in fact a trondhjemite. Ries (1979) and Barrière et al (1971) have calculated K/Ar (bi) ages for the granite of 300 Ma. However, Cabanis (1980) cites ages from zircons (U-Pb?) of 450 Ma. These pre-Variscan ages are comparable with those of similar formations in North-west Spain (see SPA 23 and SPA 29 below)

BRET 11. Pointe du Raz.
Granite de Pointe du Raz.

The sample is from the western side of the small car park which appears to occupy a small quarry, at the end of the B 784 road.

At the Pointe du Raz, another granite again showing foliation defined by the alignment of the micas, caused by deformation along the South Armorican Shear Zone. The mineralogy consists of qtz-Kfeld-pl-bi-mu and abundant apatite and zircon. The granite is part of the suite emplaced along the SASZ, dated by Vidal (1973) at 320 Ma (Rb-Sr wr isochron).

BRET 12. Anse du Loc'h.

The sample comes from the northern cliff of the cove south of the junction of the D 784 with the road to Cléden-cap-Sizun.

The outcrop is very typical Variscan bi-si gneiss. It has well developed banding, medium grainsize and is very hard.

BRET 13. Pointe de la Torche.
Granite de Pont-l'Abbé.

The sample comes from a beach outcrop on the north side of this small headland. A good, fresh Variscan medium grain sized granite rich in qtz-Kfeld-pl-mu-bi and perthite, with large amounts of apatite and zircon. Secondary chlorite and clay minerals exist. One of the South Armorican suite of granites dated by Vidal (1973) at approximately 320 Ma (Rb-Sr wr isochron).

BRET 14. Mousterlin.
Granite de Pont-l'Abbé.

Collected from the eastern promontory on the Pointe de Mousterlin.

This Variscan granite has a good relatively unaltered texture with a medium to coarse grainsize. It contains qtz-pl-Kfeld-mu-bi with perthite. Rare myrmekitic texture, apatite, zircon and rutile also exist. One of the South Armorican suite of granites dated by Vidal (1973) at approximately 320 Ma (Rb-Sr wr isochron).

BRET 17. Kerroc'h.
Granite de Guidel.

Sampled from granite outcrops on the beach at Kerroc'h, due north of the Ile-de-Groix. It is highly leucocratic, containing no mafic minerals whatsoever. It has a medium to coarse grainsize and contains qtz-plagioclase-mu and perthite, and apatite. Ries (1979) obtained a K/Ar (mu) age of 312 Ma.

BRET 18. Port Haliguen.
Granite de Quiberon.

The Port Haliguen granite outcrops at the very end of Presqu'Ile de Quiberon, where it was sampled on the beach (at the end of the D 768). It has a foliated texture with good alignment of micas. It resembles a migmatite and has evidence of microscale shearing causing the comminution of grains. The major minerals are qtz-pl-mu-bi with perthite, and some myrmekite. Ries (1979) obtained K/Ar ages (bi and mu) of 291 and 312 Ma respectively, while Vidal (1973) reported a Rb/Sr (wr isochron) age of 331±9 Ma for the granite.

BRET 19. Carnac Plage.
Granite de Carnac

The Carnac granite outcrops on the beach in the town of Carnac from where it was sampled, approximately 20 m from the western end of the car park. It is Variscan and has an unfoliated granitic texture, and appears to have been quite heavily altered, a lot of secondary minerals being present. The mineralogy is qtz-pl-Kfeld-mu-bi with perthite and micrographic texture. A radiometric age of 303 Ma (K/Ar bi) was obtained for the granite (Ries, 1979).

BRET 24. Port Hué.

St Malo Migmatites.

The sample came from the cliff to the left of the slipway on the beach at Port Hué.

The St Malo Migmatites represent a Cadomian age sedimentary sequence affected by a low pressure-high temperature (Abukuma-type) metamorphism raising them to greenschist facies. The precise age of this sedimentary sequence is not known, however south of Dinan, the metamorphosed series passes into the Brioverian sediments of southern Brittany. The metamorphism has been dated at 541±5 Ma by the U-Pb method on zircons (Peaucat, 1986). The migmatite belt is composed of three broad lithologies. The migmatised rocks forms the core of the complex and outcrops along the coast around St Malo and Dinard. This core can itself be subdivided into three main facies: gneiss injected with veins, metatexites, and diatexites with anatexic granites.

The outer parts of the belt are well differentiated paragneisses and micaschists.

BRET 27. Porz-Even.

Tufs de Treguier.

This pyroclastic deposit, 800-1000m in thickness, outcrops in a band across the Trégor region approximately three kilometres wide from the Baie de Lannion (estuary of Le Léguer) to the Baie de St Brieuc (Pointe de Porz-Even) They were sampled at this locality from a small flat lying outcrop on the beach. The tuffs are keratophyric in composition and of medium to fine grainsize. The principal minerals are al-am(altered to cl + qtz + ep)-bi, with accessory apatite and zircon in some abundance. Along with the spilites de Paimpol which outcrop to the south of the pyroclastics as massive lavas and pillows, the rocks represent a calc-alkaline series which has been given a whole-rock Rb-Sr age of 640±12 Ma.

BRET 29. Castel-Meur.

Microgranodiorite de Pleubian.

The sample was taken from directly north of the house on the shore. This is a medium grainsized granodiorite with a grannular texture with phenocrysts of plagioclase and hornblende. It is similar in composition and age to the Granodiorite de Talberg which outcrops to the east of Pleubian. Both rocks form part of the Cadomian North Trégor Batholith. All the rocks present have a calc-alkaline affinity. Some U-Pb dates on

zircon cores have been found and these are all around 615±13 Ma (Graviou et al., 1988).

BRET 30. Grande-Ile.

Granite de Ploumanac'h.

The rock was sampled from the southern side of Grande-Ile. Dated at 300 - 290 Ma (Rb-Sr, whole rock; K/Ar; Leutwein et al, 1969), this is by far the youngest intrusion in the north of the Armorican massif. It is a well exposed ring complex of three successive intrusions. The centre of the intrusion at Grande-Ile was sampled. Here the major minerals is qtz-pl-Kfeld-mu-bi-cl, with micrographic texture.

A2.2. Samples from The Channel Islands, Cotentin Peninsula, (Normandy) and the North Vendée Coast.

Samples were collected during April, 1991. No grid references are available, the IGN serie verte (1 : 100 000) maps are recommended.

JER 1.

St. Peters Granite.

A Cadomian adamellite from St. Peters Quarry, Jersey. It has a medium grainsize and no phenocrysts. The minerals are primarily qtz-Kfeld-pl-bi with microperthite. There is minor alteration to clay minerals in the feldspars. Contains accessory apatite and zircon. The rock is from the SW plutonic Complex of Jersey which has been dated between 550±12 Ma and 483±17 Ma (Rb-Sr wr isochron) by Bland (1984), revealing it as one of the youngest known Cadomian intrusions.

VEND 1. Challans.

The lithology sampled appears to be a meta-sedimentary rock which seems to correspond to the Brioverian basement, which in this area forms the edge of a Mesozoic marine basin. The rock is a schistose sandstone, quite highly folded and rich in biotite and possibly graphite, quartz and haematite. The rock is very friable.

VEND 2. La Parée Beach.

Arkose du Marais-Girard.

This is a series of arkosic schists and sandstones (the latter were sampled) which outcrop on the beach below the D 40. They form the top of the Série de Bretignolles. The rocks are dominantly green in colour but

mottled with red. They represent terrestrial deposits. The mineralogy is qtz-pl-Kfeld-mu-bi-cl. They are only slightly metamorphosed.

VEND 3. Bretignolles Quarry.
Microgranite de St-Martin-de-Brem.

The quarry is directly west of the D 80, approximately 1 km south of Brétignolles-sur-mer.

The granite has a porphyritic texture which has phenocrysts of quartz and K-feldspar in a aphyric, dominantly green-coloured matrix. This is devitrified and contains qtz-Kfeld-pl. The intrusion cross-cuts Silurian sequences which were probably folded during the Devonian. This predicts that the granite was intruded during the Carboniferous.

VEND 5. La Madelaine.
Granite de Noirmoutier.

An outcrop on the beach north of La Madelaine on the Ile-de-Noirmoutier (at the end of the D 95) is of a foliated granite. It is coarse grained with some alignment of quartz and feldspar. The rock is also rich in muscovite. It is cut by veins of pegmatite and aplite and also pods of gneiss representing the sediments into which it was intruded. It belongs to the suite of South Armorican granites dated by Vidal (1973) at approximately 320 Ma (Rb-Sr wr isochron ages).

VEND 8. Piriac.
Granite de Guerande.

A Variscan leucocratic coarse grained granite which is composed dominantly qtz-pl-Kfeld-b-mu. Sampled from the beach 1 km west of Lerat on the D 99. It belongs to the suite of South Armorican granites dated by Vidal (1973) at approximately 320 Ma (Rb-Sr wr isochron ages).

VEND 9. Pointe de Croisic.
Granite de Croisic.

The headland is also formed by a leucocratic Variscan granite. It is fine grained and cross-cut by numerous aplitic dykes. Sampled from the end of the headland. It belongs to the suite of South Armorican granites dated by Vidal (1973) at approximately 320 Ma (Rb-Sr wr isochron ages).

VEND 10. Pointe de Penchateau.

A bi-si gneiss outcrops on the beach at the end of the headland. It is finely laminated and has numerous small folds.

VEND 12. Mindin.

There is a small outcrop of a late Variscan anatexic leucogranite on the beach at Mindin. It is fine grained and has a mineralogy of qtz-Kfeld-pl-mu-bi. A small outcrop exists on the beach on the Loire estuary at the car park, 1 km west of the Pont de St-Nazaire. It belongs to the suite of South Armorican granites dated by Vidal (1973) at approximately 320 Ma (Rb-Sr wr isochron ages).

VEND 13. St-Brevin-Les-Pins.

This is a metectic bi-si gneiss of sedimentary origin (relic bedding can be observed). It also contains pods of granite and numerous veins. Collected from the south side of the headland, where there is a slipway.

VEND 15. Pointe St Gildas.

Small outcrops of a fine grained arkosic schist. collected from the north side of the headland on the D 751. The mineralogy is dominantly quartz and muscovite, with occasional plagioclase and K-feldspar forming small augen. The rocks is relatively fresh, showing only minor alteration of the feldspars.

VEND 16. Plage de la Meleu.

A meta-rhyolite outcrops on the beach. It is fine grained, but shows a foliation. There are phenocrysts of quartz and feldspar. Collected 2 km due south of la Plaine-sur-mer.

VEND 17. St Marie-sur-mer.

Again, outcrops of fine-medium grained, well foliated metasedimentary schistose rocks. Collected on the coast just below the look-out post in the village. The rock in thin section is revealed to be very fresh and of a quartz-muscovite composition.

NOR 1. Hedé.

Mancellian Batholith.

A biotite-rich rock which appears to have a volcanic texture. Fairly friable. collected from a roadside outcrop (in Brittany!) on the D 795 to Combourg, 7 km south of the town. Mineralogy is qtz-Kfeld-pl-bi and appears to be granodiorite, although in hand specimen, it is very weathered.

One of the intrusions belonging to the large Cadomian Mancellian Batholith of south-eastern Normandy. The batholith was probably intruded at 541±5 Ma, U-Pb zi (Guerrot and Peaucat, 1990).

NOR 2. Mont-Dol.
Granite de Mont-St-Michel.

A small cupola of the St-Michel batholith outcrops forming the monadnock of Mont-Dol. The granite is geochemically identical to that at Mont-St-Michel (see below). The sample came from a small quarry on the south-eastern flank of the hill. The granite was intruded post-Cadomian, during the Cambrian (approximately 550 Ma, Lameyre and Autran, 1980).

NOR 4. Mont-St-Michel.
Granite de Mont-St-Michel.

Sampled from the beach west of the Gendarmerie on the Mont. This leucogranite is the same as that which outcrops at Mont-Dol and the island of Tombelaine, intrusive in the Cadomian basement. It is a coarse-medium grained granite containing qtz-Kfeld-pl-mu-bi, with perthite. Apatite occurs as quite large crystals. Age of emplacement as above.

NOR 5. Avranches.
Granite d'Avranches.

The samples comes from a small outcrop at the western foundations of the Town Hall walls in the town centre.

The Granite d'Avranches is a poorly exposed linear intrusion aligned EW from Avranches approximately 28 km inland. It varies in thickness between 2 and 4 km. It is clearly a separate to the Granite de Vire massif to the north, although also part of the Mancellian Batholith (541±5 Ma, U-Pb zi, Guerrot and Peaucat, 1990). It contains qtz-Kfeld-pl-mu-bi with accessory apatite, zircon and rutile.

NOR 6. Les Perrieres.
Granite de Vire.

The sample comes from the disused of the two quarries accessed from the D 261, 2 km west of St-Michel-des-loups. It is extremely fresh and quarried here for tombstones. This Cadomian 'granite' is intruded in a EW lineation into Brioverian schists and greywackes and is one of the largest intrusions of the Mancellian Batholith. Chemically the composition tends towards the granodioritic with some additional leucogranites. Petrologically

the granite contains qtz-pl-bi with accessory muscovite, apatite, zircon and sphene. Dated at 541±5 Ma (U-Pb zi, Guerrot and Peaucat, 1990).

NOR 7. St-Michel-des-loups.

These Brioverian (Upper Proterozoic) meta-sands form part of the metamorphic aureole of the Granite de Vire. In other places the rocks grade into cordierite-biotite schists. The rocks are almost vertically bedded here and are a medium to fine grained arkoses, with abundant sericitization. The rocks are also criss-crossed by small quartz veins. This sampled is from the large quarry on the D 143 near St-Michel-des-loups.

NOR 9. Pointe du Thar.

A doleritic sill in the Formation de St-Pair, outcropping on the beach by the slipway, directly below the D 911. Intruded into the Upper Proterozoic St-Pair Formation meta sediments (see below).

NOR 10. Pointe du Thar.

Formation de St-Pair.

This is a fine grained flysch composed of greywackes, silts and black argillaceous sands. They are of Brioverian age, but are affected by several phases of deformation culminating in the Variscan. The sample was collected from the coarser grained greywackes.

NOR 13. Barneville-Carteret.

Grés de Moitieres-Alonne.

An arenaceous formation of lowest Llanvirnian age. It is apparently very rich in a fauna of trilobites and graptolites, *didymograptus murchisoni* being the zone fossil. Sampled from a road cutting on the D 904, by the road sign (Cherbourg, 37 km) approximately 2 km north of the Barneville-Carteret exit.

NOR 14. Les Pieux.

Grés de Rozel.

Of lower Cambrian age the Grés de Rozel are green argilites and siltstones. there is very little coarse-grained sandstone, but some horizons contain nodular calcites. The lithology is rich in sedimentary structures such as ripples and flute casts. *Planolites* ichnofacies exist along with phosphatic horizons which were probably coprolitic in origin. In thin section, the sampled horizon is of an extremely fine grained matrix with some larger clasts of lithic fragments, green biotite, pyrites, quartz and

various feldspars. Some bedding parallel lamination is apparent. Sampled from a road cutting on the D 904, 1.5 km south of the exit for Les Pieux (directly next to the road sign!).

NOR 15. Cap de la Hague.
Cap de la Hague Granodiorite.

The collected sample came from the cape itself, just to the north of Auderville, and approximately 50 m west of the coastguard hut. It is a fine to medium grained qtz-Kfeld-bi rock, strictly speaking, it is a trondhjemite. The granodiorite is a member of the Cadomian post-tectonic Northern Granites Complex, comprising seven plutonic rocks on the western tip of the Cotentin Peninsula. Power et al. (1990) calculated a Rb-Sr wr isochron age of 477±8 Ma for the Cap de la Hague Granodiorite.

NOR 16. Goury.
Granite de St Germain.

Sample collected from the south side of the harbour in the village of Goury. This is a fresh, medium grained leucogranite, with qtz-Kfeld-pl-mu-bi with perthite representing the major mineral assemblage. Acicular accessory apatite occurs, and the biotite is a green variety. Another member of the Cadomian Northern Granite Complex, it yields a 515±12 Ma Rb-Sr wr isochron age (Power et al., 1990). The Granite de St Germain is possibly the largest intrusion in the complex (inland exposure is very poor, so extents of the granites are difficult to map). At Goury, the granite is enclosed by the Cap-de-la-Hague Granodiorite.

A2.3. Samples from North-west Spain.

Samples were collected during August, 1991. Grid references are from the 1:200,000 IGME geological maps.

SPA 2.

A Gzelian age sandstone of the Sabero Group, unconformably overlying the Nocedo Formation.

SPA 5. Sheet 2, "Aviles", GR 342 1001. Salave.
Plutón de Salave.

A late Variscan granodioritic intrusion. The intrusion is accessed from the track, across fields, to the coast approximately 2 km from the village of Salave.

This is a small stock, one of the very few intrusions in the external Western Asturian-Leonese Zone. The major minerals are pl-qtz-Kfeld-bi. Structurally it is overthrust to the West by one of the major thrusts in the WALZ and was intruded into the western flank of the Narcea Anticline into Ordovician-Silurian slates. Suarez et al., (1978) have dated it at 284±8 Ma (Rb/Sr bi).

SPA 7. Sheet 1, "La Coruña", GR 304 1014. Cabo Burela.
Granito de San Ciprián.

Collected from the bay just on the west side of the headland Cabo Burela. Again this is a relatively undeformed Variscan two-mica granite of medium to coarse grainsize, with major minerals qtz-Kfeld-pl-mu-bi. It is intruded into the western margin of the WALZ into the Mondoñedo Nappe. The intrusion has a characteristically irregular shape, which is dominantly primary. The intrusion occurred during Phase 2 (approximately 310 Ma) of the Variscan deformation, and is anatectic.

SPA 8. Sheet 1, "La Coruña", GR 286 1017. Vivero.
Granodiorita de Vivero.

From the car park excavated outside the 'Hotel Ego', just off the C 642 (road to Faro) Another coarse to medium grained granodioritic rock of similar chemistry to the undeformed Macizo de La Tojiza (SPA 6, non-apatite yielding), but this time suffering some deformation and shows foliation. The outcrop at this locality is cross cut by very coarse pegmatite veins (10 cm grainsize). The intrusion is to the west of and directly associated with the Vivero Fault (a major N-S trending structure traceable for approximately 140 km). The granodiorite form part of a suite of intrusions often associated with faulting. The major minerals are qtz-Kfeld-pl-hb-bi, it approaches a tonalitic chemistry. The granite was deformed syntectonically by movement on the Vivero Fault. It is older than the Granito de San Ciprián, being cross-cut by it.

SPA 10. Sheet 1, "La Coruña", GR 278 1028. Punta de la Estaca de Bares.
Macizo de Estaca de Bares.

The sample was taken from the small car park quarried out from behind the old coastguard station on top of the Punta de la Estaca de Bares. An undeformed Variscan calc-alkaline granite. Here it is melanocratic, very biotite rich, with a medium grainsize. Also significant pyrite. Frequent xenoliths occur, up to 50 cm diameter. The outcrop shows very fine examples of spheroidal weathering. The Macizo de Estaca de Bares is of the

same intrusive suite as the Granodiorita de Vivero, although the rock resembles a syenite, it is lower in quartz and richer in K-feldspar. The xenoliths are also a common feature of this suite, indicating stoping as an intrusion mechanism. The intrusion cross-cuts the core of the Ollo de Sapo Anticline.

SPA 11. Sheet 1, "La Coruña", GR 277 1025. Porto de Barquero.
Granito de El Barquero.

Sample is from a small quarry on the road RN LC100 to the point, approximately 3 km from Porto do Barquero. It is a well foliated, leucocratic, medium grained granite, cross-cutting the Macizo de Estaca de Bares. It is of Variscan age and a calc-alkaline affinity. A K/Ar (biotite) age of 280 Ma for the intrusion was calculated by Ries (1979).

SPA 12. Sheet 1, "La Coruña", GR 273 1024. Picón.
Metarhyolites.

Sampled from a small bay accessed by a steep track approximately 2 km to the west of Picón in the Central Iberian Zone. The metarhyolites appear as sheets within the very fine-grained, vertically bedded slates *Las Capas de La Garganta* which are of mid-Ordovician age. The metarhyolites themselves are probably Silurian, and are part of the western flank of the Ollo de Sapo Antifom. They are fine grained, pale green rocks containing small quartz augen. The metarhyolites outcrop on the west side of the bay.

SPA 13. Sheet 1, "La Coruña", GR 273 1024. Picón.
Porphyry sill.

The sample location is as above, but from the East side of the bay. The sill is quite distinctive weathering out from the slates. It is of a very hard rock and has not taken any cleavage. It appears to be around 2 m in thickness. It has a fine grained matrix with phenocrysts. There is no metamorphic texture visible.

SPA 14. Sheet 1, "La Coruña", GR 264 1025. Cariño.
Gneiss de Cariño.

The rock was sampled from the cliffs forming the foundation of the harbour wall to the north of Cariño. A nicely banded paragneiss, although it forms part of the Cabo Ortegal ultrabasic complex (Capelada Unit), it contains no inclusions of ultramafic rocks. It contains biotite, garnet, staurolite, quartz, plagioclase and epidote.

SPA 15. Sheet 1, "La Coruña", GR 264 1027. Cabo Ortegal.
Neises Bandeados o de Masanteo.

A similar rock to the above, and also a member of the Capelada Unit, except that it contains ultrabasic rocks, occurring as layers, lenses and boudins (these include eclogites). Again it is very well banded.

The sample was collected from a road cutting on the road to Cabo Ortegal. The outcrop shows a set of tight, asymmetric folds.

SPA 16. Sheet 1, "La Coruña", GR 254 996. As Pontes.
Granito de Forgoselo.

Exposures of the granite on the C 641 As Pontes to Ferrol road. Approximately 1 km after the outcrop of a large quartz vein. This is a coarse grained felsic two-mica granite, with abundant, large phenocrysts of K-feldspar. The major mineral assemblage is qtz-Kfeld-pl-mu-bi. It is very weathered in its outcrops. This is a large late Variscan pluton, with an almost circular outline. It was intruded anatectically into regionally metamorphosed country rocks (at greenschist to amphibolite facies) in the CIZ, and creates an extensive metamorphic aureole within these. The granite is associated with large scale (> 10 m wide) quartz veins and other pegmatites.

The intrusion has been dated by Capdevila and Vialette (1970) at 303±6 Ma (Rb/Sr wr).

SPA 17. Sheet 1, "La Coruña", GR 233 987. Playa de Ber.
Porphyritic felsic dykes.

These outcrop on the south side of the Playa de Ber, just west of Pontedeume.

The rocks are very fine grained and leucocratic and exhibit prominent flow banding. They are intruded into the Esquitos de Ordenes (see below).

SPA 18. Sheet 1, "La Coruña", GR 233 987. Playa de Ber.
Esquitos de Ordenes.

These schists form part of the Ordenes Complex (Complejo de Ordenes), which is an extensional area in the Central to North Galician Zone. The sequence is deformed into the broad, N-S trending Frouxeira Anticline. The schists are dominantly fine grained, almost slaty. A coarser band was sampled. They are metasediments, an alternating (10-15 cm beds), cyclic sequence of pelites and psammites, originally a clastic, arenitic

sedimentary sequence. the band sampled was one of the many, localised beds of microconglomerate within the sequence.

Due to the absence of fauna within the sequence, dating has proved to be difficult, but the schists are probably Cambro-Ordovician.

SPA 19. Sheet 7, "Santiago de Compostela", GR 206 963. Mt Cedeira.
Macizo de la Coruña (locally called the Macizo de Silva).

This rock was sampled from a road cutting on the LC 401 to the east of Silva, below Mount Cedeira. It is a coarse grained granodiorite, with a mineralogy of qtz-pl-Kfeld-bi-(hb). in age it is an early Variscan granodiorite probably within the age range of 270-302 Ma, assumed from radiometric dates on similar intrusions (c.f. Ries, 1979).

SPA 20. Sheet 7, "Santiago de Compostela", GR 193 956. Anxeriz.
Macizo de Monte Castelo.

This sample was collected from a track, off to the left of the LC 402 (to Santa Comba from Anxeriz, turn off is just after the crossroads with the Portomouro - Carballo road.

This is a roughly circular and relatively undeformed gabbroic intrusion. It is medium grained, containing pl-opx-cpx-hb-bi. This largest gabbro in north-western Spain is intruded into the metasediments of the Ordenes Complex (Betanzos-Arzua Unit), immediately east of the Ordenes ultramafic rocks. This is typical of all the Spanish gabbroic rocks in that they occur exclusively in the allochthonous terranes. The intrusion occurred either just prior to or syntectonic with the second phase of Variscan deformation.

SPA 21. Sheet 7, "Santiago de Compostela", GR 192 977. W of Puerto del Razo.
Unidad de Malpica-Tuy.

Collected from outcrops on the western side of the cove at Puerto del Razo. The rock is a very hard, banded felsic gneiss. The protolith was either sedimentary and/or volcanogenic, the rock is now at amphibole granulite facies, and has suffered at least four phases of metamorphism, at least one of which (M3) was retrograde. The mineralogy is qtz-Kfeld-gt-zo-am. The Malpica-Tuy Unit is of Precambrian to Devonian age. these rocks are probably lower Palaeozoic.

SPA 22. Sheet 7, "Santiago de Compostela", GR 192 977. E of Puerto del Razo.

Macizo de Monte Neme

This is a fine grained, two-mica leucogranite from a small quarry just above the harbour wall at Puerto del Razo. The granite has suffered some late phase Variscan deformation, but was probably intruded as part of a suite around 310 Ma (c.f. Ries, 1979).

This granite is faulted against the gneiss of the Malpica-Tuy unit by a N-S trending fault along which the cove has become indented.

SPA 23. Sheet 7, "Santiago de Compostela", GR 183 984. Cabo San Adrián.
Augen gneiss.

From large disused quarry on the road to Cabo San Adrián, just north of Malpicá. A medium to coarse grained two mica gneissose granite with large feldspathic augens (5 cm diameter). This 'inhomogenous granite' has been faulted against the Malpica-Tuy unit, and forms the entire headland. It was affected by the first phase of Variscan deformation, and is therefore most likely pre-Variscan in origin. van Calsteren (1977) has dated it at 462 Ma.

The mineral assemblage is qtz-pl-Kfeld-bi-mu.

SPA 24. Sheet 7, "Santiago de Compostela", GR 179 981. Punta Nariga.
Macizo de Lage.

Collected from the Playa de Banzo, on the east side of Punta Nariga. A coarse grain size, foliated leucogranite. This granite is part of the large Lage-Dumbria Massif, forming the Blastomylonite Graben, and is part of the same intrusive suite as the Macizo de Monte Neme, and therefore can be assumed to be around 310 Ma also. The mineralogy is qtz-pl-Kfeld-bi-mu.

SPA 25. Sheet 7, "Santiago de Compostela", GR 165 968. Playa de Traba.
Migmatized granitoid.

From the north east side of the Playa de Traba, where it outcrops on the beach in weathered outcrops. It is clearly migmatised and cross cut by pegmatitic veins. It is recorded to contain lenses of migmatised sediment. It has a fairly inhomogenous texture with large variations in grainsize. Petrologically it is composed of qtz-pl-Kfeld-bi-mu.

SPA 26. Sheet 7, "Santiago de Compostela", GR 165 966. Sierra de Peña Forcada.
Macizo de Traba.

The sample was collected from a roadside cutting on coastal lane to Camelle. The granite forms the Sierra de Peña Forcada, and is relatively undeformed and quite fresh. it is pink in colour, with a major mineral assemblage of qtz-pl-Kfeld-bi-mu. Dated at 280±11 Ma (Ries, 1979).

SPA 27. Sheet 7, "Santiago de Compostela", GR 151 958. Muxia.
Macizo de Muxia.

Samples were both collected from a small quarry, just off the LC 440 just before the bay at Muxia. There appear to be two types of granite in the quarry. Sample 27 is from the west side of the quarry and is essentially leucocratic with white feldspars. It is medium grained with phenocrysts of K-feldspar, and a mineralogy of qtz-pl-Kfeld-bi-mu. Again the massif is part of the same suite as the Macizo de Monte Neme (~310 Ma).

SPA 28. Sheet 7, "Santiago de Compostela", GR 151 958. Muxia.
Macizo de Muxia.

This sample is from the eastern side of the quarry where the granite shows a definite pink coloration which does not appear to be caused by staining. The feldspar phenocrysts are pink and so are those in the groundmass. Otherwise, the rock is texturally identical.

SPA 29. Sheet 7, "Santiago de Compostela", GR 144 934. Cabo Fisterra.
Inhomogenous granite.

The sample comes from as near the end of the cape, below the lighthouse, as was possible. The rock is a highly porphyritic and very coarse grained granite. There appear to be textural variations in grainsize, presence of and alignment of phenocrysts and so on. The rock is essentially the same as SPA 23, a pre-Variscan deformed and metamorphosed granite, probably formed around 460 Ma.

SPA 30. Sheet 7, "Santiago de Compostela", GR 144 935. Cabo Fisterra Summit.
Macizo de Finisterre.

This sample comes from the higher land north of the lighthouse, where a track leads up to the radio mast. The sample comes from a parking space approximately 500 m along this track. The rock is very similar to that from below the lighthouse, but of a finer grainsize. Despite this similarity, the rock is from a much later intrusive suite of the same age and similar chemistry to the Macizo de La Coruña. An early Variscan granite, which

although not dated is probably between 270-302 Ma (c.f. Ries, 1979). The major mineral assemblage is qtz-pl-Kfeld-mu-bi.

SPA 31. Sheet 7, "Santiago de Compostela", GR 155 935. El Pindo.
Macizo de El Pindo

The sample comes from a smashed outcrop on the north side of the beach at El Pindo. The granite is very well exposed in this area, on the surrounding hills it has about 80% exposure. It is of medium grainsize, apparently undeformed, with a pink coloration. The Macizo de El Pindo, is a later Variscan granite cross-cutting other older intrusions and clearly discordant with them. It is of the same suite as the Macizo de Traba, and therefore can also be assumed to be around 280 Ma. The massif is sampled in two localities, here and at SPA 32. The mineralogy varies abruptly across the intrusion, approaching a granodiorite at this locality (qtz-pl-Kfeld-bi).

SPA 32. Sheet 7, "Santiago de Compostela", GR 156 929. Punta de Caldebarcos.
Macizo de El Pindo

This sample is from the Punta de Caldebarcos. It is still (officially) part of the Macizo de El Pindo, although it is recognised (also officially) as having a different chemistry. Here it is a two mica granite, with a major mineral assemblage of qtz-pl-Kfeld-mu-bi.

SPA 33. Sheet 10, "Mieres", GR 474 916. Sabero.
Cuenca de Sabero.

An Upper Carboniferous (Gzelian) sandstone, possibly from one of the minor marine layers within essentially terrestrial-deltaic carbonate-rich unit. It is unconformable upon part of the Sobia-Bodon Unit, on the footwall of the Esla Nappe.

SPA 36. Sheet 10, "Mieres", GR 489 928. Riano.

The sample is Ordovician conglomerate underlying a sandstone sequence, lying in the southern part of the Tarna Nappe, part of the Ponga Nappe Complex of the Asturian Arc.

SPA 38. Sheet 10, "Mieres", GR 525 962. Linnares.

Sample is from a road cutting approximately 1 km up the road to Linnares from the N 621. It is fine to medium grained, reddened micaceous sandstone with planar bedding. Probably of Permo-Trias age. The dating on this Lower Mesozoic sequence onlapping the Variscan Massif is poorly

constrained. A basal, quartz-rich conglomerate, outcropping in the vicinity of this sample has been correlated with the Buntsandstein, but the sequence is too incomplete to ascertain a detailed stratigraphy.

Appendix 3.

Apatite standards used for IR microspectroscopy.

1. Fluorapatite from Dandaragan, Western Australia.

Opaque secondary apatite occurs replacing fossilised coniferous wood in the Early Cretaceous Dandaragan Series (Playford et al., 1975; McWhae, 1958), an iron-rich, feldspathic cross bedded sandstone. This is overlain (unconformably) by the phosphatic Molecap Greensand, possibly the source of the apatite mineralising fluids.

2. Fluorapatite from Turf Pits Mine, Grassington Moor, Yorkshire, UK.

Apatite occurs in the form of opaque, yellow crystals which are accessory to the fluorite-galena-barite-calcite hydrothermal vein systems of the Carboniferous in this part of northern England. The mineralisation from the many workings on Grassington Moor was described by Dunham, (1952 and 1974).

3. Fluorapatite from Faraday Township, Hastings County, Ontario, Canada.

These apatites are green, translucent crystals, from the Precambrian Canadian craton. Faraday was worked for Uranium ore (uraninite) in pegmatites crosscutting metagabbros and amphibolites. The apatite occurs as an accessory mineral within these pegmatites (Douglas, 1968).

4. Fluorapatite from Panasqueira Mine, Beira-Baixa, Portugal.

The apatite occurs deposited in sub-horizontal, hydrothermal veins associated with Tin-Tungsten ore deposits. The samples used in this project are milky-white fibrous crystals. Further descriptions of the apatites and there paragenesis can be found in Knutson, et al. (1985) and references therein.

5. Fluorapatite from Renfrew, Canada.

The Renfrew apatites are well known for their high fluorine contents, however the precise locality of this sample is unknown. They are associated with Precambrian pegmatitic deposits, similar to those of Kongsberg-Bamble Complex, Norway.

6. Fluorapatite from Mount Dromedary, New South Wales, Australia.

The Mount Dromedary Complex is a high level, zoned intrusion comprising an outer monzonite zone and an inner quartz-monzonite zone, probably representing a volcanic plug of late Cretaceous age (97.9±1.4 Ma, K-Ar biotite; Williams et al., 1982). The apatite from this intrusion is used as a secondary fission track age standard (Green, 1985; Hurford, 1990).

7. Fluorapatite from Wakefield, Ottawa County, Quebec, Canada.

These are blue, translucent crystals of apatite from the Precambrian apatite-phlogopite deposits of the Canadian craton. At Wakefield the apatite is associated with calcite veins, in country rock of thermally metamorphosed dolomite (brucite). The region was worked for metallic Calcium and Magnesium (Douglas, 1968; Landes, 1938).

8. Fluorapatite from Cerro de Mercado, Durango, Mexico.

The Durango apatite has been extensively described by Young, et al., (1969). It is a well known apatite both for its abundant gem-quality pale yellow crystals and its use as a phosphate standard by the United States Geological Survey and consequently many other research establishments. Durango is also one of the primary age standards used by apatite fission track analysis for the calculation of the zeta calibration factor (Hurford, 1990).

Apatite from Cerro de Mercado, near Durango, is associated with a large Tertiary iron ore deposit. The apatite occurs in veins and vugs within the ore-body and occasionally as inclusions within the ore or associated with quartz.

9. Fluorapatite from Gållivare, Norrbotten, Sweden.

These green, translucent apatite crystals are from the Kiiruna-type Gållivare iron ore body in Northern Sweden(Ekström, 1972, 1973).

10. Fluorapatite from South Burgess, Leeds County, Ontario, Canada.

This crystal has well formed faces, a pale blue colour and is translucent. There are no available details of the precise locality or paragenesis of this sample, although it is probably associated with Precambrian pegmatitic mineral deposits.

11. Fluorapatite from the Fish Canyon Tuff, Colorado, USA.

The Fish Canyon Tuff is one of the largest known ash flow tuffs, erupted during the Oligocene in the San Juan Volcanic field. The tuff is phenocryst rich, and welded. Apatite occurs as inclusions in all the phenocryst phases (Whitney and Stormer, 1985). The size and homogeneity of the tuff have made the abundant apatites useful as a primary age standard for fission track analysis (Hurford, 1990).

12. Fluorapatite from Arendal, Aust-Agder, Norway.

These apatites probably come from the Gloserheia granite pegmatite in the Proterozoic Kongsberg-Bamble Formation. The blue-green translucent crystals analysed are characteristic of the intermediate zones of the pegmatite, where crystals have been known to reach sizes up to one metre (Åmli, 1975).

13. Fluorapatite from Bluestone Quarry, Bristol County, Massachussetts, USA.

These are colourless translucent crystals of apatite, associated with iron deposits (Cathcart, 1991).

14. Fluorapatite from a pegmatite.

Sample 'PFG201', the locality and paragenesis of this sample is unknown.

15. Fluor-Chlorapatite from SW Utah, USA.

The apatite is a separate from the uppermost of eight bentonite units within the middle Jurassic Carmel Formation (a shallow marine/sabkha type facies), known as Gunlock-F. The abundant apatites have a distinctly unusual composition (Kowallis, et al., 1992).

16. Fluorapatite from Snarum, Buskerud, Norway.

A sample of milky white, vein apatite. There are no details of its precise locality or paragenesis, although it is probably associated with the Precambrian Kongsberg-Bamble Complex.

17. Chlorapatite from Skaaland Mine, Arendal, Aust-Agder, Norway.

Pale brown translucent crystals of apatite are associated with the iron ores mined at Skaaland. There are two species of chlorapatite present, this sample with approximately 6 weight percentage Cl, and another with approximately 1.7 weight percentage Cl (Bugge, 1978).

18. Chlorapatite from a meta-pegmatite, Norway.

The precise locality and paragenesis of this sample is unknown, however, it is possibly from Ødegårdens Verk (see next sample).

19. Chlorapatite from Ødegårdens Verk, Bamble, Telemark, Norway.

Ødegårdens Verk was mined for apatite and other phosphate-bearing minerals. The apatite occurs in pegmatitic dykes, the products of chlorine-rich pneumatolysis and scapolitisation, crosscutting the Ødegårdite (scapolite-hornblende metagabbro) metasomatised country rock (Starmer, *pers. comm.*; Morton, 1960.)

20. Chlorapatite from Bamble, Brevik, Telemark, Norway.

This is yellow, opaque vein apatite, associated with the Kongsberg-Bamble Complex. The precise location of the sample is unknown.

Appendix 4.

Symbols

A4.1. Fission track age calculations

λ_{D8}	total decay constant for ^{238}U = 1.55125 x 10^{-10} yr^{-1}
λ_{f8}	fission decay constant for ^{238}U = 6.9 - 8.7 x 10^{-17} yr^{-1}
ρs	density of spontaneous fission tracks in the crystal
ρi	density of induced fission tracks in the detector
ρig	density of induced fission tracks in the dosimeter
ζ	personal zeta calibration factor = 356.67±5.56

A4.2. Infrared spectroscopy

F	restoring force of a spring.
r	bond length
r_0	bond length at equilibrium
m_1, m_2	atomic masses
c	velocity of light in a vacuum
λ	wavelength
v	frequency
ν	vibrational energy level
T	transmittance
R	reflectance
A	absorbance
κ	emission
n	refractive index
ε	dielectric constant

A4.3. Mineralogy

al	albite	mu	muscovite
am	amphibole	opx	orthopyroxene
bi	biotite	pl	plagioclase feldspar
cl	chlorite	qtz	quartz
cpx	clinopyroxene	sa	sanidine
ep	epidote	si	sillimanite
gt	garnet	wr	whole rock
hb	hornblende	zo	zoisite
Kfeld	potassic feldspar		